EXPLORING THE ROLE OF GLYCANS: A NEW FRONTIER IN DISEASE BIOMARKER RESEARCH

Beatrix Paton Jimenez

UNIVERSITAT ROVIRA i VIRGILI

Exploring the role of glycans: A new frontier in disease biomarker research

Beatrix Paton Jimenez

DOCTORAL THESIS 2023

UNIVERSITAT ROVIRA I VIRGILI
EXPLORING THE ROLE OF GLYCANS: A NEW FRONTIER IN DISEASE BIOMARKER RESEARCH
Beatrix Paton Jimenez

UNIVERSITAT ROVIRA I VIRGILI
EXPLORING THE ROLE OF GLYCANS: A NEW FRONTIER IN DISEASE BIOMARKER RESEARCH
Beatrix Paton Jimenez

Beatrix Paton Jimenez

Exploring the role of glycans: A new frontier in disease biomarker research

DOCTORAL THESIS

Supervised by Dr. Núria Canela Canela,

Dr. Pol Herrero Gil and Dr. Manuel Suárez Recio

Eurecat, Centre de Ciències Òmiques

Departament de Bioquímica i Biotecnologia

UNIVERSITAT ROVIRA i VIRGILI

eurecat
Centre Tecnològic de Catalunya

Reus 2023

UNIVERSITAT ROVIRA I VIRGILI
EXPLORING THE ROLE OF GLYCANS: A NEW FRONTIER IN DISEASE BIOMARKER RESEARCH
Beatrix Paton Jimenez

UNIVERSITAT ROVIRA i VIRGILI

DEPARTAMENT DE BIOQUÍMICA I BIOTECNOLOGIA
Campus Sescelades
C/ Marcel·lí Domingo, 1
43007 Tarragona
Tel. +34 977 55 95 21
Fax +34 977 55 82 32

FEM CONSTAR que aquest treball, titulat **Exploring the role of glycans: A new frontier in disease biomarker research**, que presenta **Beatrix Paton Jimenez** per a l'obtenció del títol de doctorat, ha estat realitzat sota la nostra direcció al Departament de Bioquímica i Biotecnologia de la Universitat Rovira i Virgili i que compleix els requisits per a l'obtenció de la Menció Internacional de Doctorat.

WE STATE that the present study, entitled **Exploring the role of glycans: A new frontier in disease biomarker research**, presented by **Beatrix Paton Jimenez** for the award of the degree of Doctor, has been carried out under our supervision at the Departament de Bioquímica i Biotecnologia from the Universitat Rovira i Virgili and that is eligible to apply for the International Doctoral Mention.

Tarragona, 5 de Setembre de 2023

Els directors de la tesi doctoral

Doctoral thesis supervisors



Dr. Núria Canela Canela Dr. Pol Herrero Gil Dr. Manuel Suárez Recio

UNIVERSITAT ROVIRA I VIRGILI
EXPLORING THE ROLE OF GLYCANS: A NEW FRONTIER IN DISEASE BIOMARKER RESEARCH
Beatrix Paton Jimenez

This thesis has been carried out in the Centre for Omic Sciences, a Joint Unit between Eurecat and Universitat Rovira i Virgili (URV), and supported by the Vicente López fellowship (Eurecat). The studies performed were financially supported by the Catalan Government through the funding grant ACCIÓ-Eurecat (Projects PRIV-NUTRIAGE and PRIV-COVIDOMICS). They were also supported by the Centre for the Development of Industrial Technology (CDTI) of the Spanish Ministry of Science and Innovation under a grant agreement: TECNOMIFOOD project CER-2019-1010. The international stay was partially financed by the Erasmus Plus grant.

UNIVERSITAT ROVIRA I VIRGILI
EXPLORING THE ROLE OF GLYCANS: A NEW FRONTIER IN DISEASE BIOMARKER RESEARCH
Beatrix Paton Jimenez

INDEX

SUMMARY

Glycans play a crucial role in several biological processes and have emerged as potential biomarkers in biomedical research and clinical applications. These carbohydrates are involved in cellular communication, immune responses, and disease progression. The study and analysis of glycans as biomarkers provide valuable insights into the physiological and pathological states of an organism, enabling the development of novel diagnostic tools and therapeutic interventions. Altered glycosylation patterns have been observed in numerous diseases, including cancer, cardiovascular disorders, autoimmune diseases, and infectious diseases. Such changes can be indicative of disease initiation, progression or prognosis. Moreover, glycans often exhibit alterations in the early stages of the disease, making them valuable for early detection and stratification.

In this regard, the studies included in this thesis were performed to gain a deeper understanding and provide insights into various biological processes such as ageing, age-related diseases, metabolic disorders and infectious diseases. Each study focused on analysing the glycome and its connection to these processes with the help of multi-omics approaches and advanced mass spectrometry analysis techniques. By conducting these studies, we aimed to investigate the impact of different factors, including high-glucose and high-fat diets, as well as COVID-19, on the glycome composition, with a particular focus on the N-glycome.

The integration of glycan analysis into the study of any disease, can potentially uncover novel avenues for therapeutic intervention and diagnostic tools, as well as fostering a more comprehensive understanding of the intricate relationship between glycans and disease pathogenesis.

RESUM

Els glicans juguen un paper crucial en diversos processos biològics i han emergit com a potencials biomarcadors en la recerca biomèdica i les aplicacions clíniques. Aquests carbohidrats estan implicats en la comunicació cel·lular, les respostes immunitàries i la progressió de malalties. L'estudi i l'anàlisi dels glicans com a biomarcadors proporcionen valuosos coneixements sobre els estats fisiològics i patològics d'un organisme, permetent el desenvolupament de noves eines de diagnòstic i intervencions terapèutiques. S'han observat patrons de glicosilació alterats en nombroses malalties, com el càncer, les malalties cardiovasculars, les malalties autoimmunitàries i les malalties infeccioses. Aquests canvis poden ser indicatius de l'inici, la progressió o el pronòstic de la malaltia. A més, sovint els glicans mostren alteracions en les primeres etapes de la malaltia, convertint-los en valuosos per a la detecció i la estratificació precoç.

En aquest sentit, els estudis inclosos en aquesta tesi es van realitzar per obtenir una comprensió més profunda i proporcionar coneixements sobre diversos processos biològics com l'envelliment, les malalties relacionades amb l'edat, els trastorns metabòlics i les malalties infeccioses. Cada estudi es va centrar en analitzar el glicoma i la seva connexió amb aquests processos mitjançant l'ús d'aproximacions multiòmiques i tècniques avançades d'anàlisi de l'espectrometria de masses. Mitjançant la realització d'aquests estudis, vam tenir com a objectiu investigar l'impacte de diferents factors, com les dietes riques en glucosa i greix, així com la COVID-19, en la composició del glicoma, amb un enfocament particular en el N-glicoma.

La integració de l'anàlisi de glicans en l'estudi de qualsevol malaltia pot ajudar a descobrir nous camins per a la intervenció terapèutica i eines de diagnòstic, així com fomentar una comprensió més completa de la intricada relació entre els glicans i la patogènesi de la malaltia.

ABBREVIATIONS

GPI	Glycosylphosphatidylinositol
GSLs	Glycosphingolipids
ER	Endoplasmatic reticulum
GlcNAc	N-acetylglucosamine
Asn	Asparagine
Man	Mannose
Dol-P	Dolicholpyrophosphate
Ser	Serine
Thr	Threonine
Pro	Proline
NeuAc	N-acetylneuraminic acid
GalNAc	N-acetylgalactosamine
NCDs	Noncommunicable diseases
CVDs	Cardiovascular diseases
MD	Mediterranean Diet
PTMs	Post-translational modifications
IgG	Immunoglobulin G
mRNA	Messenger RNA
MS	Mass spectrometry
LC	Liquid chromatography
TMT	Tandem mass tag

qTOF	Quadrupole time-of-flight
CE	Capillary electrophoresis
NMR	Nuclear magnetic resonance
HILIC	Hydrophilic interaction liquid chromatography
IMS	Ion mobility spectrometry
T2DM	Type 2 diabetes mellitus
AD	Alzheimer's disease
RA	Rheumatoid arthritis
ALS	Amyotrophic lateral sclerosis
IBS	Inflammatory bowel disease
HGD	High-glucose diet
PC	Phosphatidylcholines
TG	Triglycerides
HFD	High-fat diet
MED	Mediterranean-like diet
hFet	Human fetuin-A

UNIVERSITAT ROVIRA I VIRGILI
EXPLORING THE ROLE OF GLYCANS: A NEW FRONTIER IN DISEASE BIOMARKER RESEARCH
Beatrix Paton Jimenez

INTRODUCTION

UNIVERSITAT ROVIRA I VIRGILI
EXPLORING THE ROLE OF GLYCANS: A NEW FRONTIER IN DISEASE BIOMARKER RESEARCH
Beatrix Paton Jimenez

INTRODUCTION

1 GLYCOSYLATION

Glycosylation is a fundamental and highly prevalent post-translational modification that plays a crucial role in various biological processes. It involves the addition of sugar molecules, known as glycans, to proteins and lipids. Glycosylation has a significant impact on the structure, stability, function, and trafficking of these molecules, contributing to their diversity and functionality. Most glycans are located on the outermost surfaces of cellular and secreted macromolecules and are remarkably diverse. Protein-bound glycans are also abundant in the nucleus and cytoplasm of cells, where they play regulatory roles [1]. Beyond their structural significance, the sugar components of glycoconjugates have a broad range of functions in physiological and pathophysiological states [2]. Additionally, glycoproteins and polysaccharides have important functions in bacterial cells, while glycoproteins also have central roles in the biology of most viruses.[1].

A plethora of naturally occurring sugars can be combined, resulting in a wide range of distinct glycan structures on lipid and protein molecules, which modulate their function. Enzymatic site preferences and the use of stereochemical α or β linkages contribute to the complexity of where and how these sugars are linked to one another. In total, these factors suggest the possible existence of approximately 10^{12} distinct branched glycan structures [3].

Protein glycosylation involves the addition of N-linked glycans, O-linked glycans, phosphorylated glycans, glycosaminoglycans, and glycosylphosphatidylinositol (GPI) anchors to peptide backbones and C-mannosylation of tryptophan residues [4]. One the other hand, glycolipids are generated by attaching sugars to lipids; this class of glycoconjugate comprises glycosphingolipids (GSLs) [1]. The resulting glycoproteins or

glycolipids exhibit a wide range of structural variations, including the composition, length, and branching patterns of the attached glycans. These structural variations, often referred to as glycan heterogeneity, are critical determinants of their properties and functions.

1.1 Glycan biosynthesis

Glycosylation of proteins and lipids takes place in the endoplasmatic reticulum (ER) and Golgi apparatus, with most of the terminal processing occurring in the cis-, medial- and trans-Golgi compartments. In these organelles, glycosyltransferases and glycosidases construct carbohydrate structures through a series of steps controlled by factors such as substrate availability, enzyme activity, gene transcription levels, and enzyme location within the organelles. In fact, the glycome of a particular cell reflects its unique gene-expression pattern, which regulates the levels of the enzymes responsible for glycoconjugation. Unlike the genome, exome or proteome, the glycome is synthesised in a non-templated manner and is intricately controlled at multiple levels in the ER and Golgi apparatus.

1.2 N-glycosylation

N-glycosylation is a common modification of proteins, characterised by the attachment of N-acetylglucosamine (GlcNAc) to the nitrogen atom of an Asparagine (Asn) side chain through a β-1N linkage. These Asn-linked glycoconjugates, possess a core structure of $GlcNAc_2$ mannose $(Man)_3$. Additional monosaccharides can be added or removed from this core, including galactose, GlcNAc, sialic acid, and fucose, resulting in the formation of high-mannose, hybrid, or complex N-glycans (Figure 1). N-glycans are present in various organisms and play a crucial role in regulating both intracellular and extracellular functions [1]. The process of N-glycosylation relies firstly on the creation of a lipid precursor within the ER. The initial N-glycan structure consists of 14 sugar residues (Glc3Man9GlcNAc2) that are first synthesised in the ER as a branched structure on a lipid anchor, dolicholpyrophosphate (Dol-P) [5]. Once the

Dol-P-carbohydrate structure is completed, an oligosaccharyltransferase enzyme attaches the carbohydrate chain to a protein at an asparagine-X-serine/threonine (Asn-X-Ser/Thr) site (where X represents any amino acid except proline (Pro)). The nascent carbohydrate-protein conjugate undergoes further processing in the ER, typically involving the removal of glucose residues ("trimming") as part of a quality-control mechanism. Following ER processing, re-glycosylation with additional sugar residues ("processing") occurs in the Golgi apparatus, where complex N-glycans are produced through the addition of GlcNAc, galactose, sialic acid and fucose sugars, constituting complex N-glycoproteins [1,5].

1.3 O-glycosylation

Glycosylation also occurs on amino acids with functional hydroxyl groups, which are most often Ser and Thr [1]. The resulting modifications are known as *O*-glycans, which are associated with proteins in a much more ambiguous way compared to N-glycans. Lacking a common glycan core, *O*-glycosylation can occur through initial monosaccharide linkage of mannose, galactose, fucose, glucose, xylose or GlcNAc [6]. The most common *O*-glycosylation pathway is through GalNAc-*O*-glycosylation (commonly referred to as mucin-type O-glycosylation), which occurs in the Golgi apparatus, after protein folding [7]. This process eventually gives eight core structures (Figure 1), depending on the second sugar and its sugar linkage, of which cores 1-6 and core 8 have been described in humans [8]. Besides these 7 core structures, two additional epitopes can be differentiated: Tn (GalNAcα1-Ser/Thr) and sialyl Tn [NeuAcα2–6GalNAcα1-Ser/Thr; where NeuAc represents N-acetylneuraminic acid, a type of sialic acid [9]. The core structures can undergo further modifications, giving rise to heterogeneity and resulting in a range of glycan structures with varying topologies, ranging from linear to extensively branched glycan structures [6].

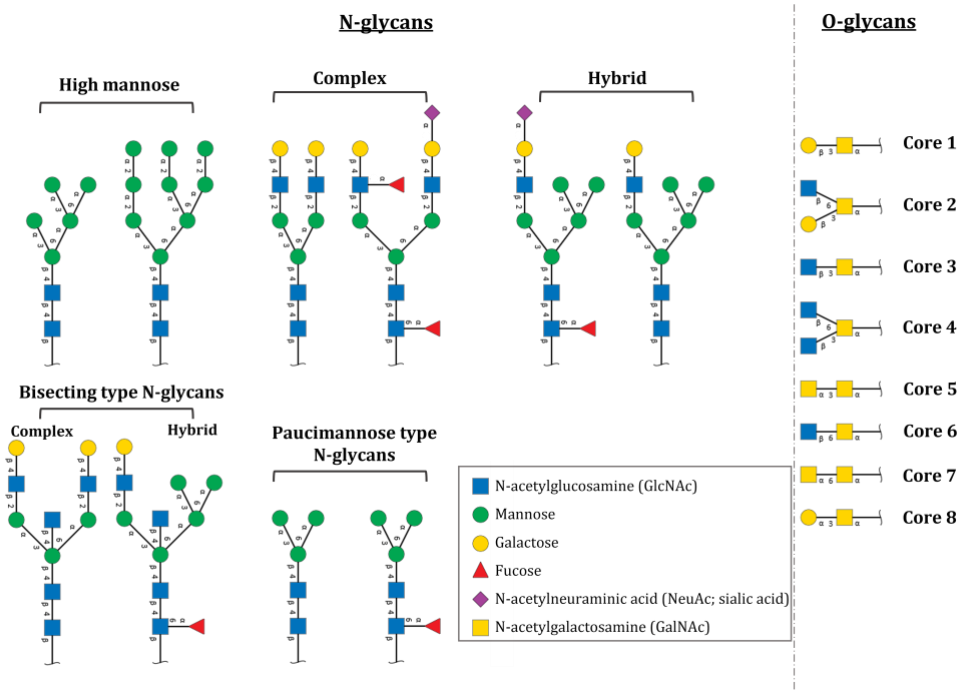

Figure 1. Major N-glycan and O-glycan structure types in mammals. Three main N-glycan structures in a mature glycoprotein include high mannose, complex and hybrid type. All classes share a common core, which may receive α 1,6-fucosylation, bisecting β 1,4-GlcNAcylation or other glycol determinants of the complex and hybrid type. Paucimannosidic type structures belong to an unusual (fourth) type of N-glycans in humans that may be truncated from the N-glycan core. Eight core structures exist for O-GalNAc-initiated glycans. Adapted from Sethi et al. [10]

2 GLYCOSYLATION IN HEALTH AND DISEASE

Glycosylation is a highly regulated process where glycoproteins play a vital role in various cellular mechanisms involved in the maintenance of health. These mechanisms include cell signalling, protein recognition, and promotion or inhibition of endocytosis [11]. Aberrant glycosylation patterns can serve as diagnostic markers and contribute to disease progression, highlighting the importance of studying glycosylation in a clinical context. Disruptions in any of these processes can contribute to the development of metabolic diseases [12,13]. Glycosylation has been associated with several diseases, such as cancer [14,15], diabetes [16],

neurodegenerative diseases [17,18] and chronic inflammatory disorders [19,20]. Additionally, glycan changes have also been associated with the process of ageing [21,22]. Several glycans are considered key factors in distinguishing between diseased and healthy states. For instance, fucosylated N-glycans (addition of 5-carbon fucose as a terminal glycan) have important implications for cancer biology [23] or galactosylation is known to decrease in type 2 diabetes mellitus patients [24–26]. Sialylated proteins (addition of 9-carbon sugar: e.g., neuraminic acid, as a terminal glycan) also play critical roles in innate immunity, ranging from antigen detection to maintaining the balance between suppression or activation of immune responses [27].

2.1 Role of nutrition

The significance of nutrition and diet in promoting and maintaining good health is widely acknowledged. In fact, both factors play a crucial role in the development and progression of noncommunicable diseases (NCDs), also known as chronic diseases. This group of pathologies includes cardiovascular diseases (CVDs), cancer, chronic respiratory diseases and diabetes, among others. NCDs account for the deaths of 41 million individuals each year, representing 74% of all deaths globally. Several risk factors contribute to the development of NCDs, including obesity, hypertension, dyslipidaemia, and hyperglycemia [28]. While further research is needed to fully comprehend the mechanisms linking diet to the onset of these conditions, it is widely recognised that NCDs can be prevented, to some extent, through proper dietary practices. Research has shown that adopting a healthy lifestyle, which includes consuming the correct intake of nutrients and bioactive foods, is closely linked to a decreased risk of morbidity/mortality, as well as an extended lifespan [29,30]. Particularly, the Mediterranean Diet (MD) is associated with a delay in ageing/death by providing antioxidant molecules and lowering the levels of inflammatory cytokines that contribute to various diseases, such as CVDs [31,32].

As stated before, nutrition plays a fundamental role in the prevention of certain diseases, however little is known about how it affects glycosylation processes. Existing reports suggest that dietary patterns can affect post-translational modifications (PTMs), specifically N-glycosylation. For instance, higher sialylation has been observed in patients after following a diet based on the Dietary Guidelines for Americans [33]. Future nutrition studies, particularly in the field of precision nutrition [34], should include nutritional physiology and biochemistry knowledge within a systems biology framework. Additionally, comprehensive phenotyping tools should be used to assess and analyse inter-individual variability. Among these tools, glycomic and glycoproteomic analyses have the potential to enhance the accuracy of analysis and assessment, potentially improving our comprehension of how individuals respond to different dietary interventions and tailor nutritional recommendations to specific needs.

2.2 Age-related diseases

Glycosylation is known to undergo changes during the process of ageing. For instance, protein N-glycosylation can be modified, resulting in an increase in certain glycoforms or the emergence of new ones after the age of 40 [35]. Traditionally, ageing has been viewed as a physiological state that promotes the development of many diseases. However, the relationship between ageing and these diseases is intricate, as they share common underlying mechanisms such as metabolism derangement, macromolecular damage, epigenetic modifications and inflammation [36,37]. This relationship led to the creation of the term “age-related diseases”. Ageing is characterised by a gradual decline in physiological well-being, which leads to impaired function and increased susceptibility to death [38]. This process is influenced both by genetic and non-genetic factors, including individuals' nutritional habits.

2.3 Dyslipidaemia

Dyslipidaemia, a well-acknowledged condition, is closely linked to an increased risk of coronary artery disease, stroke, and heart failure [39].

However, the precise mechanisms through which dyslipidaemia increases the risk of these diseases are yet to be fully understood. Notably, dyslipidaemia is influenced by alterations in systemic inflammation, a recognised underlying factor of cardiovascular and cerebrovascular diseases [40,41]. Similar to many other diseases, many glycosylation changes have been associated with dyslipidaemia. For instance, Immunoglobulin G (IgG), which plays a critical role in cardiovascular function, exhibits glycan patterns that allow distinguishing patients with dyslipidaemia from the controls. Additionally, changes in blood lipids levels have been linked to the reduction of galactose and sialic acid, along with the addition of bisecting GlcNAcs. These alterations are thought to be associated with the chronic inflammation that accompanies the development of dyslipidaemia [42].

2.4 Infectious diseases

Protein glycosylation plays a crucial role in modulating host-pathogen interactions by mediating adhesion, recognition, invasion, and immune evasion of pathogens in host cells. This intricate process influences the virulence of pathogens and the resistance of host cells [43]. Antibodies play a crucial role in the protective immune response against numerous infectious diseases and serve as primary indicators of protection for most approved vaccines. Thus, the determination of antibody glycosylation is of great interest as infectious diseases have pointed to the significant immunologic control over antibody glycosylation. Studies have revealed how glycosylation is shaped by inflammation, and importantly, how it can be controlled to direct immune function [44].

A few cross-pathogen patterns exist related to how antibody glycosylation is affected by the immune response to infection [44]. Firstly, distinct glycosylation changes occur on antibodies in an antigen-specific manner. For instance, HIV-specific antibodies exhibit distinctive IgG Fc-glycan patterns compared to influenza-specific antibodies from the same individuals [45]. Moreover, notable similarities can be observed between

antibody glycosylation in autoimmune diseases and chronic infectious diseases, both characterised by prolonged and acute inflammation. Chronic manifestations of tuberculosis and HIV infection display autoimmune like profiles, characterised by similar glycan changes, most notably, in the increased levels of agalactosylation and asialylation [46–48]. These findings suggest that chronic inflammation in both infectious and noninfectious diseases may lead to the same agalactosylated IgG Fc glycosylation profile. It is probable that in the case of autoimmunity and certain infectious diseases, the inclination towards agalactosylated and asialylated IgG is a consequence of similar inflamed immunologic pathways and thus serves as a humoral marker of inflammation [44].

As reported, antibody Fc glycosylation can influence immune response, leading to effective microbial control, highlighting the therapeutic potential of using antibodies that harness Fc glycosylation to combat infectious diseases.

3 MULTIOMIC TECHNOLOGIES FOR BIOMARKER RESEARCH

Multiomic technologies play a crucial role in biomarker research by providing a comprehensive and integrated view of biological systems. The term genomics originated from the availability of complete genome sequences, but only a small fraction of genes in the human genome (less than 2%) encodes proteins [49]. When transcribed into messenger RNAs (mRNAs), making up the “transcriptome”, approximately 30% are assigned to protein coding. The complete set of proteins expressed by a cell is known as the "proteome” and its study, “proteomics”. In eukaryotic organisms, most proteins undergo post-translational modifications (i.e phosphorylation, sulfation, oxidation, ubiquitination, acetylation, methylation, lipidation, or glycosylation) [50,51]. These modifications, combined with alternative RNA splicing, significantly increase the complexity of the proteome compared to the transcriptome. The proteome, like the transcriptome, is highly dynamic and varies depending on tissue type, microenvironment, and life cycle stage. External and internal cues such as growth factors, hormones, metabolites, or cell-to-cell interactions can modulate gene expression, resulting in a wide range of mRNA and protein levels, ranging from silence to millions of copies and protein molecules per cell [52,53]. Consequently, proteomes and their modifications undergo changes during processes such as cell differentiation, activation, trafficking, and malignant transformation. Another key omics field is “metabolomics”. It addresses the intricate and complex chemical reactions within living organisms, and it examines how these processes can be altered by external or internal disruptions. Positioned at the core of omics profiling technologies, metabolomics serves as the underlying biochemical stratum that captures insights conveyed by the genome, transcriptome, and proteome [54]. Additional types of omics data have emerged in recent years, however, no systems-level analysis of a biological process is complete without “glycomics”, which aims to

understand the structure, biosynthesis, and function of the glycome. The glycome encompasses the entire collection of glycan structures produced by cells, whether they are bound to proteins or lipids or exist in a free form. Thus, to achieve a systems-level understanding of a biological system, it is necessary to study not only the genome, transcriptome, proteome, lipidome, and metabolome but also the glycome [53]. Glycans, metabolites, and proteins are intricately interconnected through a multitude of biochemical pathways and cellular processes. Glycans have the capability to modify proteins, influencing their functions, whereas metabolites frequently function as substrates or products in enzymatic reactions involving proteins. The integration of multiple omics datasets aids in extracting valuable information and gaining a more holistic understanding of biological systems and molecular processes [54]. Additionally, integrative analyses can help identify novel biomarkers or combinations of biomarkers that exhibit stronger predictive power or diagnostic accuracy.

3.1 Role of omics in the search of novel biomarkers

Some of the main applications and benefits of omics technologies include disease research and biomarker discovery, contribution to precision medicine or aid in drug discovery and development [55–57]. The impact of omics technologies on some of these fields relies on the discovery of relevant biomarkers. A biomarker is any substance, structure or process that can be measured accurately and reproducibly in the body or its products and influence or predict the incidence or outcome of a disease [58]. Firstly, omics technologies allow generating extensive amounts of data on specific molecules (e.g., DNA, metabolites) in individuals with a particular condition [59]. This data is then analysed to determine whether specific biomarkers are associated with the presence of the disease, prognosis, or response to a specific therapeutic intervention. Lastly, biomarkers undergo multiple rounds of analytical and clinical validation before being approved for clinical use. Ultimately, the integration of biomarker-driven precision medicine and high-throughput analyses propelled by omics technologies is

expected to improve patient care [60]. However, the intricate nature of pathological conditions presents significant challenges, and omics technologies still face technical issues such as reproducibility and a high false positive rate. Nevertheless, the collaboration between clinicians, chemists, researchers, bioinformaticians, and biostatisticians in both academic and industrial settings will undoubtedly advance the development of reliable predictive, prognostic, and diagnostic biomarkers that are sensitive and specific [61].

3.2 Proteomics

As previously explained, proteomics is the study of the complete set of proteins expressed in a cell, tissue, or individual [62]. Large-scale protein analyses are widely performed thanks to the current mass spectrometry-based (MS-based) protein analysis methods [63]. A wide range of processes are included in proteomics, such as protein expression profiling, protein modifications, protein-protein interactions, protein structure, and protein function [64,65]. The outcomes obtained from these measurements contribute to unravelling disease mechanisms, facilitating disease diagnosis and prognosis, aiding in drug development, and delivering the basis for biological discovery [66–68]. Proteomics has served as a successful tool for biomarker discovery in many studies, such as diabetic kidney disease, cancer or ageing research [63,66,69–71].

Several liquid chromatography-mass spectrometry-based (LC-MS-based) proteomics strategies can be employed for the study of the proteome of biological systems, including top-down proteomics which involves the analysis of intact proteins by directly ionizing the protein [72]. On the other hand, bottom-up or shotgun proteomics, implies the digestion of intact proteins from a simple or complex sample to examine the whole proteome [73]. Differently, targeted proteomics is used to verify, validate, and absolutely quantify candidate biomarkers[74–76]. Widely used in the study of patient cohorts, shotgun proteomics workflows are comprised of an extraction of the biological sample, usually preserving the cellular state of

the system to be characterised. Sample processing also includes steps to chemically protect cysteines by reduction followed by alkylation, which cleaves existing disulfide bonds. Proteins are then cleaved into peptides by sequence-specific proteases that offer the best overall sequence coverage of proteins or that generate the particularly relevant peptides for certain PTMs. After digestion, the resulting peptides are purified and concentrated [77]. For precise quantitation, isobaric labelling, such as the tandem mass tag (TMT) is frequently used to quantify relative protein abundances in proteomic studies [78]. After labelling with this amino-reactive reagent, a combination of LC or nanoscale LC (nano LC) coupled to high-resolution MS are commonly used for the separation and detection of the peptides. To ensure precise identification and quantification of peptides from complex mixtures derived from total cell lysates, high-resolution MS is essential [77]. A high resolution analyser, such as a quadrupole time-of-flight (qTOF) or an Orbitrap analyser, in combination with higher-energy collision-induced dissociation is routinely employed to efficiently fragment peptide ions [79]. Following this proteomics pipeline, tens of thousands of unique peptides from several thousand proteins can be quantified and identified.

Proteomics plays an increasingly vital role in systems biology, as proteome composition is the result of the information that comes from genomics, epigenomics, transcriptomics, and PTMs. Consequently, the increasingly large amounts of data will demand for advances computing power [80]. Further improvements in the sensitivity and speed of MS instruments will increase the proteome coverage, eliminating the need for extensive pre-fractionation [63]. These improvements will facilitate the expansion of clinical proteomics to minimal input material and single-cell proteomics [81]. Furthermore, the development of data analysis pipelines will enable the identification of protein panels and signatures that offer superior diagnostics and prognostic accuracy compared to individual markers. These advancements are crucial for MS-based clinical proteomics to fully unleash

its potential in translating research findings into tangible improvements in clinical practice [63].

3.3 Glycomics

Glycomics focuses on the comprehensive analysis and characterization of glycans and their biological functions. It encompasses the study of the structure, biosynthesis, interactions, and roles of glycans in various biological systems [82]. This field of study plays a crucial role in understanding the roles of carbohydrates in health and disease, as well as their potential applications in the discovery of disease biomarkers and new therapeutic targets.

The genome, transcriptome, and proteome of a cell provide valuable clues about the composition and complexity of the glycome. For instance, the reduced expression of a single glycosyltransferase can disrupt the biosynthesis of numerous glycans [11]. Additionally, unlike the genome, the glycome is sensitive to external nutrient levels and metabolic fluxes, including salvage pathways. Therefore, variations in dietary monosaccharides, such as glucose, galactose, glucosamine, fucose, mannose, and N-glycolylneuraminic acid, can impact the composition of the glycome. It is this remarkable structural flexibility in response to cellular and environmental conditions that underlies the crucial roles of glycans in processes such as development, communication, and disease progression [53].

The glycome, influenced by genetic and environmental factors, provides valuable insights into both intra- and interspecies variations. Therefore, comparative glycomics, which involves comparing glycome profiles from different individuals, tissues, or conditions of interest, is an exciting frontier in biology and medicine [83]. For instance, changes in the glycome have been associated with different diseases. Any significant changes in the glycome that show a strong correlation with malignancy or other diseases may serve as a potential diagnostic marker. Notably, disease-related

alterations in the glycome might reflect downstream effects of the disease on certain organs, changes in the patient's immune system, or other disease-related effects [37,84]. However, a major challenge lies in understanding the natural variations within human glycomes. The glycome is known to respond to dietary and environmental changes and exhibits elusive variations with age, gender, and acquired susceptibility to diseases [37,85].

Overall, the study of the glycome and its variations opens up new avenues for understanding diseases, developing diagnostic tools, and uncovering the intricate connections between glycans, immune responses, and evolutionary processes.

Glycomic methods and analyses have been mostly directed toward protein glycosylation due to its biological significance. A typical experiment consists of releasing glycans from a glycoprotein-enriched sample and analysing it by LC and/or MS with or without exoglycosidase treatments (Figure 2) [86]. The most commonly used techniques for the analysis of N-glycans include LC-MS, capillary electrophoresis (CE), lectin microarray and nuclear magnetic resonance (NMR) [87]. O-glycans may be released chemically and sequenced in a similar manner to the N-glycans. However, due to their extensive heterogeneity resulting from the lack of a common glycan core, the analysis of O-glycans is particularly challenging [6].

Based on the desired level of detail, glycomic analyses can be categorised into three techniques: glycoprofiling, glycan class characterisation, and full structural analysis of the glycans released from protein(s). Glycoprofiling provides a signature to give a simple overview of the glycans in the sample, whereas glycan class characterisation uses technologies to separate glycan mixtures into types of glycans based on structural features. Differently, a detailed structural analysis involves determining the sequence and modifications of the monosaccharides, branch points, anomericity, and glycosidic linkages of the glycans present in a glycome. Orthogonal technologies are required to firstly assign preliminary structures and then

confirm the assignments [53]. For instance, a separation of glycan classes using hydrophilic interaction liquid chromatography (HILIC) can be complemented with a digestion by exoglycosidases, to help determine the sequence, anomericity, and linkage of different glycans. With MS, compositions that are consistent with the mass data can be assigned, and structural details can be resolved, by (LC) MS/MS or MS^n fragmentation [88].

Full structural analysis of glycans poses challenges due to the existence of structurally diverse glycans with identical masses, which often coelute on separation systems, and often require detailed manual annotation of MS/MS spectra. Usually, initial structural assignments are made using one technology and then validated through at least one orthogonal technology [89]. To address this bottleneck, bioinformatic tools are being developed to assist in the analysis and verification of glycan structures [83].

N-linked and O-linked glycomics are still the only techniques for comprehensively characterising the overall glycan structural landscape of the surface of a cell. These approaches will continue to be valuable in the foreseeable future for understanding cell-cell interactions [90], discovering disease biomarkers, and identifying new therapeutic targets. For the structural assignment of glycans, the use of fragmentation libraries to match fragment spectra is a promising and fast approach, which allows researchers to focus on only validating biologically relevant structures [83].

Advancements such as novel fragmentation techniques, ion mobility spectrometry (IMS), and the incorporation of heavy isotopic monosaccharides or tags offer opportunities for improved isomeric glycan characterization, quantitation, and visualization, addressing limitations in current glycomic MS techniques [89,91].

3.4 Glycoproteomics

The study of glycans as they appear on the cellular proteome is known as glycoproteomics [92]. It involves the identification and quantification of

glycosylation sites on each glycoprotein within a cell, as well as the characterization of the diverse glycan structures present at each site (Figure 2). While protein glycosylation is influenced by the collaboration of various glycosyltransferases and glycoside hydrolases [93], it might be assumed that all glycoproteins passing through the secretory pathway undergo similar modifications. However, protein- and site-specific glycosylation are well-established aspects of protein glycosylation. The exact molecular mechanisms behind protein- and site-specific glycosylation remain partly unknown, but potential factors include shared sequence motifs, protein structural conformation, unique physicochemical patches around the glycosylation site, or other yet-to-be-discovered traits. Collectively, these factors enable individual proteins to be selectively targeted among numerous others and undergo specific glycosylation processes. Since the genome, transcriptome, and proteome alone cannot accurately predict the dynamically expressed protein-linked glycans, the analysis of not only the glycome but also the glycoproteome, is necessary [53,94].

N-glycosylation sites of a complex protein sample are mapped using conventional proteomic approaches. Glycosylated proteins are subjected to proteolytic digestion and LC-MS/MS analysis, followed by the identification of the glycopeptides using the MS/MS data searched against proteomic databases [95]. Nevertheless, the available workflows for the analysis of unmodified peptides or peptides carrying simple modifications, are comparably not as developed as the corresponding proteomics methods.

In glycoproteomics, the aim is to identify all glycoproteins in a sample, including the specific sites of glycosylation occupancy (macroheterogeneity), as well as quantifying and characterising the various glycoforms at each glycosylation site (microheterogeneity) [96–98]. The ultimate goal is to capture real-time snapshots of the diverse glycan distribution on each glycoprotein within a cell, enabling insights into how site-specific glycosylation influences cellular interactions and signaling events. To fully understand the biological significance of protein glycoforms,

it is necessary to define the population of each molecular species resulting from combinations of site-specific glycan diversity across multiple sites.

A current limitation in glycoproteomics is that the glycopeptide fragment data lacks detailed information regarding glycan topology, linkage, and stereochemistry of the attached glycans. Further advancements are needed in selective enrichment and preseparation techniques for specific subsets of glycopeptides, as no single LC-MS^n method or instrument can adequately handle the full dynamic range of the entire glycopeptide pool derived from a complete glycoproteome. Current glycoproteomics methods have limitations in identifying the complete repertoire of glycans at each glycosylation site in a mixture of glycoproteins, particularly in cases of multiply glycosylated peptides with N- and O-linked structures [53,99]. Determining the relative proportions of different intact glycoform populations is crucial for understanding their biological functions, but this has been achieved in only a few cases, such as intact IgG glycoprotein analysis by MS [100]. Promising informatics initiatives have emerged to automate glycopeptide identification, aid quantitation, and support data interpretation. However, manual validation of glycopeptide assignments is still recommended to ensure confidence in the reported identifications, as false positives and non-validated glycopeptides remain a challenge. Further improvements in computational solutions are necessary to advance the field of glycoproteomics and facilitate its integration with other disciplines in the field of glycosciences [53].

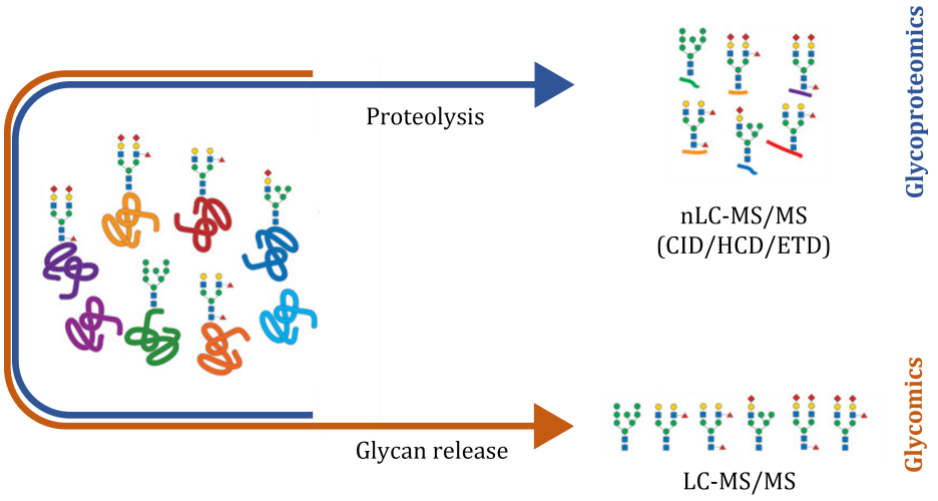

Figure 2. Simplified workflow for a glycomics and glycoproteomics procedure. Adapted from Rudd et al. [53]

REFERENCES

1. Reily C, Stewart TJ, Renfrow MB, Novak J. Glycosylation in health and disease. Nat Rev Nephrol 2019 156. 2019;15: 346–366. doi:10.1038/s41581-019-0129-4

2. Varki A. Biological roles of glycans. Glycobiology. 2017;27: 3. doi:10.1093/GLYCOB/CWW086

3. Laine RA. A calculation of all possible oligosaccharide isomers both branched and linear yields 1.05 x 10(12) structures for a reducing hexasaccharide: the Isomer Barrier to development of single-method saccharide sequencing or synthesis systems. Glycobiology. 1994;4: 759–767. doi:10.1093/GLYCOB/4.6.759

4. Spiro RG. Protein glycosylation: nature, distribution, enzymatic formation, and disease implications of glycopeptide bonds. Glycobiology. 2002;12: 43R-56R. doi:10.1093/GLYCOB/12.4.43R

5. Bieberich E. Synthesis, processing, and function of N-glycans in N-glycoproteins. Adv Neurobiol. 2014;9: 47. doi:10.1007/978-1-4939-1154-7_3

6. Saldova R, Wilkinson H. Current methods for the characterization of o-glycans. J Proteome Res. 2020;19: 3890–3905. doi:10.1021/ACS.JPROTEOME.0C00435/ASSET/IMAGES/LARGE/PR0C00435_0005.JPEG

7. Tuccillo FM, De Laurentiis A, Palmieri C, Fiume G, Bonelli P, Borrelli A, et al. Aberrant Glycosylation as Biomarker for Cancer: Focus on CD43. Biomed Res Int. 2014;2014. doi:10.1155/2014/742831

8. Brockhausen I. Pathways of O-glycan biosynthesis in cancer cells. Biochim Biophys Acta - Gen Subj. 1999;1473: 67–95. doi:10.1016/S0304-4165(99)00170-1

9. Wopereis S, Lefeber DJ, Morava É, Wevers RA. Mechanisms in Protein O-Glycan Biosynthesis and Clinical and Molecular Aspects of Protein O-Glycan Biosynthesis Defects: A Review. Clin Chem. 2006;52: 574–600. doi:10.1373/CLINCHEM.2005.063040

10. Sethi MK, Fanayan S. Mass Spectrometry-Based N-Glycomics of Colorectal Cancer. Int J Mol Sci 2015, Vol 16, Pages 29278-29304. 2015;16: 29278–29304. doi:10.3390/IJMS161226165

11. Ohtsubo K, Marth JD. Glycosylation in cellular mechanisms of health and disease. Cell. 2006;126: 855–867. doi:10.1016/J.CELL.2006.08.019

12. Mukherjee A, Morales-Scheihing D, Butler PC, Soto C. Type 2 Diabetes as a Protein Misfolding Disease. Trends Mol Med. 2015;21: 439. doi:10.1016/J.MOLMED.2015.04.005

13. Shental-Bechor D, Levy Y. Effect of glycosylation on protein folding: a close look at thermodynamic stabilization. Proc Natl Acad Sci U S A. 2008;105: 8256–8261. doi:10.1073/PNAS.0801340105

14. Hu Y, Ferdosi S, Kapuruge EP, Diaz de Leon JA, Stücker I, Radoï L, et al. Diagnostic and Prognostic Performance of Blood Plasma Glycan Features in the Women Epidemiology Lung Cancer (WELCA) Study. J Proteome Res. 2019. doi:10.1021/acs.jproteome.9b00457

15. Li Q, Li G, Zhou Y, Zhang X, Sun M, Jiang H, et al. Comprehensive N-Glycome Profiling of Cells and Tissues for Breast Cancer Diagnosis. J Proteome Res. 2019;18: 2559–2570. doi:10.1021/acs.jproteome.9b00073

16. Rudman N, Gornik O, Lauc G. Altered N-glycosylation profiles as potential biomarkers and drug targets in diabetes. FEBS Lett. 2019;593: 1598–1615. doi:10.1002/1873-3468.13495

17. Costa J, Streich L, Pinto S, Pronto-Laborinho A, Nimtz M, Conradt HS, et al. Exploring Cerebrospinal Fluid IgG N-Glycosylation as Potential Biomarker for Amyotrophic Lateral Sclerosis. Mol Neurobiol. 2019;56: 5729–5739. doi:10.1007/s12035-019-1482-9

18. Lundström SL, Yang H, Lyutvinskiy Y, Rutishauser D, Herukka SK, Soininen H, et al. Blood plasma IgG Fc glycans are significantly altered in Alzheimer's disease and progressive mild cognitive impairment. J Alzheimer's Dis. 2014;38: 567–579. doi:10.3233/JAD-131088

19. Fernandes-Cerqueira C, Renard N, Notarnicola A, Wigren E, Gräslund S, Zubarev RA, et al. Patients with anti-Jo1 antibodies display a characteristic

IgG Fc-glycan profile which is further enhanced in anti-Jo1 autoantibodies. Sci Rep. 2018;8: 1–11. doi:10.1038/s41598-018-36395-z

20. Sebastian A, Alzain MA, Asweto CO, Song H, Cui L, Yu X, et al. Glycan Biomarkers for Rheumatoid Arthritis and Its Remission Status in Han Chinese Patients. Omi A J Integr Biol. 2016;20: 343–351. doi:10.1089/omi.2016.0050

21. Šunderić M, Križáková M, Malenković V, Ćujić D, Katrlík J, Nedić O. Changes Due to Ageing in the Glycan Structure of Alpha-2-Macroglobulin and Its Reactivity with Ligands. Protein J. 2019;38: 23–29. doi:10.1007/s10930-018-9806-6

22. Krištić J, Vučković F, Menni C, Klarić L, Keser T, Beceheli I, et al. Glycans are a novel biomarker of chronological and biological ages. Journals Gerontol - Ser A Biol Sci Med Sci. 2014;69: 779–789. doi:10.1093/gerona/glt190

23. Keeley TS, Yang S, Lau E. The Diverse Contributions of Fucose Linkages in Cancer. Cancers (Basel). 2019;11: 1241. doi:10.3390/CANCERS11091241

24. Li X, Wang H, Russell A, Cao W, Wang X, Ge S, et al. Type 2 Diabetes Mellitus is Associated with the Immunoglobulin G N-Glycome through Putative Proinflammatory Mechanisms in an Australian Population. Omi A J Integr Biol. 2019;23. doi:10.1089/omi.2019.0075

25. Lemmers RFH, Vilaj M, Urda D, Agakov F, Šimurina M, Klaric L, et al. IgG glycan patterns are associated with type 2 diabetes in independent European populations. Biochim Biophys acta Gen Subj. 2017;1861: 2240–2249. doi:10.1016/j.bbagen.2017.06.020

26. Testa R, Vanhooren V, Bonfigli AR, Boemi M, Olivieri F, Ceriello A, et al. N-Glycomic changes in serum proteins in type 2 diabetes mellitus correlate with complications and with metabolic syndrome parameters. PLoS One. 2015;10: 1–16. doi:10.1371/journal.pone.0119983

27. Varki A, Gagneux P. Multifarious roles of sialic acids in immunity. Ann N Y Acad Sci. 2012;1253: 16–36. doi:10.1111/J.1749-6632.2012.06517.X

28. World Health Organization. Noncommunicable diseases. In: WHO [Internet]. 2022 [cited 20 Jun 2023]. Available:

https://www.who.int/news-room/fact-sheets/detail/noncommunicable-diseases

29. Cardelli M, Marchegiani F, Cavallone L, Olivieri F, Giovagnetti S, Mugianesi E, et al. Calorie Restriction and Aging: The Ultimate "Cleansing Diet." Journals Gerontol Ser A. 2008;63: 547–549. doi:10.1093/GERONA/63.6.547

30. Mancuso C, Scapagnini G, Currò D, Giuffrida Stella AM, De Marco C, Butterfield DA, et al. Mitochondrial dysfunction, free radical generation and cellular stress response in neurodegenerative disorders. Front Biosci. 2007;12: 1107–1123. doi:10.2741/2130

31. Capurso C, Bellanti F, Buglio A Lo, Vendemiale G. The Mediterranean Diet Slows Down the Progression of Aging and Helps to Prevent the Onset of Frailty: A Narrative Review. Nutrients. 2020;12. doi:10.3390/NU12010035

32. Dedoussis G V., Kanoni S, Mariani E, Cattini L, Herbein G, Fulop T, et al. Mediterranean diet and plasma concentration of inflammatory markers in old and very old subjects in the ZINCAGE population study. Clin Chem Lab Med. 2008;46: 990–996. doi:10.1515/CCLM.2008.191

33. Kim T, Xie Y, Li Q, Artegoitia VM, Lebrilla CB, Keim NL, et al. Diet affects glycosylation of serum proteins in women at risk for cardiometabolic disease. Eur J Nutr. 2021. doi:10.1007/s00394-021-02539-7

34. Alabduljabbar S, Zaidan S Al, Lakshmanan AP, Terranegra A. Personalized Nutrition Approach in Pregnancy and Early Life to Tackle Childhood and Adult Non-Communicable Diseases. Life. 2021;11. doi:10.3390/LIFE11060467

35. Vanhooren V, Dewaele S, Libert C, Engelborghs S, De Deyn PP, Toussaint O, et al. Serum N-glycan profile shift during human ageing. Exp Gerontol. 2010;45: 738–743. doi:10.1016/j.exger.2010.08.009

36. Franceschi C, Garagnani P, Morsiani C, Conte M, Santoro A, Grignolio A, et al. The continuum of aging and age-related diseases: Common mechanisms but different rates. Front Med. 2018;5. doi:10.3389/fmed.2018.00061

37. Miura Y, Endo T. Glycomics and glycoproteomics focused on aging and age-

related diseases - Glycans as a potential biomarker for physiological alterations. Biochim Biophys Acta - Gen Subj. 2016;1860: 1608–1614. doi:10.1016/j.bbagen.2016.01.013

38. López-Otín C, Blasco MA, Partridge L, Serrano M, Kroemer G. The Hallmarks of Aging Europe PMC Funders Group. Cell. 2013;153: 1194–1217. doi:10.1016/j.cell.2013.05.039

39. Maki KC, Guyton JR, Orringer CE, Hamilton-Craig I, Alexander DD, Davidson MH. Triglyceride-lowering therapies reduce cardiovascular disease event risk in subjects with hypertriglyceridemia. J Clin Lipidol. 2016;10: 905–914. doi:10.1016/J.JACL.2016.03.008

40. Aravindhan V, Madhumitha H. Metainflammation in Diabetic Coronary Artery Disease: Emerging Role of Innate and Adaptive Immune Responses. J Diabetes Res. 2016;2016. doi:10.1155/2016/6264149

41. Zheng J, Wu J, Chen J, Liu J, Lu Y, Huang C, et al. Therapeutic effects of quercetin on early inflammation in hypertriglyceridemia-related acute pancreatitis and its mechanism. Pancreatology. 2016;16: 200–210. doi:10.1016/J.PAN.2016.01.005

42. Liu D, Chu X, Wang H, Dong J, Ge SQ, Zhao ZY, et al. The changes of immunoglobulin G N-glycosylation in blood lipids and dyslipidaemia. J Transl Med. 2018;16: 1–10. doi:10.1186/S12967-018-1616-2/FIGURES/3

43. Lin B, Qing X, Liao J, Zhuo K. Role of Protein Glycosylation in Host-Pathogen Interaction. Cells. 2020;9. doi:10.3390/CELLS9041022

44. Irvine EB, Alter G. Understanding the role of antibody glycosylation through the lens of severe viral and bacterial diseases. Glycobiology. 2020;30: 241–253. doi:10.1093/GLYCOB/CWAA018

45. Mahan AE, Jennewein MF, Suscovich T, Dionne K, Tedesco J, Chung AW, et al. Antigen-Specific Antibody Glycosylation Is Regulated via Vaccination. PLoS Pathog. 2016;12. doi:10.1371/JOURNAL.PPAT.1005456

46. Vadrevu SK, Trbojevic-Akmacic I, Kossenkov A V., Colomb F, Giron LB, Anzurez A, et al. Frontline Science: Plasma and immunoglobulin G galactosylation associate with HIV persistence during antiretroviral

therapy. J Leukoc Biol. 2018;104: 461–471. doi:10.1002/JLB.3HI1217-500R

47. Parekh R, Isenberg D, Rook G, Roitt I, Dwek R, Rademacher T. A comparative analysis of disease-associated changes in the galactosylation of serum IgG. J Autoimmun. 1989;2: 101–114. doi:10.1016/0896-8411(89)90148-0

48. Moore JS, Wu X, Kulhavy R, Tomana M, Novak J, Moldoveanu Z, et al. Increased levels of galactose-deficient IgG in sera of HIV-1-infected individuals. AIDS. 2005;19: 381–389. doi:10.1097/01.AIDS.0000161767.21405.68

49. Carninci P, Kasukawa T, Katayama S, Gough J, Frith MC, Maeda N, et al. The transcriptional landscape of the mammalian genome. Science. 2005;309: 1559–1563. doi:10.1126/SCIENCE.1112014

50. Woods AS, Wang HYJ, Jackson SN. Sulfation, the Up-and-Coming Post-Translational Modification: Its Role and Mechanism in Protein–Protein Interaction. J Proteome Res. 2007;6: 1176. doi:10.1021/PR060529G

51. Chen L, Kashina A. Post-translational Modifications of the Protein Termini. Front Cell Dev Biol. 2021;9: 719590. doi:10.3389/FCELL.2021.719590/BIBTEX

52. Lemmon MA, Schlessinger J. Cell signaling by receptor-tyrosine kinases. Cell. 2010;141: 1117. doi:10.1016/J.CELL.2010.06.011

53. Rudd PM, Karlsson NG, Khoo K-H, Thaysen-Andersen M, Wells L, Packer NH. Glycomics and Glycoproteomics. Essentials Glycobiol. 2022 [cited 31 May 2023]. doi:10.1101/GLYCOBIOLOGY.4E.51

54. Jendoubi T. Approaches to Integrating Metabolomics and Multi-Omics Data: A Primer. Metabolites. 2021;11. doi:10.3390/METABO11030184

55. Ahmed Z. Precision medicine with multi-omics strategies, deep phenotyping, and predictive analysis. Prog Mol Biol Transl Sci. 2022;190: 101–125. doi:10.1016/BS.PMBTS.2022.02.002

56. Paananen J, Fortino V. An omics perspective on drug target discovery platforms. Brief Bioinform. 2020;21: 1937–1953. doi:10.1093/BIB/BBZ122

57. Montaner J, Ramiro L, Simats A, Tiedt S, Makris K, Jickling GC, et al. Multilevel

omics for the discovery of biomarkers and therapeutic targets for stroke. Nat Rev Neurol 2020 165. 2020;16: 247–264. doi:10.1038/s41582-020-0350-6

58. Strimbu K, Tavel JA. What are Biomarkers? Curr Opin HIV AIDS. 2010;5: 463. doi:10.1097/COH.0B013E32833ED177

59. McShane LM, Polley MYC. Development of omics-based clinical tests for prognosis and therapy selection: the challenge of achieving statistical robustness and clinical utility. Clin Trials. 2013;10: 653–665. doi:10.1177/1740774513499458

60. Karczewski KJ, Snyder MP. Integrative omics for health and disease. Nat Rev Genet. 2018;19: 299. doi:10.1038/NRG.2018.4

61. Quezada H, Guzmán-Ortiz AL, Díaz-Sánchez H, Valle-Rios R, Aguirre-Hernández J. Omics-based biomarkers: current status and potential use in the clinic. Boletín Médico Del Hosp Infant México (English Ed. 2017;74: 219–226. doi:10.1016/J.BMHIME.2017.11.030

62. Graves PR, Haystead TAJ. Molecular Biologist's Guide to Proteomics. Microbiol Mol Biol Rev. 2002;66: 39. doi:10.1128/MMBR.66.1.39-63.2002

63. Macklin A, Khan S, Kislinger T. Recent advances in mass spectrometry based clinical proteomics: applications to cancer research. Clin Proteomics 2020 171. 2020;17: 1–25. doi:10.1186/S12014-020-09283-W

64. Hyung SJ, Ruotolo BT. Integrating Mass Spectrometry of Intact Protein Complexes into Structural Proteomics. Proteomics. 2012;12: 1547. doi:10.1002/PMIC.201100520

65. Pandey A, Mann M. Proteomics to study genes and genomes. Nature. 2000;405: 837–846. doi:10.1038/35015709

66. Kwon YW, Jo HS, Bae S, Seo Y, Song P, Song M, et al. Application of Proteomics in Cancer: Recent Trends and Approaches for Biomarkers Discovery. Front Med. 2021;8: 747333. doi:10.3389/FMED.2021.747333/BIBTEX

67. Prieto P, JaÉn RI, Calle D, Gómez-Serrano M, Núñez E, Fernández-Velasco M, et al. Interplay between post-translational cyclooxygenase-2 modifications

and the metabolic and proteomic profile in a colorectal cancer cohort. World J Gastroenterol. 2019;25: 433–446. doi:10.3748/WJG.V25.I4.433

68. Zaslavsky BY, Uversky VN, Chait A. Solvent interaction analysis as a proteomic approach to structure-based biomarker discovery and clinical diagnostics. Expert Rev Proteomics. 2016;13: 9–17. doi:10.1586/14789450.2016.1116945

69. Wu J, Chen YD, Gu W. Review: Urinary proteomics as a novel tool for biomarker discovery in kidney diseases. J Zhejiang Univ Sci B. 2010;11: 227. doi:10.1631/JZUS.B0900327

70. Moresco RN, De Carvalho JAM. Applying proteomics to diagnosis of diabetic kidney disease. Expert Rev Proteomics. 2017;14: 841–843. doi:10.1080/14789450.2017.1378100

71. Tanaka T, Basisty N, Fantoni G, Candia J, Moore AZ, Biancotto A, et al. Plasma proteomic biomarker signature of age predicts health and life span. Elife. 2020;9: 1–24. doi:10.7554/ELIFE.61073

72. Carrillo-Rodriguez P, Selheim F, Hernandez-Valladares M. Mass Spectrometry-Based Proteomics Workflows in Cancer Research: The Relevance of Choosing the Right Steps. Cancers 2023, Vol 15, Page 555. 2023;15: 555. doi:10.3390/CANCERS15020555

73. Catherman AD, Skinner OS, Kelleher NL. Top Down Proteomics: Facts and Perspectives. Biochem Biophys Res Commun. 2014;445: 683. doi:10.1016/J.BBRC.2014.02.041

74. Lee H, Kim S Il. Review of Liquid Chromatography-Mass Spectrometry-Based Proteomic Analyses of Body Fluids to Diagnose Infectious Diseases. Int J Mol Sci. 2022;23. doi:10.3390/IJMS23042187

75. van Bentum M, Selbach M. An Introduction to Advanced Targeted Acquisition Methods. Mol Cell Proteomics. 2021;20: 100165. doi:10.1016/J.MCPRO.2021.100165

76. Toby TK, Fornelli L, Srzentić K, DeHart CJ, Levitsky J, Friedewald J, et al. A comprehensive pipeline for translational top-down proteomics from a single blood draw. Nat Protoc 2018 141. 2018;14: 119–152.

doi:10.1038/s41596-018-0085-7

77. Meissner F, Mann M. Quantitative shotgun proteomics: considerations for a high-quality workflow in immunology. Nat Immunol 2014 152. 2014;15: 112–117. doi:10.1038/ni.2781

78. Thompson A, Schäfer J, Kuhn K, Kienle S, Schwarz J, Schmidt G, et al. Tandem Mass Tags: A Novel Quantification Strategy for Comparative Analysis of Complex Protein Mixtures by MS/MS. Anal Chem. 2003;75: 1895–1904. doi:10.1021/AC0262560

79. Geiger T, Cox J, Mann M. Proteomics on an Orbitrap Benchtop Mass Spectrometer Using All-ion Fragmentation. Mol Cell Proteomics. 2010;9: 2252. doi:10.1074/MCP.M110.001537

80. Gracia KC, Husi H. Computational Approaches in Proteomics. Comput Biol. 2019; 119–142. doi:10.15586/COMPUTATIONALBIOLOGY.2019.CH8

81. Bennett HM, Stephenson W, Rose CM, Darmanis S. Single-cell proteomics enabled by next-generation sequencing or mass spectrometry. Nat Methods 2023 203. 2023;20: 363–374. doi:10.1038/s41592-023-01791-5

82. Cosgrave EFJ, Struwe WB, Kattla JJ, Campbell MP, Wormald MR, Rudd PM. Glycomics. Compr Biotechnol Second Ed. 2011;1: 427–446. doi:10.1016/B978-0-08-088504-9.00051-9

83. Rojas-Macias MA, Mariethoz J, Andersson P, Jin C, Venkatakrishnan V, Aoki NP, et al. Towards a standardized bioinformatics infrastructure for N- and O-glycomics. Nat Commun. 2019;10. doi:10.1038/S41467-019-11131-X

84. Kolarich D, Lepenies B, Seeberger PH. Glycomics, glycoproteomics and the immune system. Curr Opin Chem Biol. 2012;16: 214–220. doi:10.1016/J.CBPA.2011.12.006

85. Merleev AA, Park D, Xie Y, Kailemia MJ, Xu G, Ruhaak LR, et al. A site-specific map of the human plasma glycome and its age and gender-associated alterations. Sci Reports 2020 101. 2020;10: 1–11. doi:10.1038/s41598-020-73588-x

86. Trbojević-Akmačić I, Lageveen-Kammeijer GSM, Heijs B, Petrović T, Deriš H,

Wuhrer M, et al. High-Throughput Glycomic Methods. Chem Rev. 2022;122: 15865–15913. doi:10.1021/ACS.CHEMREV.1C01031/ASSET/IMAGES/LARGE/CR1C01031_0016.JPEG

87. Trbojević-Akmačić I, Lageveen-Kammeijer GSM, Heijs B, Petrović T, Deriš H, Wuhrer M, et al. High-Throughput Glycomic Methods. Chem Rev. 2022;122: 15865–15913. doi:10.1021/ACS.CHEMREV.1C01031/ASSET/IMAGES/LARGE/CR1C01031_0016.JPEG

88. Huang Y, Nie Y, Boyes B, Orlando R. Resolving isomeric glycopeptide glycoforms with hydrophilic interaction chromatography (HILIC). J Biomol Tech. 2016;27: 98–104. doi:10.7171/JBT.16-2703-003/-/DC1

89. Sastre Toraño J, Aizpurua-Olaizola O, Wei N, Li T, Unione L, Jiménez-Osés G, et al. Identification of Isomeric N-Glycans by Conformer Distribution Fingerprinting using Ion Mobility Mass Spectrometry. Chem – A Eur J. 2021;27: 2149–2154. doi:10.1002/CHEM.202004522

90. Kaltner H, Abad-Rodríguez J, Corfield AP, Kopitz J, Gabius HJ. The sugar code: letters and vocabulary, writers, editors and readers and biosignificance of functional glycan-lectin pairing. Biochem J. 2019;476: 2623–2655. doi:10.1042/BCJ20170853

91. Delafield DG, Li L. Recent Advances in Analytical Approaches for Glycan and Glycopeptide Quantitation. Mol Cell Proteomics. 2021;20: 100054. doi:10.1074/MCP.R120.002095

92. Thomas DR, Scott NE. Glycoproteomics: growing up fast. Curr Opin Struct Biol. 2021;68: 18–25. doi:10.1016/J.SBI.2020.10.028

93. Cantarel BI, Coutinho PM, Rancurel C, Bernard T, Lombard V, Henrissat B. The Carbohydrate-Active EnZymes database (CAZy): an expert resource for Glycogenomics. Nucleic Acids Res. 2009;37: D233. doi:10.1093/NAR/GKN663

94. Bagdonaite I, Malaker SA, Polasky DA, Riley NM, Schjoldager K, Vakhrushev SY, et al. Glycoproteomics. Nat Rev Methods Prim 2022 21. 2022;2: 1–29.

doi:10.1038/s43586-022-00128-4

95. Bagdonaite I, Malaker SA, Polasky DA, Riley NM, Schjoldager K, Vakhrushev SY, et al. Glycoproteomics. Nat Rev Methods Prim 2022 21. 2022;2: 1–29. doi:10.1038/s43586-022-00128-4

96. Rudd PM, Dwek RA. Glycosylation: heterogeneity and the 3D structure of proteins. Crit Rev Biochem Mol Biol. 1997;32: 1–100. doi:10.3109/10409239709085144

97. Thaysen-Andersen M, Packer NH. Site-specific glycoproteomics confirms that protein structure dictates formation of N-glycan type, core fucosylation and branching. Glycobiology. 2012;22: 1440–1452. doi:10.1093/GLYCOB/CWS110

98. Thaysen-Andersen M, Packer NH, Schulz BL. Maturing Glycoproteomics Technologies Provide Unique Structural Insights into the N-glycoproteome and Its Regulation in Health and Disease. Mol Cell Proteomics. 2016;15: 1773. doi:10.1074/MCP.O115.057638

99. Narimatsu H, Kaji H, Vakhrushev SY, Clausen H, Zhang H, Noro E, et al. Current Technologies for Complex Glycoproteomics and Their Applications to Biology/Disease-Driven Glycoproteomics. J Proteome Res. 2018;17: 4097–4112. doi:10.1021/ACS.JPROTEOME.8B00515/SUPPL_FILE/PR8B00515_SI_001.XLSX

100. Zauner G, Selman MHJ, Bondt A, Rombouts Y, Blank D, Deelder AM, et al. Glycoproteomic Analysis of Antibodies. Mol Cell Proteomics. 2013;12: 856–865. doi:10.1074/MCP.R112.026005

UNIVERSITAT ROVIRA I VIRGILI
EXPLORING THE ROLE OF GLYCANS: A NEW FRONTIER IN DISEASE BIOMARKER RESEARCH
Beatrix Paton Jimenez

HYPOTHESIS AND OBJECTIVES

UNIVERSITAT ROVIRA I VIRGILI
EXPLORING THE ROLE OF GLYCANS: A NEW FRONTIER IN DISEASE BIOMARKER RESEARCH
Beatrix Paton Jimenez

HYPOTHESIS AND OBJECTIVES

Glycans play a crucial role in several biological processes and are involved in cellular communication, immune responses, and disease progression. The study and analysis of glycans provide valuable insights into the physiological and pathological states of an organism, enabling the development of novel diagnostic tools and therapeutic interventions. Altered glycosylation patterns have been observed in numerous diseases, including cancer, cardiovascular disorders, autoimmune diseases, and infectious diseases. Such changes can be indicative of disease initiation, progression or prognosis. Moreover, glycans often exhibit alterations in the early stages of the disease, making them valuable for early detection and stratification, aiding in identifying therapeutic targets for drug development. Nevertheless, the study and analysis of glycans frequently centre around the post-translational modifications (PTMs) of a single protein target, often falling short of a comprehensive omic perspective akin to metabolomics, proteomics, or genomics. Furthermore, while the analytical techniques employed for glycan analysis have witnessed notable advancements in their capacity to deeply characterise complex biological samples, their application as an omic approach remains less explored.

In this context, we **hypothesise** that **glycome signatures hold significant potential as biomarkers for various diseases. Additionally, by incorporating data from complementary omics disciplines, the predictive value of these glycan-based biomarkers can be increased**.

Thus, the **main objective** of this thesis is **to identify glycome signatures associated with different diseases that can serve as robust and informative biomarkers.** By analysing the glycome composition, specifically the N-glycome, we aimed to identify distinct patterns or alterations that could differentiate disease states and potentially provide valuable diagnostic or prognostic information. This holds particular

promise in addressing areas such as ageing, age-related diseases and infectious diseases, where a deeper understanding of the underlying biological mechanisms is needed.

To verify the confidence of this hypothesis, several specific objectives with their correspondent sub-objectives have been proposed:

1. **To explore the alterations in the N-glycome, related to the process of ageing and age-related conditions (Chapter 1).**

1.1 To discuss the available reported alterations in the N-glycome, specifically related to the process of ageing and age-related conditions such as cancer, type 2 diabetes mellitus, metabolic syndrome, and chronic inflammatory diseases, as well as describe the available techniques for N-glycan analysis (**Manuscript 1**).

1.2 To explore the effects of a high-glucose diet on ageing, employing the animal model *C. elegans* (**Manuscript 2**).

Within this sub-objective, we aim to gain a deeper understanding of the intricate molecular mechanisms underlying various biological processes such as development and ageing, by examining the N-glycosylation patterns. To obtain a comprehensive understanding of the N-glycome and potentially provide complementary data, we will determine the proteome of *C. elegans*. Additionally, we will evaluate the lifespan, perform lipidome profiling, and explore the participation of transcriptional regulators associated with longevity, lipid accumulation, and oxidative stress. By conducting this multi-omics study, our overarching goal is to investigate the effects of dietary glucose on N2, short-lived CF1038, and long-lived CB1370 worms.

2. **To examine how a high-fat diet (HFD) can alter the brain N-glycan and lipid profile and evaluate the potential of a**

Mediterranean-like diet (MED) to reverse this situation (Chapter 2).

With the aim of attaining a comprehensive understanding of brain protein N-glycosylation, we seek to investigate how a HFD can impact the N-glycan and lipid profiles of the brain. Furthermore, we aim to evaluate the changes that occur when transitioning from a HFD to a healthier regimen based on a MED. This research holds the potential to provide valuable insights into the brain's plasticity and its ability to recover when subjected to contrasting and sequential lifestyle patterns. N-glycosylation is a crucial player in the development, organization, and regulation of the brain, remarking the importance of identifying and comprehending the specific N-glycan species involved and their alteration under different conditions (**Manuscript 3**).

3. **To determine glycan signatures for reliable risk stratification of COVID-19 patients and to identify patients who are more likely to progress to a critical stage (Chapter 3).**

3.1 To analyse the total plasma N-glycome composition from COVID-19 patients and evaluate whether it can act as a biomarker for the development of the disease.

The pathological mechanisms of SARS-CoV-2 in humans are still not fully understood, and the unpredictability of COVID-19 progression may be attributed to the lack of biomarkers that can contribute to the disease prognosis. For this, this study focuses on analysing the plasma N-glycome composition at diagnosis and 4 weeks postdiagnosis, to assess if it can enable reliable risk stratification and identify individuals who are at a higher risk of progressing to a critical stage of the disease (**Manuscript 4**).

3.2 To perform a site-specific glycan analysis of human fetuin-A in COVID-19 patients.

Fetuin-A has been reported to be an accurate biomarker of the critical clinical progression of COVID-19, decreasing with increasing severity. To potentially obtain a deeper understanding of the functional significance of glycosylation, we will perform a site-specific glycan analysis of human fetuin-A, aiming to look for differences in the glycosylation pattern between groups of severity (**Manuscript 5**).

Additionally, **two cross-cutting objectives have been assessed in this thesis**.

4. **To perform a comprehensive analysis of the total glycome, adopting a streamlined approach that offers a global perspective of the total glycosignature**. To achieve this, we have chosen mass spectrometry as the technique of preference in all our studies, based on its optimal suitability for glycan analysis.
5. **To examine glycans across diverse animal models** (*C. elegans*, golden Syrian hamster and humans) and different matrices (worm culture, plasma and brain), assessing the viability of glycomic studies in different organisms.

UNIVERSITAT ROVIRA I VIRGILI
EXPLORING THE ROLE OF GLYCANS: A NEW FRONTIER IN DISEASE BIOMARKER RESEARCH
Beatrix Paton Jimenez

RESULTS

UNIVERSITAT ROVIRA I VIRGILI
EXPLORING THE ROLE OF GLYCANS: A NEW FRONTIER IN DISEASE BIOMARKER RESEARCH
Beatrix Paton Jimenez

Chapter 1

To explore the alterations in the N-glycome,

related to the process of ageing

and age-related conditions

PREFACE

In this first chapter, we aimed to explore the alterations in the N-glycome, related to the process of ageing and age-related conditions. As discussed in the introduction, the integration of glycome analyses with other omics datasets can help identify novel biomarkers or combinations of biomarkers that exhibit stronger predictive power or diagnostic accuracy.

To accomplish this, we conducted a state-of-the-art review (**Manuscript 1**) focused on the reported N-glycan alterations reported in ageing and age-related conditions, including cancer, type 2 diabetes mellitus, metabolic syndrome, and chronic inflammatory diseases. We also evaluated the techniques employed for N-glycan analysis, aiding us in determining the most suitable technique for the subsequent studies. Following that, we proposed the elaboration of the work compiled in **Manuscript 2** after identifying a research gap pertaining to how dietary glucose influences N-glycome changes during ageing. In this pursuit, we selected *C. elegans* for its exceptional value for ageing research. Our study encompassed a multi-omics approach, involving N-glycomics, proteomics and lipidomics analyses. Additionally, we examined lifespan and the participation of transcriptional regulators associated with longevity, lipid accumulation and oxidative stress. Three different *C. elegans* strains were used in this research: wild-type N2, short-lived CF1038, and long-lived CB1370 worms. In both manuscripts, we assessed the two cross-cutting objectives by examining glycans across diverse animal models, in this case *C. elegans.* Secondly, we established mass spectrometry as the technique of preference for the analysis of N-glycans.

Manuscript 1

Glycosylation biomarkers associated with age-related diseases and current methods for glycan analysis

Beatrix Paton, Manuel Suarez, Pol Herrero and Núria Canela

Review

Published in the International Journal of Molecular Sciences

Impact Factor: 5.923; Q1, Biochemistry & Molecular Biology

(2021) 22(11), 5788;

doi: 10.3390/ijms22115788

Glycosylation biomarkers associated with age-related diseases and current methods for glycan analysis

Beatrix Paton [1], Manuel Suarez [2,*], Pol Herrero [1,*] and Núria Canela [1]

[1] Eurecat, Centre Tecnològic de Catalunya, Centre for Omic Sciences, Joint Unit Eurecat-Universitat Rovira I Virgili, Unique Scientific and Technical Infrastructure (ICTS), 43204 Reus, Spain;

[2] Nutrigenomics Research Group, Departament de Bioquímica I Biotecnologia, Universitat Rovira i Virgili, 43007 Tarragona, Spain

* Correspondence: Dr Manuel Suárez and Dr Pol Herrero

ABSTRACT

Ageing is a complex process which implies the accumulation of molecular, cellular and organ damage, leading to an increased vulnerability to disease. In Western societies, the increase in the elderly population, which is accompanied by ageing-associated pathologies such as cardiovascular and mental diseases, is becoming an increasing economic and social burden for governments. In order to prevent, treat and determine which subjects are more likely to develop these age-related diseases, predictive biomarkers are required. In this sense, some studies suggest that glycans have a potential role as disease biomarkers, as they modify the functions of proteins and take part in intra- and intercellular biological processes. As the glycome reflects the real-time status of these interactions, its characterisation can provide potential diagnostic and prognostic biomarkers for multifactorial diseases. This review gathers the alterations in protein glycosylation profiles that are associated with ageing and age-related diseases, such as cancer, type 2 diabetes mellitus, metabolic syndrome and several chronic inflammatory diseases. Furthermore, the review includes the available techniques for the determination and characterisation of glycans, such as liquid chromatography, electrophoresis, nuclear magnetic resonance and mass spectrometry.

1. INTRODUCTION

Protein glycosylation is the biochemical process for which a carbohydrate molecule is covalently attached to a protein functional group. In biology, glycosylation mainly refers to the enzymatic process that binds glycans to proteins, affecting intracellular processes like folding and transport, and playing an important role in many cellular signaling and communication events. The two most common types of protein glycosylation are N-linked and O-linked glycosylation. Regarding n-linked glycosylation, the glycan is added at the Asn residue on a nascent polypeptide within the consensus sequence Asn-X-Ser/Thr, even though this does not occur at every potential glycosylation site. On the other hand, O-linked glycosylation can occur at any hydroxyl group of a Ser or Thr residue within the protein sequence [1,2], although very few sites are occupied [3].

Many studies suggest that glycans modify the functions of proteins and take part in intra- and intercellular biological processes. Most cell-surface and secreted proteins have glycans attached to them [4] that are involved in molecular recognition processes that occur in viral infections, cell adhesion in inflammation and tumour metastasis, amongst other events [2]. Furthermore, protein-glycan interactions are also known to play a role in many processes affecting disease progression [5]. For instance, aberrant glycosylation is often present in patients with cancer [6,7], diabetes and inflammation [8,9].

Diseases are also driven by many diverse factors, including genetic variants, epigenetic dysregulation and environmental influences. Glycosylation, among other post-translational modifications (PTMs), can reflect the real-time status of these complex interactions and can provide potential diagnostic and prognostic biomarkers for multifactorial diseases [8,10]. Glycosylation is known to be altered in the process of ageing. For example, modifications in protein n-glycosylation can lead to an increase in certain types of glycoforms or even the formation of new ones, after surpassing the age of 40 years [11]. For many years, ageing has been considered to be a physiological condition that favours the onset of many

diseases. However, the relationship between ageing and these diseases is more complex, as they share basic mechanisms, such as metabolism derangement, macromolecular damage, epigenetic modifications or inflammation [2,12]. This relationship resulted in the introduction of the term age-related diseases.

Ageing is characterised by a progressive loss of physiological integrity, leading to impaired function and increased vulnerability to death [13] This process is partially modulated by genetic factors and non-genetic factors, including the nutritional habits of individuals. There is evidence indicating that dietary patterns play a central role and are recognised as major factors in the onset of chronic diseases, including cardiovascular diseases, diabetes and cancer. A better understanding of the interaction between nutrition and ageing is essential to unravel the mechanisms responsible for these positive/negative effects, to identify diet components promoting the quality of life in old age and to contribute to the prevention of late-life disabilities [14]. Few studies have shown how the dietary patterns in humans affect glycosylation, however there is evidence that diet may influence disease state by altering glycosylation [15].

The analysis of protein glycosylation is a challenging task due to the primary structure of glycans. Glycans are biopolymers composed of monosaccharides with many chiral centres that are connected by glyosidic linkages [16]. They can have complex three-dimensional structures and the function of the glycans can be considerably influenced by their stereoisomerism [17]. The structural complexity of glycans is due to their variable composition, linkage, branching and anomericity of the constituent monosaccharides, in combination with the general heterogeneity caused by the indirect control of their biosynthesis [18]. Consequently, the combination of different techniques is often necessary to determine the structure of a glycan, either alone or in association with a protein. Amongst the available techniques, electrophoresis [19,20,21,22], liquid chromatography coupled to mass spectrometry (LC-MS) [7,23,24,25,26] and nuclear magnetic resonance (NMR) [27,28] are the

most frequently used. Differently from n-glycans, the determination of O-glycans has advanced slower because these have less, or none, defined sequence patterns and arrangements [29,30] limiting the research studies focused on them.

The main objective of this review is to gather the alterations in glycosylation profiles that have been stated and associated with age-related diseases. This includes both n- and O- glycosylation events, although studies regarding O-glycosylation are limited. In addition, the most frequently used techniques for the determination and characterisation of protein glycosylation will also be briefly discussed.

2. GLYCANS ASSOCIATED WITH AGEING AND AGE-RELATED DISEASES

Age-related diseases share common mechanisms with natural ageing. These mechanisms include adaptation to stress, loss of proteostasis, stem cell exhaustion, metabolism derangement, macromolecular damage, epigenetic modifications and inflammation [31]. If age-related diseases are manifestations of accelerated ageing, it is urgent to identify markers capable of distinguishing between biological and chronological age, in order to identify subjects that are more likely to develop age-related diseases [12].

Glycomic alterations related to specific disease states such as cancer [10], inflammation [32], neuronal diseases [33] and diabetes [34] have been reviewed elsewhere, however, less information about glycomic changes associated with age and ageing-related diseases has been published—Miura and Endo have reviewed up until 2016 [2]. Some articles focus on disorders that induce or hasten the ageing process, such as Alzheimer's disease (AD) [35] or posttraumatic stress disorder in which stress exposure can influence the immune system and accelerate cellular ageing [36]. These alterations can affect the n-glycan profile as well as the metabolome in animals and humans [36]. Data on glycan-based

biomarkers used for diagnosis of diabetes, cancers and other complex diseases have been gathered in a review by Hu et al. [37]. This review summarises the clinically used glycan and glycoprotein-based biomarkers as well as the potential serum/plasma-derived n- and O-linked glycans as new biomarkers. Similarly, Zhang et al. described and categorised into different groups the clinically used glycan-based biomarkers, specifying as well whether the median values of glycan-related biomarkers are increased or decreased in cancer and other diseases compared to that of healthy controls [38].

Plasma and serum are the most frequently used sample on studies that determine glycan alterations in age-related diseases. Approximately 20% of all plasma proteins are immunoglobulins, a group of glycoproteins involved in innate and adaptive immunity. Immunoglobulin G (IgG) is the most abundant immunoglobulin and is very frequently measured in the study of the n-glycome. It is involved in anti-inflammatory and pro-inflammatory responses throughout the body. These properties are modulated by the n-glycans that are attached to the conserved Asn 297 of both heavy chains in the fragment crystallisable (Fc) portion of IgG. By changing the conformation of the Fc portion and the affinity for a number of receptors and lectins, the n-glycans control the inflammatory properties of Immunoglobulin G (IgG) [39,40]. More than 30 IgG glycoforms have been identified in human serum [41,42]. The majority of Fc n-glycans in human IgGs are galactosylated: the neutral IgG glycome consists of a percentage of approximately 40% of neutral glycans without galactose, above 40% of neutral glycans with one terminal galactose and 20% of neutral glycans with two terminal galactoses [43]. Decreasing levels of galactosylated glycoforms have been directly linked to ageing and to immune activation [43,44].

Different glycomic methodologies are used depending on each research, leading to a low comparability between studies which does not allow to draw clear conclusions on whether there are plasma glycome signatures specific to a certain disease [45]. Only a few studies show the potential of

plasma glycans in differential diagnosis on larger sample sets, as stated by Dotz and Wuhrer [45].

The following sections summarise the existing glycan alterations found in recent studies focused on the determination of the glycosylation profile in ageing and several age-related diseases.

2.1 Chronological ageing

Ageing is a complex process which implies the accumulation of molecular, cellular and organ damage, leading to a loss of function and increased vulnerability to disease and eventually to death [46]. The determination of molecular markers of age is of special interest in order to be able to predict, monitor and provide insight into age-associated physiological decline and disease [47]. Table 1 shows some of the reported glycan alterations related to chronological ageing.

Table 1. Glycan alterations on chronological ageing.

Sample type	Glycan alteration	Technique	Sample treatment	Citation
Serum	Increase in under-galactosylated glycans and decrease in a core α-1,6-fucosylated bigalactosylated biantennary structure in individuals with more than 40-50 years of age.	DSA-FACE	Purification of immunoglobulins with protein L, denaturation, N-glycan release with PNGase F, sialidase treatment and APTS labelling	[22]
Plasma	Increase of nongalactosylated glycans (A2 and FA2) and decrease of digalactosylated glycans (A2G2, FA2G2, A2BG2, and FA2BG2). Monogalactosylated glycans increase or decrease depending on the position of the galactose and the presence of bisecting GlcNAc.	HILIC-FLR	IgG isolation using protein G monolithic plates, “in gel” N-glycan release with PNGase F and 2-AB labelling.	[48]

Sample type	Glycan alteration	Technique	Sample treatment	Citation
Plasma	Nongalactosylated (A2, FA2, and FA2B) and monogalactosylated (FA2[6]BG1 and FA2[3]BG1) glycans steadily increase with age, compared to digalactosylated glycans (A2BG2, FA2G2, FA2G2S1, and FA2BG2S2) which decrease.	HPLC-FLR/MS	IgG isolation using protein G monolithic plates, denaturation, "in solution" N-glycan release, 2-AB labelling and HILIC-SPE purification	[49]
Serum	Increased α2,6 sialic acid, mannose, N-acetylglucosamine and multiantennary complex type N-glycans.	Lectin-Based Protein Microarray	Isolation of α2M using a Co-Immunoprecipitation Kit, incubation with 8 different lectins and labelling with CF647-streptavidin conjugate	[50]
Serum	The log of the ratio of two glycans (NGA2F and NA2F), named GlycoAgeTest, remains steady up to the age of 40 years and thereafter gradually increases. Patients with dementia or Cockayne syndrome have a higher GlycoAgeTest level than age-matched healthy individuals.	DSA-FACE	Denaturation, N-glycan release with PNGase F, APTS labelling and desialylation	[11]
Plasma	Significant differences in glycan microheterogeneity, with an increased sialic acid content released from newborn umbilical cord (NUCP) α-2-macroglobulin (A2M).	FACE	Neuraminidase digestion, and use of electrophoresis, western blotting and immunostaining to determine the degree of sialylation and terminal galactosylation. N-glycan profile: A2M purification with immunoprecipitation, denaturation, N-glycan	[51]

Sample type	Glycan alteration	Technique	Sample treatment	Citation
			release with PNGase F, protein precipitation, evaporation and 7-amino-1,3-naphthalenedisulfonic acid (ANDS) labelling	
Placenta	Differences in the abundance of high mannose N-glycans, 2-sialylated biantennary N-glycans, 3- (core)fucosylated biantennary N-glycans, 4-highly fucosylated N-glycans, 5- bisected N-glycans and 6-multiantennary N-glycans	MALDI-TOF MS	Denaturation, reduction, alkylation, N-glycan release with PNGase F, glycan purification with porous graphic carbon columns, permethylation for the stabilization of sialic acids, further purification with C18 columns and mixture with 2,5-DHB matrix.	[52]
Serum and pituitary extracts	Most TSH molecules are low-N-glycosylated, highsulfonated, and low-sialylated in children up to 18 months, compared with older children and adults. The degree of N-glycosylation is similar in serum and pituitary extracts up to 3 months of age and after that is higher in serum than in pituitary extracts.	Competitive binding radioimmunoassay and noncompetitive time-resolved sandwich fluoroimmunoassay	Use of electrophoresis to measure frequencies of glycoforms and neuraminidase treatment to determine sialic acids in serum and pituitary extracts. Homogenization of pituitary extracts and quantification of TSH with the two immunoassays.	[53]
Skin	Significant quantitative decreases in high mannose glycans in aged skin .	HILIC-FLR	-	[54]
Plasma	Galactosylation and sialylation decrease with increasing age and show	MALDI-TOF-MS and HILIC-FLR	IgG isolation using protein G monolithic plates. N-glycan	[55]

Sample type	Glycan alteration	Technique	Sample treatment	Citation
	significant sex dependence. Females in their 45 to 60 years show the most prominent drop in the levels of galactosylated and sialylated glycoforms. The incidence of bisecting N-acetylglucosamine increases in younger individuals and reaches a plateau at older age.		release with PNGase F and 2-AB labelling.	
Plasma	Galactosylation tends to decrease with age as di-galactosylated glycopeptides are less abundant in older participants, while nongalactosylated glycopeptides are more abundant in older participants.	MALDI-TOF-MS	Glycopeptides: IgG isolation using a protein A affinity purification step, trypsin digestion and purification with C18-SPE plate and mixture with a-cyano-4-hydroxy-cinnamic acid matrix	[56]
Plasma	Bisection, galactosylation, sialylation of diantennary species and tetraantennary species, as well as the size of high-mannose species are important plasma characteristics associated with inflammation and metabolic health.	MALDI-FTICR-MS	Protein denaturation, N-glycan release with PNGase F, 2-aminobenzoic acid (2-AA) labelling, HILIC-SPE purification and carbon-SPE desalting.	[57]
Plasma	Glycosylation patterns of α1-antitrypsin (αAT) enriched fractions are associated with chronological age and differ between females and males. Pronounced differences exist between males and females in the glycosylation profiles of immunoglobulin A enriched fractions.	CE-LIF	Protein denaturation, N-glycan release with PNGase F, APTS labelling and HILIC-SPE purification	[58]

Sample type	Glycan alteration	Technique	Sample treatment	Citation
Serum	Age-related changes are observed in N-glycans NGA2F, NGA2FB and NA2F (agalactosylated core-α-1,6-fucosylated biantennary glycan, core-α-1,6-fucosylated bisecting biantennary glycan and bigalactosylated core-α-1,6-fucosylated biantennary glycan, respectively). Furthermore, fucosylation of N-glycans is significantly different between men and women: more core-α-1,6-fucosylated glycans are detected in women, whereas more branching-α-1,3-fucosylated N-glycans are seen in men.	DSA-FACE	Protein denaturation, N-glycan release with PNGase F, sialidase treatment (neuraminidase) and APTS labelling.	[59]

Three major n-glycan structures present in human blood glycoproteins (serum, plasma and immunoglobulins fraction) have shown clear changes with ageing. Agalactosyl n-linked oligosaccharides (NG0A2F and NG0A2FB) increase with age whereas core-fucosylated biantennary n-glycans (NA2F) decrease with age [22]. A similar trend was observed in a study which aimed to evaluate the effects of the age and gender on the human serum n-glycans profiles: NGA2F and NGA2FB increased gradually with ageing whereas NA2F decreased [59]. Additionally, before the age of 50 years these three glycans changed only slightly with age, but the difference between age groups 41–50 and 51–60 years was statistically significant, indicating that the age-related physiological changes occurred in the fifties [59]. These findings suggest that galactosylation and fucosylation of human sera n-linked oligosaccharides are considered to be an age-related molecular parameter [22]. More specifically, galactosylation tends to decrease with ageing, as digalactosylated glycopeptides are less

abundant in older individuals. Additionally, nongalactosylated glycopeptides are more abundant in older individuals and decreased levels of nongalactosylated glycopeptides from IgG containing a bisecting GlcNAc are considered an early feature of familial longevity detectable at middle age [56].

As well as galactosylation, sialylation also decreases with age in the adult population, showing significant sex dependence. Furthermore, females around the age of 45 to 60 years show the most prominent drop in the levels of galactosylated and sialylated glycoforms, which is the same age in which females usually enter menopause. [55] In younger individuals, the incidence of bisecting n-acetylglucosamine is increased and reaches a plateau at older age [55]. Differently, in children, Fc galactosylation remains relatively constant with age, while bisection increases and fucosylation and sialylation decrease [60]. Figure 1 displays the general trends observed in the aforementioned studies regarding glycosylation associated with ageing.

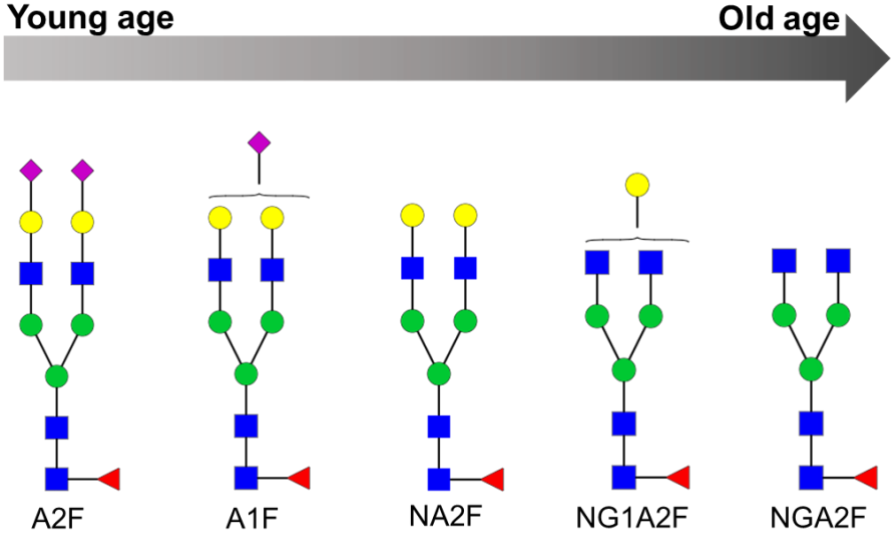

Figure 1. Decrease of galactosylated and sialylated structures with age (disialogalactosylated core-α-1,6-fucosylated biantennary, A2F; sialogalactosylated core-α-1,6-fucosylated biantennary, A1F; bigalactosylated core-α-1,6-fucosylated biantennary, NA2F; galactosylated core-α-1,6-fucosylated

biantennary, NG1A2F; agalactosylated core-α-1,6-fucosylated biantennary, NGA2F).

An ageing biomarker named GlycoAgeTest has been developed, which could possibly forecast disease progression during ageing. This marker is the log of the ratio of two glycans (NGA2F and NA2F), which remains steady up to the age of 40 years and thereafter gradually increases to reach its highest level in nonagenarians, as stated by Vanhooren et al. [11]. Furthermore, patients with dementia or Cockayne syndrome have shown to have a higher GlycoAgeTest level than age-matched healthy individuals. They concluded that the value of GlycoAgeTest is better than chronological age for estimating the physiological age of a human individual, and that it could be used as an ageing biomarker for healthy humans [11].

Several studies have focused on determining specific proteins that might show variations of glycosylation with age. For instance, advancing age has been associated with changes in IgG glycosylation, inducing pro-inflammatory modifications in this glycoprotein [48,49]. These modifications are capable of fuelling an inflammatory vicious loop and may induce apoptosis of cells in surrounding tissues [32]. Furthermore, glycosylation patterns of α1-antitrypsin (αAT) enriched fractions have been found to be associated with chronological age. Moreover, several glycans in the αAT enriched fraction are associated with physiological parameters marking cardiovascular and metabolic diseases [58]. Other examples of proteins that differ with age are protein C, plasminogen [61,62] and α-2-macroglobulin (α2M) [51]. Specifically, α2M is a glycosylated broad-spectrum inhibitor of numerous proteases, including those involved in blood coagulation. Glycosylation characteristics can affect protein structure and function. This fact was evaluated in a study that compared glycosylation characteristics of α2M in newborn umbilical cord (NUCP) and adult pooled plasmas. No significant difference was reported in n-glycan macroheterogeneity between α2M obtained from NUCP and adult plasma. Nevertheless, differences were observed in glycan

microheterogeneity, with an increased sialic acid content released from NUCP α2M [51]. In addition, glycans attached to α2M have been analysed in a human population of different ages, obtaining increased levels of α2,6-linked sialic acid, mannose, n-acetylglucosamine and multiantennary complex type n-glycans [50].

Other specific proteins of interest for their n-glycan composition are often determined. For instance, n-glycan composition of circulating molecules from the glycoprotein hormone thyrotropin (TSH) have been characterised in young children [53]. The TSH molecules are post-translationally modified in the Golgi apparatus within the cell where the branching of the n-glycans and their decoration with the terminal anionic monosaccharide residues occurs. TSH molecules modulate the biological properties of TSH in different physiological and clinical situations. Compared to adults, children have shown a lower degree of n-glycosylation and the lowest levels of sialylation have been determined in younger children [53].

Most studies determine the n-glycome in plasma, which is characteristic for a significant decrease of complex n-glycans observed with ageing. Differently, in skin glycomics, the epidermis has an abundance of high mannose n-glycosylated proteins, which play a role in stratum corneum lipid remodelling, desquamation and barrier function. Significant quantitative decreases have been observed in high mannose glycans in the stratum corneum from aged skin compared to young skin [54].

n-glycans have also been measured in the gut microbiomes of patients, showing that the proportion of various types of n-glycan biosynthesis is higher in the gut microbiomes of centenarians than in the elderly and adults. Therefore, n-glycan biosynthesis can be associated with the stability of gut microbiome in centenarians [63].

2.2 Neurodegenerative diseases

Neurodegenerative diseases are characterised by the functional loss and death of neurons, leading to symptoms that affect the daily lives of patients [64]. Glycan alterations have been observed in several neurodegenerative

diseases, such as AD, amyotrophic lateral sclerosis (ALS) or Parkinson's disease (PD). AD is a common age-related chronic neurodegenerative disease [65] characterised by its cognitive impairment [2]. Several alterations are related to the development of this disease, such as the increase in brain deposits of aggregated amyloid-β and hyperphosphorylated tau proteins [66] or the upregulation of receptors for advanced glycation end product, which is the primary mechanism by which amyloid-β traverses the blood-brain barrier [67]. Considering that altered immune responses in AD are not only related to brain but also to peripheral blood, the measurement of IgG Fc glycosylation could be potentially used as a clinical marker of inflammation and/or impaired immune responses for monitoring AD progression [24]. Table 2 shows select examples of glycan alterations related to several neurodegenerative diseases.

Table 2. Glycan alterations on neurodegenerative diseases.

Disease	Sample type	Glycan alteration	Technique	Sample treatment	Citation
Alzheimer's disease	Plasma	Lower abundance of complex galactosylated and sialylated forms in patients with AD	NanoLC-MS/MS (Orbitrap)	Reduction, alkylation, trypsin digestion and sialidase digestion.	[24]
Amyotrophic lateral sclerosis	Serum	High levels of sialylated glycans and low levels of core fucosylated glycans in patients with ALS, compared to healthy volunteer sera.	MALDI-TOF MS, HPLC-FLR	IgG purification with protein G beads, reduction, IgG separation with SDS-PAGE, N-glycan release with PNGase F, N-glycan extraction from gel pieces, decontamination with ion-exchange resin,	[68]

Disease	Sample type	Glycan alteration	Technique	Sample treatment	Citation
				2-AB labelling and further exoglycosidase digestion. Desalting and mixture with DHB for MALDI-TOF MS analysis	
Amyotrophic lateral sclerosis	Cerebrospinal fluid	Detection of diantennary N-glycans predominantly with proximal fucose and some bisecting GlcNAc; agalacto-, mono-, and digalactosylated as well as α2,6-sialylated structures in ALS patients. Furthermore, increased levels of galactosylated structures in ALS patients	HPLC-FLR, MALDI-TOF-MS	IgG isolation with protein G cartridge, evaporation, protein precipitation and denaturation, N-glycan release with PNGase F, purification with porous graphitic carbon cartridges, evaporation and 2-AB labelling. Further exoglycosidase treatment for structure elucidation. Mixture with DHB for MALDI-TOF-MS analysis.	[69]
Amyotrophic	Cerebrospinal	Determination of	HPLC-FLR,	Protein	[70]

Disease	Sample type	Glycan alteration	Technique	Sample treatment	Citation
lateral sclerosis	fluid	complex diantennary structures with sialic acid in α2,3- and α2,6-linkage, bisecting N-acetylglucosamine-containing structures as well as peripherally 30 fucosylated structures. Increase of monosialylated diantennary glycans A2G2S[6]1 and FA2G2S[3]1 in ALS.	RP-HPLC/MS/MS	precipitation, denaturation, reduction, trypsin digestion, purification with C18 cartridges, evaporation, N-glycan release with PNGase F, separation and desalting of N-glycans with C18 and porous graphitic carbon cartridges respectively. 2-AB labelling and purification by gel filtration. Further exoglycosidase treatment for structure elucidation.	
Parkinson's disease	Plasma	PD patients showed a reduced relative abundance of a high-mannose N-glycan structure, a monosialylated N-glycan structure and a core fucosylated monosialylated N-glycan structure with an additional fucose attached to one antenna, as well as an increased relative abundance	HILIC-FLR	IgG isolation using protein G monolithic plates, evaporation, denaturation, N-glycan release with PNGase F, 2-AB labelling and HILIC-SPE purification.	[40]

Disease	Sample type	Glycan alteration	Technique	Sample treatment	Citation
		of a core fucosylated monogalactosylated N-glycan structure.			
Parkinson's disease	Serum	Low sialylation and increased fucosylation is increased in PD patients on tri-antennary glycans with 2 and 3 terminal sialic acids	CE-MS/MS	Denaturation, reduction, alkylation, N-glycan release with PNGase, filtering, evaporation, hydrolysis of the glycosylamines, 2-AA labelling and HILIC purification.	[71]

Individuals with AD show an elevated proinflammatory activity in blood, shown through increased levels of inflammation mediating proteins and pro-inflammatory IgG Fc glycoforms [24]. Low abundance of complex galactosylated and sialylated forms in AD has been found, as well as differences between genders. Prior to the AD onset, declining galactosylation observed in females was inversed in males. This may indicate that females could have a lower ability to suppress peripheral inflammation compared to male patients [24]. Further studies need to address the pathological meaning of protein glycosylation changes in AD patients.

The glycosylation of collapsin response mediator protein 2 (CRMP-2) has been shown to be reduced in AD, while the glycosylation of glial fibrillary acidic protein is increased. CRMP-2 regulates the assembly and polymerisation of microtubules and is associated with neurofibrillary tangles in AD. These aberrant glycosylations in AD may help understand the mechanisms of neurodegenerative diseases [72].

ALS is another fatal disease characterised by the selective loss of motor neurons in the spinal cord, brain stem and motor cortex which leads to progressive muscle weakness, paralysis, respiratory muscle failure and death, usually within 2–5 years [73]. Neuroinflammation occurs in ALS, implying the activation of glial cells and infiltration of peripheral immune cells [73]. High levels of sialylated glycans and low levels of core fucosylated glycans have been measured in serum derived n-glycans of patients with ALS, compared to healthy volunteer sera. A distinct glycan was measured in all ALS patients, A2BG2, a galactosylated structure with a bisecting GlcNAc lacking the core fucose. This glycan increases the affinity of IgG to the activating receptor CD16 on effector cells, consequently enhancing Antibody-Dependent Cellular Cytotoxicity (ADCC). These results suggest that glycans of ALS-IgG may serve as a biomarker for the disease and may be involved in neuronal damage [68].

The IgG n-glycosylation profile has also been measured in cerebrospinal fluid of ALS patients. Diantennary n-glycans predominantly with proximal fucose and some bisecting GlcNAc; agalacto-, mono- and digalactosylated as well as α2,6-sialylated structures have been detected [69,70]. The same study established the Gal-Index parameter, a representation of the levels of galactosylated n-glycans, which could be further explored as a potential ALS biomarker [69]. Furthermore, increased levels of galactosylated structures [69] and monosialylated diantennary glycans A2G2S(6)1 and FA2G2S(3)1 have been measured in ALS patients [70]. A useful future approach would be to measure IgG galactosylation in blood samples (either serum or plasma) in order to explore differences between ALS patients and healthy population [69].

Similar to AD, altered sialylation has been determined in PD patients. Specifically, low sialylation on tri-antennary glycans with 2 and 3 terminal sialic acids and increased fucosylation have been measured [71]. Furthermore, as patients with PD age, the propensity to become more pro-inflammatory increases faster than what would be expected [40].

2.3 Cancer

There is a current interest in determining glycoproteins, and their corresponding glycans, which have critical importance in cancer. No general cancer-associated n-glycans currently exist but all of tetraantennary n-glycans in cancer patient sera are increased except in pancreatic cancer, indicating that increased tetraantennary n-glycans are a common n-glycan structural feature in different types of cancer. However, no comparable pattern of n-glycan profiles is observed among other cancers, reaching the conclusion that each type of cancer is unique and aberrant n-glycans in serum could help distinguish different classes of cancer [37]. In Table 3, several glycan alterations reported in cancer are displayed.

Table 3. Glycan alterations on cancer.

Disease	Sample type	Glycan alteration	Technique	Treatment	Citation
Hepatocellular carcinoma	Serum	One triantennary glycan (NA3Fb) is correlated with tumour stage in HCC patients.	DSA-FACE	Purification of immunoglobulins with protein L, denaturation, N-glycan release with PNGase F, sialidase treatment and APTS labelling	[74]
Breast cancer	Serum	Increases in sialylation and fucosylation of glycan structures appear to be indicative of cancer progression. Changes in the relative intensities of 8 N-glycans are characteristic of breast cancer (N-glycans sialylated to a different degree (mono-, di-, tri-, and tetrasialylated) and 5	MALDI-MS	Reduction, alkylation, trypsin digestion, N-glycan release with PNGase F, purification with activated charcoal microcolumns, permethylation and mixture with 2,5-DHB matrix	[75]

Disease	Sample type	Glycan alteration	Technique	Treatment	Citation
		of these structures are fucosylated (2 of them difucosylated))			
Breast cancer	Serum	Increase in siaylation and changes in fucosylation in breast cancer patient sera compared to that from controls. Furthermore, patients show elevated levels of the sLex-carrying triantennary structure, A3FG1, derived from the monofucosylated trisialylated triantennary N-glycan (A3FG3S3).	CapLC-QTOF	In-gel N-glycan release with PNGase F and 2AB labelling/reduction, alkylation, N-glycan release with PNGase F and in-gel trypsin digestion.	[76]
Breast cancer	Serum	Presence of 15 unique serum glycan markers in all patients but absent in normal individuals	MALDI-FT-ICR	β-elimination, glycan purification with a graphitized carbon cartridge and mixture with a DHB and DHAP matrix	[77]
Breast cancer	Serum	Increased levels of α2,3 sialylation in breast cancer samples	MALDI-TOF-MS	Trypsin digestion, denaturation, reduction, N-glycan release with PNGase F, purification with C18 micro-spin columns and Graphite micro-spin columns, sialic acid amidation and clean-up, and solid-phase permethylation	[78]
Breast cancer	Serum	Breast cancer patients exhibit a characteristic pattern of IgG Fc region N-	MALDI-MS	IgG isolation, SDS-PAGE, enzymatic glycan release, methylamidation of	[26]

Disease	Sample type	Glycan alteration	Technique	Treatment	Citation
		glycosylation.		N-glycan sialic acid and AQ-labeling	
Gastric cancer	Serum	Increased hybrid and multi-branched type (tri-, tetra-antennnary glycans) N-glycans in GC and decreased monoantennary, galactose, bisecting type and core fucose N-glycans	MALDI-TOF MS	Denaturation, PNGase F digestion, ethyl esterification, purification with sepharose beads and mixture with DHB	[225]
Gastric cancer	Serum	9 N-glycan structures altered and decrease of core-fucosylated structures.	DSA-FACE	Enzymatic glycan release, 8-aminonaphthalene-1,3,6-trisulfonic acid disodium salt (ANTS) labelling and sialidase digestion.	[79]
Pancreatic cancer	Serum	Aberrant glycosylation in four proteins (LIFR, CE350, VP13A, HPT) found in sera from pancreatic cancer patients compared to those of controls.	NanoLC-MS/MS	Immunodepletion, incubation with PHA-L lectin, reduction, alkylation, PNGase F and trypsin digestion.	[80]
Lung cancer	Plasma and serum	Significant elevation of α2−6 sialylation, β1−4 branching, β1−6 branching, antennary fucosylation, and total N-glycosylation level in almost every stage of lung cancer relative to control groups.	GC-MS	Permethylation, nonreductive release, purification, hydrolysis, reduction and acetylation	[81]
Colorectal cancer	Serum	Increased degree of fucosylation in CRC patients	Lectin Based Protein Microarray	Transferrin isolation, incubation with fourteen biotinylated lectins, wash with PBST and exposition to CF647-	[82]

Disease	Sample type	Glycan alteration	Technique	Treatment	Citation
				streptavidin conjugate	
Colorectal cancer	Plasma	Increased levels of sialylation and fucosylation	Lectin blot analysis	Delipidation, immunodepletion and incubation with agarose-bound lectins.	[83]
Colorectal cancer	Serum	Decreased levels of total core fucose residues.	DSA-FACE	Enzymatic glycan release, 8-Aminonaphthalene-1,3,6-trisulfonic acid disodium salt (ANTS) labelling and sialidase digestion.	[84]
Colorectal cancer	Serum	Increased α2,6Sia, GlcNAc and mannose (Man) residues, as well as increased multiantennary complex type N-glycans	Lectin Based Protein Microarray	α2M isolation by immunoprecipitation, incubation with set of lectins and streptavidin labelling	[85]
Prostate cancer	Serum	Four high-mannose (Man6-Man9) type, one neutral and one acidic complex-type glycans are down-regulated in the patient group while one acidic complex-type glycan is up-regulated in the patient group with active disease	MALDI-FT-ICR	Denaturation, enzymatic release, ethanol precipitation and SPE purification	[86]
Ovarian cancer	Plasma	Up-regulated fucosylated glycans in healthy samples when compared to cancerous and benign tumour control	MALDI-FT-ICR MS and NanoLC-MS/MS (Orbitrap)	Dialysis, b-elimination, SPE with graphitized carbon cartridges and pronase digestion	[87]

Disease	Sample type	Glycan alteration	Technique	Treatment	Citation
		samples			
Cancer	Serum	Significantly increased monofucosylated N-glycans at all glycosylation sites in all cancer samples. Increased core-type fucosylated N-glycans in gastroenterological cancer samples, increased core-type fucosylated N-glycan in prostate cancer samples and increased Lewis-type fucosylated N-glycan in metastatic prostate cancer and gastroenterological cancer.	HPLC-MS	Haptoglobin purification, reduction, alkylation, lysylendopeptidase, trypsin and endoprotease Glu-C digestion, affinity separation with Sepharose CL4B and desialylation.	[88]

Fucosylation is one of the most important types of glycosylation in cancer and it regulates the biological functions of adhesion molecules and growth factor receptors. Therefore, it is thought that changes in fucosylation could provide a novel strategy for cancer therapy [89].

For instance, significant changes in high-mannose and fucosylated biantennary complex n-glycans have been observed in the serum of prostate cancer patients [86], as shown in Table 3. Similarly, preliminary data states that there are pronounced age-associated changes at the level of fucosylation and branching of glycans in transferrin, as well as an increased degree of fucosylation in colorectal carcinoma [82]. These findings are consistent with previous studies in which colorectal cancer patients had dramatically higher levels of sialylation and fucosylation [83]. The changes in fucosylation levels are also present in breast cancer, where

increased levels of high-mannose and core-fucosylated glycans, as well as decreased levels of bisected and sialylated glycans were detected on breast cancer tissues compared to para-carcinoma tissues. Furthermore, six n-glycans have been associated with breast cancer and three high-mannose n-glycans (F0H6N2S0, F0H7N2S0, F0H8N2S0) have been shown to exhibit significant diagnostic accuracy in both breast cancer tissues and cells. Moreover, a negative correlation between sialylated glycans and the age of patients has been identified [90].

The glycosylation state of various types of cancer during the progression or evolution of the disease has also been stated. For instance, the serum n-glycan profile has claimed to be altered during the development of gastric cancer in a study where nine n-glycan structures were compared. The abundance of individual n-glycan structures was analysed, determining that the abundance of core-fucosylated structures decreased significantly in gastric cancer, similar to what occurs in colorectal cancer [84]. This finding could aid with the diagnose of gastric cancer in its early stages and further studies focused on the changes in glycosylation in each step of cancer development and progression could improve the diagnosis, monitoring and screening of gastric cancer [79].

n-glycans could have a potential diagnostic ability in breast cancer, improving the understanding of its underlying molecular and cellular mechanisms [90]. More specifically, targeted blood plasma glycomics is thought to be a promising source of noninvasively diagnostic and prognostic biomarkers for lung cancer. Several glycan features have been quantified and distinguished from controls, predicting survival in patients at all stages, including 2-linked mannose, α2–6 sialylation, β1–4 branching, β1–6 branching, 4-linked GlcNAc and antennary fucosylation. Furthermore, most of these identified glycans are independent of smoking status, age, gender and histological subtypes of lung cancer [81].

A limitation in most studies focused on the study of plasma or serum glycosylation is to assess if the altered glycans are either from

glycoproteins made in the liver, from immunoglobulins made by immune cells or products from cancer cells. In order to address this issue, Hu et al. purified several serum glycoproteins that are not produced by cancer cells from both healthy controls and different types of cancer patients [37]. One of these glycoproteins is IgG, which is the most prevalent serum immunoglobulin with concentrations of approximately 10–15 mg/mL. IgG is produced by B lymphocytes but not from cancer cells. A total of 36 n-glycan structures have been characterised from IgG purified from the sera of gastric, ovarian, breast and lung cancer patients, exhibiting different n-glycan structures compared to cancer-free patients [37]. Another study focused on obtaining a detailed profile of IgG n-glycans in breast cancer patients, claimed that n-glycan structures of IgG in the sera of breast cancer patients had better sensitivity and specificity compared to cancer biomarkers used in the clinical area [26]. Most importantly, serum IgG n-glycans of stage 0 breast cancer patients are already different from cancer-free controls, indicating that cancer might be accompanied by abnormal B lymphocyte-produced n-glycans of IgGs from the earliest stages of the disease [37].

Haptoglobin is another relevant glycoprotein found to be a biomarker for different cancers, including esophageal, gastric, colon, gallbladder, pancreatic, prostate and ovarian. This protein is produced in the liver and contains four glycosylation sites (Asn 184, Asn 207, Asn 211 and Asn 241). All its biantennary n-glycans have been reported to be increased, triantennary n-glycans without core fucose are decreased, and core-fucosylated glycans are increased in the sera of gastric, ovarian and pancreatic cancer patients [37]. A study focused on the characterisation of fucosylation on haptoglobin among different cancer types, showed that relevant differences in the structure or fucosylation of n-glycan were not detected in esophageal, gastric, colon, gallbladder, pancreatic and prostate cancers, suggesting that haptoglobin in the sera of cancer patients might be produced in the liver [88]. These results suggest that glycan structures

in liver are similarly affected when different types of cancer are present [37].

Glycans attached to α2M are also of interest since it is a glycoprotein associated with chronic inflammation. Previous reports stated that α2M isolated from patients with colorectal cancer contained more α2,6Sia, GlcNAc and mannose residues, as well as more multiantennary complex type n-glycans, compared to α2M isolated from healthy participants [85].

Many other n-glycosylations have been associated with other types of cancer, such as the presence of bisecting n-acetyl-glucosamine n-glycans, increased levels of α2-6 sialylated and n,N'-diacetyl-lactosamine n-glycans, which have been identified as characteristic glycan features that are unique to ovarian cancer membrane proteins [7] or the abundance of β1,6-branched oligosaccharides which is found in breast carcinoma nodal metastasis [6].

2.4 Type 2 diabetes mellitus

New evidence of glycosylation diversity in Type 2 diabetes mellitus (T2DM) has been found, where IgG glycan traits have been associated with this disease, reflecting an increased proinflammatory and biological ageing status. These associations are in concordance with a decrease of agaloctosylated glycans without galactose and an increase of monogalactosylated glycans and fucosylated structures with bisecting GlcNAc [8]. These results show that lower levels of agalactosylation could increase the risk of T2DM, which matches with previous results on T2DM [9]. A few selected glycan alterations associated with T2DM are shown in Table 4.

Table 4. Glycan alterations on T2DM.

Sample type	Glycan alteration	Technique	Treatment	Citation
Plasma	Decreased agaloctosylated glycans without galactose and increased monogalactosylated glycans and	HPLC-FLR	IgG isolation using protein G monolithic plates,	[8]

Sample type	Glycan alteration	Technique	Treatment	Citation
	fucosylated structures with bisecting GlcNAc.		"in solution" and "in gel" glycan release and labelling using PNGase F and 2-aminobenzamide (2-AB) respectively.	
Plasma	Decreased galactosylation and sialyation, increase in fucosylated structures with bisecting GlcNAc and decrease in fucosylated structures without bisecting GlcNAc	HPLC-FLR	IgG isolation using protein G monolithic plates, denaturation, glycan release, 2-AB labelling and HILIC-SPE purification	[9]
Serum	Reduced α(1,6)-linked arm monogalactosylated and core-fucosylated diantennary N-glycans (NG1[6]A2F).	DSA-FACE	Denaturation, N-glycan release with PNGase F, APTS labelling and sialidase digestion	[19]
Plasma	Decreased galactosylated glycan structures and increased agalactosylated glycan structures.	HPLC-FLR	IgG isolation using protein G monolithic plates, denaturation, "in solution" glycan release, 2-AB labelling and HILIC-SPE purification	[25]
Plasma	Compared to controls, T2DM patients show decreased core fucosylated glycans, decreased levels of low-branching and increased levels of high branching plasma N-glycans, as well as statistically significantly increased levels of di (S2) and trisialylated (S3) plasma N-glycans.	HILIC-FLR	Denaturation, N-glycan release with PNGase F, 2-AB labelling and HILIC-SPE purification.	[91]
Plasma	Eighteen glycosylation features are significantly associated with T2DM. Fucosylation and bisection of diantennary glycans are decreased in diabetes, α2,6-linked sialylation is increased and α2,3-linked sialylation of triantennary glycans is decreased.	MALDI-TOF MS	Denaturation, N-glycan release with PNGase F, ethyl-esterification of sialic acids, purification with GHP membrane	[92]

Sample type	Glycan alteration	Technique	Treatment	Citation
			plate and mixture with super-DHB matrix.	
Plasma	GlycA, a glycoprotein biomarker, is associated with incident T2DM.	NMR	Separation of proteins from lipoproteins with the addition of sodium bromide and further centrifugation and filtering with 10kDa filters.	[93]

The following particular n-glycans have been found to be significantly reduced in T2DM patients: α(1,6)-linked arm monogalactosylated and core-fucosylated diantennary n-glycans (NG1A2F) [19]. This tendency is also present in other studies where T2DM patients have shown decreased core fucosylated glycans and significantly decreased levels of low-branching plasma n-glycans. On the other hand, T2DM patients also show increased levels of high branching plasma n-glycans as well as statistically significantly increased levels of di (S2) and trisialylated (S3) n-glycans.

Galactosylation has also been associated with ageing in both controls and T2DM cases [91]. When correlating n-glycans and age in T2DM, levels of FA2G2 and FA2BG2 (both neutral glycans) decreased with age, whereas A2[3] BG1S[3]1 (monosialylated glycan) [91] increased with age. These findings are consistent with previous reports, where significant correlations were found between plasma n-glycans and age [9,40,49]. In addition, increased levels of fucosylated bisecting GlcNac have also been identified in studies of biological age in distinct populations [48,49], suggesting that this tendency in T2DM patients may be a chronic inflammatory condition as well as a biological ageing condition [8].

Some specific glycosylation changes are reflective of inflammation, such as increased α2,6-linked sialylation. Nevertheless, a study determined

thatα2,3-linked sialylation decreased in T2DM patients, which differs from reports on acute and chronic inflammation [92]. This study also found that levels of α2,3-linked and α2,6-linked sialylation fucosylated glycans increased with age, whereas non-fucosylated glycans decreased with age.

2.5 Metabolic syndrome and related diseases

Metabolic syndrome (MetS) is a cluster of metabolic abnormalities that includes hypertension, central obesity, insulin resistance and atherogenic dyslipidemia. MetS is strongly associated with an increased risk of developing atherosclerotic Cardiovascular disease (CVD) and even though characteristics of the MetS occur in some children and adolescents, the prevalence of MetS increases with age [94]. Table 5 shows reported glycan alterations associated with several MetS and related diseases.

Table 5. Glycan alterations on metabolic syndrome.

Disease	Sample type	Glycan alteration	Technique	Treatment	Citation
Metabolic Syndrome	Plasma	Specific N-glycan structural features (trigalactosylated, biantennary, triantennar, core-fucosylate, monosialylated, disialylated and trisialylated glycans) are significantly correlated with MetS related risk factors.	HILIC-FLR	Reduction, N-glycan release with PNGase F, 2AB labelling and sialydase digestion	[95]
Metabolic Syndrome	Serum	Significantly elevated levels of NGA2FB and NA3F and lower level of the α(1,6)-arm monogalactosylated glycan (NG1(6)A2F) in women with MetS.	DSA-FACE	Denaturation, N-glycan release with PNGase F, APTS labelling and sialidase digestion	[20]
Hypertension	Plasma	Decrease of	NanoHPLC-	IgG isolation	[96]

Disease	Sample type	Glycan alteration	Technique	Treatment	Citation
		galactosylation in IgG subclasses IgG1, IgG2/3, and IgG4 with increasing blood pressure	MS	using protein G monolithic plates, trypsin digestion, reverse-phase desalting and purification	
Hypertension	Plasma	Five glycans (IgG with digalactosylated glycans) significantly differ in participants with prehypertension or hypertension compared to those with normal blood pressure, while 17 other glycan traits significantly differ in participants with hypertension compared to those of normal blood pressure.	HILIC-FLR	"In solution" denaturation, "in gel" enzymatic glycan release with PNGase F and 2-aminobenzamide labelling.	[97]
Hypertension	Plasma	Ten IgG N-glycan traits (i.e., IgG1G0F, IgG2G0F, IgG2G1FN, IgG2G1FS, IgG2G2S, IgG4G0F, IgG4G1FS, IgG4G1S, IgG4G2FS, and IgG4G2N) representing galactosylation and sialylation are significantly associated with hypertension.	NanoRP-HPLC-MS	IgG isolation by affinity chromatography and trypsin digestion	[98]
Cardiometabolic disease	Plasma	Two agalactosylated glycans and a glycan containing a bisecting GlcNAc are significantly higher in participants with MetS compared to controls, whereas a higher level of a digalactosylated N-	HILIC-MS	IgG isolation using protein G monolithic plates, denaturation, "in solution" N-glycan release, 2-AB labelling and HILIC-SPE	[21]

Disease	Sample type	Glycan alteration	Technique	Treatment	Citation
		glycan is present in participants without MetS.		purification	
Atherosclerotic cardiovascular disease	Serum	A large number of N-glycan traits related to core-fucose and bisecting GlcNAc are strongly associated with atherosclerotic plaque. One specific trait related to the sialylated N-glycan appears to be strongly negatively related to circulating VLDL and is supportive of a role of IgG glycosylation in VLDL metabolism and arterial lesion formation also in humans.	HILIC-FLR	IgG isolation using protein G monolithic plates, denaturation, N-glycan release with PNGase F, 2-AB labelling and HILIC-SPE purification.	[99]
Chronic kidney disease	Plasma	Altered glycans with galactosylation, sialylation and bisecting N-acetylglucosamine features.	HPLC-FLR	IgG isolation using protein G monolithic plates, denaturation, glycan release, 2-AB labelling and HILIC-SPE purification	[100]
Dyslipidaemia	Plasma	Possible association between blood lipids and the loss of galactose and sialic acid. Moreover, the addition of bisecting GlcNAcs might be related to the chronic inflammation accompanied with the development and	HILIC–UPLC	IgG isolation using protein G monolithic plates, “in solution” N-glycan release with PNGase F and 2-AB labelling.	[101]

Disease	Sample type	Glycan alteration	Technique	Treatment	Citation
		procession of dyslipidaemia.			

Significantly elevated levels of NGA2FB and NA3F have been determined in women with MetS, while the level of the α(1,6)-arm monogalactosylated glycan (NG1A2F) was significantly lower in women with MetS compared to their healthier peers. The effect of physical exercise was also tested in patients with MetS, resulting in increased levels of NGA2FB and NA3F and lower levels of NG1A2F compared to those without MetS. This study confirmed the existence of n-glycans linked to metabolic risk in older adults. Furthermore, the results indicated that physical activity is related to a specific n-glycan profile despite the metabolic risk status [20]. Previous reports have similar changes in levels of n-glycans, such as those reported by Testa et al., claiming increased levels of NGA2FB and NA3F and decreased levels of NG1A2F in older women with MetS [19]. Moreover, reduced levels of NA3 and NA4 have been associated with the adherence to the physical activity [20], which is an alteration that has already been associated with metabolic abnormalities [19]

n-glycans have also been studied in specific populations. For instance, a research focused on the correlation between n-glycan structures and MetS components in Chinese Han individuals and Caucasian individuals from the Croatian island Korčula. The most prominent observation was the consistent positive correlations between different forms of triantennary glycans and negative correlations between glycans containing core-fucose with MetS components in both populations. The successful replication of these observations in the population of a Croatian island indicates that n-glycans of human plasma could reliably reflect alterations of human metabolism and could be potential biomarkers of MetS [95].

Metabolic syndrome is associated with an increased risk for CVD [102], which results in 40% of all deaths and ranks as the leading cause in population aged 65 or older [103]. As well as metabolic syndrome, other

conditions such as insulin resistance, MetS and prediabetes can lead to a set of metabolic abnormalities (cardiometabolic disease) which can eventually lead to CVD [21]. Several risk factors such as abdominal obesity, dyslipidemia, hyperglycemia and hypertension are related to cardiometabolic disease [104]. Previous reports have shown that IgG n-glycans are associated with some of these risk factors, including hypertension [96,97,98], T2DM [9,25] and dyslipidemia [101].

IgG glycosylation traits have been correlated with the atherosclerotic CVD risk score determined by the GlycA test. This test measures plasma glycoprotein acetylation by Nuclear Magnetic Resonance (NMR) and is able to predict higher cardiovascular risks by reflecting inflammatory pathways. The data obtained has comprehensive measures of protein glycosylation, which highlights the potential value of glycomics in identifying such pathways of disease, the reproducibility of results across different cohorts and the extent to which CVD risk can be captured by these measures [56]. Even though some IgG glycans have been reported to be associated with higher CVD risk, others are associated with lower CVD risk. Specifically, glycans that contain three exposed GlcNAcs or glycans that contain both bisecting GlcNAc and one sialic acid, are positively associated with CVD risk (consistent with the previous GlycA reports), while sialylated glycans without a bisecting GlcNAc are negatively associated. Furthermore, increased levels of non-galactosylated glycoforms with a bisecting GlcNac are reported to associate with higher age while decreased levels are associated with longevity [56]. However, results regarding the association between glycosylation traits and CVD risk showed that this association was not dependent on the presence of other sugar residues, as agalactosylated, monogalactosylated and sialylated n-glycans with a bisecting GlcNAc were positively associated with CVD risk [99].

Age and T2D are factors included in the 10-year ASCVD cardiovascular risk score assessment and have a positive association with a bisecting GlcNAc that increases ADCC mediated by the binding of the antibody to the Fc γ -

receptor, which is regulated by IgG glycosylation [105]. ADCC is increased by the same glycan traits that are involved in the pro-inflammatory pathway and inflammation is known to be the underlying mechanism of CVD's development [106]. Differently to bisecting GlcNAc which is related to pro-inflammatory activity, sialylation and core-fucosylation are consistently associated with anti-inflammatory activity [107]. For instance, a core-fucosylated digalactosylated monosialylated glycan remains strongly associated with the 10-year ASCVD risk score and has been found to be strongly negatively correlated with VLDL levels [99]. VLDL itself is a risk factor for CVD being associated with hypertriglyceridemia and dyslipidemia in general [108]. Further studies are needed which focus on the role of glycosylated structures in predicting cardiovascular events, and in particular their interaction with VLDL [99].

Hypertension is also a risk factor associated with MetS. It is a prevalent condition with numerous health risks, and its incidence is greatest among older adults [109]. n-glycosylation alteration of IgG has been associated with blood pressure status as galactosylation has been found to decrease with increasing blood pressure [96], consistent with results from Wang et al. [97]. These exact same associations have been made in studies about inflammatory bowel disease (IBD) [110] and AD [24]. Individuals with AD manifest an elevated proinflammatory activity in blood, shown through increased levels of inflammation mediating proteins and pro-inflammatory IgG Fc glycoforms. Moreover, the inflammatory status in the periphery is known to be different depending on the gender [24]. Therefore, robust associations of subclass-specific IgG Fc n-glycosylation profiles may become informative biomarker indicatives of the proinflammatory and biological state induced by hypertension [98].

As well as hypertension, dyslipidemia is also a MetS risk factor. In dyslipidemia patients, blood lipids have been associated with the loss of galactose and sialic acid, as well as the addition of bisecting GlcNAcs, which is thought to be related to the chronic inflammation accompanying the development of dyslipidaemia. Furthermore, due to the alterations of IgG

n-glycosylation profiles, they are considered to be potential biomarkers for dyslipidemia [101].

A few of the aforementioned risk factors and conditions, such as diabetes, hypertension and ageing can induce the development of chronic kidney disease [100,111]. Fourteen glycan traits with galactosylation, sialylation and bisecting n-acetylglucosamine features have been associated with renal damage, showing the role of IgG glycosylation in kidney function [100]. Moreover, this finding provides novel insight into the pathophysiology of chronic kidney disease as well as potential diagnostic and therapeutic targets [100].

2.6 Chronic inflammatory diseases

Glycan composition is altered in patients suffering from acute and chronic inflammatory diseases, such as IBD, RA and idiopathic inflammatory myopathies (IIM). A select amount of glycan alterations associated with these diseases are shown in Table 6. Changes in glycosylation have been found in IBD, a term used to define a group of inflammatory conditions of the colon and small intestine, which is divided into two forms, Crohn's disease (CD) and ulcerative colitis (UC). Patients with CD or UC show lower levels of IgG galactosylation than controls [23] which has also been observed in other studies focused on IBD [110]. More specifically, plasma samples from patients with IBD have been found to have a higher abundance of large-size glycans compared with controls, a decreased relative abundance of hybrid and high-mannose structures, lower fucosylation and galactosylation and higher sialylation (α2,3- and α2,6-linked). Patients with CD can be differentiated from UC patients due to a higher bisection, lower galactosylation and higher sialylation (α2,3-linked) [112]. To our knowledge, this same study was also the first to present novel associations of sialic acid linkages with age for both healthy population and IBD patients [112]. The linkage of sialic acids, which can be of α2,3- or α2,6- type, is reported to affect various biological processes, such as the immune response in tumour cells [113]. Therefore, sialic acid

linkages in the context of IBD were evaluated in order to provide insights into disease mechanisms and help the development of targeted treatment strategies [114]. Compared with healthy population, general sialylation was found to be significantly increased in UC, and even more in CD patients. CD and UC patients had higher relative levels of both α2,3- and α2,6- linked sialic acids compared with healthy controls in all traits, except for the α2,6-sialylation of tetra-antennary structures, which was lower in IBD. The strongest association distinguishing UC from CD was found in the sialylation per galactose in diantennary fucosylated glycans [112]. Patients with IBD share several immunologic similarities with rheumatoid arthritis (RA) patients. As the latter ones have increased levels of serum agalactosyl IgG, a study focused on measuring the oligosaccharide structure of serum IgG in patients with IBD. Results showed that the agalactosyl fraction of the fucosylated IgG oligosaccharides was significantly greater in IBD patients compared to healthy volunteers. Most importantly, the extent of agalactosylation of IgG correlated with disease activity of IBD and is a potentially effective diagnostic marker for IBD [115].

Table 6. Glycan alterations on chronic inflammatory diseases.

Disease	Sample type	Glycan alteration	Technique	Treatment	Citation
Inflammatory bowel disease	Plasma	Lower levels of IgG galactosylation compared to controls.	nanoLC-MS	IgG purification by Protein G affinity chromatography and tryptic digestion	[23]
Inflammatory bowel disease	Serum	Decreased IgG galactosylation and proportion of sialylated structures	HILIC-UPLC	IgG isolation using protein G monolithic plates, denaturation, “in solution” denaturation, N-	[110]

Disease	Sample type	Glycan alteration	Technique	Treatment	Citation
				glycan release with PNGase F, 2-AB labelling and HILIC-SPE purification	
Inflammatory Bowel Diseases	Plasma	Higher abundance of large-size glycans in IBD patients compared with controls, a decreased relative abundance of hybrid and high-mannose structures, lower fucosylation, lower galactosylation, and higher sialylation (α2,3- and α2,6-linked).	MALDI-TOF-MS	Denaturation, N-glycan release with PNGase F, esterification of sialic acids, HILIC purification with a GHP membrane and mixture with super-DHB matrix or DHB matrix.	[112]
Inflammatory Bowel Disease	Serum	The agalactosyl fraction of the fucosylated IgG oligosaccharides is significantly greater in IBD patients compared to healthy volunteers. The extent of agalactosylation of IgG correlates with disease activity of IBD and is a potentially effective diagnostic marker for IBD.	RP HPLC-FLR	IgG purification using protein G sepharose, N-glycan release with PNGase F and 2-aminopyridine labelling.	[115]
Rheumatoid arthritis	Serum	Treatment with methotrexate or/and Remicade indicates an increase of IgG galactosylation.	Modified ELISA-plate test, biosensor BIAcore, GC-MS	Isolation of IgG by affinity chromatography on Protein A-Sepharose column, protein denaturation, reduction and dialysis. Hydrolization, evaporation and neutralization for	[116]

Disease	Sample type	Glycan alteration	Technique	Treatment	Citation
				GC-MS analysis. Elisa-plate test: Reduction of purified IgG, interaction with two lectins and ExtrAvidin-AP conjugation. Biosensor BIAcore: Lectin immobilization and measurement of the binding.	
Rheumatoid arthritis	Serum	Peaks of glycans with agalactosylated glycan structures are increased in Rheumatoid arthritis cases.	HILIC -FLR	IgG isolation using protein G monolithic plates, denaturation, N-glycan release with PNGase F, 2-AB labelling and HILIC-SPE purification	[117]
Rheumatoid arthritis	Serum	Statistically significant increases in bisecting glycans FA2BG2 and FABG2S1 seropositive RA, accompanied by decrease of bisecting monogalactosylated glycan FA2[6]G1 and non-bisecting monosialylated glycan FA2[3]G1S1.	CE-LIF	Isolate IgG with protein A microwell plate, N-glycan release with PNGase F, APTS labelling and clean-up.	[118]
Rheumatoid arthritis	Serum	Aberrant galactosylation of IgG in RA compared to healthy controls. Significant correlation between levels of aberrant IgG galactosylation and disease activity (higher	HPLC-FLR	Purify IgG using a protein G HP column, reduce, alkylate and immobilize in SDS-polyacrylamide gel matrix.	[119]

Disease	Sample type	Glycan alteration	Technique	Treatment	Citation
		in females than males).		Release glycans with PNGase F and label with 2-aminobenzamide	
Rheumatoid arthritis	Serum	Patients with RA have a decrease in galactose content in IgG, which is associated with the disease activity, disease duration, and stage of joint destruction.	GC	Purification of IgG, evaluation of neutral monosaccharides through phenolsulfuric acid method, methanolysis and silylation.	[120]
Rheumatoid Arthritis	Plasma	Structure GP1 (agalactosylated glycan) might have potential as a putative biomarker for RA in the Han Chinese population, while the change in IgG glycosylation shows association with the RA active and remission states.	HPLC-FLR	IgG isolation with protein G plate, reduction, alkylation, in-gel N-glycan release with PNGase F, 2-AB labelling, SPE purification.	[121,122]
Idiopathic infammatory myopathies	Serum	IIM patients contain less galactosylated epitopes compared to healthy controls and the Fc-glycan profile of Jo1+ patients contains less bisected and afucosylated glycans compared to Jo1− patients.	nanoRP-LC-MS/MS (Orbitrap)	Glycopeptides: IgG isolation, reduction, alkylation, trypsin digestion, desalting with C18 plates and evaporation.	[123]

RA is another chronic autoimmune, inflammatory disease, which affects mainly the diarthrodial joints [124]. The disease affects about 1% of white population and can occur at any age. Nevertheless, most patients are between 40–70 years old [116]. Glycosylation, citrullination and

carbamylation PTMs have been strongly associated with RA. The role of these PTMs in the pathogenesis of RA has been reviewed by Mastrangelo et al. [125]. Moreover, recent advances in glycan analysis for RA cases have also been reviewed [126]. The aim to perform glycomic analyses in RA patients has been led by the lack of robust diagnostics of RA and its remission status. A study reported that the presence of two agalactosylated glycans (FA1 and A2) and a di-sialylated, galactosylated biantennary glycan (FA2BG2S2) increased the likelihood of occurrence of RA, whereas the presence of glycan A2BG2S2 (digalactosylated and disialylated glycan) indicated a low chance of occurrence of the disease [121]. It has been well documented that RA patients exhibit decreased galactosylation of its conservative n-glycans (Asn 297) in CH2 domains of the heavy chains. This decrease of galactosylation is proportional to disease severity [116] and is correlated with the risk of developing the disease [116,117,126,127].

In order to improve RA treatment, the effectiveness of the treatment has been correlated with IgG galactosylation. In this approach, the use of therapeutic agents such as methotrexate and remicade indicated the improvement of IgG galactosylation during therapy of RA patients [116]. Another study showed that IgG n-glycosylation correlates with RA years before RA diagnosis and indicates that n-glycans are involved actively in the disease pathology [117]. These findings correlate with another study which reported evidence on dysregulated humoral immunity in RA by examining aberrant glycosylation of IgG. This dysregulation began at least 3.5 years prior to onset of symptoms. Findings suggest that aberrant IgG galactosylation substantially predates onset of arthritis and the diagnosis of RA, and resides selectively in the anti-citrullinated peptide autoantibody fraction [119]. These early changes in the n-glycome could be useful for the creation of a specific test for early diagnosis of RA, as well as being adequate for the evaluation of disease progression, remission and proper treatment [117]. Furthermore, galactosylation of IgG in patients with rheumatoid arthritis has been correlated with severity and duration of

illness. A significant decrease of galactose ratio has been observed in patients with long duration of RA (more than 15 years) compared to patients who have had arthritis for less than 5 years. Moreover, decreased galactosylation of IgG is observed in RA patients, which correlates with severity and duration of RA and could be used in monitoring the progression in early arthritis [120].

IIM are chronic, autoimmune conditions characterised by weakness and inflammation of skeletal muscle. Extra-muscular organs, such as skin, joints and lung, are usually affected. Interstitial lung disease often occurs, which is a major cause of morbidity and mortality [123,128]. Autoantibodies are frequently found in patients with IIM, the most common being anti-Jo1 antibodies targeting histidyl transfer RNA synthetase (HisRS or Jo1). As IgG Fc-glycans affect IgG function and are altered in autoimmune diseases and autoantibodies, a study hypothesised that the total-IgG Fc-glycans from Jo1+ versus Jo1− patients and anti-Jo1-IgG would show characteristic differences, and that particular Fc-glycan features would be associated with specific clinical manifestations [123]. It was confirmed that the Fc-glycan profile of IgG1 in IIM patients contained less galactosylated epitopes compared to healthy controls, which is a feature associated with pro-inflammation. Moreover, the lower abundance in bisected and afucosylated forms was linked to anti-Jo1 autoimmune IgG [123].

3. GLYCOMICS TECHNIQUES

As reviewed, protein glycosylation is a fundamental process that controls essential biological pathways. Therefore, the analysis of glycans is ultimately important. Several methods are available for the high-throughput separation and analysis of glycans. However, the low abundance of glycans hinders their identification, as well as the structural elucidation and quantitation of the glycome. Hence, pre-treatment of the sample is required to successfully characterise the full glycome. Regarding the determination techniques, a broad range of analytical platforms can be applied for the profiling, characterisation and analysis of glycans, being the

most widely used liquid chromatography coupled with fluorescence detection (LC-FLR) [9,48,97,100], lectin-based microarray [50,82,85], capillary electrophoresis (CE) [58,71,118], matrix-assisted laser desorption/ionisation mass spectrometry (MALDI-MS) [52,75,92,112], LC-MS [23,24,49,96], DNA sequencer-aided fluorophore-assisted carbohydrate electrophoresis (DSA-FACE) [19,22,74,79], ion mobility (IM) and NMR [93]. Several reviews focus exclusively on describing the available techniques used for glycan analysis [129,130,131]. This review summarises the most commonly used techniques, focusing only on the determination of n-glycans, as O-glycans are less documented. Table 1 to 6 briefly describes the sample treatments and determination techniques used in several studies for the determination of n-glycans.

3.1 Sample preparation

Reviews by Zhang et al. [132] and Xiao et al. [133] have specifically focused on describing the developments and advancements of sample preparation strategies for MS-based qualitative and quantitative n-glycans analysis. Briefly, these pre-treatment approaches include the release, separation, enrichment and derivatisation of n-glycans.

The procedure starts with the detachment of n-glycans from the protein or peptide backbone. Two different approaches can be used for this step, a chemical release procedure or an enzymatic release procedure. The use of chemical release procedures, including hydrazinolysis [134] or β-elimination by alkaline borohydride [135] were mainly used in early studies of oligosaccharides. Nowadays, enzymatic methods are more commonly used [132]. Amongst the available endoglycosidases, PNGase F is the most frequently used for treating mammalian proteins. It cleaves the glycosidic bond between the side chain of the asparagine residue and the reducing end of an oligosaccharide, creating an aspartic acid residue and a free glycosylamine [132]. Endoglycosidases F1-F3 and H are also used in n-glycome studies. Briefly, endo F and H catalyse dissociation of the β-1,4-glycosidic bond formed between two GlcNAc units of the n-glycan core [136].

Extended digestion time is often needed due to the high complexity and wide dynamic range of glycoproteins within a biological system [132]. Therefore, several modifications to the deglycosylation procedure have been made in order to achieve a faster digestion: the deglycosylation of 15 µg of glycoproteins using an enzyme-friendly surfactant, RapiGest SF and a 50 °C incubation step, accelerates the PNGase F induced digestion, completing the process in 7 min [137]. Other approaches have been employed to accelerate the glycan release process, such as microwave-assisted digestion [138], high-pressure cycling reactor [139] and immobilised enzyme reactor [140].

Usually, a purification step or enrichment-oriented pretreatment is recommended to reduce the complexity of the sample and facilitate the determination of n-glycans [132] since the abundance of glycoprotein is low in many biological samples [132]. Moreover, some glycoforms reach down to the limit of detection of many analytical methods, hampering their identification and quantification [141]. For instance, lectin affinity chromatography is widely used in the field of isolation, fractionation and enrichment, due to the capacity of lectins to recognise and capture carbohydrates with certain motifs [142]. Other common enrichment methods are porous graphitised carbon, hydrophilic interaction chromatography (HILIC) and size exclusion capture [133].

3.2 Determination techniques

3.2.1 Fluorescence detection

Lectin-based microarray

Lectin-based protein microarray is a method that enables the determination of released n-glycans in their native form. It has been reported that a very sensitive lectin-based protein microarray assay can be formulated and used to detect changes in glycan structures which accompany ageing or a disease [82]. Lectin-based microarrays are optimal for the determination of glycosylation changes and fits very well with biomarker research requirements [143], replacing conventional lectin-based analytical methods such as lectin blotting [85]. Moreover, they are

also a useful tool for quantitative analysis of lectin-glycoprotein interactions.

Briefly, this technique consists of immobilising on a glass slide a panel of lectins (>20), for which specificity has been well documented. A fluorescent-labelled probe molecule is then added, which simultaneously interacts with the lectins. After performing extensive washing to remove the unbound probe, the resulting fluorescence (FLR) intensity on each lectin spot is measured, most commonly with a confocal-type FLR scanner [130,144]. By using this method, a fast analysis of a sample glycopattern can be obtained, rather than a precise identification of the glycan structures, which is the domain of Mass Spectrometry (MS) techniques [85].

Liquid chromatography

LC is one of the mostly used separation techniques for the determination of glycans. It is commonly combined with FLR detection as its glycan quantification is considered to be better than the quantification that MS offers [145].

Specifically, HILIC is widely used for the separation of glycans. It was first introduced as a variant of normal phase chromatography in which analytes interact with a hydrophilic stationary phase. Analytes are retained on the hydrophilic stationary phase by hydrogen bonding, ionic interactions and dipole-dipole interactions [146]. HILIC differs from normal-phase chromatography because it uses polar aqueous mobile phases, eluting analytes in order of increasing hydrophilicity [147,148]. Accordingly, this technique is widely used for the analysis of very polar compounds [147], as hydrophilic compounds strongly retain on the stationary phase [146]. This chromatography is the most efficient separation method for native or reducing end labelled glycans which provides efficient separation of different isomers [147]. These advantages have permitted that HILIC-based enrichment techniques for glycans and glycopeptides become valuable tools in glycoproteomics [149]. This separation technique can be combined with FLR detection or MS [149]. Since larger glycans elute later

(due to its large number hydrogen bonding groups), HILIC of glycans is sometimes known as “size fractionation”. As well as the size of the glycan, its charge and steric properties influence HILIC retention, resulting in the separation of isomers [149]. Often a single HILIC run may not be sufficient for structural assignment, hence additional anion exchange-LC and reversed phase liquid chromatography (RP-LC) separation steps may be used to obtain two- or three-dimensional mapping of glycans [150].

Reversed-phase chromatography is also widely used for the separation of glycans, as shown by Vreeker et al. by presenting an overview of the literature on reversed-phase separation of carbohydrates [16]. This technique is based on a noncovalent association between the nonpolar stationary phase and the nonpolar moieties of an analyte [16]. Most methods using reversed-phase columns are based on C18 separation. Characteristics can differ between columns, from column length, internal diameter and particle size which influence on the separation efficiency [16], to the density and nature of the nonpolar groups immobilised on the silica surface which influence the selectivity [151]. Oligosaccharides generally exhibit poor retention on C18-RP-LC, therefore derivatisation with a hydrophobic agent is required to allow their efficient separation. The chosen tag will not only influence the retention behaviour on the particular stationary phase, but also improve the sensitive and selective detection by UV absorption or FLR, as well as enhancing the ionisation and fragmentation behaviour in MS [18,152].

Two of the most used labelling reagents for Liquid Chromatography (LC) analysis are 2-aminobenzamide (2-AB) and procainamide [145]. Both labels use the same mechanism to bind to glycans: the primary amine group of the label reacts with the aldehyde group of the glycan, resulting in an imine, which will then be reduced to form a stable secondary amine. Using this approach, one molecule of label is stoichiometrically attached to one molecule of glycan, allowing the relative quantification of different glycans based on FLR intensity [153]. A third labelling compound is RapiFluor MS (RFMS). It uses a different binding chemistry that contains n-

hydroxysuccinimide, which modifies the n-glycan glycosylamine, producing a n-glycan with a urea linked RFMS label. In addition, it contains a quinoline fluorophore for FLR detection and a basic tertiary amine to enhance positive mode electrospray ionisation (ESI) [145]. 6-aminoquinolyl-n-hydroxysuccinimidyl carbamate (AQC) uses a similar binding chemistry to RFMS, containing a n-hydroxysuccinimide carbamate and a quinoline fluorophore but lacking the basic tertiary amine. They react with both primary and secondary amines in aqueous solution and yields derivatives that are stable at room temperature for several days. Moreover, it has unique FLR properties which allow the LC-FLR analysis of derivatised samples without prior reagent removal and with minimal reagent interference [154,155].

Capillary electrophoresis

CE is a high-resolution method that can separate complex carbohydrate molecules while offering excellent sensitivity. This method, in conjunction with laser-induced fluorescence (LIF) detection, can reach detection limits in the femtomolar range [156] and is optimal for profiling fluorophore-labelled oligosaccharides [157]. Briefly, this analytical system used for carbohydrate profiling separates and analyses oligosaccharides released from glycoproteins. Once the oligosaccharides have been released, the fluorophore 8-aminopyrene-1,3,6-trisulphonate (APTS) is used for labelling the oligosaccharides at their reducing terminus by reductive amination. Subsequently, the APTS derivatives of oligosaccharides are readily separated by CE [158]. Amongst other labels, APTS remains the method of choice for CE separations [159,160]. Glycan labelling with APTS through reductive amination is well-established and preferred over other strategies, such as hydraside or Michael addition [153].

CE provides fast and efficient separations, as well as a high degree of automation [158]. This technique is accessible to researchers through commercially available solutions to interface CE with MS, as well as improving the databases and software that will ease the data analysis [156]. By using instruments with 16-capillary arrays, exceptional

throughput can be achieved compared to LC methods. Regarding the cost of the instrument, it is on par with LC and low-end MS approaches, and the cost of the sample is significantly low. The limitations of the technique include poor acceptance by the glycomics community and the lack of large structural databases [156].

Comparisons between various separation techniques have been carried out. It has been reported that CE and HILIC have similar performance and are both better suited to resolve complex mixtures compared to RP-LC [161]. Another study demonstrated that CE and HILIC showed comparable results, however electrophoresis was more cost-effective, consumed less sample and was operated with higher throughput [159].

Another electrophoresis-based technique is DSA-FACE, a high throughput technology platform that offers an accurate fingerprint of the glycan composition in serum, plasma and other body fluids [11,162]. This procedure requires only 2 μL of sample and involves the labelling of glycans, profiling and read-out [11]. It is robust, reproducible, sensitive and quantitative, as well as non-invasive. Furthermore, the method is easy and can be learned rapidly. None of the reagents are expensive and a DNA sequencer is the only specialised equipment required. Nevertheless, this technique does have a couple of limitations. Firstly, it misses information about the sialic acid distribution, as it does not profile desialylated n-glycans. Secondly, it lacks information about the sugar structures, which can be solved by carrying out exoglycosidase digestions to obtain more information about the structure of the glycan [162].

3.2.2 Mass spectrometry detection

MS is becoming increasingly more important for structural determination and quantitative glycomic analysis due to its speed, simplicity, resolution and information content [163,164].

At present, MALDI and ESI are the most widely-used MS ionisation techniques for the analyses of carbohydrates [129,164]. In both MALDI and ESI, free glycans tend to be detected as metal (usually sodium) adducts in the positive ion mode, and as deprotonated or anion-adducted species in

the negative-ion mode [129]. Even though native glycans can be analysed by MS, low sensitivity in positive mode MS and potential insource fragmentation leads to the inability to directly analyse native glycans [152]. To address this issue, several derivatisation methods have been used, such as reductive amination, permethylation and peracetylation [165]. Parameters of interest such as reproducibility and quantification can be measured using MS even though they can be compromised by ion suppression in complex samples, fluctuations in spectrometer performance or variability in matrix crystallisation for specifically MALDI-TOF MS applications [163].

Various mass analysers, available for the separation of ions in MS, are used in glycosylation studies. For instance, some of the most common are the quadrupole mass analyser [166], time of flight mass analyser [167], quadrupole ion trap mass analysers [168] and Fourier-transform ion cyclotron resonance [169,170]. Several parameters differ depending on the used mass analyser, such as the extent of glycan dissociation, which is lower in ion traps compared to quadrupole time-of-flight, triple quadrupole and Fourier Transform mass spectrometers with external dissociation cells [171].

Matrix-Assisted Laser Desorption/Ionisation Mass Spectrometry

MALDI-MS is a soft ionisation technique in which a sample is embedded in a low molecular weight ultraviolet-absorbing matrix. Ionisation is affected by a pulsed laser which will be absorbed by the matrix. This energy is then transferred to the compounds present on the sample and enables the predominant formation of singly charged quasi-molecular ions [172]. For the analysis of n-glycans, 2,5-diydroxybenzoic acid (DHB) is the most frequently used matrix for the suspension and co-crystallisation of the oligosaccharides, permitting their efficient ionisation. Other matrices, such as oxidised carbon nanotubes with short and open-end structures produce strong signals from small carbohydrates and amino acids [173]. Both of these matrices generally generate [M + Na]+ ions [174]. Many other matrices have been tested for the analysis of carbohydrates and

glycoconjugates using MALDI-MS [174]. Figure 2B shows a characteristic MALDI-TOF MS spectra of n-glycans.

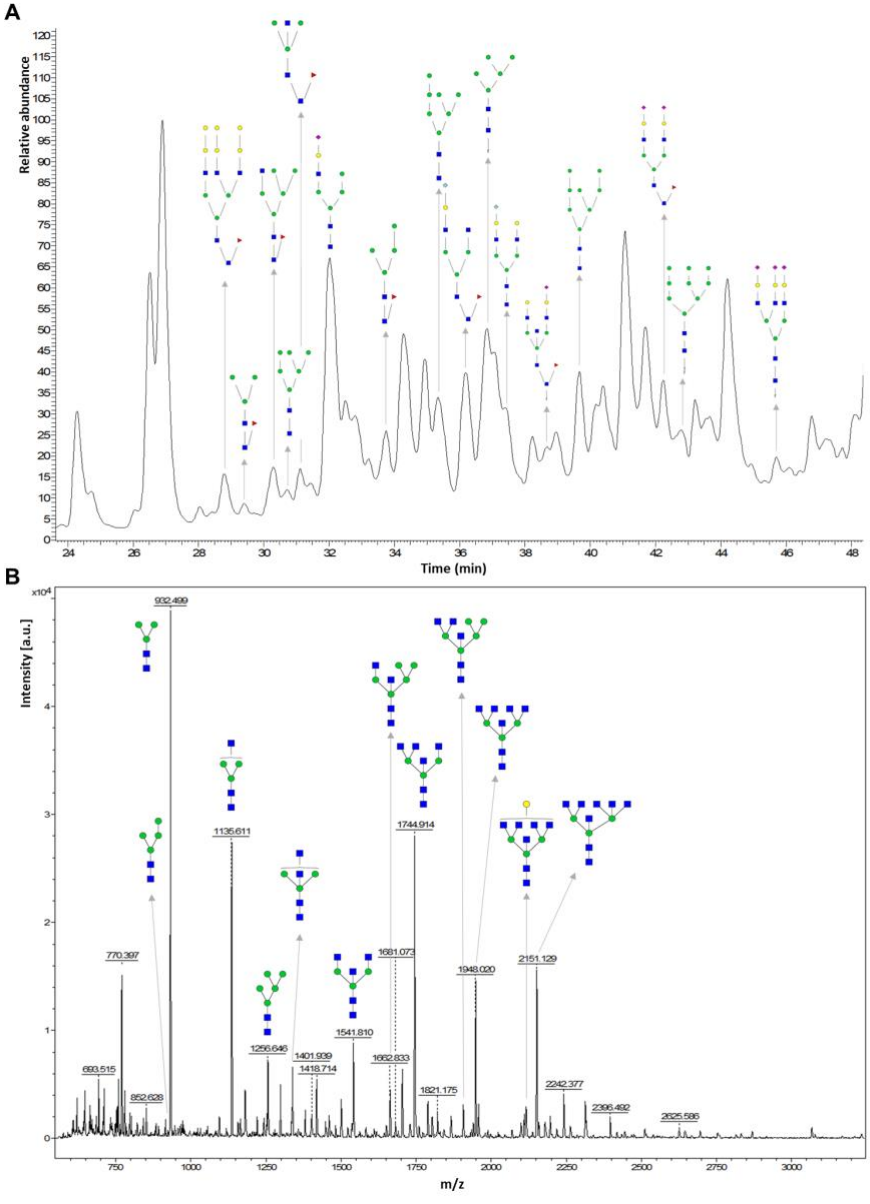

Figure 2. (A) HPLC-MS Orbitrap chromatogram of mouse brain n-glycans released with PNGase F and labelled with RFMS. (B) Positive ion MALDI-TOF spectra of n-glycans from ovalbumin released by treatment with PNGase F and recorded in 2,5-DHB matrix. The symbol nomenclature used for each glycan structure is shown in Figure 1.

The use of MALDI offers several advantages compared with ESI. It has a higher salt tolerance to contaminants (for instance, salts in buffers) [164] and little susceptibility to suppression effects. However, it also has a few disadvantages, like the variations between spectra performance at different positions in the sample spots, which are often observed. In order to overcome this drawback, a spot has to be sampled in several locations until the best signal to noise ratio is obtained [175]. In addition, MALDI-MS cannot resolve isobaric compounds unless MS/MS is employed [163] and the presence of abundant ions derived from the matrix often limits the utility of MALDI-MS for the analysis of small molecules [174]. Although positive-ion MALDI-MS is predominantly used to profile glycans, negative-ion MALDI-MS has recently gained interest as it can provide advantageous fragmentation. Its main difficulty is the formation of the deprotonated ion [M-H]-, which is very successful for ESI but not for MALDI. The formation of [M+Cl]- has been proved to be a useful alternative as it produces similar fragmentation for sequencing neutral oligosaccharides using MALDI-MS/MS [176].

MALDI can also be used as a mass spectrometry imaging technique (MALDI-IMS), a well-developed tool that enables high throughput reporting of molecules localised within a single formalin-fixed, paraffin embedded (FFPE) tissue section. By using the enzyme PNGase F to release the n-glycans from thin tissue sections, MALDI-IMS is routinely used to examine the distribution of n-glycosylation [177,178].

Liquid chromatography coupled to mass spectrometry

MS is commonly coupled to separation techniques, mainly LC, in order to significantly improve the identification and quantitation of low abundant glycans by reducing competitive ionisation and detector saturation [179]. In addition, LC-MS is sometimes further combined with FLR for the detection of glycans for their extended dynamic range and more comparable response between released glycans. Thus, MS provides poorer quantification but is slightly more sensitive [145] compared to FLR. In positive ESI-MS there is the tendency of forming adducts with protons,

sodium, potassium and ammonium, which splits the glycan signal into multiple peaks and makes quantification less robust [180]. Nevertheless, ESI-MS is optimal for the measurement of the ratio of different glycans which coelute in the same peak. Therefore, FLR and MS are two complementary detection techniques [145]. Figure 2A shows a typical LC-MS chromatogram of n-glycans.

As well as MALDI-MS, ESI-MS is a soft ionisation technique commonly applied to obtain a glycosylation profile. This technique consists in the nebulisation of a sample solution into electrically charged droplets, the liberation of ions from droplets, followed by the transportation of ions from the atmospheric pressure ionisation source region into the vacuum and mass analyser of the mass spectrometer [181]. ESI has a few drawbacks compared to other ionisation techniques. Its ionisation efficiency decreases when the molecular weight increases, unlike MALDI, which maintains a constant ionisation efficiency when the size of the molecule increases. Furthermore, ESI generates multiply charged ions which complicates spectral analysis. Nevertheless, the instrument software can perform a deconvolution of the multiple charge states to produce a spectrum that shows a single molecular weight distribution. This approach will solve the issue but will affect the ability to detect low-abundance species as the signal will be distributed over multiple charge states [129].

Amongst the different types of LC that can be used in the determination of glycans, nanoscale reversed-phase columns are also used [7,16,23,80,87]. These columns typically have a dimension of 75 μm × 150 mm and a flow rate of around 300 nL/min. The reduction of the internal diameter of the column limits the amount of the sample that can be injected, which is a drawback. In order to inject larger volumes, trapping columns are used [16]. The reduction of the internal diameter increases the sensitivity of the measurements with MS detection, achieving sensitivities in the low femtomole range [18]. Coupling nanoscale columns with MS detection is optimal for glycan analysis as the samples are often complex and full

chromatographic separation is not obtained. In order to further improve the chromatographic separation, two-dimensional LC can be used, which is characteristic for successfully achieving the separation of isomers [182,183]. In the first dimension, separation is performed in HILIC mode at analytical scale, resulting in an incomplete separation of the different glycans in the samples. Using nanoscale reversed phase in the second dimension allows the separation of complex samples and isomer mixtures. Altogether, a two-dimensional separation is achieved obtaining detailed characterisation of complex glycan mixtures [16,182,183].

As previously mentioned, the derivatisation of glycans not only enables the optical detection of glycans but also enhances the ionisation and fragmentation behaviour in MS [18]. The aforementioned tags show differences between them. For instance, even though procainamide and 2-AB have the same mechanism, procainamide shows increased FLR and ionisation over 2-AB, as it contains a basic tertiary amine tail with high proton affinity, exhibiting a higher sensitivity in positive mode ESI-MS [184].

MS fragmentation methods

Even though glycans can be identified using high resolution MS (HRMS), the lack of characteristic fragment ions can be a problem for detailed structural elucidation of glycans. This can be solved by making molecular ions more energetic by inducing fragmentation, which can be achieved by employing tandem MS [129,152]. Among the existing fragmentation techniques, collision-induced dissociation (CID) is employed for the generation of tandem mass spectra of oligosaccharides [185], in which analyte molecules are accelerated and collided with a neutral gas, resulting in the fragmentation of molecular bonds and the creation of tandem mass spectra [186]. Dissociation of protonated glycan or glycopeptides ions is not recommended because monosaccharide rearrangements may result. On the contrary, the use of sodium (or other metal) cationised ions is more recommended since rearrangements of this kind of ions have not been reported [171].

Generally, glycans undergo two types of cleavage upon CID: glycosidic cleavages (for instance, B-/Y- and C-/Z-types) result from the rupture between the two neighbouring residues which provide information on the composition and sequence, whereas cross-ring cleavages (A-/X- types) provide linkage information due to the fragmentation of a sugar ring [129,176]. This type of fragmentation is shown in both positive and negative ion modes, hence a common nomenclature is used, as illustrated in Figure 3. When the charge is retained on the carbohydrate portion, fragments are designated as Ai, Bi and Ci, where i represents the number of the glycosidic bond cleaved, counted from the non-reducing end (except for branched oligosaccharides, which follow a different rule). Differently, those ions containing the reducing sugar unit are labelled as Xj, Yj and Zj, where j corresponds to the number of the interglycosidic bond counted from the reducing end. The glycosidic bond linking to the reducing end is numbered 0 [187]. Focusing on the sugar ring fragmentation, in which carbon-carbon bonds are cleaved, the cross-ring cleavages are designated with Aj and Xj labels. Two superscripts, k and l (i.e., k,lAi and k,lXj) are used to indicate the sugar ring bonds that have been broken. Each ring bond is encoded with a number, as shown in Figure 3 [129].

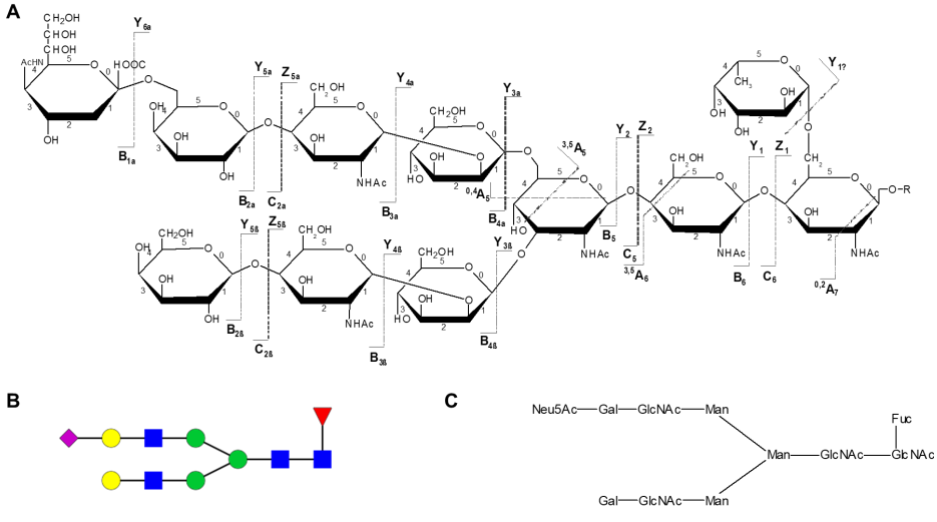

Figure 3. Three types of structural representations for one specific glycan. (A) Diagram with some of the main cleavage sites ivolved in fragment ion formation.

(B) Symbolic representation of the glycan structure. (C) Tree abstraction of the glycan structure.

As previously mentioned, branched oligosaccharides do not have the same nomenclature. Their carbohydrate portion is known as the "core" unit and the branches as "antennae". Each antenna is represented by a Greek letter (α, β and γ), which are assigned with decreasing molecular (fragment) weight ($\alpha \geq \beta \geq \gamma$). This nomenclature is then applied to branched carbohydrates [187]. When fragmentations take place on the α- and β-antennae, they are represented as Aiα, Biα, Ciα, Xjα and Zjα, respectively. Ions resulting from the core unit are designated without a Greek letter, but the numbering begun in the core continues into the antennae, and vice versa [187].

On the other hand, higher-energy collision dissociation (HCD), introduced following the development of the Orbitrap MS, is a CID related fragmentation technique in which beam-type fragmentation spectra are created inside the HCD cell. This technique can be used for the detection of individual monosaccharide fragments as it does not have the "1/3 rule" which establishes a lower range m/z cut-off which is what limits ion-trap CID [188].

Some of the existing automated analysis tools and software used to determine glycan composition take into account the fragmentation patterns of glycans that have just been stated above.

Sialic acid containing glycan analysis

Sialic acids are a family of 9-carbon containing acidic carbohydrates, which frequently terminate the glycan structure. Sialylation affects the half-lives of many circulating glycoproteins and plays important roles in several biologic processes such as cell-cell communication, cell-matrix interaction, adhesion and protein targeting [189]. This modification occurs in approximately 20% of core-fucosylated biantennary Fc n-glycans [43]. Moreover, these carbohydrates are found on both n- and O- linked glycans

attached to either galactose or n-acetylglucosamine via α2,3- or α2,6-linkages whose syntheses are catalysed by specific enzymes [78].

The presence of sialic acids can complicate the quantification of both neutral and acidic glycans in a single sample, as neutral glycans ionise better in positive mode whereas sialylated glycans ionise better in negative mode. Sialic acid residues are highly labile on sialylated carbohydrates, hence, in source fragmentation with both MALDI and ESI can lead to sialic acid residue loss, which consequently complicates structural and quantitative analysis of these glycans [190]. To overcome this problem, several derivatisation strategies can be applied in order to neutralise sialic acid residues. These strategies allow the simultaneous analysis of neutral and acidic glycans apart from preventing the loss of the sialic acid residue due to in-source fragmentation [164].

Permethylation is the predominant derivatisation technique applied to sialylated glycans. The ionisation efficiency of glycans is improved when they become less hydrophilic by converting their polar hydroxyl and carboxylate groups into nonpolar methylated homogenous derivatives [164,191]. This derivatisation method offers several advantages regarding the analysis of glycans as it helps facilitate the determination of sequence and composition of monosaccharides in glycans, branching position and interglycosidic linkage information, as well as the presence of configurational and conformational isomers [192]. Permethylation enhances the stabilisation of sialic acid residues through neutralisation, enabling the simultaneous analysis of neutral and acidic carbohydrates in positive ion mode [164]. Moreover, this technique facilitates structure elucidation by tandem MS, through the formation of more informative fragments. However, the isomeric separation of permethylated glycans using the existing methods is not satisfactory [188].

Esterification is an alternative to permethylation, which was originally achieved by the formation of ethyl esters using methyl iodide in DMSO [193]. More recently, 3-methyl-1-p-tolytriazene (MTT) in DMSO-acetonitrile solution [194] or 4-4(4,6-dimethoxy-1,3,5-triazin-2-yl)-4-

methyl-morpholinium chloride (DMTMM) in methanol have been used. This last derivatisation method offers the advantage that α2,3- and α2,6-linked sialic acids can be differentiated, as methyl esters are produced from α2,6-linked acids and lactones from α2,3-linked acids. This fact allows linkage position to be determined by the resulting mass difference, avoiding the use of exoglycosidase digestions for the linkage determination [164,195]. 1-ethyl-3-(3-(dimethylamino) propyl) carbodiimide (EDC) and 1-hydroxybenzotriazole (HOBt) in an ethanolic solution are also employed as an esterification method. These reagents are widely used in peptide synthesis, in which EDC is responsible for initial carboxylic acid activation and HOBt catalyses the subsequent conversion to an ester or an amide [196].

Finally, amidation is another derivatisation strategy in which several reagents can be employed. Complete amidation of both α2,3- and α2,6-sialic acids can be achieved by using acetohydrazide and (EDC) as a coupling reagent in mild acidic conditions. Azetohydrazide can be easily coupled with the carboxylic acid; however, the aldehyde of the reducing end of a free glycan is also reactive to hydrazide. Therefore, permanent charge cannot be incorporated after the amidation reaction [197]. To overcome this issue, amidation can be performed on the sialylated n-glycan while it is still attached to the protein [198]. EDC, HOBt and dimethylamine in DMSO are also employed in amidation techniques [199], as well as DMT-MM in ammonium chloride [200].

Isotopic labelling

Isotopic labels are widely used for quantitative analysis. They offer a major advantage for glycan analysis as they enable the simultaneous analysis of multiple samples and comparison with an internal standard. The use of these labels provide a method for the separation of derivatised and underivatised glycans [201]. Internal standards with similar characteristics to the analytes have also been used to standardise analysis to a known quantity or to perform absolute quantitation [163,202].

However, this practice is not widely used as the availability of internal standards is limited and molar differences in glycan ionisation introduce large errors when standards of similar characteristics are used [163,164,203].

Chemical or metabolic labelling approaches incorporate a heavy isotope into a glycan for comparative analysis. These techniques help reduce some issues related to label free analysis such as instrument response and differences in ionisation efficiencies. In chemical labelling approaches, heavy isotopes are introduced during methylation or reductive amination procedures for the analysis of glycans using MALDI-MS [204] or LC-ESI-MS [205].

For instance, the reagents 13CH3I and 12CH2DI were used during methylation to analyse n-linked oligosaccharides from glycoprotein and human serum [206]. The mass difference between these compounds is only 0.002922 Da which required high resolution MS with more than m/ Δ m = 30,000 resolution in order to resolve the two isotopic species. This method is known as QUIBL, used for quantitative isobaric labelling and particularly useful for the quantitation of isomers by MS/MS [202]. Isotopic labelling is also a suitable approach for those glycans that cannot be modified by reductive amination. This is the case of O-glycans that are released through β-elimination, producing a hydroxyl group at the reducing end which impedes the use of reductive amination. In order to overcome this issue, isotopic labelling using NaBD4 during β-elimination can introduce deuterium labels [207].

Ion mobility

In recent years, IM has been used in the field of glycomics for the separation of isomeric compounds. In this technique, ions are not only separated according to their mass and charge but also according to their shape and size. Hence, ion-mobility mass spectrometry (IMMS) can be an optimal technique for the separation of glycoconjugate isomers which have different sialic acid linkage [208,209]. When IM is coupled on-line with MS,

it provides three-dimensional analytical information for each detected species: shape-to-charge, mass-to-charge and abundance, allowing reliable analyte identification [208,209].

Specifically, IM measures the time (drift time) that a particular ion takes to cross a cell filled with an inert, neutral background gas (commonly N2 or He) at a controlled pressure under the influence of a weak electric field. The drift time of a specific ion is mainly due to ion-gas collisions, hence ions are separated due to their ion-neutral collision cross-section (Ω), related to the overall shape and topology of the ion [209,210]. Furthermore, the accelerating electric force is greater when the charge of the ion is higher, meaning that the ion will cross the chamber more quickly. Taking this into account, the drift time of an ion is determined by the collision cross-section-to-charge ratio (Ω/z) [211]. In order to further expand the utility of IMMS to glycomics, separation factors will need to be augmented with multiple stages of IMMS or orthogonal analysis techniques such as gas-phase action spectroscopy [208].

MS analysis tools

There are many analysis tools used for the identification of glycans and glycopeptides from both MS and MS/MS data, as reported by Woodin et al. [3]. GlycoWorkbench is one of the most commonly used to identify both glycans and glycopeptides from MS data. It looks for matches between calculated theoretical glycan masses and the corresponding m/z values from a spectral peak list uploaded by the user [212]. Similarly, GlycoSpectrumScan identifies n- and O-linked glycoforms using MS data, as well as determining the relative abundance of these glycoforms for each glycosylation site [3,213]. Many other tools are also used, such as Glycofragment and GlycoSearchMS, both developed for glycan structure determination. Glycofragment calculates the theoretical fragmentation patterns of glycan structures and GlycoSearchMS compares the experimental data obtained with the theoretical spectra from n-linked and O-linked glycan fragmentation entries extracted from SweetDB [214].

SimGlycan is an ideal tool to increase throughput of glycan analysis. Glycan structures can be determined from MS/MS data obtained from various mass spectrometers, using a built-in database with theoretical fragmentation profiles to provide the most likely structure candidates. SimGlycan stands out from other software platforms for its capacity to report novel glycans. Glycan structures are determined, monosaccharide by monosaccharide, from the fragments observed. Furthermore, the software has been updated to perform fragmentation analysis for glycopeptides [207]. ProteinScape is another software used for the identification of glycans and glycopeptides [80,215], amongst many others that are either freely available or not [3].

In addition to the available analysis tools and software for the identification of glycans, several glycomic databases are available, which document different glycan structures. As reviewed by Hizal et al. [216], the Consortium Functional Glycomics (CFG) glycan structure database [217], Glycobase [212], Glycome DB [218], GlycoSuiteDB [219], EuroCarbDB [220] and Lectin Frontier Database [221] are a few of the publicly accessible databases.

3.2.3 Nuclear Magnetic Resonance

NMR is a very powerful tool for the analysis of complex n-glycans and has specifically been proven to be suitable for the determination of the primary sequence of glycans [27]. NMR is a nondestructive technique as it leaves the sample intact for further analyses and, with sample amounts as small as 15 pmol [215]. This technique can provide structural information for isolated glycan species, however, the quantities required to achieve actionable levels of signal to noise ratio in NMR are a significant challenge for those studies targeting low abundance glycans [208]. However, more recent studies have demonstrated that NMR can indeed be highly sensitive if water suppression and sample preparation are optimised [215].

In order to interpret the 1H-NMR spectrum of a carbohydrate chain in terms of primary structural assignments, Vliegenthart and Kamerling developed the structural reporter group (SRG) concept. The SRG concept is

based on the fact that the chemical shifts of specific glycan protons are very sensitive to the structure of a given glycan, and the comparison of structural elements allow the characterisation of the compound [222].

Therefore, NMR data offers additional information which can be tightly integrated with LC-MS and MS/MS data, achieving a complete characterisation of even isobaric glycans differing in only one linkage position or in the substitution in one branch [215].

4. CONCLUSIONS

Glycome analysis is emerging as a source of potential biomarkers in different pathological states [223]. Its analysis is not easy, as the diverse structures of glycans are complex and heterogenic. Moreover, there is a wide range of possible monosaccharide combinations and linkages, that result in structurally complex glycans, which can be attached to proteins, conforming glycosylation PTMs.

A wide variety of glycans have been reported to be altered in many studies focused on determining the glycosylation profile in ageing and several age-related diseases. Galactosylation and sialylation are altered in many diseases; however, these features specifically decrease with age, as well as in AD and RA patients, but increase in ALS patients. Fucosylation is increased in several types of cancer and decrease in IBD and T2DM patients. The glycan patterns shown amongst the different types of age-related diseases are limited, nevertheless, aberrant glycosylation could help distinguish different diseases and identify potential diagnostic and prognostic biomarkers.

In clinical studies, the comparison of glycans levels altered in specific diseases often leads to inconsistent results, which cannot be explained completely by the different statistical methods. This may be due to the diversity of the glycome in different populations and even in different environments. Diseases can show diversity among populations, justifying the inconsistency of some results. However, glycan traits can be considered as a new avenue of research in the systematic understanding of complex diseases.

Furthermore, the use of a wide range of glycomic methodologies leads to low comparability between studies which hinders the obtention of clear results. CE is characteristic for providing fast and efficient separations, as well as being highly automated, whereas IMMS is considered to be optimal for the separation of glycoconjugate isomers which have different sialic acid linkage. NMR is a nondestructive technique as it leaves the sample intact for further analyses and can provide structural information for isolated glycan species. Nevertheless, MS seems to be the most promising technique, with the possibility to use different types of chromatographic separation combined with the most appropriate ionisation technique and mass analyser.

Author Contributions

B.P. collected the information and drafted the manuscript. P.H., N.C. and M.S. made critical revisions and gave suggestions during the preparation. All authors have read and agreed to the published version of the manuscript.

Funding

This work was financially supported by the Catalan Government through the funding grant ACCIÓ-Eurecat, by the Centre for the Development of Industrial Technology (CDTI) of the Spanish Ministry of Science and Innovation under grant agreement: TECNOMIFOOD project CER-20191010.

Acknowledgments

BP is supported by a fellowship from the Vicente Lopez Program (Eurecat).

Conflicts of Interest

The authors declare no conflict of interest.

REFERENCES

1. Van Den Steen, P.; Rudd, P.M.; Dwek, R.A.; Opdenakker, G. Concepts and principles of O-linked glycosylation. *Crit. Rev. Biochem. Mol. Biol.* **1998**, *33*, 151–208, doi:10.1080/10409239891204198.

2. Miura, Y.; Endo, T. Glycomics and glycoproteomics focused on aging and age-related diseases - Glycans as a potential biomarker for physiological

alterations. *Biochim. Biophys. Acta - Gen. Subj.* **2016**, *1860*, 1608–1614, doi:10.1016/j.bbagen.2016.01.013.

3. Woodin, C.L.; Maxon, M.; Desaire, H. Software for Automated Interpretation of Mass Spectrometry Data from Glycans and Glycopeptides. *Analyst* **2014**, *138*, 2793–2803, doi:10.1039/c2an36042j.Software.

4. Ohtsubo, K.; Marth, J.D. Glycosylation in Cellular Mechanisms of Health and Disease. *Cell* **2006**, *126*, 855–867, doi:10.1016/j.cell.2006.08.019.

5. Dennis, J.W.; Granovsky, M.; Warren, C.E. Protein glycosylation in development and disease. *BioEssays* **1999**, *21*, 412–421, doi:10.1002/(SICI)1521-1878(199905)21:5<412::AID-BIES8>3.0.CO;2-5.

6. Handerson, T.; Camp, R.; Harigopal, M.; Rimm, D.; Pawelek, J. B1,6-Branched Oligosaccharides Are Increased in Lymph Node Metastases and Predict Poor Outcome in Breast Carcinoma. *Clin. Cancer Res.* **2005**, *11*, 2969–2974, doi: 10.1158/1078-0432.CCR-04-2211.

7. Anugraham, M.; Jacob, F.; Nixdorf, S.; Everest-dass, A.V.; Heinzelmann-schwarz, V.; Packer, N.H. Specific Glycosylation of Membrane Proteins in Epithelial Ovarian Cancer Cell Lines : Glycan Structures Reflect Gene Expression and DNA Methylation Status. *Mol. Cell Proteomics* **2014**, *13, 2213*–2232, doi:10.1074/mcp.M113.037085.

8. Li, X.; Wang, H.; Russell, A.; Cao, W.; Wang, X.; Ge, S.; Zheng, Y.; Guo, Z.; Hou, H.; Song, M.; et al. Type 2 Diabetes Mellitus is Associated with the Immunoglobulin G N-Glycome through Putative Proinflammatory Mechanisms in an Australian Population. *OMICS* **2019**, *23*, 631-639, doi:10.1089/omi.2019.0075.

9. Lemmers, R.F.H.; Vilaj, M.; Urda, D.; Agakov, F.; Šimurina, M.; Klaric, L.; Rudan, I.; Campbell, H.; Hayward, C.; Wilson, J.F.; et al. IgG glycan patterns are associated with type 2 diabetes in independent European populations. *Biochim. Biophys. Acta - Gen. Subj.* **2017**, *1861*, 2240–2249, doi:10.1016/j.bbagen.2017.06.020.

10. J. Kailemia, M.; Park, D.; B. Lebrilla, C. Glycans and Glycoproteins as Specific Biomarkers for Cancer. *Anal. Bioanal. Chem.* **2017**, *409*, 395–410, doi:10.1007/s00216-016-9880-6.

11. Vanhooren, V.; Dewaele, S.; Libert, C.; Engelborghs, S.; De Deyn, P.P.; Toussaint, O.; Debacq-Chainiaux, F.; Poulain, M.; Glupczynski, Y.; Franceschi, C.; et al. Serum N-glycan profile shift during human ageing. *Exp. Gerontol.* **2010**, *45*, 738–743, doi:10.1016/j.exger.2010.08.009.

12. Franceschi, C.; Garagnani, P.; Morsiani, C.; Conte, M.; Santoro, A.; Grignolio, A.; Monti, D.; Capri, M.; Salvioli, S. The continuum of aging and age-related diseases: Common mechanisms but different rates. *Front. Med.* **2018**, *5*, doi:10.3389/fmed.2018.00061.

13. López-Otín, C.; Blasco, M.A.; Partridge, L.; Serrano, M.; Kroemer, G. The Hallmarks of Aging Europe PMC Funders Group. *Cell* **2013**, *153*, 1194–1217, doi:10.1016/j.cell.2013.05.039.

14. Minuti, A.; Patrone, V.; Giuberti, G.; Spigno, G.; Pietri, A.; Battilani, P.;

Ajmone Marsan, P. Nutrition and Ageing. *Stud. Health Technol. Inform.* **2014**, *203*, 112–121, doi:10.3233/978-1-61499-425-1-112.

15. Kim, T.; Xie, Y.; Li, Q.; Artegoitia, V.M.; Lebrilla, C.B.; Keim, N.L.; Adams, S.H.; Krishnan, S. Diet affects glycosylation of serum proteins in women at risk for cardiometabolic disease. *Eur. J. Nutr.* **2021**, doi:10.1007/s00394-021-02539-7.

16. Vreeker, G.C.M.; Wuhrer, M. Reversed-phase separation methods for glycan analysis. *Anal. Bioanal. Chem.* **2017**, *409*, 359–378, doi:10.1007/s00216-016-0073-0.

17. Geyer, H.; Geyer, R. Strategies for analysis of glycoprotein glycosylation. *Biochim. Biophys. Acta - Proteins Proteomics* **2006**, *1764*, 1853–1869, doi:10.1016/j.bbapap.2006.10.007.

18. Wuhrer, M.; Deelder, A.M.; Hokke, C.H. Protein glycosylation analysis by liquid chromatography-mass spectrometry. *J. Chromatogr. B Anal. Technol. Biomed. Life Sci.* **2005**, *825*, 124–133, doi:10.1016/j.jchromb.2005.01.030.

19. Testa, R.; Vanhooren, V.; Bonfigli, A.R.; Boemi, M.; Olivieri, F.; Ceriello, A.; Genovese, S.; Spazzafumo, L.; Borelli, V.; Bacalini, M.G.; et al. N-Glycomic changes in serum proteins in type 2 diabetes mellitus correlate with complications and with metabolic syndrome parameters. *PLoS One* **2015**, *10*, 1–16, doi:10.1371/journal.pone.0119983.

20. Nilsson, A.; Santoro, A.; Franceschi, C.; Kadi, F. Detrimental links between physical inactivity, metabolic risk and N-glycomic biomarkers of aging. *Exp. Gerontol.* **2019**, *124*, 110626, doi:10.1016/j.exger.2019.05.015.

21. Wang, H.; Li, X.; Wang, X.; Liu, D.; Zhang, X.; Cao, W.; Zheng, Y.; Guo, Z.; Li, D.; Xing, W.; et al. Next-Generation (Glycomic) Biomarkers for Cardiometabolic Health: A Community-Based Study of Immunoglobulin G N -Glycans in a Chinese Han Population . *Omi. A J. Integr. Biol.* **2019**, *23*, 1–11, doi:10.1089/omi.2019.0099.

22. Vanhooren, V.; Desmyter, L.; Liu, X.E.; Cardelli, M.; Franceschi, C.; Federico, A.; Libert, C.; Laroy, W.; Dewaele, S.; Contreras, R.; et al. N-glycomic changes in serum proteins during human aging. *Rejuvenation Res.* **2007**, *10*, 521–531, doi:10.1089/rej.2007.0556.

23. Šimurina, M.; de Haan, N.; Vučković, F.; et al. Glycosylation of Immunoglobulin G Associates With Clinical Features of Inflammatory Bowel Diseases. *Gastroenterology* **2018**, *154*, 1320–1333, doi:10.1053/j.gastro.2018.01.002.

24. Lundström, S.L.; Yang, H.; Lyutvinskiy, Y.; Rutishauser, D.; Herukka, S.K.; Soininen, H.; Zubarev, R.A. Blood plasma IgG Fc glycans are significantly altered in Alzheimer's disease and progressive mild cognitive impairment. *J. Alzheimer's Dis.* **2014**, *38*, 567–579, doi:10.3233/JAD-131088.

25. Ge, S.; Wang, Y.; Song, M.; Li, X.; Yu, X.; Wang, H.; Wang, J.; Zeng, Q.; Wang, W. Type 2 diabetes mellitus: Integrative analysis of multiomics data for biomarker discovery. *Omi. A J. Integr. Biol.* **2018**, *22*, 514–523, doi:10.1089/omi.2018.0053.

26. Kawaguchi-Sakita, N.; Kaneshiro-Nakagawa, K.; Kawashima, M.; Sugimoto, M.; Tokiwa, M.; Suzuki, E.; Kajihara, S.; Fujita, Y.; Iwamoto, S.; Tanaka, K.; et al. Serum immunoglobulin G Fc region N-glycosylation profiling by matrix-assisted laser desorption/ionization mass spectrometry can distinguish breast cancer patients from cancer-free controls. *Biochem. Biophys. Res. Commun.* **2016**, *469*, 1140–1145, doi:10.1016/j.bbrc.2015.12.114.

27. Leeflang, B.R.; Vliegenthart, J.F.G. Glycoprotein Analysis: Using Nuclear Magnetic Resonance. *Encycl. Anal. Chem.* **2012**, 1–14, doi:10.1002/9780470027318.a0306.pub2.

28. Harvey, D.J. Identification of protein-bound carbohydrates by mass spectrometry. *Proteomics* **2001**, *1*, 311–328, doi:10.1002/1615-9861(200102)1:2<311::AID-PROT311>3.0.CO;2-J.

29. Mariño, K.; Bones, J.; Kattla, J.J.; Rudd, P.M. A systematic approach to protein glycosylation analysis: A path through the maze. *Nat. Chem. Biol.* **2010**, *6*, 713–723, doi:10.1038/nchembio.437.

30. Jensen, P.H.; Kolarich, D.; Packer, N.H. Mucin-type O-glycosylation - Putting the pieces together. *FEBS J.* **2010**, *277*, 81–94, doi:10.1111/j.1742-4658.2009.07429.x.

31. Kennedy, B. K.; Berger, S. L.; Brunet, A.; et al. Aging: a common driver of chronic diseases and a target for novel interventions. *Cell* **2014**, *159*, 709–713, doi:doi:10.1016/j.cell.2014.10.039.

32. Dall'Olio, F.; Vanhooren, V.; Chen, C.C.; Slagboom, P.E.; Wuhrer, M.; Franceschi, C. N-glycomic biomarkers of biological aging and longevity: A link with inflammaging. *Ageing Res. Rev.* **2013**, *12*, 685–698, doi:10.1016/j.arr.2012.02.002.

33. Everest-Dass, A. V.; Moh, E.S.X.; Ashwood, C.; Shathili, A.M.M.; Packer, N.H. Human disease glycomics: technology advances enabling protein glycosylation analysis–part 2. *Expert Rev. Proteomics* **2018**, *15*, 341–352, doi:10.1080/14789450.2018.1448710.

34. Rudman, N.; Gornik, O.; Lauc, G. Altered N-glycosylation profiles as potential biomarkers and drug targets in diabetes. *FEBS Lett.* **2019**, *593*, 1598–1615, doi:10.1002/1873-3468.13495.

35. Kizuka, Y.; Kitazume, S.; Taniguchi, N. N-glycan and Alzheimer's disease. *Biochim. Biophys. Acta - Gen. Subj.* **2017**, *1861*, 2447–2454, doi:10.1016/j.bbagen.2017.04.012.

36. Konjevod, M.; Tudor, L.; Svob Strac, D.; Nedic Erjavec, G.; Barbas, C.; Zarkovic, N.; Nikolac Perkovic, M.; Uzun, S.; Kozumplik, O.; Lauc, G.; et al. Metabolomic and glycomic findings in posttraumatic stress disorder. *Prog. Neuro-Psychopharmacology Biol. Psychiatry* **2019**, *88*, 181–193, doi:10.1016/j.pnpbp.2018.07.014.

37. Hu, M.; Lan, Y.; Lu, A.; Ma, X.; Zhang, L. *Progress in Molecular Biology and Translational Science*; 1st ed.; Elsevier Inc., 2019; Vol. 162; pp. 1-24.

38. Zhang, M.; Dou, H.; Yang, D.; Shan, M.; Li, X.; Hao, C.; Zhang, Y.; Zeng, P.; He, Y.; Liu, Y.; et al. *Retrospective analysis of glycan-related biomarkers based on*

clinical laboratory data in two medical centers during the past 6 years; 1st ed.; Elsevier Inc., 2019; Vol. 162; ISBN 9780128177389.

39. Nimmerjahn, F.; Anthony, R.M.; Ravetch, J. V. Agalactosylated IgG antibodies depend on cellular Fc receptors for in vivo activity. *Proc. Natl. Acad. Sci. U. S. A.* **2007**, *104*, 8433–8437, doi:10.1073/pnas.0702936104.

40. Russell, A.C.; Šimurina, M.; Garcia, M.T.; Novokmet, M.; Wang, Y.; Rudan, I.; Campbell, H.; Lauc, G.; Thomas, M.G.; Wang, W. The N-glycosylation of immunoglobulin G as a novel biomarker of Parkinson's disease. *Glycobiology* **2017**, *27*, 501–510, doi:10.1093/glycob/cwx022.

41. Arnold, J.N.; Wormald, M.R.; Sim, R.B.; Rudd, P.M.; Dwek, R.A. The Impact of Glycosylation on the Biological Function and Structure of Human Immunoglobulins. *Annu. Rev. Immunol.* **2007**, *25*, 21–50, doi:10.1146/annurev.immunol.25.022106.141702.

42. Shade, K.-T.; Anthony, R. Antibody Glycosylation and Inflammation. *Antibodies* **2013**, *2*, 392–414, doi:10.3390/antib2030392.

43. Pučić, M.; Knežević, A.; Vidič, J.; Adamczyk, B.; Novokmet, M.; Polašek, O.; Gornik, O.; Šupraha-Goreta, S.; Wormald, M.R.; Redžic, I.; et al. High throughput isolation and glycosylation analysis of IgG-variability and heritability of the IgG glycome in three isolated human populations. *Mol. Cell. Proteomics* **2011**, *10*, 1–15, doi:10.1074/mcp.M111.010090.

44. Parekh, R.; Isenberg, D.; Rook, G.; Roitt, I.; Dwek, R.; Rademacher, T. A comparative analysis of disease-associated changes in the galactosylation of serum IgG. *J. Autoimmun.* **1989**, *2*, 101–114, doi:10.1016/0896-8411(89)90148-0.

45. Dotz, V.; Wuhrer, M. N -glycome signatures in human plasma: associations with physiology and major diseases . *FEBS Lett.* **2019**, *593*, 2966–2976, doi:10.1002/1873-3468.13598.

46. Fontana, L.; Partridge, L.; Longo, V.D. Extending Healthy Life Span — From Yeast to Humans. *Science.* **2010**, *328*, 321-6, doi: 10.1126/science.1172539.

47. Walt, D; Aoki-Kinoshita, KF; Bendiak, B; et al. Transforming Glycoscience: A Roadmap for the Future; *Washington, DC: National Academies Press*, **2012**, doi:10.17226/13446

48. Krištić, J.; Vučković, F.; Menni, C.; Klarić, L.; Keser, T.; Beceheli, I.; Pučić-Baković, M.; Novokmet, M.; Mangino, M.; Thaqi, K.; et al. Glycans are a novel biomarker of chronological and biological ages. *Journals Gerontol. - Ser. A Biol. Sci. Med. Sci.* **2014**, *69*, 779–789, doi:10.1093/gerona/glt190.

49. Yu, X.; Wang, Y.; Kristic, J.; Dong, J.; Chu, X.; Ge, S.; Wang, H.; Fang, H.; Gao, Q.; Liu, D.; et al. Profiling IgG N-glycans as potential biomarker of chronological and biological ages: A community-based study in a Han Chinese population. *Med. (United States)* **2016**, *95*, 1–10, doi:10.1097/MD.0000000000004112.

50. Šunderić, M.; Križáková, M.; Malenković, V.; Ćujić, D.; Katrlík, J.; Nedić, O. Changes Due to Ageing in the Glycan Structure of Alpha-2-Macroglobulin

and Its Reactivity with Ligands. *Protein J.* **2019**, *38*, 23–29, doi:10.1007/s10930-018-9806-6.

51. Calvert, L.; Atkinson, H.; Berry, L.; Chan, A. Age-Dependent Variation in Glycosylation Features of Alpha-2-Macroglobulin. *Cell Biochem. Biophys.* **2019**, *77*, 335–342, doi:10.1007/s12013-019-00883-4.

52. Robajac, D.; Masnikosa, R.; Nemčovič, M.; Križáková, M.; Belická Kluková, Ľ.; Baráth, P.; Katrlík, J.; Nedić, O. Glycoanalysis of the placental membrane glycoproteins throughout placental development. *Mech. Ageing Dev.* **2019**, *183*, doi:10.1016/j.mad.2019.111151.

53. Wide, L.; Eriksson, K. Unique Pattern of N-Glycosylation, Sialylation, and Sulfonation on TSH Molecules in Serum of Children Up to 18 Months. *J. Clin. Endocrinol. Metab.* **2019**, *104*, 4651–4659, doi:10.1210/jc.2018-02576.

54. Donovan, M., Bernard, D., Simonetti, L., Nukhet Cavusoglu, Rudd, P., & Duke, R. Skin Glycomics - Characterization of the N-glycome in the Stratum Corneum of Aged and Dry skin. *Journal of Inv. Dermatology.* **2019**, *139* doi: 10.1016/j.jid.2019.07.213.

55. Baković, M.P.; Selman, M.H.J.; Hoffmann, M.; Rudan, I.; Campbell, H.; Deelder, A.M.; Lauc, G.; Wuhrer, M. High-throughput IgG Fc N-glycosylation profiling by mass spectrometry of glycopeptides. *J. Proteome Res.* **2013**, *12*, 821–831, doi:10.1021/pr300887z.

56. Ruhaak, L.R.; Uh, H.W.; Beekman, M.; Koeleman, C.A.M.; Hokke, C.H.; Westendorp, R.G.J.; Wuhrer, M.; Houwing-Duistermaat, J.J.; Slagboom, P.E.; Deelder, A.M. Decreased levels of bisecting GLcNAc glycoforms of IgG are associated with human longevity. *PLoS One* **2010**, *5*, 1–8, doi:10.1371/journal.pone.0012566.

57. Reiding, K.R.; Ruhaak, L.R.; Uh, H.; Bouhaddani, S.; Akker, E.B. Van Den; Plomp, R.; Mcdonnell, L.A.; Houwing-duistermaat, J.J.; Slagboom, P.E.; Beekman, M.; et al. Human Plasma N -glycosylation as Analyzed by Matrix-Assisted Laser Desorption / Ionization- Fourier Transform Ion Cyclotron Resonance- MS Associates with Markers of Inflammation and Metabolic Health. *Mol Cell Proteomics.* **2017**, *16, 228*–242, doi:10.1074/mcp.M116.065250.

58. Ruhaak, L.R.; Koeleman, C.A.M.; Uh, H.W.; Stam, J.C.; van Heemst, D.; Maier, A.B.; Houwing-Duistermaat, J.J.; Hensbergen, P.J.; Slagboom, P.E.; Deelder, A.M.; et al. Targeted Biomarker Discovery by High Throughput Glycosylation Profiling of Human Plasma Alpha1-Antitrypsin and Immunoglobulin A. *PLoS One* **2013**, *8*, 1–11, doi:10.1371/journal.pone.0073082.

59. Ding, N.; Sun, H.N.; Sun, W.; Qu, Y.; Liu, X.; Yao, Y.; Liang, X.; Chen, C.C.; Li, Y. Human serum N-glycan profiles are age and sex dependent. *Age Ageing* **2011**, *40*, 568–575, doi:10.1093/ageing/afr084.

60. De Haan, N.; Reiding, K.R.; Driessen, G.; Van Der Burg, M.; Wuhrer, M. Changes in healthy human IgG Fc-glycosylation after birth and during early childhood. *J. Proteome Res.* **2016**, *15*, 1853–1861, doi:10.1021/acs.jproteome.6b00038.

61. Berry, L.R.; Van Walderveen, M.C.; Atkinson, H.M.; Chan, A.K.C. Comparison of N-linked glycosylation of protein C in newborns and adults. *Carbohydr. Res.* **2013**, *365*, 32–37, doi:10.1016/j.carres.2012.10.019.

62. Edelberg, J.M.; Enghild, J.J.; Pizzo, S. V.; Gonzalez-Gronow, M. Neonatal plasminogen displays altered cell surface binding and activation kinetics: Correlation with increased glycosylation of the protein. *J. Clin. Invest.* **1990**, *86*, 107–112, doi:10.1172/JCI114671.

63. Kim, B.S.; Choi, C.W.; Shin, H.; Jin, S.P.; Bae, J.S.; Han, M.; Seo, E.Y.; Chun, J.; Chung, J.H. Comparison of the gut microbiota of centenarians in longevity villages of South Korea with those of other age groups. *J. Microbiol. Biotechnol.* **2019**, *29*, 429–440, doi:10.4014/JMB.1811.11023.

64. Wang, W.; Gopal, S.; Pocock, R.; Xiao, Z. Glycan mimetics from natural products: New therapeutic opportunities for neurodegenerative disease. *Molecules* **2019**, *24*, doi:10.3390/molecules24244604.

65. Alzheimer's Associaton Report. 2020 Alzheimer's disease facts and figures. *Alzheimer's Dement.* **2020**, *16*, 391–460, doi:10.1002/alz.12068.

66. Duyckaerts, C; Delatour, B; Potier, M.-C. Classification and basic pathology of Alzheimer disease. *Acta Neuropathol* **2009**, *118*, 5–36, doi:10.1007/s00401-009-0532-1.

67. Deane, R.; Yan, S. Du.; Submamaryan, R.K.; Larue, B.; Jovanovic, S.; Hogg, E.; Welch, D.; Manness, L.; Lin, C.; Yu, J.; et al. RAGE mediates amyloid- β peptide transport across the blood-brain barrier and accumulation in brain. *Nat Med.* **2003**, *9*, 907–913, doi: 10.1038/nm890.

68. Edri-Brami, M.; Rosental, B.; Hayoun, D.; Welt, M.; Rosen, H.; Wirguin, I.; Nefussy, B.; Drory, V.E.; Porgador, A.; Lichtenstein, R.G. Glycans in sera of amyotrophic lateral sclerosis patients and their role in killing neuronal cells. *PLoS One* **2012**, *7*, doi:10.1371/journal.pone.0035772.

69. Costa, J.; Streich, L.; Pinto, S.; Pronto-Laborinho, A.; Nimtz, M.; Conradt, H.S.; de Carvalho, M. Exploring Cerebrospinal Fluid IgG N-Glycosylation as Potential Biomarker for Amyotrophic Lateral Sclerosis. *Mol. Neurobiol.* **2019**, *56*, 5729–5739, doi:10.1007/s12035-019-1482-9.

70. Gonçalves, M.; Tillack, L.; de Carvalho, M.; Pinto, S.; Conradt, H.S.; Costa, J. Phosphoneurofilament heavy chain and N-glycomics from the cerebrospinal fluid in amyotrophic lateral sclerosis. *Clin. Chim. Acta* **2015**, *438*, 342–349, doi:10.1016/j.cca.2014.09.011.

71. Váradi, C; Nehéz, K; Hornyák, O; et al. Serum N-Glycosylation in Parkinson's Disease: A Novel Approach for Potential Alterations. *Molecules* **2019**, *24*, doi:10.3390/molecules24122220.

72. Kanninen, K.; Goldsteins, G.; Auriola, S.; Alafuzoff, I.; Koistinaho, J. Glycosylation changes in Alzheimer's disease as revealed by a proteomic approach. *Neurosci Lett.* **2004**, *367*, 235–240, doi:10.1016/j.neulet.2004.06.013.

73. Hovden, H.; Frederiksen, J.L.; Pedersen, S.W. Immune system alterations in amyotrophic lateral sclerosis. *Acta Neurol. Scand.* **2013**, *128*, 287–296,

doi:10.1111/ane.12125.

74. Vanhooren, V.; Liu, X.E.; Franceschi, C.; Gao, C.F.; Libert, C.; Contreras, R.; Chen, C. N-glycan profiles as tools in diagnosis of hepatocellular carcinoma and prediction of healthy human ageing. *Mech. Ageing Dev.* **2009**, *130*, 92–97, doi:10.1016/j.mad.2008.11.008.

75. Kyselova, Z.; Mechref, Y.; Kang, P.; et al. Breast Cancer Diagnosis and Prognosis through Quantitative Measurements of Serum Glycan Profiles. *Clin. Chem.* **2008**, *54*, 1166–1175, doi:10.1373/clinchem.2007.087148.

76. Hamid, U.; Royle, L.; Saldova, R.; et al. A strategy to reveal potential glycan markers from serum glycoproteins associated with breast cancer progression. *Glycobiology* **2008**, *18*, 1105–1118, doi:10.1093/glycob/cwn095.

77. J. An, H.; Miyamoto S.; S. Lancaster K.; et al. Profiling of Glycans in Serum for the Discovery of Potential Biomarkers for Ovarian Cancer. *J. Proteome Res.* **2006**, *5*, 1626–1635, doi:10.1021/pr060010k.

78. R. Alley Jr., W.; V. Novotny, M. Glycomic Analysis of Sialic Acid Linkages in Glycans Derived from Blood Serum Glycoproteins. *J. Proteome Res.* **2010**, *9*, 761–771, doi: 10.1021/pr901210r.

79. Liu, L.; Yan, B.; Huang, J.; Gu, Q.; Wang, L.; Fang, M.; Jiao, J.; Yue, X. The Identification and Characterization of Novel N-glycan-based Biomarkers in Gastric Cancer. *PLoS One* **2013**, *8*, 1–11, doi:10.1371/journal.pone.0077821.

80. Drabik, A.; Bodzon-Kulakowska, A.; Suder, P.; Silberring, J.; Kulig, J.; Sierzega, M. Glycosylation Changes in Serum Proteins Identify Patients with Pancreatic Cancer. *J. Proteome Res.* **2017**, *16*, 1436–1444, doi:10.1021/acs.jproteome.6b00775.

81. Hu, Y.; Ferdosi, S.; Kapuruge, E.P.; Diaz de Leon, J.A.; Stücker, I.; Radoï, L.; Guénel, P.; Borges, C.R. Diagnostic and Prognostic Performance of Blood Plasma Glycan Features in the Women Epidemiology Lung Cancer (WELCA) Study. *J. Proteome Res.* **2019**, *18,* 3985-3998, *doi*:10.1021/acs.jproteome.9b00457.

82. Penezić, A.; Križakova, M.; Miljuš, G.; Katrlik, J.; Nedić, O. Diagnostic Potential of Transferrin Glycoforms—A Lectin-Based Protein Microarray Approach. *Proteomics - Clin. Appl.* **2019**, *13*, 1–8, doi:10.1002/prca.201800185.

83. Qiu, Y.; Patwa, T.H.; Xu, L.; Shedden, K.; Misek, D.E.; Jin, G.; Ruffin, M.T.; Turgeon, D.K.; Synal, S.; Marcon, N.; et al. Plasma Glycoprotein Profiling for Colorectal Cancer Biomarker Identification by Lectin Glycoarray and Lectin Blot. *J. Proteome Res.* **2009**, *7*, 1693–1703, doi:10.1021/pr700706s.

84. Zhao, Y.P.; Ruan, C.P.; Wang, H.; Hu, Z.Q.; Fang, M.; Gu, X.; Ji, J.; Zhao, J.Y.; Gao, C.F. Identification and assessment of new biomarkers for colorectal cancer with serum N-glycan profiling. *Cancer* **2012**, *118*, 639–650, doi:10.1002/cncr.26342.

85. Šunderić, M.; Šedivá, A.; Robajac, D.; Miljuš, G.; Gemeiner, P.; Nedić, O.;

Katrlík, J. Lectin-based protein microarray analysis of differences in serum alpha-2-macroglobulin glycosylation between patients with colorectal cancer and persons without cancer. *Biotechnol. Appl. Biochem.* **2016**, *63*, 457–464, doi:10.1002/bab.1407.

86. De Leoz, M.L.A.; An, H.J.; Kronewitter, S.; Kim, J.; Beecroft, S.; Vinall, R.; Miyamoto, S.; De Vere White, R.; Lam, K.S.; Lebrilla, C. Glycomic approach for potential biomarkers on prostate cancer: Profiling of N-linked glycans in human sera and pRNS cell lines. *Dis. Markers* **2008**, *25*, 243–258, doi:10.1155/2008/515318.

87. Bereman, M.S.; Williams, T.I.; Muddiman, D.C. Development of a nanolc ltq orbitrap mass spectrometric method for profiling glycans derived from plasma from healthy, benign tumor control, and epithelial ovarian cancer patients. *Anal. Chem.* **2009**, *81*, 1130–1136, doi:10.1021/ac802262w.

88. Takahashi, S.; Sugiyama, T.; Shimomura, M.; Kamada, Y.; Fujita, K.; Nonomura, N.; Miyoshi, E.; Nakano, M. Site-specific and linkage analyses of fucosylated N-glycans on haptoglobin in sera of patients with various types of cancer: possible implication for the differential diagnosis of cancer. *Glycoconj. J.* **2016**, *33*, 471–482, doi:10.1007/s10719-016-9653-7.

89. Miyoshi, E.; Moriwaki, K.; Nakagawa, T. Biological function of fucosylation in cancer biology. *J. Biochem.* **2008**, *143*, 725–729, doi:10.1093/jb/mvn011.

90. Li, Q.; Li, G.; Zhou, Y.; Zhang, X.; Sun, M.; Jiang, H.; Yu, G. Comprehensive N-Glycome Profiling of Cells and Tissues for Breast Cancer Diagnosis. *J. Proteome Res.* **2019**, *18*, 2559–2570, doi:10.1021/acs.jproteome.9b00073.

91. Adua, E.; Memarian, E.; Russell, A.; Trbojević-Akmačić, I.; Gudelj, I.; Jurić, J.; Roberts, P.; Lauc, G.; Wang, W. High throughput profiling of whole plasma N-glycans in type II diabetes mellitus patients and healthy individuals: A perspective from a Ghanaian population. *Arch. Biochem. Biophys.* **2019**, *661*, 10–21, doi:10.1016/j.abb.2018.10.015.

92. Dotz, V.; Lemmers, R.F.H.; Reiding, K.R.; Hipgrave Ederveen, A.L.; Lieverse, A.G.; Mulder, M.T.; Sijbrands, E.J.G.; Wuhrer, M.; van Hoek, M. Plasma protein N-glycan signatures of type 2 diabetes. *Biochim. Biophys. Acta - Gen. Subj.* **2018**, *1862*, 2613–2622, doi:10.1016/j.bbagen.2018.08.005.

93. Connelly, M.A.; Gruppen, E.G.; Wolak-Dinsmore, J.; Matyus, S.P.; Riphagen, I.J.; Shalaurova, I.; Bakker, S.J.L.; Otvos, J.D.; Dullaart, R.P.F. GlycA, a marker of acute phase glycoproteins, and the risk of incident type 2 diabetes mellitus: PREVEND study. *Clin. Chim. Acta* **2016**, *452*, 10–17, doi:10.1016/j.cca.2015.11.001.

94. Grundy, S.M.; Hansen, B.; Smith, S.C.; Cleeman, J.I.; Kahn, R.A. Clinical Management of Metabolic Syndrome. *Arterioscler. Thromb. Vasc. Biol.* **2004**, *24*, 551–556, doi:10.1161/01.atv.0000112379.88385.67.

95. Lu, J.P.; Knežević, A.; Wang, Y.X.; Rudan, I.; Campbell, H.; Zou, Z.K.; Lan, J.; Lai, Q.X.; Wu, J.J.; He, Y.; et al. Screening novel biomarkers for metabolic syndrome by profiling human plasma N-glycans in Chinese han and Croatian populations. *J. Proteome Res.* **2011**, *10*, 4959–4969,

doi:10.1021/pr2004067.

96. Gao, Q.; Dolikun, M.; Štambuk, J.; Wang, H.; Zhao, F.; Yiliham, N.; Wang, Y.; Trbojević-Akmačić, I.; Zhang, J.; Fang, H.; et al. Immunoglobulin G N-Glycans as Potential Postgenomic Biomarkers for Hypertension in the Kazakh Population. *Omi. A J. Integr. Biol.* **2017**, *21*, 380–389, doi:10.1089/omi.2017.0044.

97. Wang, Y.; Klarić, L.; Yu, X.; Thaqi, K.; Dong, J.; Novokmet, M.; Wilson, J.; Polasek, O.; Liu, Y.; Krištić, J.; et al. The Association between Glycosylation of Immunoglobulin G and Hypertension. *Med. (Baltimore)* **2016**, *95*, 1–11, doi:10.1097/MD.0000000000003379.

98. Liu, J.; Dolikun, M.; Štambuk, J.; Trbojević-Akmačić, I.; Zhang, J.; Wang, H.; Zheng, D.; Zhang, X.; Peng, H.; Zhao, Z.; et al. The association between subclass-specific IgG Fc N-glycosylation profiles and hypertension in the Uygur, Kazak, Kirgiz, and Tajik populations. *J. Hum. Hypertens.* **2018**, *32*, 555–563, doi:10.1038/s41371-018-0071-0.

99. Menni, C.; Gudelj, I.; MacDonald-Dunlop, E.; Mangino, M.; Zierer, J.; Bešić, E.; Joshi, P.K.; Trbojević-Akmačić, I.; Chowienczyk, P.J.; Spector, T.D.; et al. Glycosylation Profile of Immunoglobulin G Is Cross-Sectionally Associated with Cardiovascular Disease Risk Score and Subclinical Atherosclerosis in Two Independent Cohorts. *Circ. Res.* **2018**, *122*, 1555–1564, doi:10.1161/CIRCRESAHA.117.312174.

100. Barrios, C.; Zierer, J.; Gudelj, I.; Stambuk, J.; Ugrina, I.; Rodríguez, E.; Soler, M.J.; Pavic, T.; Simurina, M.; Keser, T.; et al. Glycosylation profile of IgG in moderate kidney dysfunction. *J. Am. Soc. Nephrol.* **2016**, *27*, 933–941, doi:10.1681/ASN.2015010109.

101. Liu, D.; Chu, X.; Wang, H.; Dong, J.; Ge, S.Q.; Zhao, Z.Y.; Peng, H.L.; Sun, M.; Wu, L.J.; Song, M.S.; et al. The changes of immunoglobulin G N-glycosylation in blood lipids and dyslipidaemia. *J. Transl. Med.* **2018**, *16*, 1–10, doi:10.1186/s12967-018-1616-2.

102. Wilson, P.W.F.; D'Agostino, R.B.; Parise, H.; Sullivan, L.; Meigs, J.B. Metabolic syndrome as a precursor of cardiovascular disease and type 2 diabetes mellitus. *Circulation* **2005**, *112*, 3066–3072, doi:10.1161/CIRCULATIONAHA.105.539528.

103. Brian J. North and David A. Sinclair The Intersection Between Aging and Cardiovascular Disease. *Circ. Res.* **2012**, *110*, 1097–1108, doi:10.1161/CIRCRESAHA.111.246876.

104. Vasudevan, A.R.; Ballantyne, C.M. Cardiometabolic risk assessment: An approach to the prevention of cardiovascular disease and diabetes mellitus. *Clin. Cornerstone* **2005**, *7*, 7–16, doi:10.1016/S1098-3597(05)80063-8.

105. Umaña, P.; Jean-Mairet, J.; Moudry, R.; Amstutz, H.; Bailey, J.E. Engineered glycoforms of an antineuroblastoma IgG1 with optimized antibody-dependent cellular cytotoxic activity. *Nat. Biotechnol.* **1999**, *17*, 176–180, doi:10.1038/6179.

106. Willerson, J.T.; Ridker, P.M. Inflammation as a cardiovascular risk factor. *Circulation* **2004**, *109*, 2–11, doi:10.1161/01.cir.0000129535.04194.38.

107. Böhm, S.; Schwab, I.; Lux, A.; Nimmerjahn, F. The role of sialic acid as a modulator of the anti-inflammatory activity of IgG. *Semin. Immunopathol.* **2012**, *34*, 443–453, doi:10.1007/s00281-012-0308-x.

108. Tenenbaum, A.; Klempfner, R.; Fisman, E.Z. Hypertriglyceridemia: A too long unfairly neglected major cardiovascular risk factor. *Cardiovasc. Diabetol.* **2014**, *13*, 1–10, doi:10.1186/s12933-014-0159-y.

109. Buford, T.W. Hypertension and Aging. *Ageing Res. Rev.* **2016**, 96–111, doi:doi:10.1016/j.arr.2016.01.007.

110. Trbojevic Akmacic, I.; Ventham, N.T.; Theodoratou, E.; Vučković, F.; Kennedy, N.A.; Krištić, J.; Nimmo, E.R.; Kalla, R.; Drummond, H.; Štambuk, J.; et al. Inflammatory bowel disease associates with proinflammatory potential of the immunoglobulin G glycome. *Inflamm. Bowel Dis.* **2015**, *21*, 1237–1247, doi:10.1097/MIB.0000000000000372.

111. El Nahas, A.M.; Bello, A.K. Chronic kidney disease: The global challenge. *Lancet* **2005**, *365*, 331–340, doi:10.1016/S0140-6736(05)17789-7.

112. Clerc, F.; Novokmet, M.; Dotz, V.; Reiding, K.R.; de Haan, N.; Kammeijer, G.S.M.; Dalebout, H.; Bladergroen, M.R.; Vukovic, F.; Rapp, E.; et al. Plasma N-Glycan Signatures Are Associated With Features of Inflammatory Bowel Diseases. *Gastroenterology* **2018**, *155*, 829–843, doi:10.1053/j.gastro.2018.05.030.

113. Schultz, M.J.; Swindall, A.F.; Bellis, S.L. Regulation of the metastatic cell phenotype by sialylated glycans. *Cancer Metastasis Rev.* **2012**, *31*, 501–518, doi:10.1007/s10555-012-9359-7.

114. Dalziel, M.; Crispin, M.; Scanlan, C.N.; Zitzmann, N.; Dwek, R.A. Emerging principles for the therapeutic exploitation of glycosylation. *Science* **2014**, *343*, doi:10.1126/science.1235681.

115. Shinzaki, S.; Iijima, H.; Nakagawa, T.; Egawa, S.; Nakajima, S.; Ishii, S.; Irie, T.; Kakiuchi, Y.; Nishida, T.; Yasumaru, M.; et al. IgG oligosaccharide alterations are a novel diagnostic marker for disease activity and the clinical course of inflammatory bowel disease. *Am. J. Gastroenterol.* **2008**, *103*, 1173–1181, doi:10.1111/j.1572-0241.2007.01699.x.

116. Pasek, M.; Duk, M.; Podbielska, M.; Sokolik, R.; Szechiński, J.; Lisowska, E.; Krotkiewski, H. Galactosylation of IgG from rheumatoid arthritis (RA) patients - Changes during therapy. *Glycoconj. J.* **2006**, *23*, 463–471, doi:10.1007/s10719-006-5409-0.

117. Gudelj, I.; Salo, P.P.; Trbojević-Akmačić, I.; Albers, M.; Primorac, D.; Perola, M.; Lauc, G. Low galactosylation of IgG associates with higher risk for future diagnosis of rheumatoid arthritis during 10 years of follow-up. *Biochim. Biophys. Acta - Mol. Basis Dis.* **2018**, *1864*, 2034–2039, doi:10.1016/j.bbadis.2018.03.018.

118. Magorivska, I.; Döncző, B.; Dumych, T.; Karmash, A.; Boichuk, M.; Hychka, K.; Mihalj, M.; Szabó, M.; Csánky, E.; Rech, J.; et al. Glycosylation of random

IgG distinguishes seropositive and seronegative rheumatoid arthritis. *Autoimmunity* **2018**, *51*, 111–117, doi:10.1080/08916934.2018.1468886.

119. Ercan, A.; Cui, J.; Chatterton, D.E.W.; Deane, K.D.; Hazen, M.M.; Brintnell, W.; Donnell, C.I.O.; Derber, L.A.; Weinblatt, M.E.; Nancy, A.; et al. IgG galactosylation aberrancy precedes disease onset, correlates with disease activity and is prevalent in autoantibodies in rheumatoid arthritis. *Arthritis Rheum.* **2010**, *62*, 2239–2248, doi:10.1002/art.27533.

120. Gindzienska-Sieskiewicz, E.; Klimiuk, P.A.; Kisiel, D.G.; Gindzienski, A.; Sierakowski, S. The changes in monosaccharide composition of immunoglobulin G in the course of rheumatoid arthritis. *Clin. Rheumatol.* **2007**, *26*, 685–690, doi:10.1007/s10067-006-0370-7.

121. Sebastian, A.; Alzain, M.A.; Asweto, C.O.; Song, H.; Cui, L.; Yu, X.; Ge, S.; Dong, H.; Rao, P.; Wang, H.; et al. Glycan Biomarkers for Rheumatoid Arthritis and Its Remission Status in Han Chinese Patients. *Omi. A J. Integr. Biol.* **2016**, *20*, 343–351, doi:10.1089/omi.2016.0050.

122. Huffman, J.E.; Pučić-Baković, M.; Klarić, L.; Hennig, R.; Selman, M.H.J.; Vučković, F.; Novokmet, M.; Krištić, J.; Borowiak, M.; Muth, T.; et al. Comparative performance of four methods for high-throughput glycosylation analysis of immunoglobulin G in genetic and epidemiological research. *Mol. Cell. Proteomics* **2014**, *13*, 1598–1610, doi:10.1074/mcp.M113.037465.

123. Fernandes-Cerqueira, C.; Renard, N.; Notarnicola, A.; Wigren, E.; Gräslund, S.; Zubarev, R.A.; Lundberg, I.E.; Lundström, S.L. Patients with anti-Jo1 antibodies display a characteristic IgG Fc-glycan profile which is further enhanced in anti-Jo1 autoantibodies. *Sci. Rep.* **2018**, *8*, 1–11, doi:10.1038/s41598-018-36395-z.

124. Lee, D.M.; Weinblatt, M.E. Rheumatoid arthritis. *Lancet.* **2001**, *358*, 903–911, doi:10.1016/S0140-6736(01)06075-5.

125. Mastrangelo, A.; Colasanti, T.; Barbati, C.; Pecani, A.; Sabatinelli, D.; Pendolino, M.; Truglia, S.; Massaro, L.; Mancini, R.; Miranda, F.; et al. The Role of Posttranslational Protein Modifications in Rheumatological Diseases: Focus on Rheumatoid Arthritis. *J. Immunol. Res.* **2015**, *2015*, doi:10.1155/2015/712490.

126. Albrecht, S.; Unwin, L.; Muniyappa, M.; Rudd, P.M. Glycosylation as a marker for inflammatory arthritis. *Cancer Biomarkers* **2014**, *14*, 17–28, doi:10.3233/CBM-130373.

127. Parekh, R.B.; Dwek, R.A.; Sutton, B.J.; Fernandes, D.L.; Leung, A.; Stanworth, D.; Rademacher, T.W.; Mizuochi, T.; Taniguchi, T.; Matsuta, K.; et al. Association of rheumatoid arthritis and primary osteoarthritis with changes in the glycosylation pattern of total serum IgG. *Nature* **1985**, *316*, 452–457, doi:10.1038/316452a0.

128. Johnson, C.; Pinal-Fernandez, I.; Parikh, R.; Paik, J.; Albayda, J.; Mammen, A.L.; Christopher-Stine, L.; Danoff, S. Assessment of Mortality in Autoimmune Myositis With and Without Associated Interstitial Lung Disease. *Lung* **2016**, *194*, 733–737, doi:10.1007/s00408-016-9896-x.

129. Han, L.; Costello, C.; Mass Spectrometry of Glycans. *Biochem. (Mosc).* **2013**, *78*, 710–720, doi:10.1134/S0006297913070031.

130. Hirabayashi, J.; Yamada, M.; Kuno, A.; Tateno, H. Lectin microarrays: Concept, principle and applications. *Chem. Soc. Rev.* **2013**, *42*, 4443–4458, doi:10.1039/c3cs35419a.

131. Zhang, L.; Luo, S.; Zhang, B. The use of lectin microarray for assessing glycosylation of therapeutic proteins. *MAbs* **2016**, *8*, 524–535, doi:10.1080/19420862.2016.1149662.

132. Zhang, Y.; Peng, Y.; Yang, L.; Lu, H. Advances in sample preparation strategies for MS-based qualitative and quantitative N-Glycomics. *Trends Anal. Chem.* **2017**, *99,* 34-46, doi:10.1016/j.trac.2017.11.013.

133. Xiao, K.; Han, Y.; Yang, H.; Lu, H.; Tian, Z. Mass spectrometry-based qualitative and quantitative N-glycomics: an update of 2017-2018. *Anal. Chim. Acta* **2019**, *1091,* 1-22, doi:10.1016/j.aca.2019.10.007.

134. Takasaki, S.; Mizuochi, T.; et. al. Hydrazinolysis of Asparagine-Linked Sugar Chains to Produce Free Oligosaccharides. *Methods in Enzymology* **1982**, *83*, 263–268, doi:10.1016/0076-6879(82)83019-X.

135. Rasilo, M.; Renkonen, O. Mild alkaline borohydride treatment liberates N-acetylglucosamine linked oligosaccharide chains of glycoproteins. *FEBS Lett.* **1981**, *135*, 38–42, doi:10.1016/0014-5793(81)80938-6.

136. Maley, F.; Trimble, R. B.; Tarentino, A. L.; et. al. Characterization of Glycoproteins and Their Associated Oligosaccharides through the Use of Endoglycosidases. *Anal Biochem.* **1989**, *204*, 195–204, doi:10.1016/0003-2697(89)90115-2.

137. Lauber, M.A.; Yu, Y.; Brousmiche, D.W.; Hua, Z.; Koza, S.M.; Magnelli, P.; Guthrie, E.; Taron, C.H.; Fountain, K.J. Rapid Preparation of Released N -Glycans for HILIC Analysis Using a Labeling Reagent that Facilitates Sensitive Fluorescence and ESI-MS Detection. *Anal Chem.* **2015**, *87,* 5401-5409, doi:10.1021/acs.analchem.5b00758.

138. Sandoval, W.N.; Arellano, F.; Arnott, D.; Raab, H.; Vandlen, R.; Lill, J.R. Rapid removal of N-linked oligosaccharides using microwave assisted enzyme catalyzed deglycosylation. *Int. J. Mass Spec.* **2007**, *259*, 117–123, doi:10.1016/j.ijms.2006.09.003.

139. Szabo, Z.; Karger, B.L. Rapid Release of N-Linked Glycans from Glycoproteins by Pressure-Cycling Technology. *Anal Chem.* **2010**, *82*, 2588–2593, doi: 10.1021/ac100098e.

140. Palm, A.K.; Novotny, M. V. A monolithic PNGase F enzyme microreactor enabling glycan mass mapping of glycoproteins by mass spectrometry. **2005**, *19,* 1730–1738, doi:10.1002/rcm.1979.

141. Song, T.; Aldredge, D.; Lebrilla, C. B. A Method for In-Depth Structural Annotation of Human Serum Glycans That Yields Biological Variations. *Anal Chem.* **2017**, *87*, 7754–7762, doi:10.1021/acs.analchem.5b01340.A.

142. Fanayan, S.; Hincapie, M.; Hancock, W.S. Using lectins to harvest the

plasma/serum glycoproteome. *Electrophoresis* **2012**, *33*, 1746–1754, doi:10.1002/elps.201100567.

143. Etxebarria, J.; Calvo, J.; Martin-Lomas, M.; Reichardt, N.C. Lectin-array blotting: Profiling protein glycosylation in complex mixtures. *ACS Chem. Biol.* **2012**, *7*, 1729–1737, doi:10.1021/cb300262x.

144. Mahal, J.P.R. and L.K. Dot by dot: Analyzing the glycome using lectin microarrays João. *Curr. Opin. Chem. Biol.* **2013**, *17*, 1–9, doi:10.1016/j.cbpa.2013.06.009.

145. Keser, T.; Pavić, T.; Lauc, G.; Gornik, O. Comparison of 2-Aminobenzamide, Procainamide and RapiFluor-MS as Derivatizing Agents for High-Throughput HILIC-UPLC-FLR-MS N-glycan Analysis. *Front. Chem.* **2018**, *6*, 1–12, doi:10.3389/fchem.2018.00324.

146. Alpert, A.J. Hydrophilic-interaction chromatography for the separation of peptides, nucleic acids and other polar compounds. *J. Chromatogr. A* **1990**, *499*, 177–196, doi:10.1016/S0021-9673(00)96972-3.

147. Takegawa, Y.; Deguchi, K.; Ito, H.; Keira, T.; Nakagawa, H.; Nishimura, S.I. Simple separation of isometric sialylated N-glycopeptides by a zwitterionic type of hydrophilic interaction chromatography. *J. Sep. Sci.* **2006**, *29*, 2533–2540, doi:10.1002/jssc.200600133.

148. Buszewski, B.; Noga, S. Hydrophilic interaction liquid chromatography (HILIC)-a powerful separation technique. *Anal. Bioanal. Chem.* **2012**, *402*, 231–247, doi:10.1007/s00216-011-5308-5.

149. Wuhrer, M.; Boer, A.R.; et al. Structural glycomics using hydrophilic interaction chromatography (HILIC) with mass spectrometry. *Mass Spectrom. Rev.* **2009**, *28*, 192–206, doi:10.1002/mas.20195.

150. Takahashi, N. Three-dimensional mapping of N-linked oligosaccharides using anion-exchange, hydrophobic and hydrophilic interaction modes of high-performance liquid chromatography. *J. Chromatogr. A* **1996**, *720*, 217–225, doi: 10.1016/0021-9673(95)00328-2.

151. El Rassi, Z. *Carbohydrate analysis: high performance liquid chromatography and capillary electrophoresis,* 1st ed.; ElSevier, **1994**.

152. Zhou, S.; Veillon, L.; Dong, X.; Huang, Y.; Mechref, Y. Direct comparison of derivatization strategies for LC-MS/MS analysis of N -glycans. *Analyst* **2017**, *142*, 4446–4455, doi:10.1039/c7an01262d.

153. Ruhaak, L.R.; Deelder, A.M.; Wuhrer, M.; Zauner, G.; Bruggink, C.; Huhn, C. Glycan labeling strategies and their use in identification and quantification. *Anal. Bioanal. Chem.* **2010**, *397*, 3457–3481, doi:10.1007/s00216-010-3532-z.

154. Cohen, S.A.; Michaud, D.P. Synthesis of a fluorescent derivatizing reagent,6-aminoquinolyl-N-hydroxysuccinimidyl carbamate, and its application forthe analysis of hydrolysate amino acids via high-performance liquidchromatography. *Anal Biochem.* **1993**, *211,* 279–287, doi:10.1006/abio.1993.1270.

155. Wu, Y.; Sha, Q.; Wang, C.; Liu, B.; Wang, S.; Liu, X. Development of a filter-aided extraction method coupled with glycosylamine labeling to simplify and enhance high performance liquid chromatography-based N-glycan analysis. *J. Chromatogr. A* **2019**, *1600*, 105–111, doi:10.1016/j.chroma.2019.04.059.

156. Lu, G.; Crihfield, C.L.; Gattu, S.; Veltri, L.M.; Holland, L.A. Capillary Electrophoresis Separations of Glycans. *Chem. Rev.* **2018**, *118*, 7867–7885, doi:10.1021/acs.chemrev.7b00669.

157. Donczo, B.; Szarka, M.; Tovari, J.; et. al. Molecular glycopathology by capillary electrophoresis: Analysis of the N-glycome of formalin-fixed paraffin-embedded mouse tissue samples. *Electrophoresis* **2017**, *38,* 1–7, doi:10.1002/elps.201600558.

158. Guttman, A. High-resolution carbohydrate profiling by capillary gel electrophoresis. *Nature* **1996**, *380,* 461-462, doi: 10.1038/380461a0.

159. Mahan, A.E.; Tedesco, J.; Dionne, K.; Baruah, K.; Cheng, H.D.; De Jager, P.L.; Barouch, D.H.; Suscovich, T.; Ackerman, M.; Cripsin, M.; Alter, G. A method for high-throughput, sensitive analysis of IgG Fc and Fab glycosylation by capillary electrophoresis. *J Immunol Methods* **2015**, *417*, 34–44, doi:10.1016/j.jim.2014.12.004.

160. Reusch, D.; Haberger, M.; Kailich, T.; Heidenreich, A.K.; Kampe, M.; Bulau, P.; Wuhrer, M. High-throughput glycosylation analysis of therapeutic immunoglobulin G by capillary gel electrophoresis using a DNA analyzer. *MAbs* **2014**, *6*, 185–196, doi:10.4161/mabs.26712.

161. Adamczyk, B.; Tharmalingam-Jaikaran, T.; Schomberg, M.; Szekrényes, Á.; Kelly, R.M.; Karlsson, N.G.; Guttman, A.; Rudd, P.M. Comparison of separation techniques for the elucidation of IgG N-glycans pooled from healthy mammalian species. *Carbohydr. Res.* **2014**, *389*, 174–185, doi:10.1016/j.carres.2014.01.018.

162. Vanhooren, V.; Laroy, W.; Libert, C.; Chen, C. N-Glycan profiling in the study of human aging. *Biogerontology* **2008**, *9*, 351–356, doi:10.1007/s10522-008-9140-z.

163. Echeverria, B.; Etxebarria, J.; Ruiz, N.; Hernandez, Á.; Calvo, J.; Haberger, M.; Reusch, D.; Reichardt, N.C. Chemo-Enzymatic Synthesis of 13C Labeled Complex N-Glycans As Internal Standards for the Absolute Glycan Quantification by Mass Spectrometry. *Anal. Chem.* **2015**, *87*, 11460–11467, doi:10.1021/acs.analchem.5b03135.

164. Smith, J.; Mittermayr, S.; Váradi, C.; Bones, J. Quantitative glycomics using liquid phase separations coupled to mass spectrometry. *Analyst* **2017**, *142*, 700–720, doi:10.1039/c6an02715f.

165. Han, L.; Costello, C.E. Mass Spectrometry of Glycans. *Biochem. (Mosc).* **2014**, *78*, 710–720, doi:10.1134/S0006297913070031.Mass.

166. Chen, J.E.; Glover, G.H. Functional Magnetic Resonance Imaging Methods. *Neuropsychology Review* **2016**, *25*, 289–313, doi:10.1007/s11065-015-9294-9.

167. Zhou, S.; Hu, Y.; DeSantos-Garcia, J.L.; Mechref, Y. Quantitation of Permethylated N-Glycans through Multiple- Reaction Monitoring (MRM) LC-MS/MS. *J Am Soc Mass Spectrom.* **2015**, *26*, 596–603, doi:10.1007/s13361-014-1054-1.

168. Wu, S.; Salcedo, J.; Tang, N.; Waddell, K.; Grimm, R.; German, J.B.; Lebrilla, C.B. Employment of tandem mass spectrometry for the accurate and specific identification of oligosaccharide structures. *Anal. Chem.* **2012**, *84*, 7456–7462, doi:10.1021/ac301398h.

169. Sandra, K.; Devreese, B.; Van Beeumen, J.; Stals, I.; Claeyssens, M. The Q-Trap mass spectrometer, a novel tool in the study of protein glycosylation. *J. Am. Soc. Mass Spectrom.* **2004**, *15*, 413–423, doi:10.1016/j.jasms.2003.11.003.

170. Zhou, W.; Hakansson, K. Structural Characterization of Carbohydrates by Fourier Transform Tandem Mass Spectrometry. *Curr. Proteomics* **2011**, *8*, 297–308, doi:10.2174/157016411798220826.

171. Mechref, Y.; Novotny, M. V.; Krishnan, C. Structural characterization of oligosaccharides using MALDI-TOF/TOF tandem mass spectrometry. *Anal. Chem.* **2003**, *75*, 4895–4903, doi:10.1021/ac0341968.

172. Leymarie, N.; Zaia, J. Effective use of mass spectrometry for glycan and glycopeptide structural analysis. *Anal. Chem.* **2012**, *84*, 3040–3048, doi:10.1021/ac3000573.

173. Dell, A. Glycoprotein Structure Determination by Mass Spectrometry. *Science* **2002**, *291*, 2351–2356, doi:10.1126/science.1058890.

174. Wang, C. hong; Li, J.; Yao, S. jun; Guo, Y. long; Xia, X. hua High-sensitivity matrix-assisted laser desorption/ionization Fourier transform mass spectrometry analyses of small carbohydrates and amino acids using oxidized carbon nanotubes prepared by chemical vapor deposition as matrix. *Anal. Chim. Acta* **2007**, *604*, 158–164, doi:10.1016/j.aca.2007.10.001.

175. Harvey, D.J. Analysis of carbohydrates and glycoconjugates by matrix-assisted laser desorption/ionization mass spectrometry: an update for 2007-2008. *Mass Spectrom. Rev.* **2012**, *31*, 183–311, doi:DOI 10.1002/mas.20333.

176. Borowsky, A.D.; Clowers, B.H.; Lebrilla, C.B.; Miyamoto, S.; Ferrige, A.; An, H.J.; Lam, K.S.; Kirmiz, C.; Li, B.; Alecio, R.; et al. A Serum Glycomics Approach to Breast Cancer Biomarkers. *Mol. Cell. Proteomics* **2006**, *6*, 43–55, doi:10.1074/mcp.m600171-mcp200.

177. Huang, C.; Yan, J.; Zhan, L.; Zhao, M.; Zhou, J. Linkage and sequence analysis of neutral oligosaccharides by negative-ion MALDI tandem mass spectrometry with laser-induced dissociation. *Anal. Chim. Acta* **2019**, *1071*, 25–35, doi:10.1016/j.aca.2019.04.067.

178. Briggs, M.T.; Kuliwaba, J.S.; Muratovic, D.; Everest-Dass, A. V.; Packer, N.H.; Findlay, D.M.; Hoffmann, P. MALDI mass spectrometry imaging of N-glycans on tibial cartilage and subchondral bone proteins in knee

osteoarthritis. *Proteomics* **2016**, *16*, 1736–1741, doi:10.1002/pmic.201500461.

179. Angel, P.M.; Mehta, A.; et al. MALDI Imaging Mass Spectrometry of N-glycans and Tryptic Peptides from the Same Formalin-Fixed, Paraffin-Embedded Tissue Section. *Methods Mol. Biol.* **2018**, *1788,* 255–241, doi:10.1007/7651_2017_81.

180. Zhou, S.; Wooding, K.; Mechref, Y. Analysis of Permethylated Glycan by Liquid Chromatography (LC) and Mass Spectrometry (MS). *Methods Mol. Biol. Glycomics Methods Protoc.* **2017**, *1503*, 83–96, doi:10.1007/978-1-4939-6493-2_7.

181. Grünwald-Gruber, C.; Thader, A.; Maresch, D.; Dalik, T.; Altmann, F. Determination of true ratios of different N-glycan structures in electrospray ionization mass spectrometry. *Anal. Bioanal. Chem.* **2017**, *409*, 2519–2530, doi:10.1007/s00216-017-0235-8.

182. Bruins, A.P. Mechanistic aspects of electrospray ionization. *J. Chromatogr. A* **1998**, *794*, 345–357, doi:10.1016/S0021-9673(97)01110-2.

183. Wuhrer, M.; Koeleman, C.A.; Deelder, A.M. Two-Dimensional HPLC Separation with Reverse- Phase-Nano-LC-MS/MS for the Characterization of Glycan Pools After Labeling with 2-Aminobenzamide. *Glycomics Methods Protoc.* **2009**, *534*, 133–145, doi:10.1007/978-1-59745-022-5.

184. Wuhrer, M.; Koeleman, C.A.M.; Fitzpatrick, J.M.; Hoffmann, K.F.; Deelder, A.M.; Hokke, C.H. Gender-specific expression of complex-type N-glycans in schistosomes. *Glycobiology* **2006**, *16*, 991–1006, doi:10.1093/glycob/cwl020.

185. Kozak, R.P.; Tortosa, C.B.; Fernandes, D.L.; Spencer, D.I.R. Comparison of procainamide and 2-aminobenzamide labeling for profiling and identification of glycans liquid chromatography with fluorescence detection coupled to electrospray ionization-mass spectrometry. *Anal. Biochem.* **2015**, *486*, 38–40, doi:10.1016/j.ab.2015.06.006.

186. Li, B.; An, H.J.; Hedrick, J.L.; Lebrilla, C.B. Collision-Induced Dissociation Tandem Mass Spectrometry for Structural Elucidation of Glycans. *Methods Mol. Biol. Glycomics Methods Protoc.* **2009**, *534*, 75–89, doi:10.1007/978-3-7091-1416-2_3.

187. Sleno, L.; Volmer, D.A. Ion activation methods for tandem mass spectrometry. *J. Mass Spectrom.* **2004**, *39*, 1091–1112, doi:10.1002/jms.703.

188. Domon, B.; Costello, C.E. A systematic nomenclature for carbohydrate fragmentations in FAB-MS/MS spectra of glycoconjugates. *Glycoconj. J.* **1988**, *5*, 397–409, doi:10.1007/BF01049915.

189. Zhou. S.; Dong, X.; Veillon, L.; Huang, Y.; Mechref, Y. LC-MS/MS analysis of permethylated N-glycans facilitating isomeric characterization. *Anal Bioanal Chem.* **2017**, *409*, 453–466, doi:10.1007/s00216-016-9996-8.

190. Wang, P. Altered glycosylation in cancer : Sialic acids and sialyltransferases. **2005,** doi:10.29685/JCM.200512.0001.

191. Wada, Y.; Azadi, P.; Costello, C.E.; Dell, A.; Dwek, R.A.; Geyer, H.; Geyer, R.; Kakehi, K.; Karlsson, N.G.; Kato, K.; et al. Comparison of the methods for profiling glycoprotein glycans - HUPO human disease glycomics/proteome initiative multi-institutional study. *Glycobiology* **2007**, *17*, 411–422, doi:10.1093/glycob/cwl086.

192. Mechref, Y.; Hu, Y.; Desantos-Garcia, J.L.; Hussein, A.; Tang, H. Quantitative glycomics strategies. *Mol. Cell. Proteomics* **2013**, *12*, 874–884, doi:10.1074/mcp.R112.026310.

193. Hu, Y.; Borges, C.R. A spin column-free approach to sodium hydroxide-based glycan permethylation. *Analyst* **2017**, *142*, 2748–2759, doi:10.1039/c7an00396j.

194. Powell, A.K.; Harvey, D.J. Stabilization of sialic acids in N-linked oligosaccharides and gangliosides for analysis by positive ion matrix-assisted laser desorption/ionization mass spectrometry. *Rapid Commun. Mass Spectrom.* **1996**, *10*, 1027–1032, doi:10.1002/(SICI)1097-0231(19960715)10:9<1027::AID-RCM634>3.0.CO;2-Y.

195. Kita, Y.; Miura, Y.; Furukawa, J.; Nakano, M.; Shinohara, Y.; Ohno, M.; Takimoto, A.; Nishimura, S.-I. Quantitative Glycomics of Human Whole Serum Glycoproteins Based on the Standardized Protocol for Liberating N -Glycans . *Mol. Cell. Proteomics* **2007**, *6*, 1437–1445, doi:10.1074/mcp.t600063-mcp200.

196. Wheeler, S.F.; Domann, P.; Harvey, D.J. Derivatization of sialic acids for stabilization in matrix-assisted laser desorption/ionization mass spectrometry and concomitant differentiation of alpha(2 --> 3)- and alpha(2 --> 6)-isomers. *Rapid Commun. Mass Spectrom.* **2009**, *23*, 303-12, doi:10.1002/rcm.3867.

197. Reiding, K.R.; Blank, D.; Kuijper, D.M.; Deelder, A.M.; Wuhrer, M. High-Throughput Profiling of Protein N-Glycosylation by MALDI-TOF-MS Employing Linkage-Specific Sialic Acid Esterification. **2014,** *86,* 5784-5793, doi:10.1021/ac500335t.

198. Toyoda, M.; Ito, H.; Matsuno, Y.K.; Narimatsu, H.; Kameyama, A. Quantitative derivatization of sialic acids for the detection of sialoglycans by MALDI MS. *Anal. Chem.* **2008**, *80*, 5211–5218, doi:10.1021/ac800457a.

199. Gil, G.; Iliff, B.; Cerny, R.; Velander, W.H.; Van Cott, K.E. High throughput quantification of N-glycans using one-pot sialic acid modification and matrix assisted laser desorption ionization time of flight mass spectrometry. *Anal. Chem.* **2010**, *82*, 6613–6620, doi: 10.1021/ac1011377.

200. De Haan, N.; Reiding, K.R.; Haberger, M.; Reusch, D.; Falck, D.; Wuhrer, M. Linkage-Specific Sialic Acid Derivatization for MALDI-TOF-MS Profiling of IgG Glycopeptides. *Anal. Chem.* **2015**, *87*, 8284–8291, doi:10.1021/acs.analchem.5b02426.

201. Sekiya, S.; Wada, Y.; Tanaka, K. Derivatization for Stabilizing Sialic Acids in MALDI-MS. *Society* **2005**, *77*, 4962–4968.

202. Cummings, R.D.; Pierce, J.M. *Handbook of Glycomics*; 2009.

203. Kailemia, M.J.; Ruhaak, L.R.; Lebrilla, C.B.; Amster, I.J. Oligosaccharide Analysis By Mass Spectrometry: A Review Of Recent Developments. *Anal. Chem.* **2015**, *86*, 196–212, doi:10.1021/ac403969n.

204. Kohler, J.J.; Patrie, S.M. *Mass Spectrometry of Glycoproteins: Methods and Protocols.* Springer Protoc. 2013; pp.197–215.

205. Kang, P.; Mechref, Y.; Kyselova, Z.; Goetz, J.A.; Novotny, M. V. Comparative glycomic mapping through quantitative permethylation and stable-isotope labeling. *Anal. Chem.* **2007**, *79*, 6064–6073, doi:10.1021/ac062098r.

206. Ma, H.; Miao, X.; Ma, Q.; Zheng, W.; Zhou, H.; Jia, L. Functional roles of glycogene and N-glycan in multidrug resistance of human breast cancer cells. *IUBMB Life* **2013**, *65*, 409–422, doi:10.1002/iub.1133.

207. Atwood, J.A.; Cheng, L.; Alvarez-manilla, G.; Warren, N.L.; York, W.S.; Orlando, R. Quantitation by Isobaric Labeling: Applications to Glycomics James. *J. Proteome Res.* **2008**, *7,* 367–374, doi:10.1021/pr070476i.

208. Apte, A.; Meitei, N.S. Bioinformatics in Glycomics: Glycan Characterization with Mass Spectrometric Data Using SimGlycan. *Methods Mol Biol.* **2010,** *600*, 269–281, doi:10.1007/978-1-60761-454-8.

209. Morrison, K.A.; Clowers, B.H. Contemporary glycomic approaches using ion mobility–mass spectrometry. *Curr. Opin. Chem. Biol.* **2018**, *42*, 119–129, doi:10.1016/j.cbpa.2017.11.020.

210. Barroso, A.; Giménez, E.; Konijnenberg, A.; Sancho, J.; Sanz-Nebot, V.; Sobott, F. Evaluation of ion mobility for the separation of glycoconjugate isomers due to different types of sialic acid linkage, at the intact glycoprotein, glycopeptide and glycan level. *J. Proteomics* **2018**, *173*, 22–31, doi:10.1016/j.jprot.2017.11.020.

211. Ruotolo, B.T.; Benesch, J.L.P.; Sandercock, A.M.; Hyung, S.J.; Robinson, C. V. Ion mobility-mass spectrometry analysis of large protein complexes. *Nat. Protoc.* **2008**, *3*, 1139–1152, doi:10.1038/nprot.2008.78.

212. Bush, M.F.; Hall, Z.; Giles, K.; Hoyes, J.; Robinson, C. V.; Ruotolo, B.T. Collision cross sections of proteins and their complexes: A calibration framework and database for gas-phase structural biology. *Anal. Chem.* **2010**, *82*, 9557–9565, doi:10.1021/ac1022953.

213. Campbell, M.P.; Royle, L.; Radcliffe, C.M.; Dwek, R.A.; Rudd, P.M. GlycoBase and autoGU : tools for HPLC-based glycan analysis. **2008**, *24*, 1214–1216, doi:10.1093/bioinformatics/btn090.

214. Deshpande, N.; Jensen, P.H.; Packer, N.H.; Kolarich, D. GlycoSpectrumScan : Fishing Glycopeptides from MS Spectra of Protease Digests of Human Colostrum sIgA research articles. **2010**, *9,* 1063–1075, doi:10.1021/pr900956x.

215. Lohmann, K.K.; von der Lieth, C.W. GlycoFragment and GlycoSearchMS: Web tools to support the interpretation of mass spectra of complex carbohydrates. *Nucleic Acids Res.* **2004**, *32*, 261–266, doi:10.1093/nar/gkh392.

216. Fellenberg, M.; Behnken, H.N.; Nagel, T.; Wiegandt, A.; Baerenfaenger, M.; Meyer, B. Glycan analysis: Scope and limitations of different techniques - A case for integrated use of LC-MS(/MS) and NMR techniques. *Anal. Bioanal. Chem.* **2013**, *405*, 7291–7305, doi:10.1007/s00216-013-7164-y.

217. Hizal, D.B.; Wolozny, D.; Colao, J.; Jacobson, E.; Tian, Y.; Krag, S.S.; Betenbaugh, M.J.; Zhang, H. Glycoproteomic and glycomic databases. *Clin. Proteomics* **2014**, *11*, 1–10, doi:10.1186/1559-0275-11-15.

218. Functional Glycomics Gateway. Available online: http://www.functionalglycomics.org/ (accessed on 15 May 2020).

219. Ranzinger, R.; Herget, S.; Wetter, T.; Von der Lieth, W. GlycomeDB - Integration of open-access carbohydrate structure databases. *BMC Bioinformatics* **2008**, *9*, 1–13, doi:10.1186/1471-2105-9-384.

220. Cooper, C.A.; Joshi, H.J.; Harrison, M.J.; Wilkins, M.R.; Packer, N.H. GlycoSuiteDB: A curated relational database of glycoprotein glycan structures and their biological sources. 2003 update. *Nucleic Acids Res.* **2003**, *31*, 511–513, doi:10.1093/nar/gkg099.

221. Von Der Lieth, C.W.; Freire, A.A.; Blank, D.; Campbell, M.P.; Ceroni, A.; Damerell, D.R.; Dell, A.; Dwek, R.A.; Ernst, B.; Fogh, R.; et al. EUROCarbDB: An open-access platform for glycoinformatics. *Glycobiology* **2011**, *21*, 493–502, doi:10.1093/glycob/cwq188.

222. Hirabayashi, J.; Tateno, H.; Shikanai, T.; Aoki-Kinoshita, K.F.; Narimatsu, H. The lectin frontier database (LfDB), and data generation based on frontal affinity chromatography. *Molecules* **2015**, *20*, 951–973, doi:10.3390/molecules20010951.

223. Johannes F. G. Vliegenthart, Lambertus Dorland, et al. High-resolution, 1H-nuclear magnetic resonance spectrometry as a tool in the structural analysis of carbohydrates related to glycoproteins. *Adv. Carbohydr. Chem. Biochem.* **1983**, *41*.

224. Kam, R.K.T.; Poon, T.C.W. The potentials of glycomics in biomarker discovery. *Clin. Proteomics* **2008**, *4*, 67–79, doi:10.1007/s12014-008-9017-9.

225. Qin, R.; Zhao, J.; Qin, W.; Zhang, Z.; Zhao, R.; Han. J.; et al. Discovery of Non-invasive Glycan Biomarkers for Detection and Surveillance of Gastric Cancer. *J Cancer* **2017,** *10,* 1908-1916, doi:10.7150/jca.17900.

Manuscript 2

Decoding the glycosylation signatures of ageing in *C. elegans* under a high-glucose diet: A multi-omics perspective

Beatrix Paton, Pol Herrero, Trisha Arora, Lorena García, Manuel Suárez and Núria Canela

Article

In preparation

Decoding the glycosylation signatures of ageing in *C. elegans* under a high-glucose diet: A multi-omics perspective

Beatrix Paton[1], Pol Herrero[1], Trisha Arora[1], Lorena García[1], Manuel Suárez[2] and Núria Canela[1]*

[1] Eurecat, Centre Tecnològic de Catalunya, Centre for Omic Sciences (Joint Unit Eurecat- Universitat Rovira i Virgili), Unique Scientific and Technical Infrastructure (ICTS), Reus, Spain.

[2] Universitat Rovira i Virgili, Departament de Bioquímica i Biotecnologia, Nutrigenomics Research Group, Tarragona, Spain

ABSTRACT

Sugar intake is known to be too high in industralised nations. High-glucose diets (HGDs), linked to obesity, type 2 diabetes, and cardiovascular diseases, are closely related to oxidative stress, which is a contributing factor to the development of several diseases. To study the impact of a HGD, three different *Caenorhabditis elegans* strains were employed: wild type N2, short-lived CF1038 [*daf-16(mu86)*] and long-lived CB1370 [*daf-2(e1370)*]. The N-glycome, proteome and lipidome were analysed, as well as evaluating the lifespan and assessing the participation of transcriptional regulators known to be involved in longevity, lipid accumulation and oxidative stress, to potentially observe the changes induced by dietary glycose on the development and ageing of *C. elegans.* The effect of a HGD was revealed through shorter lifespans in all strains and significant differences in the N-glycome, proteome and lipidome, mainly observed on day 12 (aged worms). The N-glycome was especially affected by a HGD in N2 and CB1370 strains. The response to elevated glucose levels included modifications in protein pathways involved in catabolic processes, energy production, translation, and RNA processing. Through an integrative analysis, positive correlations between proteins involved in lipid transport and phosphatidylcholine (PCs) and triglyceride (TG) lipid families were observed in HGD-fed groups. Overall, this study sheds light on the intricate relationship between nutrition, multi-omics responses, gene expression, and lifespan in *C. elegans*.

1. INTRODUCTION

Diets in industrialised countries often have high glycemic index values, as they are characterised for having processed carbohydrates or sugars, which are easily metabolised to glucose, quickly raising blood glucose levels. High-glucose diets (HGDs) have been associated with obesity, type 2 diabetes and cardiovascular diseases [1–3]. The hormone insulin mediates some of the effects of a HGD on human health and abrupt changes in its levels can lead to insulin resistance and ultimately to type 2 diabetes [3]. In addition, HGDs are known to produce reactive oxygen species (ROS), that include both radical and non-radical oxygen species such as hydroxyl radical ($HO^{\cdot}$), superoxide anion ($O_2^{\cdot-}$), and hydrogen peroxide (H_2O_2). These ROS have the potential to damage lipids, proteins and nucleic acids, thereby contributing to cell death [4,5]. Consequently, oxidative stress has been proposed as a contributing factor to the development of several diseases, including obesity and diabetes [6].

An optimal model to investigate the impact of high glucose concentrations is *Caenorhabditis elegans* [7]. As one of the top non-mammalian eukaryotic model organisms, *C. elegans* is extensively used in studies related to development and ageing [8,9]. This anatomically simple nematode consists of an intestine surrounded by muscle, nerve and reproductive tissue, with a defined number of nuclei and rapid lifespan [10]. This model has been extensively used in studies concerning the toxicity induced by glucose [3,4,7,11,12], providing evidence that HGDs have an impact on growth, fertility, ageing and lifespan. Precisely, high glucose concentrations can reduce lifespan, which is known to be partially attributed to the activation of the insulin/IGF-1 signalling (IIS) pathway [3]. In this pathway, insulin-like peptides bind to their receptor (IGF-1 receptor/DAF-2), which recruits an insulin receptor substrate. This triggers the activation of the phosphatidylinositol-3-OH kinase AGE-1/PI3K, leading to an increase in phosphatidylinositol (3,4,5)-triphosphate (PIP3) levels. PIP3, in turn, initiates a kinase cascade which phosphorylates and inactivates the

transcription factor (TF) DAF-16/FOXO, by promoting its translocation from the nucleus to the cytosol. Conversely, in unfavourable conditions, IIS is down-regulated, leading to the activation of DAF-16/FOXO. This occurs by enhancing its translocation from the cytoplasm to the nucleus, where it triggers the activation of genes that promote longevity. The three primary downstream TFs associated with IIS, which are crucial for regulating lifespan, include DAF-16/FOXO, heat shock TF 1 (HSF-1), and SKN-1/nuclear factor erythroid 2 (NRF2), as identified thus far [13].

In this study, three different *C elegans* strains were examined: wild type N2, short-lived CF1038 [*daf-16(mu86)*] and long-lived CB1370 [*daf-2(e1370)*]. CB1370 was selected for its deletion in the allele e1370 of the *daf-2* gene, an insulin/insulin-like growth factor (IGF) receptor orthologue. This deletion causes DAF-16 to not be negatively regulated by DAF-2, causing DAF-16 to stay in the nucleus. As a result, the organism undergoes significant alterations on the phenotype, including prolonged lifespan and lipid content, as well as drastic changes to adult size, morphology, pumping rate, and gonad morphology [14,15]. The interest in the DAF-2 signalling pathway is partly due to its involvement in fat and carbohydrate metabolism, as it is an orthologue of insulin, and its connection to ageing and crucial function in reproduction in *C. elegans* [16]. The strain CF1038 was selected for its unfunctional DAF-16 protein. The TF DAF-16 regulates multiple biological processes including lifespan, stress response, dauer formation, and metabolism in *C. elegans* [17]. Since DAF-16 regulates many genes involved in cellular stress response [18], CF1038 could potentially be more sensitive to a HGD than the N2 strain. Moreover, DAF-16 influences the rate of ageing in response to insulin/insulin-like growth factor 1 (IGF-1) signalling, hence *daf-16* null mutants have shortened lifespans [19].

Chronic exposure to high glucose levels can lead to oxidative stress, inflammation, and impaired cellular function, which contribute to ageing processes [4,5,20,21]. HGDs may also impact protein glycosylation

patterns, including N-glycosylation. N-glycosylation is a post-translational modification (PTM) in proteins and its patterns can be influenced by various factors, including nutrient availability and metabolic status [22]. Changes in N-glycosylation have been associated with age-related diseases and the ageing process itself [23]. However, changes in protein N-glycosylation due to high glucose levels and their impact on *C. elegans* longevity remain little explored.

To gain a deeper understanding of the molecular mechanisms underlying several biological processes, including development and ageing, in the present study we aimed to examine N-glycosylation patterns. Furthermore, to potentially provide complementary data and a more comprehensive understanding of the N-glycome, the *C. elegans* proteome was also studied. We also evaluated the lifespan, lipidome profile and assessed the participation of transcriptional regulators known to be involved in longevity, lipid accumulation and oxidative stress, to ultimately observe the changes that dietary glucose induces in wild type N2, short-lived CF1038 and long-lived CB1370 worms.

While N-glycosylation, *C. elegans* longevity, and HGDs have been individually studied in the context of ageing and age-related diseases [23–25], their direct correlation and specific implications for *C. elegans* longevity under HGD require further investigation. Understanding the influence of N-glycosylation on *C. elegans* lifespan and its relationship with HGDs would involve exploring the effects of altered N-glycosylation patterns and related cellular processes. Findings from a multi-omics study on *C. elegans* fed a HGD can unravel the precise connections among these factors and provide insights that could be translated to understanding human metabolic diseases.

2. RESULTS

Nematodes were harvested on days 1 (L1 larvae), 5 (adults in egg laying stage) and 12 (ageing). Time points after day 12 were not considered, as

phenotypes associated with ageing can already be observed at this time point [26–28]. As in this study time points involving fertile worms are included, worms were treated with 50 μM 5-Fluoro-2′-deoxyuridine (FUdR) at the mid-late L4 larval stage (day 3) to eliminate bias from progeny in the assay. Although worms were unviable with this FUdR dose, they were healthy, not prone to bursting and with a lifespan similar to that of untreated control worms, as reported in previous studies [29].

2.1 Lifespan and stress-responsive transcription factors are altered with glucose exposure

Lifespan has been reported to be affected by a HGD [3,7]. We determined how lifespan was affected in N2, CF1038 and CB1370 worms in media supplemented with 80 mM of glucose. With the addition of glucose, lifespan was reduced in a 29%, 12% and 19% in N2, CF1038 and CB1370 strains, respectively, compared to the correspondent controls (Figure 1A and Supplementary Table 2). To investigate the potential involvement of some key regulators in the glucose-dependent reduction of lifespan observed in these strains, TFs of carbohydrate and lipid metabolism, oxidative stress and longevity [4] were measured: HIF-1/HIF1α, CRH-1/CREB, CEP-1/p53, SKN-1/NRF2, SBP-1/SREBP, and DAF-16/FOXO. When evaluating the expression of these TFs on day 12 in all strains, no statistically significant differences were observed between diets for *crh-1*, *skn-1* and *sbp-1*. For *daf-16*, mRNA was decreased in HGD-fed N2 worms, increased in HGD-fed CB1370 worms and absent in CF1038 worms. A similar trend was observed for skn-1, *crh-1* and *cep-1*, decreasing in N2 worms, but increasing in CF1038 and CB1370, when fed a HGD, compared to their correspondent CD-fed worms. In the case of *hif-1*, mRNA was increased in all strains fed a HGD, compared to the correspondent controls (Figure 1B). Taken together, the HGD treatment significantly modulated stress-responsive TFs *daf-16*, *cep-1* and *hif-1*.

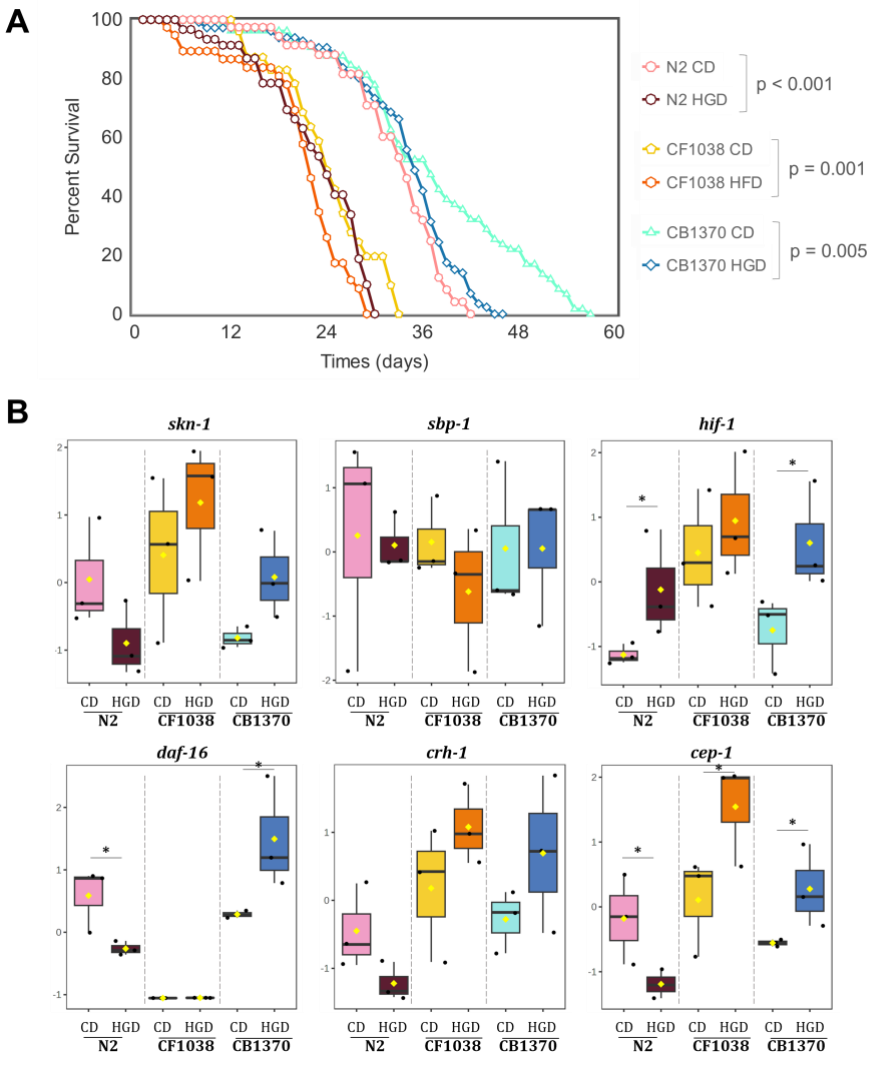

Figure 1. A) Effects of a HGD on lifespan of N2, CF1038 and CB1370 strains. Survival curves were analysed using log-rank tests (OASIS2). B) mRNA abundance of stress-responsive TFs of worms grown in glucose-supplemented media. Significant differences (* $p < 0.05$) between diets were determined using Kruskal Wallis and Mann-Whitney tests.

2.2 N-glycan analysis

Worms were mixed and lysed, followed by N-glycan release and derivatization using Rapifluor-MS (RFMS), enabling their detection through liquid chromatography-tandem mass spectrometry (LC-MS/MS). For the N-glycan release, PNGase F was employed to cleave N-glycans from

glycopeptides, although it has been proved to be insufficient for the release of more highly core-modified N-glycans [30]. As a result, oligomannosidic, paucimannosidic, complex, truncated complex and phosphorylcholine-rich N-glycans were identified in this study, making up a total of 25 identified N-glycans (Supplementary Table 1). As observed in Figure 2, principal component analysis (PCA) shows that diet-induced differences are larger with the increase of time, specially in N2 and CF1038 strains.

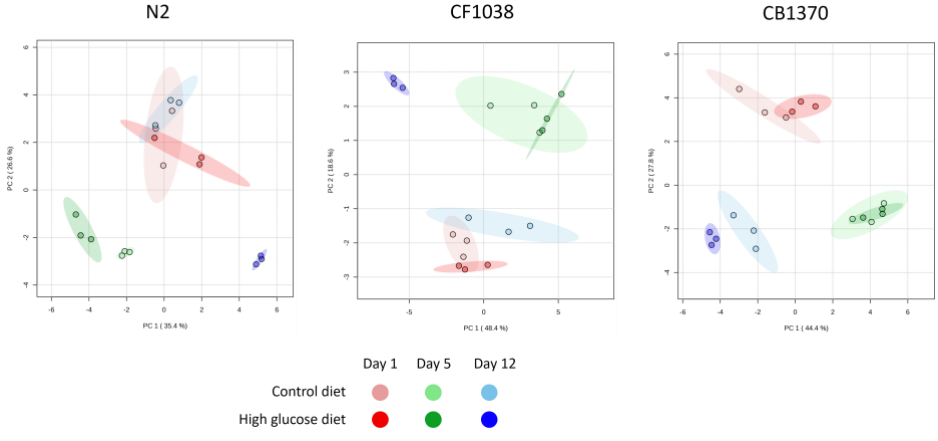

Figure 2. Principal component analysis (PCA) score plots representing N-glycomics data from all samples, comparing diets (Control diet (CD) and high-glucose diet (HGD)) in different developmental stages (day 1, day 5 and day 12), in three different *C. elegans* mutants (N2, CF1038 and CB1370).

N-glycan compositions detected by MS were reported as follows: Hex [hexose, either glucose (Glc), galactose (Gal), or mannose (Man)], HexNAc [N-acetylhexosamine, either N-acetylglucosamine (GlcNAc) or N-acetylgalactosamine (GalNAc)], Fuc [fucose], Pc [phosphorylcholine] and Me [methyl]. In the three strains, the most abundant structures identified belong to the oligomannosidic (or high-mannose, containing $Hex_{5-10}HexNAc_2$) and paucimannosidic ($dHex_{0-2}Hex_{2-4}HexNAc_2$) subgroups, constituting approximately 70% and 23% of the identified N-glycome. The most abundant oligomannose structure was $Hex_5HexNAc_2$ (GLY13), followed by $Hex_6HexNAc_2$ (GLY17). Of the paucimannose structures, $Hex_3HexNAc_2$ (GLY2) and $Fuc_1Hex_4HexNAc_2$ (GLY8) were of the highest

abundance. In lower abundance, two fucose-rich structures were determined ($Fuc_{1-2}Hex_6HexNAc_2$) (GLY18 and GLY20), as well as 7 truncated complex- and hybrid/complex-type structures. As differences in the N-glycome related to the development have been previously reported [31], we focused on assessing the comprehensive changes in the N-glycome caused by the diet (CD vs HGD) in the development of N2, CB1370 and CF1038.

In N2, a total of 16 N-glycans significantly changed between diets along the developmental stages ($p<0.05$), generally decreasing with a HGD at all time points. Overall, significant differences between diets were mainly observed on day 12 ($p<0.05$). Most N-glycans increased with development (Figure 3A), except for those N-glycans included in cluster a, which generally decreased with time, especially when fed a HGD (i.e complex N-glycan $Hex_6HexNAc_3$ (GLY19)). Several trends in N-glycan levels can be distinguished regarding time and diets: in cluster a (Figure 3A), for instance, N-glycans from CD groups decreased from day 1 to day 5 and then increased until day 12. Differently, in Cluster b, the only two identified fucose-rich N-glycans (Fuc1-2Hex6HexNAc2 (GLY18 and GLY20)) increased with time in CD-fed worms but decreased in HGD-fed worms).

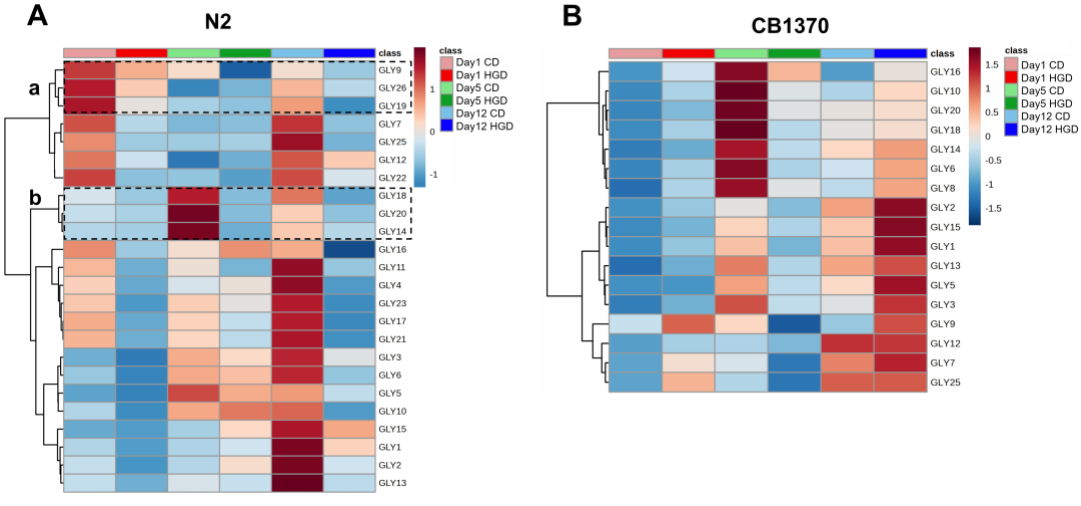

Figure 3. Heatmaps plotting changes between diets. A) Significant relative abundances of N-glycans in N2 increasing or decreasing along the different developmental stages (day 1, day 5 and day 12) according to the diet (CD or HGD). a) cluster of N-glycans decreasing with development, especially when fed a HGD b) cluster with fucose-rich N-glycans increasing with time in CD-fed worms but decreasing in HGD-fed worms. B) Significant relative abundances of N-glycans in CB1370 increasing or decreasing along the different developmental stages (day 1, day 5 and day 12) according to the diet (CD or HGD).

In the CB1370 strain, 14 N-glycans statistically changed between treatments in the three different developmental stages. Few differences were observed on day 1 between diets, however, on day 5, 13 N-glycans were decreased ($p<0.05$) in HGD-fed worms compared to CD-fed ones. This tendency switched at 12 weeks, where all the statistically significant N-glycans (8 in total, $p<0.05$) were increased in the HGD group compared to the CD one (Figure 3B).Fucose-rich N-glycans ($Fuc_{1-2}Hex_6HexNAc_2$ (GLY18 and 20)) and paucimannosidic species $Fuc_1Hex_5HexNAc_2$ (GLY14) showed a similar trend in N2 and CB1370 strains, decreasing significantly on day 5 in HGD-fed worms compared to CD-fed ones (Figure 4A).

Regarding mutant CF1038, only 3 N-glycans were statistically changed between diets along the developmental stages: $Hex_4HexNAc_2$ (GLY5), $Hex_{10}HexNAc_2$ (GLY26) and $Fuc_1Hex_5NAc_2Me_1$ (GLY9).

Methylated N-glycan $Fuc_1Hex_5HexNAc_2Me_1$ (GLY9) was particularly of interest for being the only statistically significant species between diets in all strains (Figure 4B). This methylated N-glycan showed a similar behaviour until day 5 in the mutant strains. However, in aged worms (day 12), it was significantly increased when fed a HGD only in CB1370. In aged N2 worms, the tendency was the opposite, decreasing in HGD-fed worms compared to CD ones.

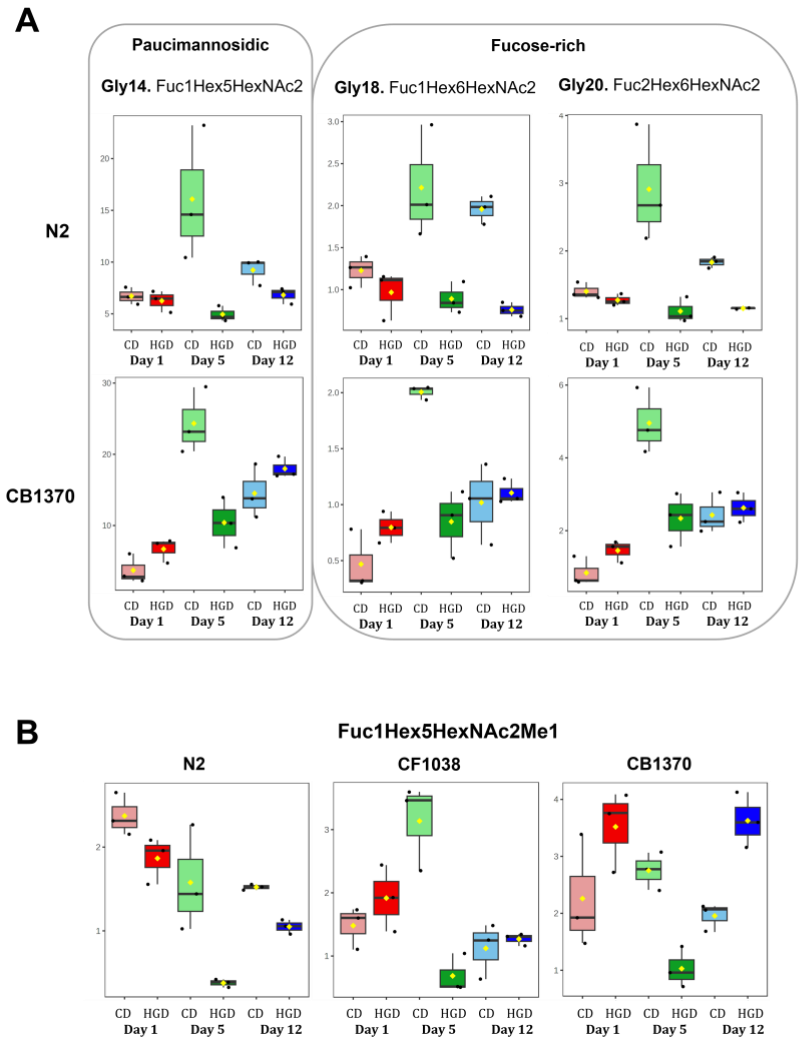

Figure 4. A) Box plots showing differences between diets (CD vs HGD) in three different developmental stages (day 1, day 5 and day 12) for three statistically significant N-glycans ($p<0.05$). B) Box plots showing differences between diets (CD vs HGD) in three different developmental stages (day 1, day 5 and day 12) for methylated N-glycan Fuc1Hex5HexNAc2Me1 (GLY9) ($p<0.05$). CD, control diet; HGD, high-glucose diet.

Differences between strains and diets at 12 weeks were also evaluated, to address the changes caused by a HGD in aged worms with different lifespans. More significant differences were observed between strains fed a HGD compared to a CD. In HGD-fed worms, all statistically significant N-

glycans were increased in CB1370 compared to CF1038 and N2, except for fucose-rich $Fuc_1Hex_6HexNAc_2$ (GLY18) which was increased in CF1038 compared to CB1370 and N2 (Figure 5).

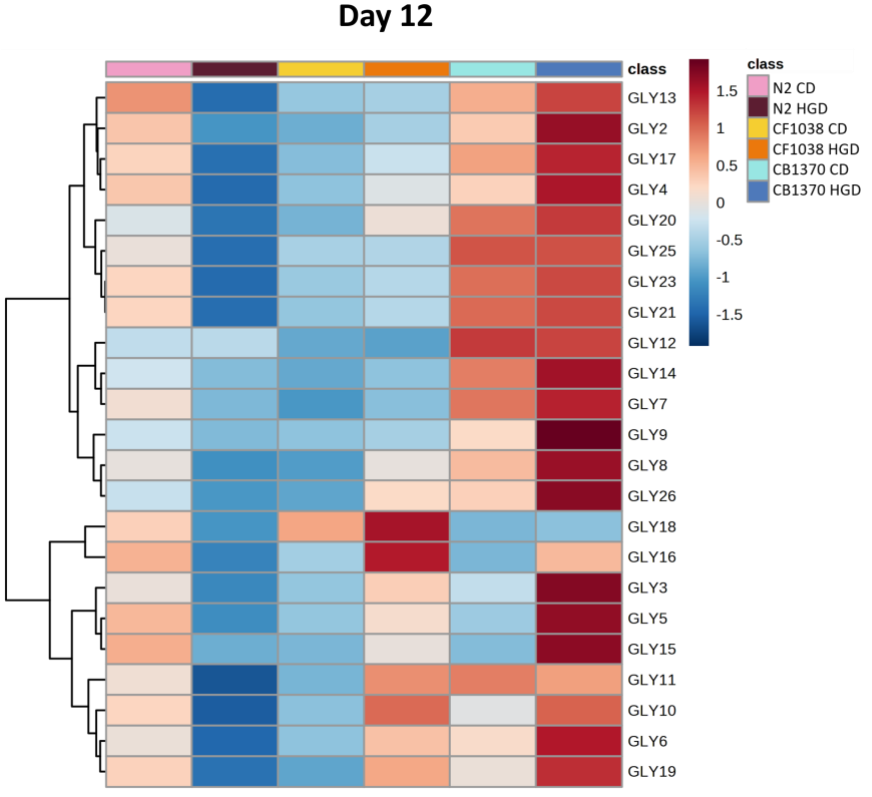

Figure 5. Significant relative abundances of N-glycans on day 12 in all strains (CB1370, CF1038 and N2) increasing or decreasing according to the diet (CD or HGD). For the three tests, significant differences ($p<0.05$) between treatments were determined using Kruskal Wallis and Mann-Whitney tests. The colour-coding is based on the relative abundance of each compound, low (blue) and high (red). CD, control diet; HGD, high-glucose diet.

2.3 Proteomics analysis

Worms were mixed and lysed, followed by trypsin digestion and tandem mass tags (TMT) peptide labelling, prior to analysis by LC-MS/MS. Three independent biological replicates were analysed. Identifications were highly reproducible, with 3061 of proteins identified in all groups, in at least two of three biological replicates. Relative protein quantification

among the three biological replicates was very reproducible in each condition studied within every individual strain, as shown in the PCA plot (Figure 6). As observed in Figure 6, diet-induced differences are larger with the increase of time in all strains. The HGD-fed groups differ from the CD-fed ones especially when reaching day 12 (aged worms), except for CB1370, which already shows an evident separation on day 5.

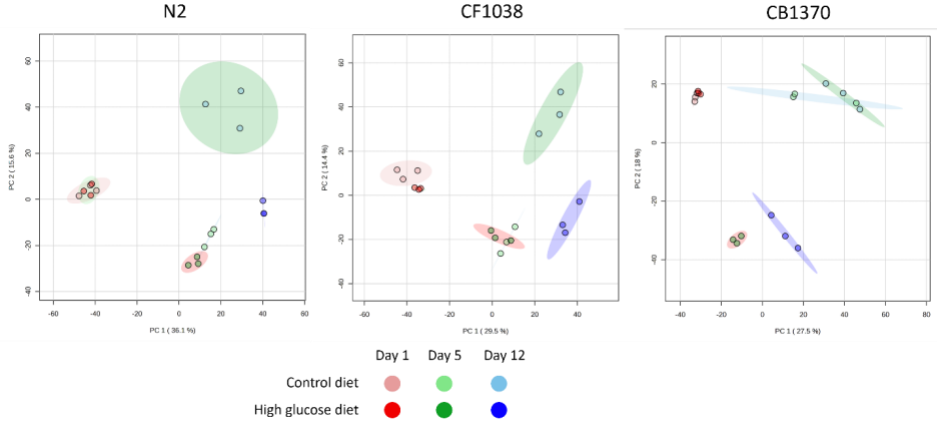

Figure 6. Principal component analysis (PCA) score plots representing proteomics data from all samples, comparing diets (Control diet (CD) and high-glucose diet (HGD)) in different developmental stages (day 1, day 5 and day 12), in three different *C. elegans* mutants (N2, CF1038 and CB1370).

Altered biological process with ageing in N2 worms fed a HGD

Differences according to the diet were evaluated along the developmental stages in N2 worms. A total of 35, 55 and 311 proteins were found to be significantly altered in abundance between diets (CD vs HGD) on day 1, 5 and 12, respectively, with p-values less than 0.05 considered significant and a fold change (FC) superior to 1.5. For these proteins, GO term analyses to characterise the most affected biological processes were performed in N2 on day 5 and day 12 by profiling the differences according to the diet using the Database for Annotation, Visualization and Integrated Discovery (DAVID) [32] and REVIGO [33]. The day 5 analysis revealed an enrichment of GO terms including translation, heterochromatin formation, protein N-linked glycosylation via asparagine,

DNA repair and proteolysis (Figure 7A). Differently, day 12 enriched GO terms included response to stress, lipid transport, cysteine biosynthetic process tricarboxylic acid cycle and protein deglutathionylation (Figure 7B). Interestingly, protein N-linked glycosylation related pathways were only enriched in day 5 worms.

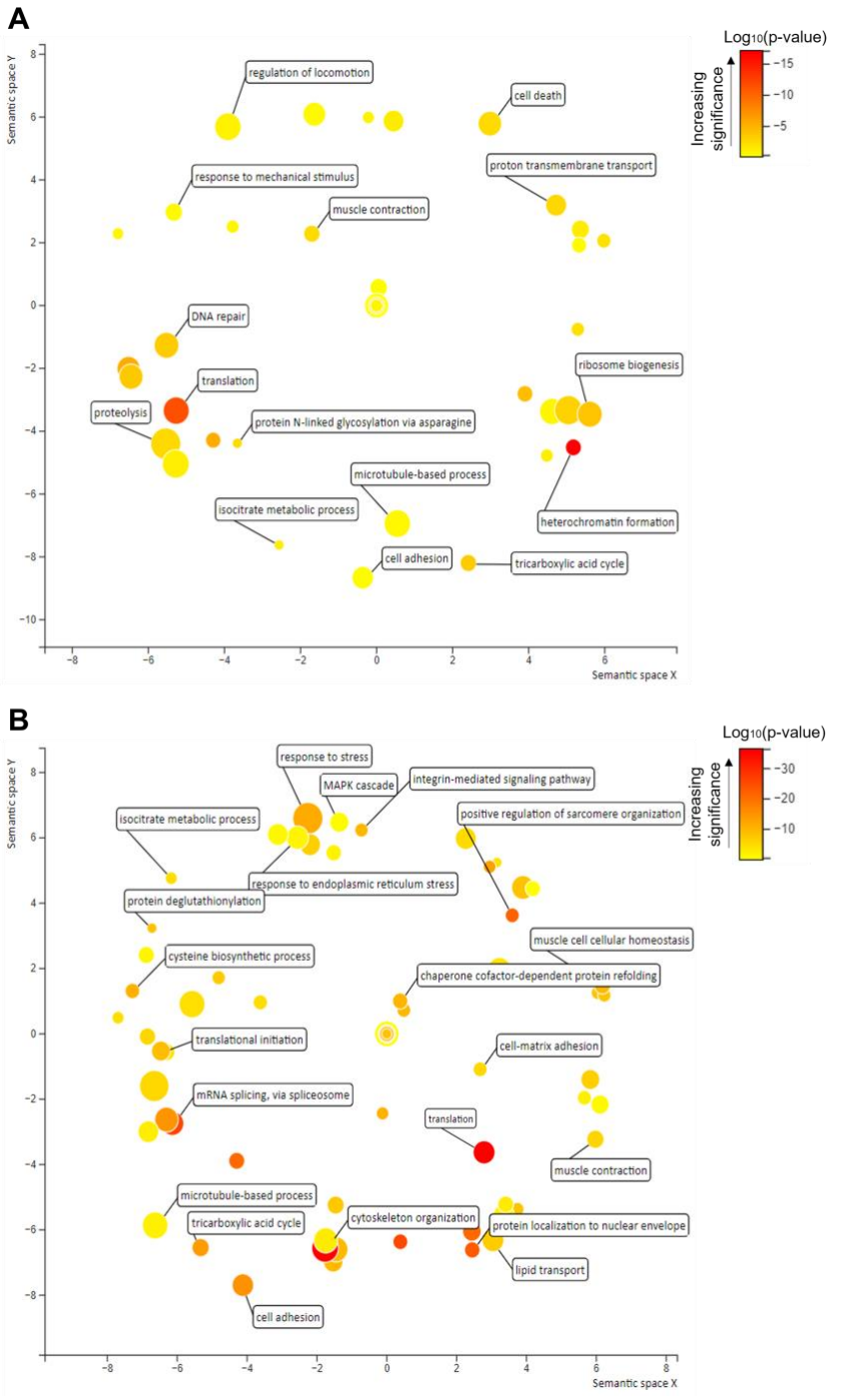

Figure 7. GO term enrichment (biological process) of the A) 619 diet-variant proteins in N2 adult worms (day 5) and B) 928 diet-variant proteins in N2 aged worms (day 12) between CD and HGD groups (p values < 0.05). Analyses were performed using DAVID and plotted using REVIGO. The size of the bubbles is

indicative of the number of proteins annotated with that GO term, and bubbles are colour coded according to significance.

Altered biological process in aged mutants fed a HGD

Differences according to the diet were evaluated on day 12 for all the studied strains. A total of 311 (as previously mentioned), 98 and 498 proteins were found to be significantly altered in abundance between diets (CD vs HGD) on day 12 in N2, CF1038 and CB1370, respectively, with p-values less than 0.05 considered significant and a FC superior to 1.5. Out of these statistically significant proteins, a set of 202, altered in at least 2 out of 3 of the evaluated strains, were further probed performing a GO term enrichment analysis (using DAVID), taking into account the direction of changes (Figure 8). Proteins from cluster 1, related to translation, ribosome and ribonucleoprotein complex GO terms, showed a similar tendency in N2 and CF1038, mostly decreasing in HGD-fed worms. Differently, proteins in CB1370 either showed the opposite tendency to the other two strains or simply did not show a statistically significant difference between diets (grey coloured cells). A similar tendency was observed in the remaining clusters, in which proteins generally behaved in a similar manner in N2 and CF1038, and showed the opposite behaviour in CB1370. Cluster 2 constituted of nutrient reservoir activity and lipid transport activity GO terms. Involved in these pathways, vitellogenins 1, 2, 3, 4 and 5 were decreased in N2 and CF1038 in HGD-fed worms compared to CD-fed ones. Inversely, when worms were fed a HGD, vitellogenin levels were increased in CB1370 compared to all the other groups (Figure 9A). The enrichment analysis also revealed an enrichment of GO term ageing. A heatmap was created to plot the 17 altered proteins from this pathway, whose levels showed the significant changes between the diets in each strain (Figure 9B). All of these decreased in CF1038 and increased in CB1370 with a HGD, when compared to the respective CD-fed group. Differently, in N2, some of these proteins increased and others decreased.

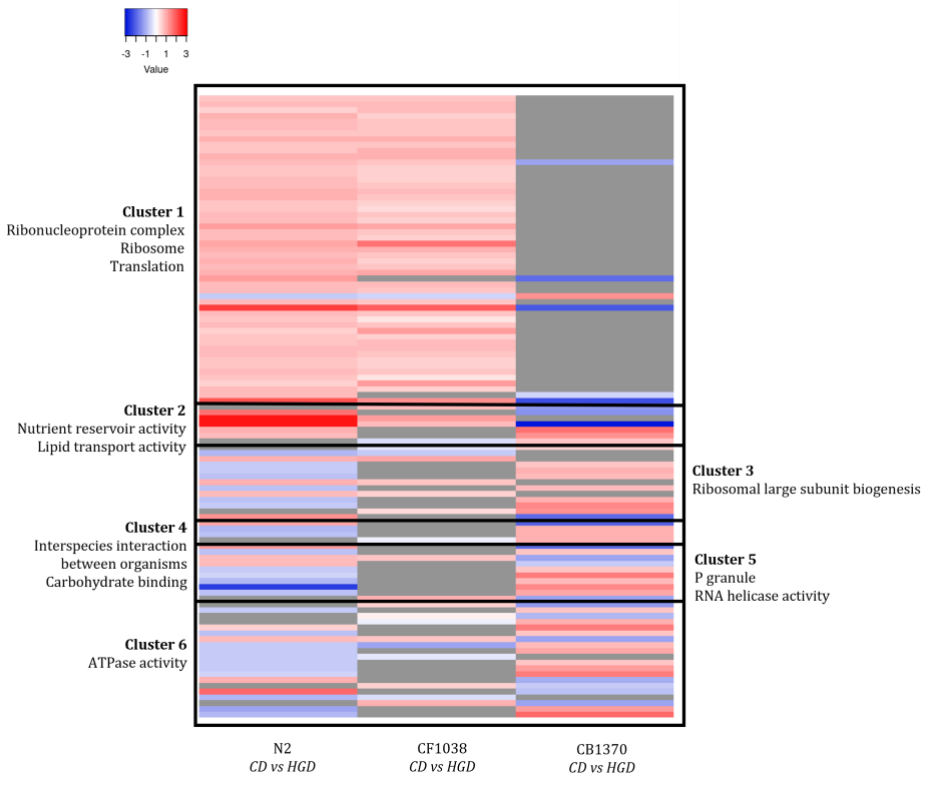

Figure 8. Heatmap of the 202 statistically significant proteins between diets (CD vs HGD) on day 12 in at least 2 of 3 three strains (N2, CF1038 and CB1370). Clusters were generated from GO term enrichment analysis ($p<0.05$) using DAVID. All GO terms (except cluster 5 and 6) remained significant ($p<0.05$) after multiple hypothesis correction (Benjamini-Hochberg). CD, control diet; HGD, high-glucose diet. Grey coloured cells indicate no statistically significant alteration.

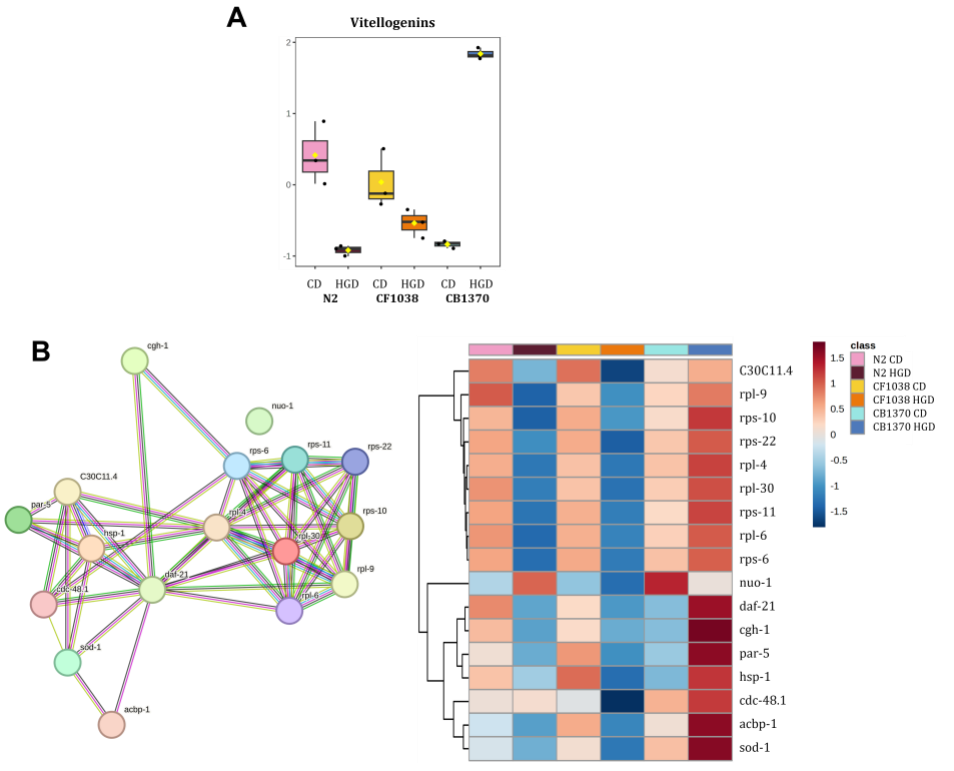

Figure 9. A) Ageing Gene Ontology (GO) term output of the CD versus HGD changes in protein abundance in all strains on day 12 (aged worms), obtained from STRING. Heatmap shows diet-dependent changes in abundance of these proteins. B) Box plots showing differences in vitellogenins between strains (N2, CB1370 and CF1038) increasing or decreasing according to the diet (CD or HGD), on day 12 ($p<0.05$). CD, control diet; HGD, high-glucose diet.

2.4 Lipidomics analysis

A total of 261 lipids were detected in positive ionisation mode (Supplementary Table 4). The most detectable lipid classes were triglycerides (TG), phosphatidylcholines (PC) and diglycerides (DG), which constituted 58%, 16% and 10%, respectively, of the total lipids detected. Lysophosphatidylcholines (LPC), sphingomyelins (SM) and phosphatidylethanolamines (PE) were the remaining lipid classes detected. As shown in the PCA plots (Figure 10A), a clear separation was observed for the lipid profiles between developmental stages in all strains. Differences between diets were only significant ($p<0.05$) on day 5 and day

12 for CF1038. Changes were evaluated on day 12 for all strains and diets, observing statistically significant differences ($p<0.05$) between diets mainly for CF1038 (Figure 10B). Lipids were grouped together according to their families, showing different tendencies along the developmental stages and between diets in all strains. The tendencies observed for TG and PC were generally the opposite in N2 and CF1038; TG increased in N2 but decreased in CF1038 HGD-fed worms ($p<0.05$) compared to their correspondent controls. However, PC decreased in N2, but increased in CF1038. No evident tendencies were observed in CB1370 for any lipid families.

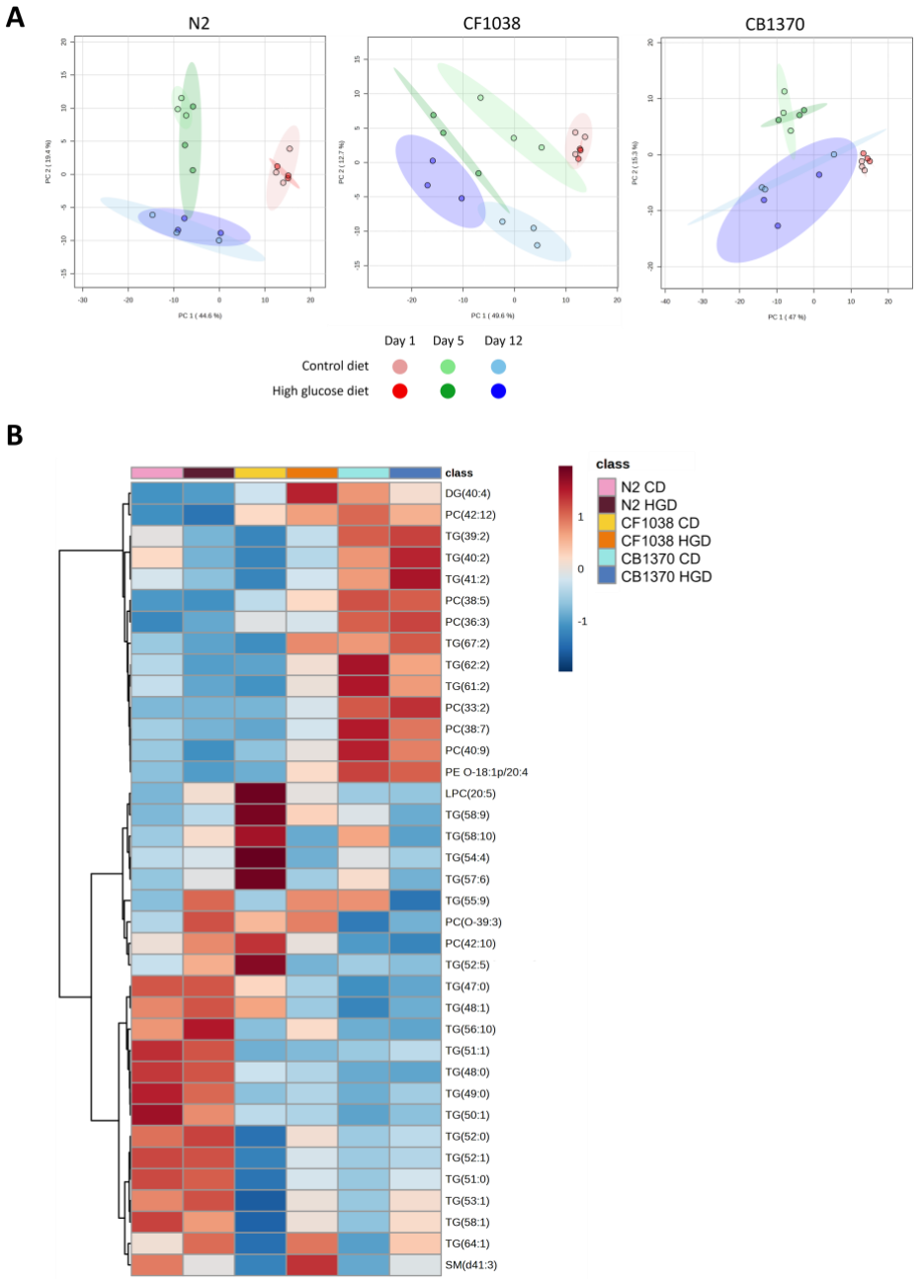

Figure 10. A) Principal component analysis (PCA) score plots representing lipidomics data from all samples, comparing diets (CD and HGD) in different developmental stages (day 1, day 5 and day 12), in three different *C. elegans* mutants (N2, CF1038 and CB1370). B) Heatmap plotting the significant relative abundance of N-glycans on day 12 in all strains (N2, CF1038 and CB1370) increasing or decreasing according to the diet (CD or HGD). Significant differences

($p<0.05$) between treatments were determined using Kruskal Wallis and Mann-Whitney tests. Columns indicate the strain and diet: CD, control diet; HGD, high-glucose diet. The colour-coding is based on the relative abundance of each compound, low (blue) and high (red).

2.5 Integrative analysis

An integrative analysis was performed to assess the connection between proteins, N-glycans and lipids. Firstly, correlation heatmaps were created to visualise the strength of correlation between N-glycans and proteins and between N-glycans and lipids. A general trend was observed, where higher correlations were observed in the HGD-fed groups from all strains on day 12, compared to the control groups (Figure 11 and 12). Proteins were clustered from GO term enrichment analysis ($p<0.05$) using DAVID. Interestingly, cluster 1 proteins, related to the ribonucleoprotein complex, ribosome and translation, were positively correlated with most N-glycans in HGD groups on day 12, while they were negatively correlated in the control groups (Figure 11). Generally, for most proteins and N-glycans, opposite correlations were observed between control and HGD groups on day 12. Differently, correlations between N-glycans and lipids for control and HGD groups on day 12 were similar.

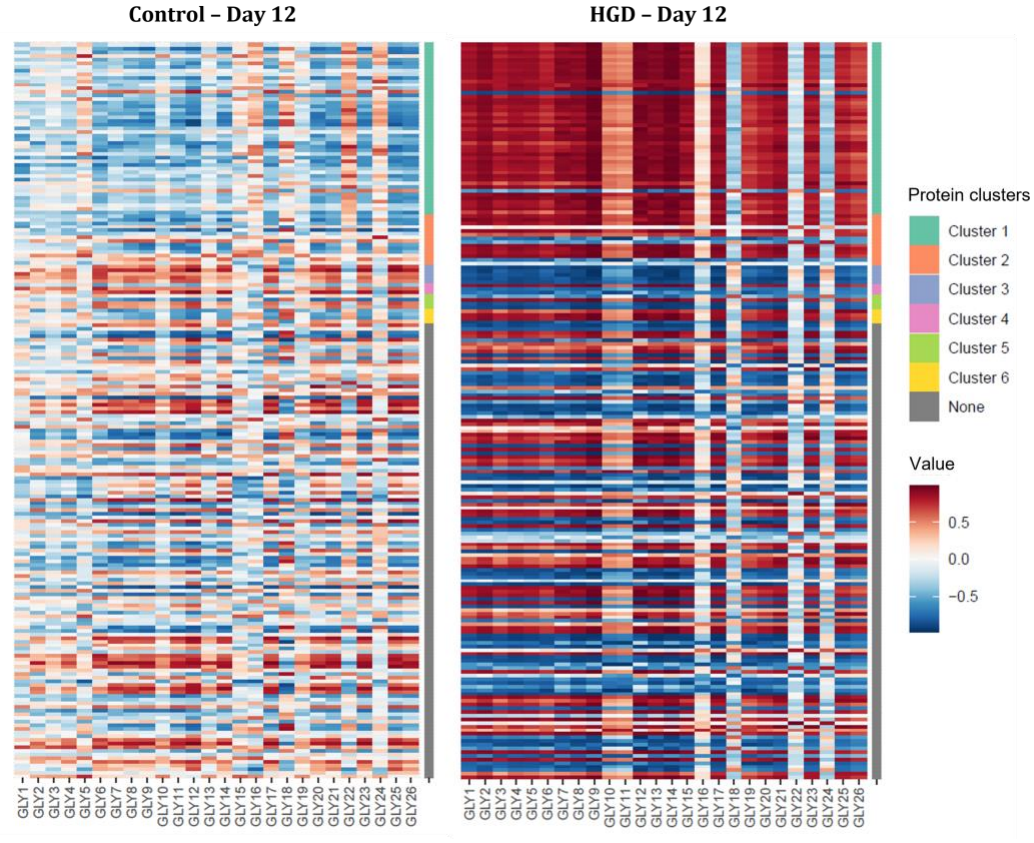

Figure 11. Correlation heatmaps between the 26 identified N-glycans and a selection of 202 proteins that were statistically significant between diets on day 12 in at least 2 of 3 strains (see Figure 8). Proteins were clustered from GO term enrichment analysis ($p<0.05$) using DAVID. Top left heatmap corresponds to control groups (all strains) on day 12, whereas top right heatmap correspond to HGD groups (all strains) on day 12. Cluster 1, ribonucleoprotein complex, ribosome and translation; cluster 2, nutrient reservoir activity and lipid transport activity; cluster 3, ribosomal large subunit biogenesis; cluster 4, interspecies interaction between organisms and carbohydrate binding; cluster 5, P granule and RNA helicase activity; cluster 6, ATPase activity.

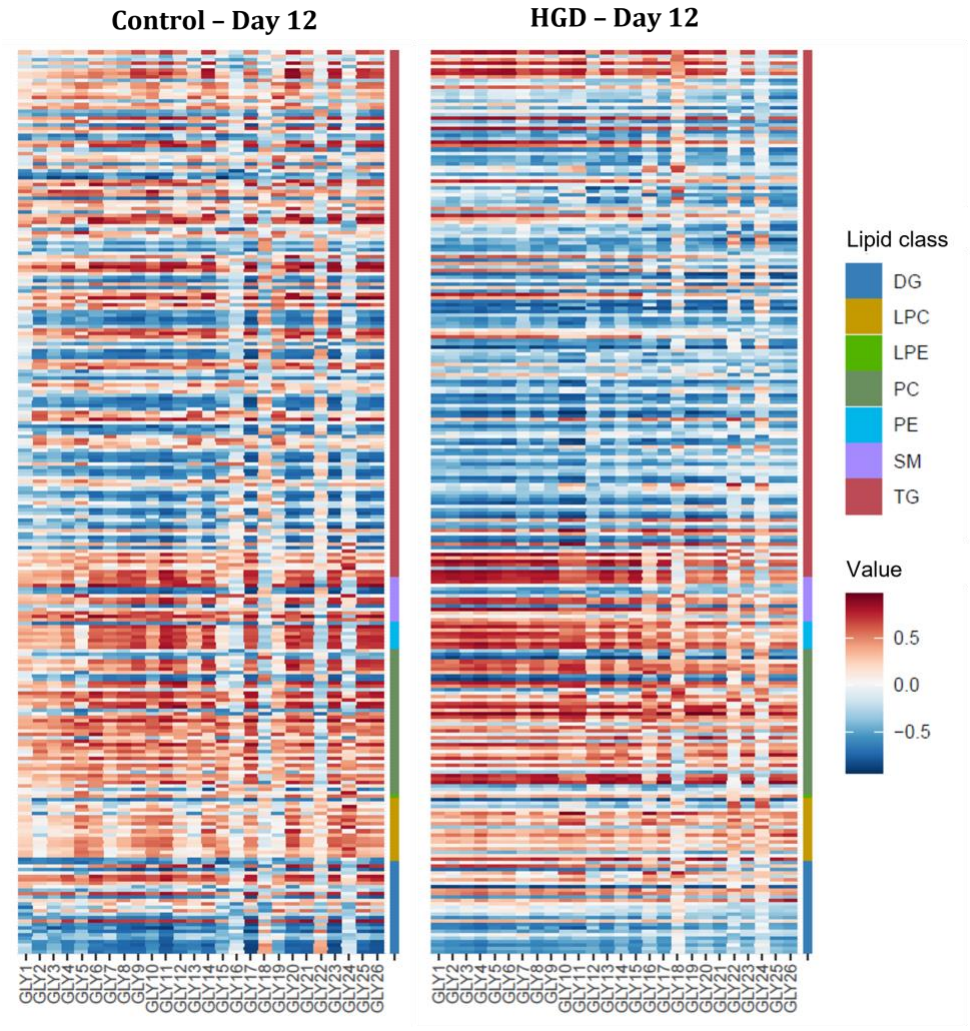

Figure 12. Correlation heatmaps between the 26 identified N-glycans and a selection of 261 identified lipids. Proteins were clustered according to the lipid class. Top left heatmap corresponds to control groups (all strains) on day 12, whereas top right heatmap correspond to HGD groups (all strains) on day 12. DG, diglycerides; LPC, lysophosphatidylcholines; LPE, lysophosphatidylethanolamines; PC, phosphatidylcholines; PE, phosphatidylethanolamines; SM, sphingomyelins; TG, triglycerides.

Following up, correlation networks were created between N-glycans, proteins and lipids on day 12 in N2 and CF1038. As these two strains overall showed similar behaviours in the separate N-glycome, proteome and lipidome analyses, we examined correlations in these two strains

together to ensure the robustness of the correlation network analysis. In the CD group (Figure 13), mostly positive correlations were observed between the majority of TG and the respective proteins and N-glycans. Transthyretin-like protein 2 (TTR-2, P4500, from cluster 2) showed many strong positive correlations with a wide variety of lipids, mainly PC. Additional proteins showing strong correlations include ribosomal protein RPL-43 (Q9U2A8 from cluster 1), showing a negative correlation with N-glycan $Hex_4HexNAc_2$ (GLY5). Intermediate filament protein ifa-2 MUA-6 (O02365), which is critical in the formation of aggresomes that form in response to protein misfolding [34], showed several strong correlations with PC, as well as with TTR-2. Similarly, in the HGD group (Figure 14), many positive correlations were observed for the TG lipid family. Furthermore, unlike the limited correlations observed within the CD group, the HGD group exhibited significant correlations involving 17 N-glycans, among themselves and with various proteins and lipids. Additionally, several vitellogenins (P18947, P55155 and P05690) showed positive correlations with PC and TG lipid families. Lastly, many proteins from cluster 1, related to the ribonucleoprotein complex, ribosome and translation, were negatively correlated with mostly PC and TG. One of the proteins showing more correlations in the HGD group was a DEAD-box helicase required for larval development (O17157), previously reported to change with age [35], which was mostly negatively correlated with TG, PC and other proteins related to protein clusters 1 and 2.

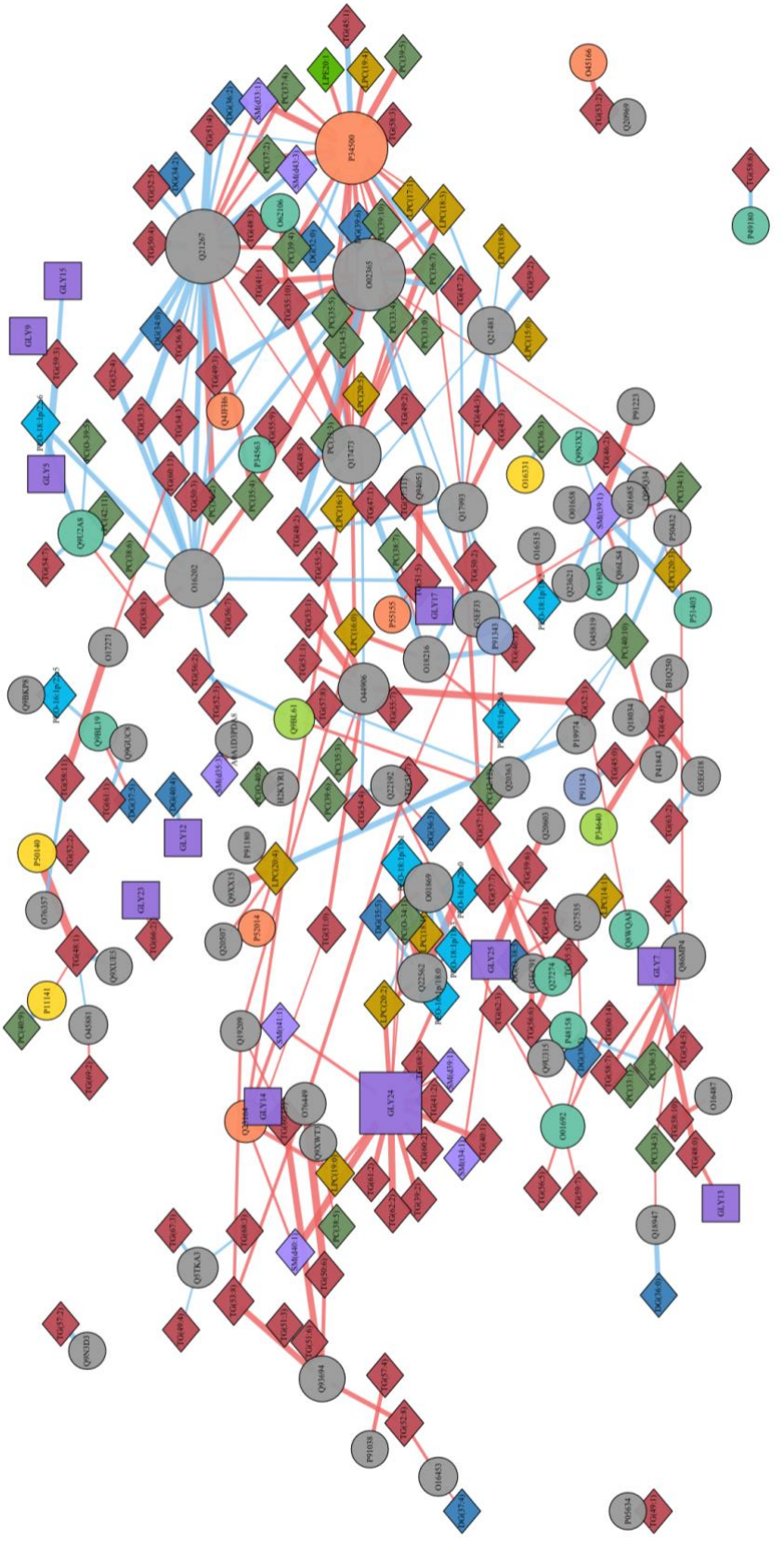

Figure 13. Correlation network between N-glycans, proteins and lipids for the CD groups of N2 and CF1038 strains on Day 12. Pearson's correlation coefficient was used to analyse correlations. The Pearson correlation coefficient threshold was set to 0.95. Network nodes were shaped based on the type of molecule (squares for N-glycans, circles for proteins and rhombi for lipids) and coloured according to the chemical classification (lipids) and GO term enrichment analysis clusters (proteins). Red and blue lines represent positive and negative correlations between pairs, respectively. The thickness of the lines represents the Pearson coefficient between a pair, and the node sizes were adjusted for their degree of centrality.

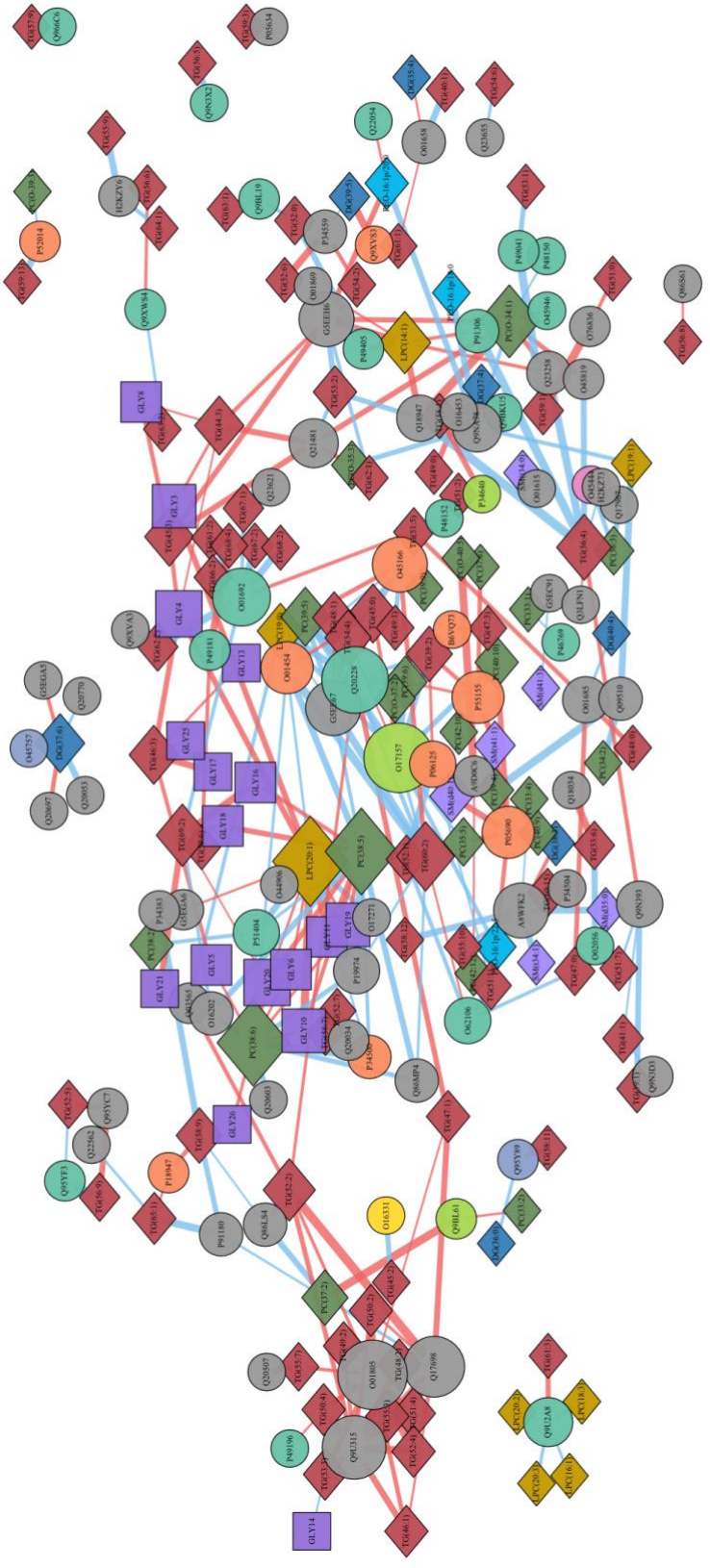

Figure 14. Correlation network between N-glycans, proteins and lipids for the HGD groups of N2 and CF1038 strains on Day 12. Pearson's correlation coefficient was used to analyse correlations. The Pearson correlation coefficient threshold was set to 0.95. Network nodes were shaped based on the type of molecule (squares for N-glycans, circles for proteins and rhombi for lipids) and coloured according to the chemical classification (lipids) and GO term enrichment analysis clusters (proteins). Red and blue lines represent positive and negative correlations between pairs, respectively. The thickness of the lines represents the Pearson coefficient between a pair, and the node sizes were adjusted for their degree of centrality.

3. DISCUSSION

In this study we explored the effect of a HGD on the lifespan of three different *C. elegans* strains: wild type N2, short-lived CF1038 and long-lived CB1370. We aimed to gain a holistic understanding of how the animal model *C. elegans* responds to a HGD by performing a multi-omics study including N-glycomics, proteomics and lipidomics, as well as looking at the changes in the expression of a selection of genes and determining the lifespan of the three strains.

Lifespan was reduced in a 29%, 12% and 19% in HGD-fed N2, CF1038 and CB1370, respectively, compared to the correspondent controls. Similar results have been observed in HGD related studies [4,36]. To examine the potential involvement of some key TFs related to cellular metabolism, antioxidant resistance and ageing, in the glucose-dependent reduction of lifespan observed in these strains, mRNA expression of *hif-1*, *crh-1*, *cep-1*, *skn-1*, *sbp-1* and *daf-16* were measured. In aged worms (day 12) no presence was shown for *daf-16* in CF1038, due to its unfunctional *daf-16*. Differently, aged N2 worms were unable to mount an adaptive response to oxidative stress, justifying the reduced expression of *daf-16* and *skn-1* in HGD-fed worms. The effect of a HGD on CB1370 was the opposite to N2, suggesting that high glucose levels may trigger the upregulation of *daf-16* gene expression to compensate for the decreased nuclear DAF-16 protein

levels. The inactivation of *hif-1*, *crh-1*, *cep-1* and *skn*-1 has been reported to have a protective effect on the lifespan of glucose-fed worms [4,37], explaining why these genes were decreased in our N2 HGD-fed worms. However, the *daf*-2 and *daf-16* mutant strains (CB1370 and CF1038, respectively) showed the opposite tendency, increasing the expression of those genes in HGD-fed mutants.

As previously reported in the *C. elegans* proteome, a weak correlation exists between mRNA-level and protein-level changes during ageing, suggesting that PTMs are responsible for a significant proportion of age-related functional changes in proteins [38]. N-glycosylation, among the most prevalent PTMs, can be subject to diverse influences, including factors such as nutrient availability and metabolic conditions [22]. To date, the N-glycome of *C. elegans* is not fully elucidated and the role of its many glycosylation relevant genes is still unclear [39]. Its N-glycans are characteristic for containing a range of galactose and fucose modifications associated with the asparagine-linked $Man_{2-3}GlcNAc_2$ core region [10,30]. Some of the modifications are the galactosylation of fucose, fucosylation of galactose and methylation of mannose or fucose residues as well as phosphorylcholine on antennal (non-reducing) N-acetylglucosamine. Even though *C. elegans* can be used as a model for some aspects of N-glycan function, its glycome has some particularities, that makes it different to those of other organisms. Various reports describe the N-, O- and lipid-linked glycans in *C. elegans*, even though new variants are still being discovered. In contrast to the well-defined genome, the complex glycome of this nematode and its synthesis is still not fully understood [10]. We compared N-glycans of N2 with those of two mutants, CB1370 and CF1038. Additionally, in these three strains, we determined changes in the N-glycan profile along the developmental stages (on day 1, day 5 and day 12) when worms were fed a HGD, ultimately aiming to determine how a HGD can alter the N-glycome and how this is related to the ageing process of *C. elegans.*

Oligomannosidic and paucimannosidic structures were the most abundant subgroups of N-glycans detected in all groups and strains, consistent with previous reports [31,40–44]. More specifically, oligomannose structures $Hex_5HexNAc_2$ (GLY13) and $Hex_6HexNAc_2$ (GLY17) were the most abundant species present, consistent with glucose and mannose trimming via the activities of α-glucosidases and α1,2-mannosidases, respectively, occurring in the endoplasmic reticulum. Moreover, this process correlates with the $Man_5GlcNAc_2$ structure serving as a major checkpoint in N-glycan processing [31,43,45,46]. In CB1370 fed either a CD or HGD, $Hex_6HexNAc_2$ (GLY17) was increased compared to CF1038 and N2 strains. Differently, N2 worms showed increased levels of $Hex_6HexNAc_2$ (GLY17) when fed a CD but decreased levels when fed a HGD, compared to CF1038.

Several N-glycans shared a similar trend along the developmental stages in all strains. When N-glycans showed an increase or decrease from day 1 to day 5, the respectively inversed alteration was observed from day 5 to day 12 (i.e., an increased N-glycan from day 1 to day 5 decreases from day 5 to day 12). This tendency was observed in both diets, indicating that it is likely related to significant lifestyle changes in the worm. L1 larvae (day 1) have exited embryonic development [47] and egg-laying adults (day 5) will likely have altered behaviour, while ageing worms (day 12) have reduced activity. Changes along the developmental stages may be related to alterations in the development of the nematode, innate immunity or processes in the secretory system required for the stage status [47]. It has been previously reported that the unfolded protein response is highly active in the L1 through the L2 stage, suggesting a high rate of glycoprotein biosynthesis.

Methylation of either α1,2-fucose (on the bisecting Gal or on the GalFuc) or mannose is a signature of some “mature” glycan structures [10] and can also be indicative markers of stress in the organism [48]. In aged worms (day 12), methylated $Fuc_1Hex_5HexNAc_2Me_1$ (GLY9) was increased in CB1370 but decreased in N2 strains when fed a HGD.

The difficulty concerning *C. elegans* lies in the fact that the enzymatic processes underlying the N-glycome remain insufficiently explored. As previously stated, our understanding is limited regarding the characteristics of the majority of β-GALTs and α-GALTs, along with methyltransferases, α1,2-FUTs, and phosphorylcholinyltransferases that alter N-glycans within this organism [48].

The IIS pathway, extensively studied in *C. elegans*, is essential in the organism's response to environmental stimuli, including nutrient availability and various stressor [49]. The orthologous to the human insulin receptor, DAF-2, binds to numerous insulin-like peptides, acting as both agonists and antagonists [50]. This binding leads to the activation of a phosphatidylinositol (3,4,5)-trisphosphate (PIP3) signalling cascade, which represses DAF-16 activity through phosphorylation and cytoplasmic retention [19]. When DAF-2 signalling is absent, DAF-16 enters the nucleus and directly or indirectly regulates the expression of its target genes, increasing lifespan [50]. The IIS pathway functions as a vitellogenin repressor. Vitellogenins are precursors of yolk proteins, crucial for lipid transport to oocytes, and are known to increase with age [51]. *daf-2* mutants have been reported to exhibit reduced vitellogenin transcription and accumulation in older worms [52]. In fact, RNAi-induced knockdown of vitellogenin has been shown to extend the lifespan of *daf-2* worms, suggesting that reduced vitellogenin expression may partially mediate their longevity [18]. Accordingly, in our study, vitellogenins 1, 2, 3, 4 and 5 were decreased at day 12 in CB1370, compared to N2 and CF1038, when fed a CD. Conversely, when worms were fed a HGD, vitellogenin levels were increased in CB1370 and decreased in N2 and CF1038. The significant increase in HGD-fed CB1370 worms is indicative of the reduced lifespan caused by a HGD. Additionally, vitellogenins play crucial roles in lipid transport and control trafficking of lipids, either for energy production in the starving hermaphrodite or for reproduction in the oocytes [53].

Many proteins related to the "ribonucleoprotein complex", "ribosome" and "translation" pathways (Cluster 1 in Figure 8) were enriched. Taken together, these data suggest that with high glucose levels, there is an overall increase in the activation of catabolic, energy-producing pathways. Additionally, there is a significant rewiring of translation and RNA processing, highlighting the adaptive response to high glucose levels.

To further visualise the alterations in protein levels, we evaluated the enrichment of GO terms on days 5 and 12. Interestingly, protein N-linked glycosylation via asparagine was only enriched in day 5 worms. Precisely, several N-glycans presented the most significant differences on day 5 (i.e., methylated and fucosylated N-glycans shown in Figure 4). We also closely evaluated the behaviour of several age-related proteins on day 12 when fed a CD vs a HGD (Figure 9A). Remarkably, these 18 proteins were generally decreased in N2 and CF1038 but increased in CB1370 when fed a HGD, compared to their control counterparts. DAF-21, a longevity regulator, followed this trend, likely increasing under conditions of oxidative stress (caused by a HGD), to maintain protein folding and prevent protein aggregation [54]. Why the opposite alteration is observed in strains N2 and CF1038 needs to be further explored. SOD-1, a major contributor to ageing [55] showed the same tendency than DAF-21 in the different strains and conditions. Decreased levels of SOD-1 were determined in HGD-fed N2 and CF1038 strains, which would indicate a reduction in the lifespans, consistent with our lifespan results. Protein NUO-1 was of special interest for showing an opposite behaviour compared to the other evaluated age-related proteins. The function of NUO-1 is primarily related to energy production and mitochondrial function, as it is closely tied to its participation in Complex I of the electron transport chain, leading to ATP production [56]. While decreased in the two mutant strains and increased in N2 when fed a HGD, the relationship between NUO-1, ageing and glucose availability is complex, hence further research is needed to better understand the molecular mechanisms involved.

Lipids are essential for physiological activities, energy metabolism, membrane integrity, and signalling pathways. Lipid metabolism dysregulation has been linked to a variety of age-related illnesses and effects lifespan in several organisms [57]. HGD can also affect lipid metabolism, altering lipid content, storage, and utilisation. Such changes in lipid metabolism may have an impact on cellular functions and lead to changes in longevity. In the present study we focused on observing the tendencies of TG in glucose-fed worms as glucose is a known precursor of triglycerides [4]. Interestingly, HGD-fed N2 worms showed increased TG levels from day 5 onwards, but HGD-fed CF1038 worms showed decreased levels, compared to CD worms. High glucose levels can activate insulin signalling, which can inhibit DAF-16 activity and promote breakdown. Results obtained for CF1038 suggest that high glucose levels may activate signalling pathways that promote lipid breakdown and inhibit triglyceride synthesis to maintain lipid homeostasis. This feedback mechanism would ensure that the organism adjusts its lipid metabolism according to nutrient availability. Further research should focus on why the tendency observed in N2 is the opposite, as the results suggest that N2 does not have the same feedback mechanism as CF1038.

Integrative analyses were performed to potentially identify groups of molecules that are co-regulated across different omics analyses. This integration can help reveal more comprehensive insights into biological processes and potential crosstalk between different molecular levels. In the network analyses, abundant positive correlations were observed between TG and N-glycans in HGD-fed N2 and CF strains, compared to the respective control groups. In CD groups, transthyretin-like protein 2 (P34500), involved in lipid transport, showed a high number of correlations, mostly positive, with different lipid families. Interestingly, this correlation was not seen in the HGD groups, possibly indicating a disruption in the lipid transport activity. In the HGD groups, some molecules with a high degree of centrality include PCs 28:5 and 38:6, LPC

20:1 and proteins ATP-dependent RNA helicase (O17157) related to ATPase activity, and small ribosomal subunit protein uS4 (Q20228) related to the ribosome. These hub nodes could potentially represent key regulatory players in the response to a HGD.

4. CONCLUSION

We aimed to gain a holistic understanding of how lifespan processes are affected by a HGD on the animal model *C. elegans,* by performing a multi-omics study including N-glycomics, proteomics and lipidomics, along with gene expression analysis and lifespan determination. In comparison to their respective controls, N2, CF1038, and CB1370 worms fed an HGD had a 29%, 12%, and 19% shorter lifetime. Similar findings have been observed in other HGD research. In all strains and conditions, the most abundant subgroups of N-glycans found were oligomannosidic and paucimannosidic structures. Most significant differences between diets were observed on day 12, specially in N2 and CB1370. Furthermore, variations in N-glycan profiles followed a pattern throughout the embryonic phases, implying important lifestyle changes and developmental processes in the worm. Similarly, we discovered that the expression of vitellogenins, which play important roles in lipid transport and reproduction, changed across strains and diets, indicating their function in lifespan regulation and response to a HGD. The proteomic data analysis revealed modifications in protein pathways involved in catabolic processes, energy production, translation, and RNA processing, indicating an adaptive response to elevated glucose levels. Finally, a HGD impacted lipid metabolism, with strain-specific changes in TG levels found.These findings demonstrate that lipid metabolism is differentially regulated in response to glucose availability, implying the involvement of feedback mechanisms to maintain lipid homeostasis.

A general trend was identified in all the analyses, where drastic alterations were observed on day 5, coinciding with the adult stage, in which worms

are capable of egg laying. These changes are likely due to the higher metabolic rates exhibited by *C. elegans* in adulthood compared to an ageing stage. Moreover, changes induced by the diet are generally prominent from day 5 to day 12. As glucose is a major energy source for *C. elegans*, the increased metabolic activity in HGD-fed adults (day 5) leads to greater glucose utilization. As a result, adult *C. elegans* are more sensitive to changes in glucose availability or alterations in glucose metabolism. An integrative analysis was also performed, revealing strong correlations in HGD-fed groups between N-glycans and proteins. Also, abundant positive correlations were observed between TGs and proteins, especially in the CD groups. Also, several vitellogenins showed positive correlations with PC and TG lipid families in the HGD-fed groups. Overall, this study sheds light on the intricate relationship between nutrition, multi-omics responses, gene expression, and lifespan in *C. elegans*. Changes in the N-glycome, proteome, and lipidome, as well as changes in critical TFs and pathways, give information on the molecular mechanisms behind the organism's reaction to HGD and its impact on ageing. More research is needed to completely comprehend the activities and relationships of individual genes, pathways, and metabolic processes in *C. elegans*.

5. MATERIALS AND METHODS

5.1 Reagents

Sodium dodecyl sulfate (SDS), ammonium bicarbonate (ABC), dithiothreitol (DTT), iodoacetamide (IAA), trichloroacetic acid (TCA), formic acid, glucose, Fud, Na2HPO4, KH2PO4, NaCl, MgSO4, ethylenediaminetetraacetic acid (EDTA), ammonium formate, trypsin, chloroform, methanol, NaCl, methyl-tert-butyl ether and 2-propanol were purchased from Sigma-Aldrich (Missouri, USA). Tris-HCl was obtained from Bio-Rad (California, USA) and urea was purchased from PlusOne (GE Healthcare, Illinois, USA). Acetone and acetonitrile (ACN) were obtained from Merck Millipore, (Massachusetts, USA). cOmplete Protease Inhibitor Cocktail and PhosSTOP were purchased from Roche Diagnostics

(Switzerland) and Pierce RIPA Buffer was obtained from Thermo Fisher Scientific (Germany).

5.2 Strains and culture conditions

The wild type Bristol (N2), CF1038 *daf-16(mu86)* and CB1370 *daf-2(e1370)* strains were cultured using Nematode Growth Medium (NGM) plates seeded with *Escherichia coli* OP50-1 and raised at 18 °C, as previously described [58]. Strains and *E. coli* OP50-1 were obtained from *Caenorhabditis* Genetics Center at the University of Minnesota. Worms were synchronised with alkaline hypochlorite solution [59], a condition in which only eggs can survive, and eggs were washed with M9 buffer solution. Once synchronised, worms were seeded on NGM plates (CD group) or glucose-supplemented plates (HGD group), and fed with *E.coli* OP50-1 during 12 days. To achieve a glucose concentration of 80mM, glucose was incorporated into the mixture of agar and salts of the NGM medium. To minimise the metabolic activity of *E. coli*, *E.coli* OP50-1 was heat-inactivated before adding to the NGM plates, as previously described [60]. Briefly, after bacterial concentration and resuspension, *E.coli* OP50 was incubated in a water bath for 30 min at 65 °C and cooled down before use. To eliminate progeny from the assays, worms were treated with 50 µM FUdR at the L4 stage until adulthood. Day 1, 5 and 12 worms were harvested and washed three times with M9 buffer (42 mM Na2HPO4, 22 mM KH2PO4, 86 mM NaCl, and 1 mM MgSO4) in order to remove all bacteria. After removing the excess of M9 buffer, worms were stored at –80 °C until analysis.

5.3 Lifespan assays

Lifespan assays were performed at 18 °C using age-synchronised worms. Worms were grown on NGM plates and seeded with inactivated OP50-1 bacteria. At the L4 stage, worms were transferred to FUdR treated plates. For each assay, worms were scored as dead or alive and transferred to new plates every other day. To determine mortality, worms were gently prodded using a wire pick (90% platinum and 10% iridium) along

different points of their body and scored as dead if they did not respond to this stimulation. Animals that exploded, bagged or were missing were censored in all cases. The number of animals used for each assay can be found in Supplementary Table 2.

5.4 Quantitative RT-PCR

For the obtention of RNA, 5,000 worms were lysed by sonication (40% amplitude with 15 sec on/off in triplicate) using 1 mL of Trizol (Invitrogen). Total RNA was further purified using the SV 96 Total RNA Isolation System (Promega). cDNA was synthesized using the High Capacity cDNA Reverse Transcription Kit (Thermo Fisher). Triplicate 8 µL quantitative real time RT-PCR (qPCR) reactions were set-up in 384-well plates and run on a 7900HT Fast Real-Time PCR System (Applied Biosystems) using POWERUP SYBR Green Master Mix (Applied Biosystems) in accordance with the manufacturer's instructions. The primer sequences can be found in Supplementary Table 3 [4]. Each qPCR reaction was performed using three biological replicates. The PCR program consisted of: 10 min at 95 °C, 40 cycles of 95 °C for 15 s, Tm (see Supplementary Table 3 for each oligonucleotide pair) for 30 s and 70 °C for 30 s. Y45F10D.4 gene served as a reference as described in [61]. The relative expression ratio of the target mRNA in relation to the expression of Y45F10D.4 mRNA was calculated using previously established methods [62].

5.5 N-glycome analysis

5.5.1 Lysis, de-N-glycosylation and labelling of N-glycans

The *C. elegans* pellet (5,000 worms per sample) was resuspended in 100 µL of lysis buffer (4% SDS, 0.1M Tris/HCl pH 8.0, 1mM EDTA and protease and phosphatase inhibitors) before incubating at 95 °C for 5 min and then subjecting the sample to bead beating procedure. Two stainless steel balls (3.2 mm diameter) were added to the samples and subjected to bead beating for 2 min at medium speed (Bullet Blender, Cultek, Barcelona, Spain); this step was performed in triplicate. Afterwards, methanol/chloroform protein precipitation was performed to isolate the

protein content before N-glycan analysis. Protein quantification was performed using the Bradford method. The method for the release and labelling of N-glycans was conducted following a previously described protocol [63]. Sample denaturation, de-N-glycosylation, labelling with Rapifluor-MS (RFMS), and purification steps were performed according to the Waters Corporation's "GlycoWorks RapiFluor-MS N-Glycan Kit Care and Use Manual" (p/n 715004793), with minor modifications. Briefly, 50 µg of protein were denatured in the presence of 5% (w/v) RapiGest at 90 °C for 3 minutes. De-N-glycosylation was then carried out by adding 1.2 µL of Rapid PNGase F and incubating at 50 °C for 5 minutes. The digested samples were directly labelled with 6 µL of RFMS reagent without requiring purification. The labelling reaction proceeded at room temperature for 5 minutes. Following this, a GlycoWorks µElution Plate was utilised for the Solid-Phase Extraction (SPE) Clean-up procedure. Glycans were eluted using 200 mM ammonium acetate in 5% acetonitrile.

5.5.2 LC-MS/MS

The LC-MS/MS analysis was carried out using a previously described analytical method [63].

After derivatisation, samples were analysed using an Agilent UHPLC 1290 Infinity Series coupled to an Agilent qTOF/MS 6550 Series (Agilent Technologies, Santa Clara, CA). N-glycans were separated on a Waters ACQUITY UPLC BEH amide column (2.1 mm × 150 mm i.d., particle size 1.7 µm) using 50 mM ammonium formate solution (mobile phase A) and 100% acetonitrile (mobile phase B). The flow rate was set to 0.4 mL/min, the injection volume was 20 µL and the column temperature was maintained at 60 °C throughout the analysis. Initially, the gradient ramped mobile phase A from 25 to 46%, over 35 min. From 35 to 36.5 min, the gradient ramped from 46 to 100% solvent A and the flow rate was lowered to 0.2 mL/min. Mobile phase A was then held at 100% from 36.5 to 39.5 min, after which the percentage of solvent A decreased to 25%, from 39.5 min to 43.1 min. The flow rate was then increased back to 0.4 mL/min from 43.1 to 47.6 minutes, and solvent A was maintained at 25% for the

remainder of the run (47.6 to 55.0 minutes). The qTOF operated in positive electrospray ionization mode (ESI+), and mass spectra were recorded in the m/z range of 300-1,700 at a rate of 1.5 spectra/s. The source conditions were set as follows: nebuliser gas at 25 psi, gas temperature at 200 °C, gas flow at 12 L/min, sheath gas temperature at 250 °C, sheath gas flow at 12 L/min, capillary voltage at 3,500 V, and nozzle voltage at 500 V. For identification purposes, tandem mass experiments (MS/MS) using data-dependent acquisition were performed, with a collision energy of 30 eV applied to the 10 most intense ions.

5.5.3 Data processing of LC-MS data and statistical analysis

The MS data were first processed using Agilent MassHunter Qualitative Analysis B.07 software. For the identification of N-glycans, total ion chromatograms (TIC) containing MS/MS fragmentation data were deconvoluted using the "find by molecular feature" algorithm, which detected chromatographic peaks considered to be N-glycans. The resulting list of entities containing the MS/MS data was exported and loaded to Simglycan software for molecular and structural elucidation. Simglycan is a high-throughput structural identification tool that uses a built-in database with theoretical fragmentation profiles to predict the structure of glycans. Following the identification process, 25 N-glycans were identified in *C. elegans*. Subsequently, the exact mass $[M+H]^+$, $[M+2H]^{2+}$ or $[M+3H]^{3+}$ of these structures were extracted on all samples using Agilent Mass Hunter Quantitative software (B.07) to create a refined matrix of quantitative data for statistical purposes. Finally, the obtained data matrix, which included the peak area for each identified N-glycan, was normalised by dividing the peak area of each N-glycan by the sum of the peak areas of all N-glycans within each respective sample.

5.6 Proteome analysis

5.6.1 Lysis, protein digestion and TMT labelling

A total of 5,000 worms were lysed in RIPA Buffer containing a protease/phosphatase inhibitor, before subjecting to bead beating combined with a freeze-thaw cycle. Two stainless steel balls (3.2 mm

diameter) were added before subjecting the samples to bead beating for 3 min at medium speed (Bullet Blender, Cultek, Barcelona, Spain); this step was performed in triplicate. Proteins in the supernatant were precipitated with TCA/acetone overnight. After discarding the supernatant, the pellet was resuspended in 6M urea in 50 mM ABC and the concentration was quantified using the Bradford method prior to the digestion procedure. Samples were reduced and alkylated using DTT and IAA, respectively, followed by overnight trypsin digestion (ratio 1:100). Digested proteins were desalted onto HLB SPE cartridges (Waters, Bedford, MA, USA) and peptides were eluted with 80% ACN, 20% water and 0.1% formic acid before drying in a SpeedVac concentrator and labelling with TMT 10-plex (Thermo Fisher Scientific) according to the manufacturer's instructions. A pool of all samples was labelled with the 126-Tag and included in each batch to normalise all samples and TMT batches. Then, the labelled peptides from each sample were mixed and desalted again on HLB SPE columns.

5.6.2 nanoLC-MS/MS analysis

After labelling with TMT 10-plex and before nano LC-MS/MS analysis, peptides were fractionated using the Pierce High pH Reversed-Phase Peptide Fractionation Kit (Thermo Fisher Scientific), following the manufacturer's instructions. The 9 fractions obtained were then loaded on a trap nanocolumn (0.01 × 2 cm, 5 µm, Thermo Fisher Scientific) coupled to a C18 reversed-phase (RP) nanocolumn (0.0075 × 12 cm 3 µm, Nikkyo Technos Co. Ltd., Japan) for chromatographic analysis. Chromatographic separation was completed with a 175-min gradient (0–1 min., 2% B isocratic; 1–26 min., 2–12% B; 26–126 min., 12–32% B; 126–146 min., 32–52% B; 146–161 min., 52–95% B; and 161–176 min., 95% B isocratic). The mobile phase consisted of Milli-Q water containing 0.1% formic acid and ACN with 0.1% formic acid, at a flow rate of 300 nL/min. MS analyses were performed on a LTQ-Orbitrap Velos Pro (Thermo Fisher Scientific) by acquiring an enhanced FT-resolution spectrum (R = 30,000 FHMW), followed by two data dependent MS/MS scans (FT—(CID)MS/MS at 35%

NCE and FT-(HCD) MS/MS R = 15,000 FHMW) of the ten most intense parent ions with a charge state rejection of one and a dynamic exclusion of 1 min.

5.6.3 Data processing of LC-MS data

Proteins were identified with Proteome Discover Software (version 1.4; Thermo Scientific, Germany) combined with the Mascot search engine (version 2.5). The *C. elegans* protein database was used to screen the data and identify proteins. Two missed cleavages for trypsin digestion and an error of 0.02 Da for the FT-MS/MS fragment ion mass, 0.8 Da for the IT-MS/MS fragment ion mass and 10.0 ppm for the FT-MS parent ion mass were allowed. TMT 10plex on lysine and the N-termini were set as quantification modifications, while oxidation of methionine and acetylation of N-termini were set as dynamic modifications and carbamidomethylation of cysteine was set as a static modification. The FDR and protein probabilities were calculated using a fixed PSM validator.

5.7 Lipidomics analysis

5.7.1 Sample preparation

Samples were extracted using an adapted Folch procedure [51–53]. A total of 5,000 worms were extracted with 1,500 µL of chloroform:methanol (2:1, v,v) containing the internal standard mixture (Lipidomic SPLASH®, Avanti Lipids) and homogenized using a bead beating method combined with a freeze-thaw cycle. Afterwards, 300 µL of water with NaCl (0.9%) were added and centrifuged at 15,000 rpm for 10 min to promote liquid phase separation. The lower phase was recovered, evaporated to dryness and reconstituted with methanol:methyl-tert-butyl ether (9:1, v,v) for LC-MS analysis.

5.7.2 LC-MS

Samples were analysed using an Agilent UHPLC 1290 Infinity Series coupled to an Agilent qTOF/MS 6550 Series (Agilent Technologies, Santa Clara, CA). The chromatographic separation consists in an elution with a ternary mobile phase containing water with 10mM ammonium formate and 0.1% formic acid (solvent A), methanol (solvent B) and 2-propanol

(solvent C). The stationary phase was a C18 column (Kinetex EVO C18 Column, 2.6 µm, 2.1 mm X 100 mm) that allows the sequential elution of the more hydrophobic lipids such as lysophospho-lipids, sphingomyelins, phospholipids, diglycerides, triglycerides and cholesteryl esters, among others. The flow rate was 0.6 mL min/min, the injection volume was 2 µL, and the column temperature was set to 60 °C. The gradient employed was 0–0.5 min, 55–45% A + 10% B; 0.5–1.5 min, 45–42.8% A + 10–9.5% B; 1.5–1.6 min, 42.8–34% A + 9.5–7.5% B; 1.6–5 min, 34–31.8% A + 7.5–7% B; 5–5.1 min, 31.8–18.6% A + 7–4% B; 5.1–7.5 min, 18.6–16.4% A + 4–3.5% B; 7.5–9 min, 16.4% A + 3.5% B; 9–9.5 min, 16.4–0% A + 3.5–0% B; 9.5–11.5min, 0% A + 0% B; 11.5–11.6 min, 0–45% A + 0–10% B; and 24.75–29.25, 55–45% A + 10% B. The qTOF operated in positive electrospray ionisation mode (ESI+), and mass spectra were recorded between m/z 300–1,700 at 3 spectra/s. The source conditions were 35 psi for nebuliser gas, 225 °C for gas temperature, 11 L/min for gas flow, 300 °C for sheath gas temperature, 12 L/min for sheath gas flow, 3,500 V for capillary voltage and 500 V for nozzle voltage.

5.7.3 Data processing of LC-MS data

The MS data were processed using both Agilent MassHunter Qualitative and Quantitative Analysis B.07 software. The identification of lipid species was performed by matching their accurate mass and tandem mass spectrum, when available, to Metlin-PCDL from Agilent containing more than 40,000 metabolites and lipids. LipidCreator workbench was also used for targeted exact mass list generation [54]. In addition, chromatographic behaviour of pure standards for each family and bibliographic information was used to ensure their putative identification. After putative identification of lipids, these were quantified in terms of internal standard response ratio using one internal standard for each lipid family by using Agilent Mass Hunter Quantitative software (B.07) to create a refined matrix of quantitative data for statistical purposes.

5.8 Statistical analysis

Lifespan data were plotted as Kaplan–Meier survival curves and statistical analyses were performed using the logrank (Mantel–Cox) test in OASIS2 [64]. Non-parametric Kruskal-Wallis and Mann-Whitney tests were used to assess significant differences between time points and diets in all strains, in glycomics, proteomics, lipidomics and gene expression analyses. For these analyses, Metaboanalyst 5.0. [65] and Mass Profiler Professional (MPP) software v.15.1 (Agilent Technologies, Massachusetts, USA) were employed. For the proteomics data, enrichment analyses were conducted using STRING [66] and DAVID [32], before plotting using REVIGO [33]. Additional graphical representations were generated with Metaboanalyst 5.0. Results were considered statistically significant at $p < 0.05$.

5.9 Correlation network analysis

The correlation heatmaps and networks were constructed with R (version 4.2.0). Pearson correlation was calculated for each molecular pair to assess linear relationships under different conditions. The Pearson correlation coefficient for each pair of molecular species was used to plot the heatmap with R package ggplot. Correlation network analysis was performed to combine correlations from proteomics, glycomics and lipidomics data for various conditions. Only the molecular pairs with Pearson coefficient > 0.95 were used to visualise the network, done using R package igraph.

REFERENCES

1. Aston, L.M. Glycaemic index and metabolic disease risk. *Proc. Nutr. Soc.* **2006**, *65*, 125–134, doi:10.1079/PNS2005485.

2. Venn, B.J.; Green, T.J. Glycemic index and glycemic load: measurement issues and their effect on diet-disease relationships. *Eur. J. Clin. Nutr.* **2007**, *61 Suppl 1*, S122–S131, doi:10.1038/SJ.EJCN.1602942.

3. Lee, S.J.; Murphy, C.T.; Kenyon, C. Glucose Shortens the Lifespan of Caenorhabditis elegans by Down-Regulating Aquaporin Gene Expression. *Cell Metab.* **2009**, *10*, 379, doi:10.1016/J.CMET.2009.10.003.

4. Alcántar-Fernández, J.; Navarro, R.E.; Salazar-Martínez, A.M.; Pérez-Andrade, M.E.; Miranda-Ríos, J. Caenorhabditis elegans respond to high-glucose diets through a network of stress-responsive transcription factors. *PLoS One* **2018**, *13*, 1–24, doi:10.1371/journal.pone.0199888.

5. Ray, P.D.; Huang, B.W.; Tsuji, Y. Reactive oxygen species (ROS) homeostasis and redox regulation in cellular signaling. *Cell. Signal.* **2012**, *24*, 981–990, doi:10.1016/J.CELLSIG.2012.01.008.

6. Bonomini, F.; Rodella, L.F.; Rezzani, R. Metabolic syndrome, aging and involvement of oxidative stress. *Aging Dis.* **2015**, *6*, 109–120, doi:10.14336/AD.2014.0305.

7. Schlotterer, A.; Kukudov, G.; Bozorgmehr, F.; Hutter, H.; Du, X.; Oikonomou, D.; Ibrahim, Y.; Pfisterer, F.; Rabbani, N.; Thornalley, P.; et al. C. elegans as Model for the Study of High Glucose– Mediated Life Span Reduction. *Diabetes* **2009**, *58*, 2450, doi:10.2337/DB09-0567.

8. Corsi, A.K.; Wightman, B.; Chalfie, M. A Transparent Window into Biology: A Primer on Caenorhabditis elegans. *Genetics* **2015**, *200*, 387–407, doi:10.1534/GENETICS.115.176099.

9. Maglioni, S.; Arsalan, N.; Ventura, N. C. elegans screening strategies to identify pro-longevity interventions. *Mech. Ageing Dev.* **2016**, *157*, 60–69, doi:10.1016/J.MAD.2016.07.010.

10. Paschinger, K.; Yan, S.; Wilson, I.B.H. N-glycomic complexity in anatomical simplicity: Caenorhabditis elegans as a non-model nematode? *Front. Mol. Biosci.* **2019**, *6*, 9, doi:10.3389/FMOLB.2019.00009/BIBTEX.

11. Mondoux, M.A.; Love, D.C.; Ghosh, S.K.; Fukushige, T.; Bond, M.; Weerasinghe, G.R.; Hanover, J.A.; Krause, M.W. O-linked-N-acetylglucosamine cycling and insulin signaling are required for the glucose stress response in Caenorhabditis elegans. *Genetics* **2011**, *188*, 369–382, doi:10.1534/GENETICS.111.126490.

12. Choi, S.S. High glucose diets shorten lifespan of Caenorhabditis elegans via ectopic apoptosis induction. *Nutr. Res. Pract.* **2011**, *5*, 214–218, doi:10.4162/NRP.2011.5.3.214.

13. Altintas, O.; Park, S.; Lee, S.J. V. The role of insulin/IGF-1 signaling in the longevity of model invertebrates, C. elegans and D. melanogaster. *BMB Rep.* **2016**, *49*, 81–92, doi:10.5483/BMBREP.2016.49.2.261.

14. Kenyon, C.; Chang, J.; Gensch, E.; Rudner, A.; Tabtiang, R. A C. elegans mutant that lives twice as long as wild type. *Nature* **1993**, *366*, 461–464, doi:10.1038/366461A0.

15. Kimura, K.D.; Tissenbaum, H.A.; Liu, Y.; Ruvkun, G. daf-2, an insulin receptor-like gene that regulates longevity and diapause in Caenorhabditis elegans. *Science* **1997**, *277*, 942–946, doi:10.1126/SCIENCE.277.5328.942.

16. Castro, C.; Krumsiek, J.; Lehrbach, N.J.; Murfitt, S.A.; Miska, E.A.; Griffin, J.L. A study of Caenorhabditis elegans DAF-2 mutants by metabolomics and differential correlation networks. *Mol. Biosyst.* **2013**, *9*, 1632, doi:10.1039/C3MB25539E.

17. Baumeister, R.; Schaffitzel, E.; Hertweck, M. Endocrine signaling in Caenorhabditis elegans controls stress response and longevity. *J. Endocrinol.* **2006**, *190*, 191–202, doi:10.1677/joe.1.06856.

18. Murphy, C.T.; McCarroll, S.A.; Bargmann, C.I.; Fraser, A.; Kamath, R.S.; Ahringer, J.; Li, H.; Kenyon, C. Genes that act downstream of DAF-16 to influence the lifespan of Caenorhabditis elegans. *Nat. 2003 4246946* **2003**, *424*, 277–283, doi:10.1038/nature01789.

19. Lin, K.; Hsin, H.; Libina, N.; Kenyon, C. Regulation of the Caenorhabditis elegans longevity protein DAF-16 by insulin/IGF-1 and germline signaling. *Nat. Genet. 2001 282* **2001**, *28*, 139–145, doi:10.1038/88850.

20. Oguntibeju, O.O. Type 2 diabetes mellitus, oxidative stress and inflammation: examining the links. *Int. J. Physiol. Pathophysiol. Pharmacol.* **2019**, *11*, 45.

21. Liu, J.; Chen, S.; Biswas, S.; Nagrani, N.; Chu, Y.; Chakrabarti, S.; Feng, B. Glucose-induced oxidative stress and accelerated aging in endothelial cells are mediated by the depletion of mitochondrial SIRTs. *Physiol. Rep.* **2020**, *8*, doi:10.14814/PHY2.14331.

22. Jiménez del Val, I.; Constantinou, A.; Dell, A.; Haslam, S.; Polizzi, K.M.; Kontoravdi, C. A quantitative and mechanistic model for monoclonal antibody glycosylation as a function of nutrient availability during cell culture. *BMC Proc. 2013 76* **2013**, *7*, 1–3, doi:10.1186/1753-6561-7-S6-O10.

23. Paton, B.; Suarez, M.; Herrero, P.; Canela, N.; Cairo, W.; Garozzo, D.; Pshezhetsky, A. V Glycosylation Biomarkers Associated with Age-Related Diseases and Current Methods for Glycan Analysis. *Int. J. Mol. Sci. 2021, Vol. 22, Page 5788* **2021**, *22*, 5788, doi:10.3390/IJMS22115788.

24. Brewer, R.A.; Gibbs, V.K.; Daniel L. Smith, J. Targeting glucose metabolism for healthy aging. *Nutr. Heal. Aging* **2016**, *4*, 31, doi:10.3233/NHA-160007.

25. Zhang, S.; Li, F.; Zhou, T.; Wang, G.; Li, Z. Caenorhabditis elegans as a Useful Model for Studying Aging Mutations. *Front. Endocrinol. (Lausanne).* **2020**, *11*, 554994, doi:10.3389/FENDO.2020.554994.

26. Croll, N.A.; Smith, J.M.; Zuckerman, B.M. The aging process of the nematode Caenorhabditis elegans in bacterial and axenic culture. *Exp. Aging Res.* **1977**, *3*, 175–189, doi:10.1080/03610737708257101.

27. Huang, C.; Xiong, C.; Kornfeld, K. Measurements of age-related changes of physiological processes that predict lifespan of Caenorhabditis elegans. *Proc. Natl. Acad. Sci. U. S. A.* **2004**, *101*, 8084, doi:10.1073/PNAS.0400848101.

28. Jiang, H.C.; Hsu, J.M.; Yen, C.P.; Chao, C.C.; Chen, R.H.; Pan, C.L. Neural activity and CaMKII protect mitochondria from fragmentation in aging Caenorhabditis elegans neurons. *Proc. Natl. Acad. Sci. U. S. A.* **2015**, *112*, 8768–8773, doi:10.1073/PNAS.1501831112/-/DCSUPPLEMENTAL.

29. Narayan, V.; Ly, T.; Pourkarimi, E.; Murillo, A.B.; Gartner, A.; Lamond, A.I.; Kenyon, C. Deep Proteome Analysis Identifies Age-Related Processes in C. elegans. *Cell Syst.* **2016**, *3*, 144–159, doi:10.1016/j.cels.2016.06.011.

30. Yan, S.; Vanbeselaere, J.; Jin, C.; Blaukopf, M.; Wöls, F.; Wilson, I.B.H.; Paschinger, K. Core Richness of N-Glycans of Caenorhabditis elegans: A

Case Study on Chemical and Enzymatic Release. *Anal. Chem.* **2018**, *90*, 928–935, doi:10.1021/ACS.ANALCHEM.7B03898/ASSET/IMAGES/LARGE/AC-2017-03898Q_0005.JPEG.

31. Sheikh, M.O.; Tayyari, F.; Zhang, S.; Judge, M.T.; Weatherly, D.B.; Ponce, F. V.; Wells, L.; Edison, A.S. Correlations between LC-MS/MS-detected glycomics and NMR-detected metabolomics in Caenorhabditis elegans development. *Front. Mol. Biosci.* **2019**, *6*, 49, doi:10.3389/FMOLB.2019.00049/BIBTEX.

32. Huang, D.W.; Sherman, B.T.; Lempicki, R.A. Systematic and integrative analysis of large gene lists using DAVID bioinformatics resources. *Nat. Protoc. 2009 41* **2008**, *4*, 44–57, doi:10.1038/nprot.2008.211.

33. Supek, F.; Bošnjak, M.; Škunca, N.; Šmuc, T. REVIGO Summarizes and Visualizes Long Lists of Gene Ontology Terms. *PLoS One* **2011**, *6*, e21800, doi:10.1371/JOURNAL.PONE.0021800.

34. Kopito, R.R. Aggresomes, inclusion bodies and protein aggregation. *Trends Cell Biol.* **2000**, *10*, 524–530, doi:10.1016/S0962-8924(00)01852-3.

35. Copes, N.; Edwards, C.; Chaput, D.; Saifee, M.; Barjuca, I.; Nelson, D.; Paraggio, A.; Saad, P.; Lipps, D.; Stevens, S.M.; et al. Metabolome and proteome changes with aging in Caenorhabditis elegans. *Exp. Gerontol.* **2015**, *72*, 67, doi:10.1016/J.EXGER.2015.09.013.

36. De Guzman, A.C. V.; Kang, S.; Kim, E.J.; Kim, J.H.; Jang, N.; Cho, J.H.; Choi, S.S. High-Glucose Diet Attenuates the Dopaminergic Neuronal Function in C. elegans, Leading to the Acceleration of the Aging Process. *ACS Omega* **2022**, *7*, 32339–32348, doi:10.1021/ACSOMEGA.2C03384/ASSET/IMAGES/LARGE/AO2C03384_0009.JPEG.

37. Zhu, G.; Yin, F.; Wang, L.; Wei, W.; Jiang, L.; Qin, J. Modeling type 2 diabetes-like hyperglycemia in C. elegans on a microdevice. *Integr. Biol.* **2016**, *8*, 30–38, doi:10.1039/C5IB00243E.

38. Walther, D.M.; Kasturi, P.; Zheng, M.; Pinkert, S.; Vecchi, G.; Ciryam, P.; Morimoto, R.I.; Dobson, C.M.; Vendruscolo, M.; Mann, M.; et al. Widespread Proteome Remodeling and Aggregation in Aging C. elegans. *Cell* **2015**, *161*, 919–932, doi:10.1016/J.CELL.2015.03.032.

39. Paschinger, K.; Wöls, F.; Yan, S.; Jin, C.; Vanbeselaere, J.; Dutkiewicz, Z.; Arcalis, E.; Malzl, D.; Wilson, I.B.H. N-glycan antennal modifications are altered in Caenorhabditis elegans lacking the HEX-4 N-acetylgalactosamine-specific hexosaminidase. *J. Biol. Chem.* **2023**, *299*, doi:10.1016/J.JBC.2023.103053.

40. Cipollo, J.F.; Costello, C.E.; Hirschberg, C.B. The fine structure of Caenorhabditis elegans N-glycans. *J. Biol. Chem.* **2002**, *277*, 49143–49157, doi:10.1074/JBC.M208020200.

41. Haslam, S.M.; Gems, D.; Morris, H.R.; Dell, A. The glycomes of Caenorhabditis elegans and other model organisms. *Biochem. Soc. Symp.*

2002, *69*, 117–134, doi:10.1042/BSS0690117/95316.

42. Natsuka, S.; Adachi, J.; Kawaguchi, M.; Nakakita, S.I.; Hase, S.; Ichikawa, A.; Ikura, K. Structural analysis of N-linked glycans in Caenorhabditis elegans. *J. Biochem.* **2002**, *131*, 807–813, doi:10.1093/OXFORDJOURNALS.JBCHEM.A003169.

43. Paschinger, K.; Gutternigg, M.; Rendić, D.; Wilson, I.B.H. The N-glycosylation pattern of Caenorhabditis elegans. *Carbohydr. Res.* **2008**, *343*, 2041–2049, doi:10.1016/J.CARRES.2007.12.018.

44. Geyer, H.; Schmidt, M.; Müller, M.; Schnabel, R.; Geyer, R. Mass spectrometric comparison of N-glycan profiles from Caenorhabditis elegans mutant embryos. *Glycoconj. J.* **2012**, *29*, 135–145, doi:10.1007/S10719-012-9371-8.

45. Schachter, H. Paucimannose N-glycans in Caenorhabditis elegans and Drosophila melanogaster. *Carbohydr. Res.* **2009**, *344*, 1391–1396, doi:10.1016/J.CARRES.2009.04.028.

46. Wilson, I.B.H. The class I α1,2-mannosidases of Caenorhabditis elegans. *Glycoconj. J.* **2012**, *29*, 173–179, doi:10.1007/S10719-012-9378-1.

47. Cipollo, J.F.; Awad, A.M.; Costello, C.E.; Hirschberg, C.B. N-Glycans of Caenorhabditis elegans are specific to developmental stages. *J. Biol. Chem.* **2005**, *280*, 26063–26072, doi:10.1074/JBC.M503828200.

48. Wilson, I.B.H.; Yan, S.; Jin, C.; Dutkiewicz, Z.; Rendić, D.; Palmberger, D.; Schnabel, R.; Paschinger, K. Increasing Complexity of the N-Glycome During Caenorhabditis Development. *Mol. Cell. Proteomics* **2023**, *22*, 100505, doi:10.1016/J.MCPRO.2023.100505.

49. Perez, M.F.; Lehner, B. Vitellogenins - Yolk Gene Function and Regulation in Caenorhabditis elegans. *Front. Physiol.* **2019**, *10*, 1067, doi:10.3389/FPHYS.2019.01067.

50. Murphy, C.T. The search for DAF-16/FOXO transcriptional targets: approaches and discoveries. *Exp. Gerontol.* **2006**, *41*, 910–921, doi:10.1016/J.EXGER.2006.06.040.

51. Liang, V.; Ullrich, M.; Lam, H.; Lian Chew, Y.; Banister, S.; Song, X.; Zaw, T.; Kassiou, M.; Götz, J.; Nicholas, H.R. Altered proteostasis in aging and heat shock response in C. elegans revealed by analysis of the global and de novo synthesized proteome. *Cell. Mol. Life Sci* **2014**, *71*, 3339–3361, doi:10.1007/s00018-014-1558-7.

52. Depina, A.S.; Iser, W.B.; Park, S.S.; Maudsley, S.; Wilson, M.A.; Wolkow, C.A. Regulation of Caenorhabditis elegans vitellogenesis by DAF-2/IIS through separable transcriptional and posttranscriptional mechanisms. *BMC Physiol.* **2011**, *11*, doi:10.1186/1472-6793-11-11.

53. Harvald, E.B.; Sprenger, R.R.; Dall, K.B.; Ejsing, C.S.; Nielsen, R.; Mandrup, S.; Murillo, A.B.; Larance, M.; Gartner, A.; Lamond, A.I.; et al. Multi-omics Analyses of Starvation Responses Reveal a Central Role for Lipoprotein Metabolism in Acute Starvation Survival in C. elegans. *Cell Syst.* **2017**, *5*, 38-52.e4, doi:10.1016/J.CELS.2017.06.004.

54. Somogyvári, M.; Gecse, E.; Sőti, C. DAF-21/Hsp90 is required for C. elegans longevity by ensuring DAF-16/FOXO isoform A function. *Sci. Rep.* **2018**, *8*, 12048, doi:10.1038/S41598-018-30592-6.

55. Cabreiro, F.; Ackerman, D.; Doonan, R.; Araiz, C.; Back, P.; Papp, D.; Braeckman, B.P.; Gems, D. Increased life span from overexpression of superoxide dismutase in Caenorhabditis elegans is not caused by decreased oxidative damage. *Free Radic. Biol. Med.* **2011**, *51*, 1575, doi:10.1016/J.FREERADBIOMED.2011.07.020.

56. Lee, S.J.; Hwang, A.B.; Kenyon, C. Inhibition of respiration extends C. elegans' lifespan via reactive oxygen species that increase HIF-1 activity. *Curr. Biol.* **2010**, *20*, 2131, doi:10.1016/J.CUB.2010.10.057.

57. Gille, B.; Galuska, C.E.; Fuchs, B.; Peleg, S. Recent Advances in Studying Age-Associated Lipids Alterations and Dietary Interventions in Mammals. *Front. Aging* **2021**, *2*, 773795, doi:10.3389/FRAGI.2021.773795/BIBTEX.

58. Brenner, S. The genetics of Caenorhabditis elegans. *Genetics* **1974**, *77*, 71–94, doi:10.1093/GENETICS/77.1.71.

59. Porta-de-la-Riva, M.; Fontrodona, L.; Villanueva, A.; Cerón, J. Basic Caenorhabditis elegans methods: Synchronization and observation. *J. Vis. Exp.* **2012**, 1–9, doi:10.3791/4019.

60. Lee, S.Y.; Kang, K. Measuring the Effect of Chemicals on the Growth and Reproduction of Caenorhabditis elegans. *J. Vis. Exp.* **2017**, *2017*, 56437, doi:10.3791/56437.

61. Hoogewijs, D.; Houthoofd, K.; Matthijssens, F.; Vandesompele, J.; Vanfleteren, J.R. Selection and validation of a set of reliable reference genes for quantitative sod gene expression analysis in C. elegans. *BMC Mol. Biol.* **2008**, *9*, 1–8, doi:10.1186/1471-2199-9-9/TABLES/3.

62. Pfaffl, M.W. A new mathematical model for relative quantification in real-time RT-PCR. *Nucleic Acids Res.* **2001**, *29*, E45, doi:10.1093/NAR/29.9.E45.

63. Paton, B.; Foguet-Romero, E.; Suarez, M.; Mayneris-Perxachs, J.; Boqué, N.; Caimari, A.; Canela, N.; Herrero, P. Brain N-Glycosylation and Lipidomic Profile Changes Induced by a High-Fat Diet in Dyslipidemic Hamsters. *Int. J. Mol. Sci.* **2023**, *24*, 2883, doi:10.3390/IJMS24032883/S1.

64. Han, S.K.; Lee, D.; Lee, H.; Kim, D.; Son, H.G.; Yang, J.-S.; Lee, S.-J. V.; Kim, S.; Han, S.K.; Lee, D.; et al. OASIS 2: online application for survival analysis 2 with features for the analysis of maximal lifespan and healthspan in aging research. *Oncotarget* **2016**, *7*, 56147–56152, doi:10.18632/ONCOTARGET.11269.

65. Pang, Z.; Chong, J.; Zhou, G.; De Lima Morais, D.A.; Chang, L.; Barrette, M.; Gauthier, C.; Jacques, P.É.; Li, S.; Xia, J. MetaboAnalyst 5.0: narrowing the gap between raw spectra and functional insights. *Nucleic Acids Res.* **2021**, *49*, W388–W396, doi:10.1093/NAR/GKAB382.

66. Szklarczyk, D.; Gable, A.L.; Lyon, D.; Junge, A.; Wyder, S.; Huerta-Cepas, J.; Simonovic, M.; Doncheva, N.T.; Morris, J.H.; Bork, P.; et al. STRING v11: protein-protein association networks with increased coverage, supporting

functional discovery in genome-wide experimental datasets. *Nucleic Acids Res.* **2019**, *47*, D607–D613, doi:10.1093/NAR/GKY1131.

SUPPLEMENTARY MATERIAL

Supplementary Table 1. List of identified N-glycans. rt, retention time.

ID	m/z	Z	glycan mass (with reducing end)	rt	Glycan composition
GLY1	603.765	2	894.336	7.670	Fuc1Hex2HexNAc2
GLY2	611.763	2	910.331	9.642	Hex3HexNAc2
GLY3	1368.553	1	1056.369	10.942	Fuc1Hex3HexNAc2
GLY4	1425.571	1	1113.386	11.525	Hex3HexNAc3
GLY5	1384.547	1	1072.362	12.376	Hex4HexNAc2
GLY6	1571.628	1	1259.443	12.825	Fuc1Hex3HexNAc3
GLY7	1628.647	1	1316.463	13.318	Hex3HexNAc4
GLY8	765.818	2	1218.441	13.855	Fuc1Hex4HexNAc2
GLY9	853.840	2	1394.485	14.124	Fuc1Hex5HexNAc2Me1
GLY10	887.858	2	1462.522	14.349	Fuc1Hex3HexNAc4
GLY11	795.819	2	1278.444	15.066	Hex3HexNAc3Pc1
GLY12	916.366	2	1519.538	15.156	Hex3HexNAc5
GLY13	773.803	2	1234.412	15.604	Hex5HexNAc2
GLY14	846.833	2	1380.471	16.456	Fuc1Hex5HexNAc2
GLY15	989.397	2	1665.598	16.500	Fuc1Hex3HexNAc5
GLY16	919.873	2	1526.552	17.934	Fuc2Hex5HexNAc2
GLY17	854.830	2	1396.465	18.517	Hex6HexNAc2
GLY18	927.871	2	1542.547	19.414	Fuc1Hex6HexNAc2
GLY19	956.380	2	1599.565	19.817	Hex6HexNAc3
GLY20	1000.886	2	1688.578	20.086	Fuc2Hex6HexNAc2
GLY21	935.855	2	1558.516	21.072	Hex7HexNAc2
GLY22	1122.426	2	1931.656	21.655	Neu5Ac1Hex5HexNAc4
GLY23	1016.882	2	1720.569	23.448	Hex8HexNAc2
GLY25	1097.908	2	1882.621	25.285	Hex9HexNAc2
GLY26	1178.932	2	2044.670	26.943	Hex10HexNAc2

Supplementary Table 2. Lifespan assays for each strain and condition. HGD, high-glucose diet; CD, control diet. The number of worms employed in each assay is specified between brackets.

% CB1370 CD [89]		% CB1370 HGD [114]		% CF1038 CD [90]		% CF1038 HFD [129]

#days	dead	censored		#days	dead	censored		#days	dead	censored		#days	dead	censored
1	0	0		1	0	0		1	0	0		1	0	9
2	0	0		2	0	0		2	0	0		2	0	3
3	0	0		3	0	0		3	0	0		3	0	3
4	0	0		4	0	0		4	0	0		4	3	0
5	0	0		5	0	0		5	0	0		5	3	3
6	0	0		6	0	0		6	0	0		6	6	0
7	0	3		7	0	0		7	0	0		7	0	0
8	0	3		8	1	8		8	0	0		8	0	0
9	0	3		9	2	10		9	0	0		9	0	0
10	0	0		10	0	0		10	0	0		10	0	0
11	1	2		11	0	0		11	0	6		11	3	6
12	2	4		12	0	0		12	0	9		12	0	0
13	0	0		13	0	0		13	3	6		13	0	0
14	0	0		14	0	3		14	6	0		14	3	0
15	0	0		15	0	3		15	0	0		15	0	0
16	0	0		16	0	0		16	0	0		16	0	0
17	0	0		17	1	0		17	3	3		17	0	0
18	0	0		18	2	0		18	0	0		18	3	0
19	0	1		19	0	0		19	0	0		19	3	0
20	2	2		20	0	0		20	3	3		20	9	0
21	1	1		21	1	0		21	6	0		21	12	0
22	1	0		22	1	0		22	3	0		22	12	0
23	1	0		23	1	0		23	3	0		23	12	0
24	1	0		24	0	0		24	6	0		24	9	0
25	0	2		25	2	2		25	4	0		25	9	0
26	0	4		26	4	1		26	5	0		26	0	0
27	2	2		27	2	0		27	4	0		27	6	0
28	1	1		28	1	0		28	2	0		28	3	0
29	1	0		29	3	0		29	3	0		29	9	0
30	2	0		30	3	0		30	0	0				
31	4	0		31	2	0		31	0	0				
32	5	0		32	2	0		32	6	0				
33	3	0		33	2	0		33	6	0				
34	3	0		34	9	0								
35	0	0		35	6	0								
36	0	0		36	6	0								

37	3	0		37	9	0								
38	3	0		38	6	0								
39	2	0		39	6	0								
40	1	0		40	2	0								
41	1	0		41	1	0								
42	2	0		42	6	0								
43	0	0		43	3	0								
44	2	0		44	1	0								
45	2	0		45	2	0								
46	1	0		46	0	0								
47	1	0												
48	0	0												
49	3	0												
50	0	0												
51	2	0												
52	1	0												
53	2	0												
54	1	0												
55	3	0												
56	0	0												
57	1	0												

% N2 CD [147]				**% N2 HGD [189]**		
#days	**dead**	**censored**		**#days**	**dead**	**censored**
1	0	0		1	0	0
2	0	0		2	0	0
3	0	0		3	0	0
4	0	0		4	0	0
5	0	0		5	0	9
6	0	9		6	6	0
7	0	9		7	0	0
8	0	9		8	3	0
9	0	0		9	3	15
10	0	0		10	0	15
11	0	3		11	3	0
12	3	0		12	0	6

13	0	0		13	0	6
14	0	3		14	6	15
15	0	15		15	0	9
16	0	0		16	9	0
17	0	0		17	0	0
18	3	0		18	0	6
19	3	0		19	9	3
20	0	0		20	3	0
21	0	0		21	3	0
22	0	6		22	6	0
23	3	0		23	3	0
24	0	0		24	6	3
25	0	0		25	6	0
26	6	3		26	0	0
27	0	0		27	6	3
28	0	3		28	12	0
29	9	0		29	7	0
30	0	0		30	8	0
31	9	0				
32	0	0				
33	6	0				
34	6	0				
35	9	0				
36	3	0				
37	6	3				
38	9	0				
39	3	0				
40	3	0				
41	0	0				
42	3	0				

Supplementary Table 3. List of primers. Pairs of primers used in the qRT-PCR analysis. Tm, primer melting temperature.

Gene	**Sequence**	**Tm (°C)**
Y45F10D.4	Fw gcgaaaacactcctgcac	60
	Rev tttcgcgggttctcgtagtg	
sbp-1	Fw CTT CTC AAT GCG ATT TTC CC	55
	Rev TCC AGA TAA TTG TTG GGT GG	

crh-1	Fw ATG GAG TCA CTG GTT TTC AAT	55
	Rev TTG TGG TCC TCC TGG AAA TA	
hif-1	Fw CGG AAA AGA AAC ATG GAA CG	55
	Rev CGA TTC TTT AGA CCG ACG AT	
cep-1	Fw CCC AAG TTT GAG CGC AGA ATG	60
	Rev CCG ATG TCC TGC GAA TCG GG	
skn-1c	Fw AAG GGC ACA CGA CAA GTG G	60
	Rev AGC ATT CTC TTC GGC AGT GAG	
daf-16	Fw AAA GAG CTC GTG GTG GGT TA	63
	Rev TTC GAG TTG AGC CTT TGT AGT CG	

Supplementary Table 4. List of identified lipids. rt, retention time; DG, diacylglycerides; LPC, lysophosphatidylcholines; PC, phosphatidylcholines; PE, phosphatidylethanolamines ;SM, sphingomyelins; TG, triglycerides.

Compound	**m/z**	**rt**		**Compound**	**m/z**	**rt**
DG(32:0) [M+NH4]+	586.541	6.243		TG(48:1) [M+NH4]+	822.755	8.261
DG(34:0) [M+NH4]+	614.572	6.515		TG(48:2) [M+NH4]+	820.739	8.084
DG(34:2)	593.514	3.765		TG(48:3) [M+NH4]+	818.724	7.845
DG(34:3)	591.499	6.238		TG(48:4) [M+NH4]+	816.708	7.668
DG(35:4)	603.499	6.165		TG(48:5) [M+NH4]+	814.692	7.563
DG(35:5)	601.483	5.661		TG(49:0) [M+NH4]+	838.787	9.009
DG(36:0) [M+NH4]+	642.604	6.885		TG(49:1) [M+NH4]+	836.771	8.444
DG(36:1) [M+NH4]+	640.588	3.526		TG(49:2) [M+NH4]+	834.755	8.206
DG(36:2)	621.546	4.303		TG(49:3) [M+NH4]+	832.739	7.978
DG(36:2) [M+NH4]+	638.572	6.426		TG(49:4) [M+NH4]+	830.724	7.818
DG(36:3)	619.530	6.498		TG(50:1) [M+NH4]+	850.787	8.903
DG(36:5)	615.499	6.104		TG(50:2) [M+NH4]+	848.771	8.582
DG(37:4)	631.530	6.470		TG(50:3) [M+NH4]+	846.755	8.139
DG(37:5)	629.514	6.265		TG(50:4) [M+NH4]+	844.739	7.956
DG(37:6)	627.499	6.027		TG(50:5) [M+NH4]+	842.724	7.773
DG(37:6) [M+NH4]+	644.525	5.937		TG(50:6) [M+NH4]+	840.708	7.657
DG(38:3)	647.561	6.896		TG(51:0) [M+NH4]+	866.818	9.187
DG(38:4)	645.545	6.730		TG(51:1) [M+NH4]+	864.802	8.810
DG(38:5)	643.530	6.575		TG(51:2) [M+NH4]+	862.787	8.610
DG(38:7)	639.499	6.170		TG(51:3) [M+NH4]+	860.771	8.383
DG(39:4)	659.561	6.857		TG(51:4) [M+NH4]+	858.755	8.084
DG(39:5)	657.545	6.663		TG(51:5) [M+NH4]+	856.739	7.923

Compound	m/z	rt		Compound	m/z	rt
DG(39:6) [M+NH4]+	672.556	6.403		TG(51:6) [M+NH4]+	854.724	7.801
DG(40:4)	673.575	6.963		TG(51:7) [M+NH4]+	852.709	7.635
DG(40:6) [M+NH4]+	686.572	2.516		TG(52:0) [M+NH4]+	880.833	9.459
DG(42:4) [M+OH]+	717.601	6.443		TG(52:1) [M+NH4]+	878.818	9.060
DG(O-38:5) [M+NH4]+	646.577	6.298		TG(52:2) [M+NH4]+	876.802	8.810
LPC(14:0)	468.309	1.990		TG(52:3) [M+NH4]+	874.787	8.538
LPC(14:1)	466.294	1.624		TG(52:4) [M+NH4]+	872.770	8.289
LPC(15:0)	482.324	2.068		TG(52:5) [M+NH4]+	870.755	8.078
LPC(16:0)	496.340	1.597		TG(52:6) [M+NH4]+	868.739	7.929
LPC(16:1)	494.324	1.991		TG(52:7) [M+NH4]+	866.724	7.729
LPC(17:0)	510.356	1.791		TG(52:8) [M+NH4]+	864.708	7.585
LPC(17:1)	508.340	1.531		TG(53:1) [M+NH4]+	892.833	9.459
LPC(18:0)	524.371	2.024		TG(53:2) [M+NH4]+	890.818	9.015
LPC(18:1)	522.356	1.702		TG(53:3) [M+NH4]+	888.802	8.627
LPC(18:2)	520.340	1.481		TG(53:6) [M+NH4]+	882.755	8.028
LPC(18:3)	518.325	1.292		TG(53:7) [M+NH4]+	880.739	7.884
LPC(19:0)	538.387	2.394		TG(53:8) [M+NH4]+	878.724	7.712
LPC(19:1)	536.372	1.935		TG(54:1) [M+NH4]+	906.849	9.592
LPC(19:4)	530.325	1.547		TG(54:2) [M+NH4]+	904.833	9.198
LPC(20:1)	550.387	2.239		TG(54:3) [M+NH4]+	902.818	8.810
LPC(20:2)	548.371	1.962		TG(54:4) [M+NH4]+	900.801	8.655
LPC(20:3)	546.356	1.641		TG(54:5) [M+NH4]+	898.786	8.405
LPC(20:4)	544.340	1.447		TG(54:6) [M+NH4]+	896.770	8.245
LPC(20:5)	542.325	1.287		TG(54:7) [M+NH4]+	894.755	8.051
LPE 20:1	508.3398	1.640		TG(54:8) [M+NH4]+	892.739	7.840
PC(31:0)	720.554	4.807		TG(55:1) [M+NH4]+	920.865	10.239
PC(32:1)	732.554	3.693		TG(55:10) [M+NH4]+	902.724	7.690
PC(33:1)	746.569	3.937		TG(55:2) [M+NH4]+	918.849	9.586
PC(33:2)	744.554	4.463		TG(55:3) [M+NH4]+	916.833	9.198
PC(33:3)	742.539	3.471		TG(55:4) [M+NH4]+	914.817	8.810
PC(33:4)	740.523	3.305		TG(55:5) [M+NH4]+	912.802	8.561
PC(33:5)	738.508	3.848		TG(55:6) [M+NH4]+	910.786	8.361
PC(34:1)	760.585	4.153		TG(55:7) [M+NH4]+	908.771	8.233
PC(34:2)	758.570	4.840		TG(55:8) [M+NH4]+	906.755	7.984
PC(34:3)	756.554	3.654		TG(55:9) [M+NH4]+	904.739	7.845
PC(34:5)	752.523	3.349		TG(56:10) [M+NH4]+	916.739	7.873
PC(35:2)	772.585	4.070		TG(56:11) [M+NH4]+	914.724	7.651
PC(35:3)	770.570	3.831		TG(56:2) [M+NH4]+	932.865	9.758

Compound	m/z	rt		Compound	m/z	rt
PC(35:4)	768.554	3.615		TG(56:4) [M+NH4]+	928.833	9.098
PC(35:5)	766.539	3.488		TG(56:5) [M+NH4]+	926.817	8.705
PC(36:2)	786.600	4.369		TG(56:6) [M+NH4]+	924.802	8.638
PC(36:3)	784.585	4.014		TG(56:7) [M+NH4]+	922.786	8.328
PC(36:5)	780.554	3.698		TG(56:8) [M+NH4]+	920.771	8.106
PC(36:7)	776.523	3.238		TG(56:9) [M+NH4]+	918.755	7.940
PC(37:2)	800.616	4.691		TG(57:1) [M+NH4]+	948.895	10.357
PC(37:4)	796.585	4.003		TG(57:11) [M+NH4]+	928.739	7.818
PC(37:6)	792.554	3.643		TG(57:12) [M+NH4]+	926.723	7.627
PC(38:2)	814.632	4.912		TG(57:2) [M+NH4]+	946.880	8.572
PC(38:5)	808.584	3.937		TG(57:3) [M+NH4]+	944.864	9.758
PC(38:6)	806.569	3.865		TG(57:4) [M+NH4]+	942.848	9.254
PC(38:7)	804.554	3.571		TG(57:5) [M+NH4]+	940.833	8.999
PC(39:10)	812.523	3.238		TG(57:6) [M+NH4]+	938.817	8.732
PC(39:4)	824.616	4.547		TG(57:7) [M+NH4]+	936.802	8.572
PC(39:5)	822.600	4.253		TG(57:8) [M+NH4]+	934.786	8.344
PC(39:6)	820.585	4.070		TG(57:9) [M+NH4]+	932.771	8.123
PC(39:9)	814.539	3.637		TG(58:1) [M+NH4]+	962.911	9.032
PC(40:10)	826.539	3.443		TG(58:10) [M+NH4]+	944.770	8.056
PC(40:9)	828.553	3.488		TG(58:11) [M+NH4]+	942.755	7.940
PC(42:10)	854.572	3.959		TG(58:12) [M+NH4]+	940.739	7.757
PC(42:11)	852.552	3.737		TG(58:13) [M+NH4]+	938.724	7.579
PC(42:12)	850.537	3.543		TG(58:2) [M+NH4]+	960.896	10.274
PC(O-34:1)	746.607	5.982		TG(58:3) [M+NH4]+	958.880	8.511
PC(O-35:3)	756.591	5.373		TG(58:4) [M+NH4]+	956.864	9.586
PC(O-37:2)	786.638	5.018		TG(58:6) [M+NH4]+	952.833	8.999
PC(O-39:3)	812.654	7.374		TG(58:7) [M+NH4]+	950.817	8.860
PC(O-39:5)	808.622	5.012		TG(58:9) [M+NH4]+	946.786	8.250
PC(O-40:5)	822.638	5.406		TG(59:1) [M+NH4]+	976.927	9.315
PE O-16:1p/20:0	732.5902	5.478		TG(59:10) [M+NH4]+	958.786	8.278
PE O-16:1p/22:5	750.5432	4.702		TG(59:11) [M+NH4]+	956.770	8.150
PE O-18:1p/18:1	730.5745	5.373		TG(59:13) [M+NH4]+	952.739	7.707
PE O-18:1p/18:2	728.5589	4.979		TG(59:2) [M+NH4]+	974.911	10.385
PE O-18:1p/18:3	726.5432	4.674		TG(59:3) [M+NH4]+	972.895	8.666
PE O-18:1p/20:4	752.5589	4.885		TG(59:4) [M+NH4]+	970.880	8.428
PE O-18:1p/22:6	776.5589	5.495		TG(59:5) [M+NH4]+	968.864	9.437
SM(d33:1)	689.559	3.437		TG(59:6) [M+NH4]+	966.848	9.403
SM(d35:0)	719.607	7.252		TG(59:7) [M+NH4]+	964.833	8.877

Compound	m/z	rt		Compound	m/z	rt
SM(d35:1)	717.591	3.654		TG(60:1)	990.944	9.603
SM(d35:3)	713.560	6.975		TG(60:1) [M+NH4]+	990.942	9.586
SM(d36:2)	729.591	7.252		TG(60:13) [M+NH4]+	966.755	7.856
SM(d39:1)	773.653	4.757		TG(60:14) [M+NH4]+	964.740	7.911
SM(d40:1)	787.669	5.134		TG(60:15) [M+NH4]+	962.724	7.579
SM(d41:3)	797.652	4.985		TG(60:2) [M+NH4]+	988.927	10.473
SM(d43:3)	825.683	8.023		TG(60:3) [M+NH4]+	986.911	8.921
SM(t34:0)	721.586	6.520		TG(60:4) [M+NH4]+	984.896	8.655
SM(t34:1)	719.570	7.258		TG(61:1) [M+NH4]+	1004.958	9.869
SM(t39:1)	789.648	4.436		TG(61:2) [M+NH4]+	1002.942	10.507
SM(t41:1)	817.679	5.179		TG(61:3) [M+NH4]+	1000.927	9.071
TG(39:1) [M+NH4]+	696.614	7.179		TG(62:1) [M+NH4]+	1018.974	10.202
TG(39:2) [M+NH4]+	694.599	7.052		TG(62:2) [M+NH4]+	1016.958	10.523
TG(40:0) [M+NH4]+	712.645	7.280		TG(62:3) [M+NH4]+	1014.942	9.503
TG(40:1) [M+NH4]+	710.630	7.108		TG(62:4) [M+NH4]+	1012.927	9.098
TG(40:2) [M+NH4]+	708.614	6.975		TG(63:1) [M+NH4]+	1032.989	10.340
TG(41:1) [M+NH4]+	724.646	7.269		TG(63:2) [M+NH4]+	1030.973	10.102
TG(41:2) [M+NH4]+	722.630	7.075		TG(63:3) [M+NH4]+	1028.958	9.753
TG(42:1) [M+NH4]+	738.661	7.551		TG(64:1) [M+NH4]+	1047.005	10.401
TG(44:1) [M+NH4]+	766.692	7.635		TG(64:2) [M+NH4]+	1044.989	10.274
TG(44:3) [M+NH4]+	762.661	7.484		TG(64:3) [M+NH4]+	1042.973	9.869
TG(45:0) [M+NH4]+	782.724	7.995		TG(65:1) [M+NH4]+	1061.021	10.468
TG(45:1) [M+NH4]+	780.708	7.773		TG(65:2) [M+NH4]+	1059.005	10.340
TG(45:2) [M+NH4]+	778.692	7.601		TG(65:3) [M+NH4]+	1056.989	10.257
TG(45:3) [M+NH4]+	776.677	7.628		TG(66:2) [M+NH4]+	1073.020	10.429
TG(46:1) [M+NH4]+	794.724	7.923		TG(67:1) [M+NH4]+	1089.052	10.551
TG(46:2) [M+NH4]+	792.708	7.707		TG(67:2) [M+NH4]+	1087.036	10.507
TG(46:3) [M+NH4]+	790.692	7.579		TG(67:3) [M+NH4]+	1085.020	10.412
TG(47:0) [M+NH4]+	810.755	8.317		TG(68:2) [M+NH4]+	1101.052	10.551
TG(47:1) [M+NH4]+	808.739	8.106		TG(68:3) [M+NH4]+	1099.036	10.484
TG(47:2) [M+NH4]+	806.724	7.862		TG(68:4) [M+NH4]+	1097.020	10.423
TG(47:3) [M+NH4]+	804.708	7.668		TG(69:2) [M+NH4]+	1115.067	10.568
TG(48:0) [M+NH4]+	824.771	8.798				

UNIVERSITAT ROVIRA I VIRGILI
EXPLORING THE ROLE OF GLYCANS: A NEW FRONTIER IN DISEASE BIOMARKER RESEARCH
Beatrix Paton Jimenez

Chapter 2

To examine how a high-fat diet can alter the brain N-glycan and lipid profile and evaluate the potential of a Mediterranean-like diet to reverse this situation

UNIVERSITAT ROVIRA I VIRGILI
EXPLORING THE ROLE OF GLYCANS: A NEW FRONTIER IN DISEASE BIOMARKER RESEARCH
Beatrix Paton Jimenez

PREFACE

Following one of the cross-cutting objectives already assessed in **Chapter 1**, we examined N-glycans on a second matrix and animal model, being brain samples from Golden Syrian hamsters. Following the line of the effect of dietary glucose on N-glycan profiles, in **Manuscript 3** we were inclined to see the effect of a high-fat diet on the brain N-glycome and lipidome, to further comprehend the role and response of N-glycans to changes in nutrition. Additionally, changes were evaluated when transitioning from a high-fat diet to a Mediterranean-like diet. This research holds the potential to provide valuable insights into the brain's plasticity and its ability to recover when subjected to contrasting and sequential lifestyle patterns.

Manuscript 3

Brain N-Glycosylation and Lipidomic Profile Changes Induced by a High-Fat Diet in Dyslipidemic Hamsters

Beatrix Paton, Elisabet Foguet-Romero, Manuel Suárez, Jordi Mayneris-Perxachs, Noemí Boqué, Antoni Caimari, Núria Canela and Pol Herrero

Article

Published in the International Journal of Molecular Sciences

Impact Factor: 6.208; Q1, Biochemistry & Molecular Biology

(2023) 24(3), 2883;

doi: 10.3390/ijms24032883

Brain N-Glycosylation and Lipidomic Profile Changes Induced by a High-Fat Diet in Dyslipidemic Hamsters

Beatrix Paton [1], Elisabet Foguet-Romero [1], Manuel Suarez [2,*], Jordi Mayneris-Perxachs [3,4], Noemí Boqué [5], Antoni Caimari [6], Núria Canela [1,*] and Pol Herrero [1]

[1] Eurecat, Centre Tecnològic de Catalunya, Centre for Omic Sciences, Joint Unit Eurecat-Universitat Rovira i Virgili, Unique Scientific and Technical Infrastructure (ICTS), 43204 Reus, Spain

[2] Nutrigenomics Research Group, Departament de Bioquímica I Biotecnologia, Universitat Rovira i Virgili, 43007 Tarragona, Spain

[3] Department of Diabetes, Endocrinology and Nutrition, Girona Biomedical Research Centre (IDIBGI), Hospital Universitari de Girona Doctor Josep Trueta, 17190 Girona, Spain

[4] CIBER Pathophysiology of Obesity and Nutrition (CIBEROBN), Instituto de Salud Carlos III, 28029 Madrid, Spain

[5] Eurecat, Centre Tecnològic de Catalunya, Technological Unit of Nutrition and Health, 43204 Reus, Spain

[6] Eurecat, Centre Tecnològic de Catalunya, Biotechnology Area, 43204 Reus, Spain

* Correspondence: Dr Manuel Suárez and Dr Núria Canela

ABSTRACT

The consumption of diets rich in saturated fats is known to be associated with higher mortality. The adoption of healthy habits, for instance adhering to a Mediterranean diet, has proved to exert a preventive effect towards cardiovascular diseases and dyslipidemia. Little is known about how a suboptimal diet can affect brain function, structure, and the mechanisms involved. The aims of this study were to examine how a high-fat diet can alter the brain N-glycan and lipid profile in male Golden Syrian hamsters and to evaluate the potential of a Mediterranean-like diet to reverse this situation. During twelve weeks, hamsters were fed a normal fat diet (CTRL group), a high-fat diet (HFD group), and a high-fat diet followed by a Mediterranean-like diet (MED group). Out of seventy-two identified N-glycans, fourteen were significant ($p < 0.05$) between HFD and CTRL groups, nine between MED and CTRL groups, and one between MED and HFD groups. Moreover, forty-nine lipids were altered between HFD and CTRL groups, seven between MED and CTRL groups, and five between MED and HFD groups. Our results suggest that brain N-glycan composition in high-fat diet-fed hamsters can produce events comparable to those found in some neurodegenerative diseases, and may promote brain ageing.

1. INTRODUCTION

A large portion of the world population has adopted unhealthy eating habits that can undermine healthcare systems unless current trends are inverted towards more sustainable lifestyle models [1]. In 2017, 11 million deaths were attributed to dietary risk factors, confirming that a suboptimal diet has an evident impact on mortality across nations [2].

A direct relationship exists between dietary patterns and obesity/overweight risk [3]. Therefore, it is important to understand the mechanisms that link diet with obesity, to find new effective preventable measures. Research has shown that obesity disturbs brain structure and function [4], and is associated with brain-level molecular changes [5]. Dietary interactions with the hypothalamus appear to be key in the development of obesity. Exposure to a high-fat diet (HFD) influences the proteome of the hypothalamus, showing cellular stress, altered synaptic plasticity, and altered mitochondrial function [6]. Moreover, the contribution of insulin resistance, essential fatty acid consumption, and oxidative stress, coordinated with inflammatory and vascular alterations, cause overall changes in brain function with the consumption of high-fat and high-glycemic index-type diets [7].

Recent evidence supports the idea that the microbiome could be poorly affected by HFDs, resulting in a state of dysbiosis, leading to increased insulin resistance and inflammation [8]. Dysbiosis is not only associated with gastrointestinal disorders but also with diseases affecting other distal organs. For instance, the nervous system and the gastrointestinal tract communicate through a bidirectional network of signaling pathways known as the gut-brain axis. However, numerous mechanisms behind the impact of the gut microbiota in neuro-development and -pathogenesis remain poorly understood [9].

An effective approach to improving lifestyle and decreasing risk factors contributing to non-communicable diseases can be obtained with

adherence to a dietary plan inspired by the principles of the Mediterranean Diet (MED) [1,10]. The MED is characterised by the high consumption of foods and nutrients presumed to be healthy for the organism and specifically for the brain, such as vegetables, fruits, fish, unsaturated fatty acids, and diverse antioxidants [11].

Adherence to the MED has been associated with a lower risk of obesity [12], cardiovascular mortality [13], and type-2 diabetes [14], amongst other diseases. Furthermore, compliance with MEDs has also been associated with slower cognitive decline [15] and a reduction in the incidence of neurodegenerative disorders such as Parkinson's disease [16] and Alzheimer's disease [17]. For instance, the increasing consumption of antioxidant-rich foods has been associated with better cognitive performance in elderly subjects at high cardiovascular risk [18].

Glycans are essential functional components that participate in numerous physiological processes aimed to maintain organ function and homeostasis in living organisms [19]. N-glycosylation has a wide variety of essential modulatory roles in glycoproteins that are involved in nervous system development and functioning [20]. This post-translational modification influences neuronal excitability and behaviour by affecting voltage-gated ion channels [21] and also alters neurotransmitter receptors, such as the α-amino-3-hydroxy-5-methyl-4-isoxazolepropionic acid receptor (AMPAR) [22] and the N-methyl-D-aspartate receptor (NMEDAR) [23]. More specifically, the loss of core fucosylation on AMPARs enhances their heteromerization, increasing sensitivity for postsynaptic depolarization and consequently activating NMEDARs. As a result, this event impairs long-term potentiation, which is closely related to learning and memory in the hippocampus [24].

Furthermore, N-glycosylation in the hippocampus is required for the consolidation and reconsolidation of contextual fear memory in mice [25]. However, research on how a HFD affects N-glycosylation is limited.

Barboza et al. suggested that chronic consumption of HFD and induced obesity results in abnormal hippocampal cell surface N-glycosylation [26].

Lipids also have essential roles in the nervous system. They are essential for cellular functioning due to their role in membrane composition, signalling, and energy metabolism. The brain is the second most abundant organ in terms of lipid concentration and diversity, only after adipose tissue [27]. The most representative lipid subtypes in the central nervous system are glycerophospholipids, sphingolipids, and sterol lipids. Altered lipid metabolism has been associated with structural damage, inflammatory processes, apoptotic signalling, and increased oxidative stress resulting in neural impairment leading to neurodegeneration [28]. Furthermore, a higher prevalence of obesity is known to increase the risk of developing several neurological disorders which have been associated with the increase of certain lipid species. For instance, in Alzheimer's disease, HIV, arteriosclerosis, and ageing, long-chain ceramides are found to be increased [29].

An unparalleled level of complexity exists in the development, organisation, and regulation of the brain, in which N-glycosylation plays a critical role, highlighting the need to identify and understand the unique N-glycan species involved. In line with our interest in obtaining a complete picture of brain protein N-glycosylation, the main aim of this study is to investigate how the brain N-glycan and lipid profile can be affected by a HFD, and evaluate the changes induced when switching to a Mediterranean-like diet after consuming a HFD. This research could shed more light on the plasticity of the brain and its capacity to recover when individuals are subjected to opposing and sequential lifestyle routines using a HFD followed by a switch to a healthy regime based on a Mediterranean-like diet. Golden Syrian hamster was selected for its similar response to humans in terms of lipoprotein metabolism and aortic lesion morphology when fed high cholesterol and saturated fat diets [30].

2. RESULTS AND DISCUSSION

In the present study, we hypothesised that the intake of a Mediterranean-like diet after the consumption of a HFD would ameliorate or reverse the alterations in the brain N-glycan and lipid profile, produced by the HFD, similar to what has been observed in liver steatosis [31]. The experimental design employed attempts to resemble, to some extent, a situation in which subjects showing a high adherence to unhealthy diets are advised to shift towards a healthier diet, such as the MED, to ameliorate alterations or diseases strongly associated with unbalanced diets.

2.1 Body composition, serum analyses, and histological evaluation

We assessed the changes in body weight, and biometric and serum variables of each hamster group at week 8 and week 12, as well as examining the phenotypic differences in all groups. Week-8 hamsters received either a NFD or HFD, whereas week-12 hamsters received either a complete HFD (HFD group), a complete NFD (CTRL group), or an 8-week HFD followed by a 4-week MED (MED group) (Figure 1A). As predicted, total cholesterol levels significantly increased in the HFD group compared to the CTRL group after 8 weeks (Table 1). No significant changes were found at this time between groups either in cumulative energy intake or in the biometric parameters (Table 1). At the endpoint (week 12), HFD hamsters displayed increased circulating levels of total cholesterol, low-density lipoprotein (LDL), and high-density lipoprotein (HDL) compared to the CTRL group (Table 2). The shift to a Mediterranean-like diet did not dampen the increase observed in the serum levels of lipids observed after the HFD challenge (Table 2). No differences were observed in final body weight ($p = 0.586$) in HFD-fed and CTRL animals, which can be partially attributed to a trend towards lower caloric intake in HFD-fed animals (Table 2). However, the HFD group showed significantly increased mesenteric white adipose tissue depot (MWAT) weight compared to the CTRL group, an increase that was also observed in the MED hamsters versus their CTRL counterparts. A higher caloric intake was observed in the MED hamsters compared to the HFD group (Table 2).

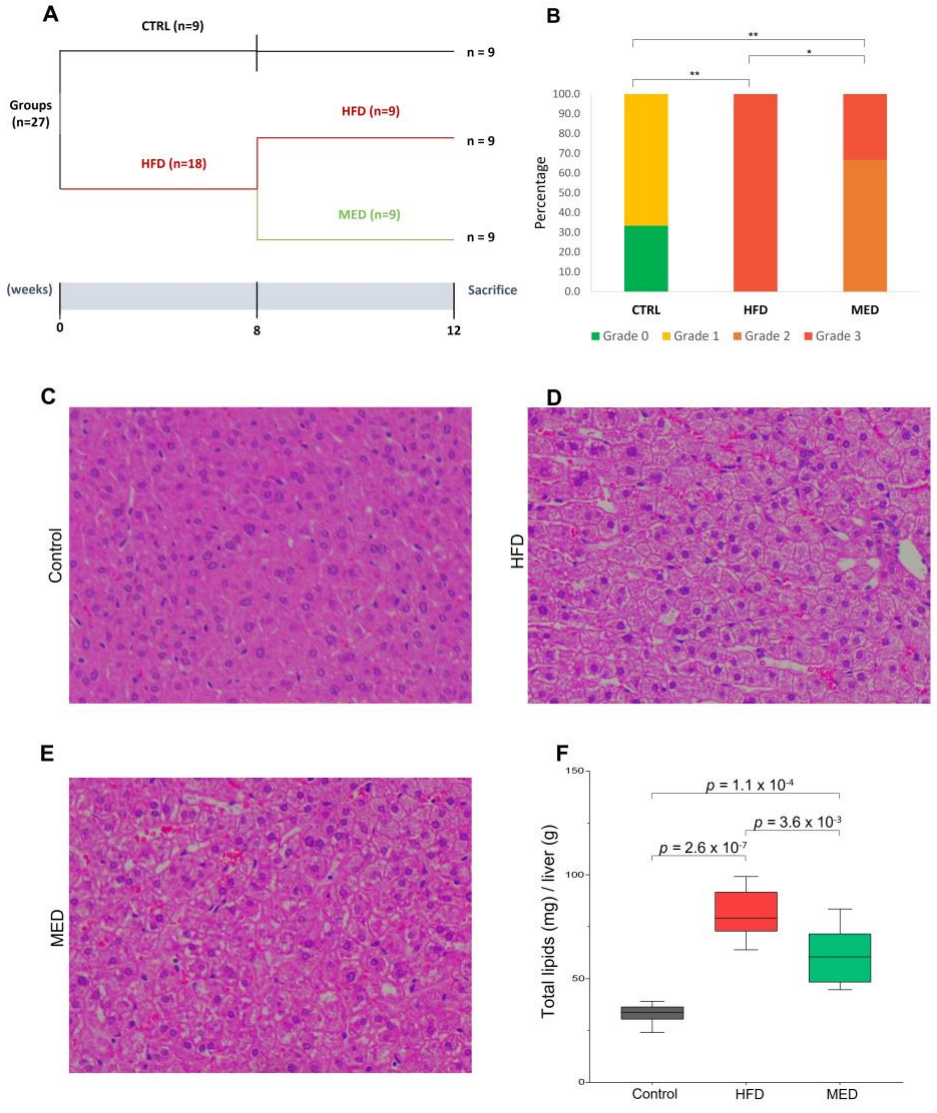

Figure 1. Effect of the HFD and MED on liver histology of Golden Syrian hamsters. (A) Outline of the experimental design. (B) Steatosis score of histological changes in the liver. Differences were detected using Fisher's exact test (* p-value < 0.05, ** p-value < 0.001). (C–E) Histological analysis of steatosis in liver sections stained with Hematoxylin and Eosin (400×). (F) Relative hepatic lipid content of hamsters in experimental groups. CTRL, normal diet; HFD, high-fat diet; MED, Mediterranean-like diet. Differences among groups in hepatic total lipid content were detected by Student t-test. All results were considered statistically significant at p-value < 0.05.

Table 1. Energy intake, body composition, and serum parameters of hamsters fed with a NFD (CTRL group) or a HFD (HFD group) in the 8th week of the study.

	Control (week 8) (n = 9)	**HFD (week 8) (n = 18)**
Cumulative food intake (kcal)	205.45 ± 14.08	198.81 ± 16.78
Biometric variables		
Body weight (g)	123.05 ± 5.14	120.76 ± 7.08
Fat mass (%)	11.94 ± 3.20	12.37 ± 2.14
Lean mass (%)	84.89 ± 3.26	84.09 ± 2.12
Lean/fat ratio	7.83 ± 3.22	7.04 ± 1.51
Serum parameters		
CHOL (mM) *	4.96 ± 0.66	8.30 ± 0.66

Data are shown as the mean ± SD. * indicates the significant difference ($p < 0.05$) between groups detected by Student's t test.

Table 2. Effects of HFD and MED on food intake and biometric and serum variables at the end of the study (week 12).

	Control (week 12) (n = 9)	**HFD (week 12) (n = 9)**	**MED (week 12) (n = 9)**
Cumulative food intake (kcal) [a]	126.8 ± 14.4	118.7 ± 8.3	133.3 ± 9.9
Biometric variables			
Body weight (g)	122.20 ± 5.62	119.60 ± 5.71	125.71 ± 10.71
Liver weight (g) [b,c]	4.23 ± 0.30	5.06 ± 0.43	5.43 ± 0.64
Liver weight (%) [b,c]	3.49 ± 0.25	4.27 ± 0.30	4.35 ± 0.25
MWAT (%) [b,c]	0.88 ± 0.24	1.13 ± 0.14	1.23 ± 0.22
MUS	0.27 ± 0.03	0.26 ± 0.03	0.26 ± 0.03
Fat mass (%)	11.28 ± 2.59	11.21 ± 2.12	13.34 ± 2.28
Lean mass (%)	85.42 ± 2.39	85.13 ± 2.17	83.32 ± 2.23
Lean/fat mass ratio	8.00 ± 2.13	7.88 ± 1.71	6.43 ± 1.21
Serum variables			
CHOL (mM) [b,c]	3.33 ± 0.49	6.01 ± 0.51	5.47 ± 0.64
HDL-C (mM) [b,c]	2.51 ± 0.50	3.78 ± 0.38	3.57 ± 0.73
LDL-C (mM) [b,c]	0.94 ± 0.27	2.03 ± 0.38	1.97 ± 0.34
TG (mM) [c]	5.83 ± 1.19	7.10 ± 4.13	10.48 ± 3.09

Data are shown as the mean ± SD. HFD, high fat diet. MED, Mediterranean-like diet. MWAT,

mesenteric white adipose tissue. MUS, gastrocnemius and soleus muscles. CHOL, total cholesterol. TG, triglyceride. Superscript letters indicate statistically significant differences detected by Student's t test ($p < 0.05$) between groups; [a] Differences for MED vs HFD, [b] differences for HFD vs CTRL, and [c] differences for MED vs CTRL.

In comparison with the CTRL group, the HFD hamsters also developed microvesicular steatosis without apparent inflammation or fibrosis (Figure 1C,D). In agreement with the histological analyses, the HFD group displayed a significant increase in lipid content compared to their control counterparts (Figure 1C). We observed that, at week 12, hamsters fed with the HFD had a significantly more severe grade of hepatic steatosis (measured as steatosis score after histological analysis) compared to those from the CTRL group ($p < 0.001$), and this HFD-induced hepatic steatosis was significantly attenuated in MED hamsters in comparison to their HFD counterparts (Fisher's exact test; p-value < 0.05) (Figure 1B). The shift to a Mediterranean-like diet for 4 weeks significantly decreased fatty liver microvesicular steatosis and, accordingly, decreased the total hepatic lipid content in the MED animals in comparison with the HFD hamsters (Figure 1F).

2.2 N-Glycosylation

Total brain N-glycan composition was determined and compared between groups. The Oxford nomenclature was used to annotate individual glycan structures where A represents the number of antennae present, F indicates the fucose, B indicates the presence of a bisecting N-acetylglucosamine, G represents galactoses, and S denotes sialic acids [32]. Figure 2 shows the N-glycan profile in brain tissue. Each identified glycan with its corresponding monoisotopic mass and composition can be found in Table S5.

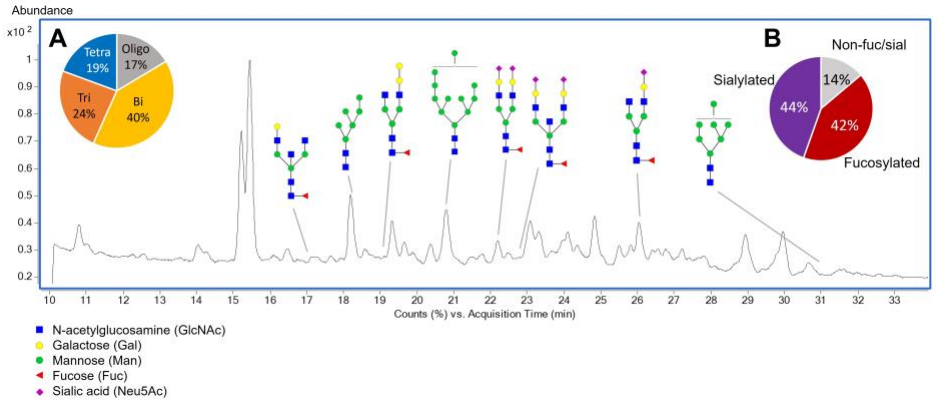

Figure 2. Representative chromatogram of the brain N-glycan profile representing selected statistically significant structures in the three groups (CTRL, HFD, and MED). (**A**) Pie chart depicting the degree of the 72 N-glycans identified in hamster brain tissue. Oligo, oligomannose; Bi, biantennary; Tri, triantennary; Tetra, tetrantennary. (**B**) Pie chart depicting the percentage of fucosylated and sialylated N-glycans in hamster brain tissue. Non-fuc/sial, non-fucosylated and non-sialylated N-glycans. Structural symbols for the N-glycans are shown below the chromatogram.

A high correlation exists between the glycosylation profiles in human and mouse brains, indicating little interspecies variation in brain glycosylation [33]. Complex/hybrid-fucosylated glycans have been reported to be the most abundant glycan class in the brain. Higher levels of fucosylation and lower levels of sialylation have been observed in the brain compared with serum [33,34]. The high content of high-mannose glycans is also characteristic of the brain glycosylation pattern. Oligomannosides tend to be eliminated during the processing of sugars to yield mature N-glycans, except in the brain, where they are carried to the cell surface on recognition molecules [35].

Several glycan classes, including mannose, complex, and tentative hybrid types were identified in our brain hamster samples. Two levels of confidence were used to assign the certainty with which a feature was assigned an N-glycan. The lowest level of confidence comprised 32 compounds, identified through Simglycan software. The composition of 2

additional compounds was determined using Simglycan and Glycostore. Lastly, with the highest degree of confidence, the composition and structure were identified for 38 N-glycans employing Simglycan and Glycostore. It is important to note that the use of the RFMS kit provided high intensities and high signal enhancement for neutral glycans, consequently allowing the identification of a large amount of N-glycans.

Regarding the research on the influence of a HFD and a MED, we found some statistically significant differences in N-glycans between HFD and MED vs. CTRL, but no relevant differences between MED and HFD. These results suggested that the HFD, which was administrated before the MED nutritional intervention, exerted a high impact on glycan composition compared to the second nutritional intervention with a MED. In more detail, the statistical analysis revealed statistically significant changes in fourteen N-glycans (p-value < 0.05) for the HFD group vs. CTRL group, nine for the MED group vs. CTRL group and, only one for the MED group vs. HFD group. The composition and structure of the statistically significant N-glycans are shown in Table 3. Complex N-glycans accounted for approximately 83% of these statistically significant features, while high mannose glycans accounted for approximately 17%.

Table 3. Statistically significant brain N-glycans by week 12 in the three different pairs of conditions: HFD vs. CTRL, MED vs. CTRL, and MED vs. HFD. HFD, high-fat diet; CTRL, normal-fat diet; MED, Mediterranean-like diet; FC, fold change.

HFD vs CTRL					
Glycan Name [1]	**Composition [2]**	**Glycan Mass**	**m/z**	**p**	**FC**
F(6)A2BG(4)2S(6,6)2	NeuAc2 Gal2 Fuc1 GlcNAc5 Man3	2571.92	1442.5620	0.0126	-1.20
A2[6]G(4)1	Gal1 GlcNAc4 Man3	1478.54	895.8720	0.0069	1.19
-	HexNAc4 Hex5 NeuAc3	2513.87	1414.0499	0.0046	-1.28
F(6)A2[3]BG(4)1	Gal1 Fuc1 GlcNAc5 Man3	1827.68	1070.4368	0.0426	1.10

-	HexNAc6 Hex5 Fuc1 NeuAc3	3066.09	1126.7695	0.0236	1.35
M11 a3D1,[D2(1),D3(1)],a2D4(2)	GlcNAc2 Man11	2206.75	1259.9943	0.0036	-1.32
F(6)A2[6]G1Ga1	Fuc1 Gal2 GlcNAc4 Man3	1786.65	1049.9261	0.0038	1.15
F(6)A2G(4)2S(6,6)2	NeuAc2 Gal2 Fuc1 GlcNAc4 Man3	2368.84	1341.0211	0.0266	-1.23
F(6)A2G(4)2S(3,3)2	NeuAc2 Gal2 Fuc1 GlcNAc4 Man3	2368.84	1341.0211	0.0215	-1.25
M6 D1	GlcNAc2 Man6	1396.49	854.8422	0.0050	1.12
-	HexNAc6 Hex5 Fuc2	2338.86	1325.9973	0.0103	-1.54
-	HexNAc5 Hex6 NeuAc3	2879.01	1064.7489	0.0366	-1.16
-	HexNAc6 Hex3 Fuc1 NeuAc2	2450.89	1382.0477	0.0146	-1.23
-	HexNAc8 Hex7	2777.01	1029.7350	0.0059	-1.24
MED vs CTRL					
Glycan Name	**Composition**	**Glycan Mass**	**m/z**	**p**	**FC**
F(6)A2BG(4)2S(6,6)2	NeuAc2 Gal2 Fuc1 GlcNAc5 Man3	2571.92	1442.5621	0.0478	-1.22
M7	GlcNAc2 Man7	1558.54	935.8692	0.0310	1.15
-	HexNAc4 Hex5 NeuAc3	2513.87	1414.0499	0.0233	-1.29
F(6)A2[3]BG(4)1	Gal1 Fuc1 GlcNAc5 Man3	1827.68	1070.4368	0.0007	1.19
F(6)A2G(4)2S(6,6)2	NeuAc2 Gal2 Fuc1 GlcNAc4 Man3	2368.84	1341.0211	0.0300	-1.26
-	HexNAc6 Hex6 Fuc1 NeuAc3	3228.15	1180.7875	0.0226	-1.41
F(6)A3G(4)3S(3,3,3)3	NeuAc3 Gal3 Fuc1 GlcNAc5 Man3	1915.69	1113.0953	0.0328	-1.50
-	HexNAc6 Hex7 NeuAc4	3535.24	1283.491	0.0495	-1.30
F(6)A2[6]G1Ga1	Fuc1 Gal2 GlcNAc4 Man3	1786.65	1049.9261	0.0073	1.11
MED vs HFD					

Glycan Name	Composition	Glycan Mass	m/z	p	FC
-	HexNAc6 Hex5 Fuc1 NeuAc3	3066.09	1126.7695	0.0285	-1.59

[1] Employed glycan nomenclature: F- Fucose; G- Galactose; S- N-Acetylneuraminic acid; Ga- a-linked Galactose; A1- Monoantennary, A2- Biantennary, B, bisecting GlcNAc linked α1-4 to α1-3 mannose. Numbers with parentheses indicate the preceding monosaccharide's linkage while those not in parentheses indicate the preceding characteristic's number. For example, F(6)A3G(4)3S(3,3,3)3 represents a core fucosylated triantennary glycan with 3 galactoses directly attached to antennae, and the three antennae terminated with an N-glycolylneuraminic acid.

[2] Employed glycan nomenclature for glycan composition: HexNAc- N-Acetylhexosamine; Hex- Hexose; NeuAc- N-Acetylneuraminic acid; Fuc- Fucose; Gal- Galactose; GlcNAc- N-Acetylglucosamine; Man- Mannose.

Remarkably, all the statistically significant sialylated glycans were increased in the CTRL group (vs. HFD and MED group), except for N-glycan HexNAc6Hex5Fuc1NeuAc3 (Table 3). Sialylated structures such as F(6)A2BG(4)2S(6,6)2 and F(6)A2G(4)2S(6,6)2 were increased in the CTRL, whereas non-sialylated structures such as F(6)A2BG(4)1 and F(6)A2G2 were decreased in the CTRL group compared to HFD and MED groups, indicating that the Mediterranean-like diet was not able to reverse the effect of the HFD. In Figure 3, boxplots of all the statistically significant N-glycans for CTRL, HFD, and MED groups are shown. A similar tendency was observed in a study where HFD-fed mice showed a significant decrease in complex tri- and tetraantennary sialofucosylated N-glycans in the hippocampus brain region. Interestingly, transcript analysis of the glycosyltransferases showed that the *MGAT2* gene, which encodes the enzyme responsible for initiating the synthesis of complex branched N-glycans, was significantly decreased in hippocampi of HFD-fed obese mice compared to lean controls [26].

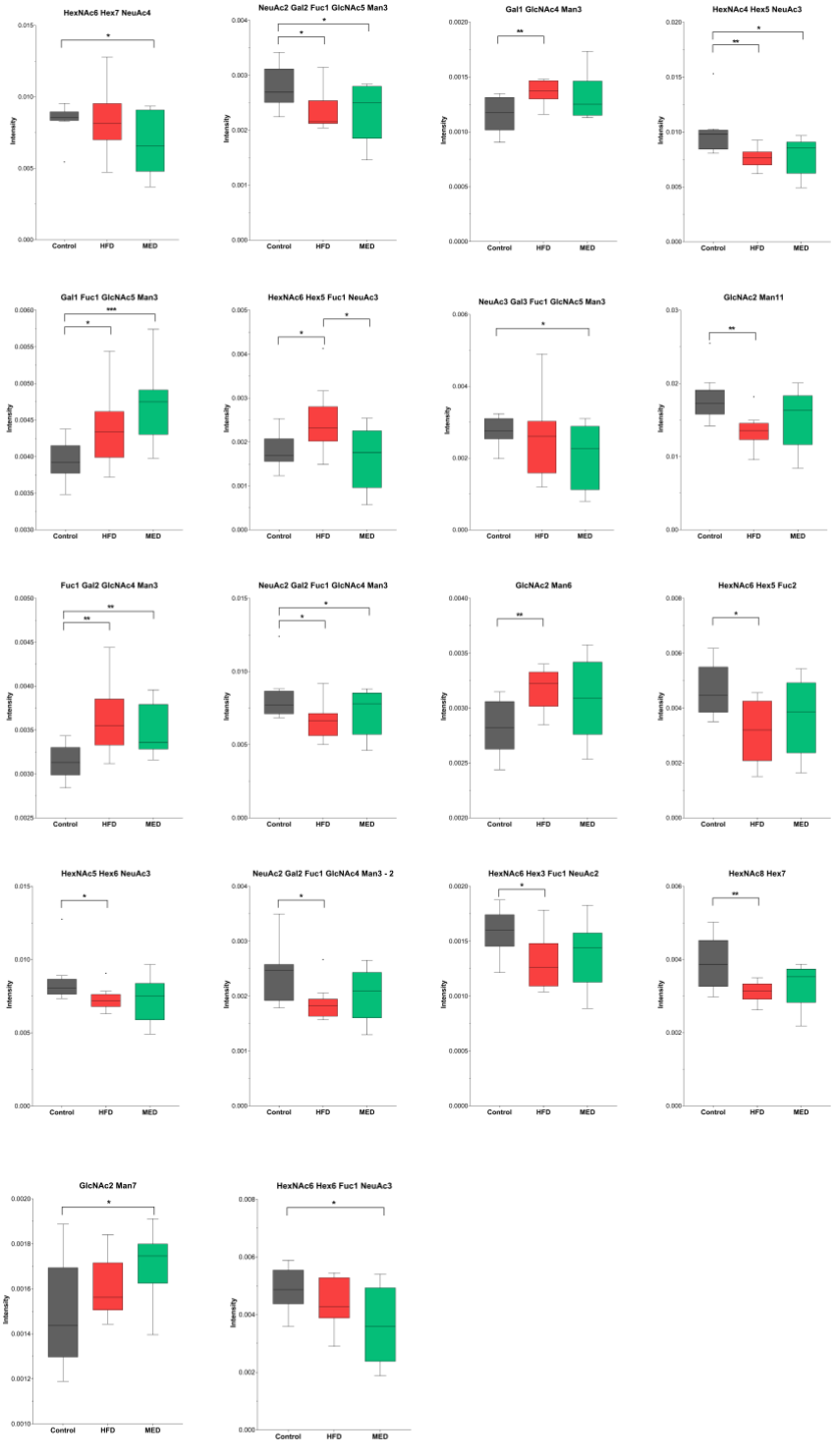
HexNAc6 Hex7 NeuAc4
NeuAc2 Gal2 Fuc1 GlcNAc5 Man3
Gal1 GlcNAc4 Man3
HexNAc4 Hex5 NeuAc3
Gal1 Fuc1 GlcNAc5 Man3
HexNAc6 Hex5 Fuc1 NeuAc3
NeuAc3 Gal3 Fuc1 GlcNAc5 Man3
GlcNAc2 Man11
Fuc1 Gal2 GlcNAc4 Man3
NeuAc2 Gal2 Fuc1 GlcNAc4 Man3
GlcNAc2 Man6
HexNAc6 Hex5 Fuc2
HexNAc5 Hex6 NeuAc3
NeuAc2 Gal2 Fuc1 GlcNAc4 Man3 - 2
HexNAc6 Hex3 Fuc1 NeuAc2
HexNAc8 Hex7
GlcNAc2 Man7
HexNAc6 Hex6 Fuc1 NeuAc3
Intensity
Control
HFD
MED

Figure 3. Boxplots showing increased and decreased abundance at week 12 for each statistically significant N-glycan (* *p*-value < 0.05, ** *p*-value < 0.01, *** *p*-value < 0.001).

Moreover, statistically significant differences were observed in three oligomannose glycans. They were increased in both the HFD group and MED group compared to the CTRL group, except for M11 which was decreased in the HFD group vs. the CTRL group. Regarding fucosylation, nine structures were increased in the CTRL group compared to the HFD and MED groups, whereas five fucosylated structures showed the opposite tendency, increasing in the HFD and MED groups compared to the CTRL group (Figure 3). Only one glycan (HexNAc6Hex5Fuc1NeuAc3) was found to be statistically significant between the MED and HFD groups. This sialylated and fucosylated glycan increased in the HFD group compared to the CTRL and MED groups, showing an opposite tendency compared to the rest of statistically significant N-glycans (Figure 3).

Overall, these results show that the four-week nutritional intervention with a MED in our study was not able to have an effect on brain N-glycan composition compared to hamsters fed with a HFD. However, the study demonstrates that the HFD influences brain N-glycan composition. Thus, most sialylated and fucosylated structures are decreased in the HFD-fed group, whereas most oligomannose N-glycans are increased. These tendencies have been observed in other studies where N-glycan galactosylation, sialylation, and fucosylation events decrease with ageing. Abnormal N-glycan alterations have previously been associated with chronic consumption of HFD and induced obesity, specifically in the hippocampal brain region [26]. Similar alterations have been determined in age-related diseases, such as Alzheimer's disease (AD), amyotrophic lateral sclerosis (ALS), or Parkinson's Disease (PD). For instance, increased levels of sialylated glycans have been found in ALS [36] but decreased in AD [37] and PD patients [38]. Similar to our results, fucosylation decreases in T2DM [39] and ALS patients [36], but increases in PD [38]. Taking this

into account, our results suggest that brain N-glycan behaviour related to adherence to a HFD can produce events similar to those found in some neurodegenerative diseases and may promote brain ageing process.

2.3 Lipidomics

In the evaluation of the brain lipid profile, 192 lipids were identified and quantified (as relative concentrations) in the different groups. The identified lipids belong to the following species: Lysophosphatidylcholines (LPC), lysophosphatidylethanolamines (LPE), phosphatidylcholines (PC), phosphatidylethanolamines (PE), sterol esters (SE), sphingomyelins (SM), triglycerides (TAG), and diacylglycerides (DAG). Each brain region has differences in the lipid pattern. Specifically, the hippocampus and the cortex have a similar pattern, however, the olfactory bulb and the hypothalamus show different lipid profiles [40]. The hypothalamus is characterised as being enriched in fatty acids as it has a high cell density, and therefore a high content of structural lipids such as phospholipids and cholesterol esters [41]. This is reflected in our data as LPC, LPE, PC, PE, and SM were the most abundant lipids found in our hamster brain samples.

Statistically significant differences ($p < 0.05$) were observed in forty-nine lipids in HFD samples vs. CTRL samples, whereas only seven lipids showed a significant change in MED samples vs. CTRL and, five lipids in MED samples vs. HFD samples (Table 4). These results suggest that a HFD clearly alters the brain lipid profile and that the 4-week MED nutritional intervention after a HFD barely modifies the lipid profile. In the present study, PC were the most abundant lipids in the brain, in concordance with previous results [40]. Two PC (34:2 and 36:5) were increased in the HFD and MED groups compared to the CTRL group. Moreover, two PE (30:1 and 38:2) were increased in the HFD group compared to the CTRL and the MED group. Both PC and PE are the most abundant phospholipids in all mammalian cell membranes. Abnormally high and low cellular PC/PE

ratios are known to influence energy metabolism and can indicate disease progression [42].

Table 4. Statistically significant differences in brain lipids by week 12 in the three different pairs of conditions. FC, fold change.

HFD vs CTRL			
Lipid species	**Compound**	**p**	**FC[1]**
Lysophosphatidylcholines	LPC 14:0	0.0476	1.34
	LPC 18:1	0.0447	1.34
Lysophosphatidylethanolamines	LPE 18:0	0.0307	1.36
	LPE 22:6	0.0239	1.43
Phosphatidylcholines	PC 17:0	0.0498	1.27
	PC 17:1	0.0285	1.30
	PC 30:0	0.0386	1.28
	PC 31:0	0.0255	1.31
	PC 31:1	0.0113	1.37
	PC 32:2	0.0436	1.29
	PC 32:3	0.0259	1.33
	PC 33:0	0.0382	1.29
	PC 34:0	0.0335	1.28
	PC 34:2	0.0057	1.36
	PC 34:5	0.0354	1.35
	PC 35:0	0.0181	1.39
	PC 36:0	0.0239	1.30
	PC 36:2	0.0428	1.26
	PC 36:5	0.0078	1.32
	PC 38:3	0.0408	1.29
	PC 38:5	0.0312	1.41
	PC 39:3	0.0491	1.27
	PC 40:6	0.0295	1.27
	PC 42:2	0.0416	1.85
	PC 42:3	0.0401	1.42
	PC 44:2	0.0167	1.44
Phosphatidylethanolamines	PE 30:1	0.0225	1.47
	PE 36:1	0.0185	1.37
	PE 38:2	0.0355	1.39
	PE 38:5	0.0302	1.33
	PE 38:6	0.0393	1.22

	PE 40:4	0.0458	1.32
	PE 40:6	0.0300	1.26
	PE 42:2	0.0259	1.30
	PE 44:5	0.0265	1.23
Sterol esters	SE 27:1/18:1	0.0196	1.37
	SE 27:1/18:2	0.0013	1.65
	SE 27:1/20:1	0.0008	1.81
	SE 27:1/20:4	0.0027	1.60
	SE 27:1/22:4	0.0339	1.57
	SE 27:1/22:6	0.0401	1.49
Sphingomyelins	SM 32:2;2	0.0434	1.46
	SM 35:1;2	0.0418	1.33
	SM 35:2;2	0.0282	1.31
	SM 40:2;2	0.0283	1.43
Triglycerides	TAG 50:1	0.0497	1.32
	TAG 52:1	0.0091	1.38
	TAG 56:5	0.0163	1.46
MED vs CTRL			
Lipid species	**Compound**	**p**	**FC**
Lysophosphatidylcholines	LPC 20:4	0.0195	-1.53
Lysophosphatidylethanolamines	LPE 20:4	0.0145	-1.58
Phosphatidylcholines	PC 34:2	0.0375	1.28
	PC 36:5	0.0351	1.27
Sterol esters	SE 27:1/16:1	0.0169	-1.34
	SE 27:1/18:2	0.0399	1.39
	SE 27:1/22:6	0.0010	2.03
MED vs HFD			
Lipid species	**Compound**	**p**	**FC**
Diacylglycerides	DAG 36:4	0.0494	-1.37
	DAG 38:4	0.0396	-1.40
Phosphatidylethanolamines	PE 30:1	0.0318	-1.36
	PE 38:2	0.0186	-1.38
Sterol esters	SE 27:1/18:3	0.0416	-1.42

Two types of glycerolipids, specifically TAG and DAG, were altered in the different groups. TAG 50:1, 52:1, and 56:5 were increased in the HFD group compared to the CTRL group, and, DAG 36:4 and 38:4 were increased in the HFD group compared to the MED group. A similar trend

has been observed in other studies which demonstrated that high-fat feeding increases the total contents of TAG and DAG in the hypothalamus [29,40]. Moreover, DAG have been reported to be the lipid species most influenced by a HFD, showing a significant increase in four different brain regions [40]. Taking this into account, our results suggest that the MED may have a positive impact on the brain DAG levels in animals previously subjected to a HFD. However, previous studies have shown that the lipid profile of the hypothalamus isnot affected by a HFD, suggesting that the hypothalamus cannot be a depot for dietary lipids, as the blood barrier serves as a metabolic shield to the brain [41]. This could explain why, in our study, DAG levels were not altered in the HFD group vs. the CTRL group. These non-consistent results between different groups could be a result of having characterised the whole brain tissue instead of focusing on profiling one specific brain region.

Lysophospholipids were increased in the HFD group compared to the CTRL group and decreased in the MED group compared to the CTRL group. This obtained data supports a different study which determined that a HFD affected lysophospholipids in the cortex and hippocampus, but did not affect the hypothalamus and olfactory bulb [40]. Moreover, circulating levels of lysophospholipids have been reported to change with the progression of dyslipidemia-related diseases [43]. In our study, brain LPC and LPE increased in the HFD group compared to the CTRL group. Similar shifts in plasma and hepatic levels of LPC and LPE have been associated with chronic intake of a HFD in obese [44] and non-obese mice [45]. More specifically, in our study, LPE 20:4, a lipid reported to exhibit early alterations in response to dyslipidemia, was decreased in the MED compared to the CTRL group. Consistent with previous reports, LPC and LPE, specifically LPE 20:4, could serve as potential biomarkers of risk of developing lipid disorders [43].

3. MATERIALS AND METHODS

3.1 Reagents

Trichloroacetic acid (TCA), acetone, ammonium bicarbonate (ABC), ammonium formate, chloroform, sodium chloride (NaCl), and formic acid (LC-MS grade) were purchased from Sigma-Aldrich (St. Louis, MO, USA). RIPA Lysis and Extraction Buffer were obtained from ThermoFisher Scientific (Waltham, MA, USA), and, 2-propanol (LC-MS grade), methanol (LC-MS grade), acetonitrile (LC-MS grade), and methyl-*tert*-butyl ether were purchased from Merck (Darmstadt, Germany). The water used throughout the study was purified with a Milli-Q system from Millipore (Burlington, MA, USA).

3.2 Diets

A normal-fat diet (NFD) and two isocaloric diets, a HFD and a ME-like diet were used (ENVIGO, Barcelona, Spain) (Table S1). The NFD contains 11% calories from fat, whereas the HFD contains 23% calories from fat and 1 g/kg cholesterol. In the MED (23% calories from fat), extra virgin olive oil (EVOO; 50 g/kg of diet), walnuts (20 g/kg of diet), and fish oil (6 g/kg of diet) were added to the HFD in place of lard. In addition, in the MED, total cholesterol content was adjusted to 250 mg/kg of diet, taking into account the amount of cholesterol present in lard and fish oil. The nutritional composition and manufacturing companies of the ingredients used in the MED are specified in Tables S2–S4.

Considering an average hamster's weight of 130 g and a daily diet intake of 7 g, the amounts of EVOO, walnuts, and fish oil included in the MED were equivalent to the daily consumption of 26.8 g, 10.7 g, and 0.97 g of these food items, respectively, for a 60 kg human. These daily amounts can be usually achieved in the context of a Mediterranean diet pattern [46]. In the MED, cholesterol was included at 0.025%, because, according to previous research, it is non-atherogenic for hamsters at this concentration [47,48]. The extrapolated daily intake using the same formula was 134 mg, which is

lower than the daily cholesterol intake estimated in the PREDIMED study (340 mg/day) [46].

3.3 Animals and experimental design

The Animal Ethics Committee of the Technological Unit of Nutrition and Health of Eurecat (Reus, Spain) and the Generalitat de Catalunya approved all procedures (DAAM 10026). The experimental protocol complied with the ARRIVE guidelines followed the 'Principles of laboratory animal care' and was carried out in accordance with the EU Directive 2010/63/EU for animal experiments. All animals were housed individually at 22 °C under a light/dark cycle of 12 h (lights on at 09:00 a.m.) and were given free access to food and water. Twenty-seven 10-week-old male Golden Syrian hamsters (Janvier Labs, Saint Berthevin, France) weighing 110–120 g were used. After an adaptation period of 1 week, hamsters were randomly assigned into two experimental groups fed with a normal fat diet (CTRL group, fed the NFD, n = 9, 11% calories from fat; Envigo, Barcelona, Spain) or a HFD (n = 18, 23% calories from fat and 1g/kg cholesterol; Envigo, Barcelona, Spain) for 8 weeks. In a previous study, using similar diets, we demonstrated that this period was useful to induce fatty liver and hypercholesterolemia in hamsters [31,49]. Afterwards, the HFD group was randomly distributed into two subgroups. The first subgroup continued receiving a HFD until week 12 (HFD group, n = 9). The second subgroup changed to the MED during the last 4 weeks of the study (MED group, n = 9) (Figure 1A). The sample size was calculated with the statistical program G*Power (version 3.1.9.4). Based on the LDL levels and their standard deviations, with a statistical power of 90%, a confidence level of 95%, and carrying out a Student *t*-test, the minimum sample size necessary to detect a difference of at least 10% in LDL cholesterol levels was eight animals per experimental group. To cover possible interferences in the response within each group, nine animals per group were finally selected.

Body weight and food intake were recorded once per week, and food was renewed daily. At 12 weeks, all experimental animals were sacrificed under anaesthesia (pentobarbital sodium, 60 mg/kg body weight) after 6 h of diurnal fasting. Blood was collected by cardiac puncture, and serum was obtained by centrifugation and stored at −20 °C until analysis. The liver, MWAT, and brain were rapidly removed, weighed, frozen in liquid nitrogen, and stored at −70 °C until analysis.

3.4 Histological evaluation

Morphometric analyses of tissues and steatosis of liver histology were carried out using the methods described in the literature [31]. Briefly, liver samples (n = 9 per group) were fixed, and subjected to dehydration and paraffin infiltration-immersion. After obtaining the tissue sections, a histological examination was carried out. The histological sections of the liver were analysed according to the Kleiner scoring system [50].

3.5 Hepatic lipid extraction and quantification

Lipid extraction and quantification were carried out using the methods previously described [31]. Briefly, liver samples (80–100 mg) were mixed with 1 mL of hexane:isopropanol (3:2, *v*/*v*). The tubes with the samples were gassed with nitrogen before being closed to minimize lipid oxidation and then left overnight under orbital agitation at room temperature protected from light. The content of each tube was transferred into a new one, and 0.3 mL of Na_2SO_4 (0.47 M) was added. Tubes were mixed for 5 min, left for 15 min in orbital agitation, and centrifuged at 1000× *g* for 10 min at 4 °C. The upper phase containing lipids was dissolved in hexane and transferred to a clean, previously weighed glass tube. The hexane extract was then dried with nitrogen gas. Once the tube was dried, the percentage of lipids was determined gravimetrically.

3.6 Body composition analyses

Body composition was analysed by Nuclear magnetic resonance (NMR). Lean and fat mass analyses were performed at the end of weeks 8 and 12 using an EchoMRI-700® device (Echo Medical Systems, L.L.C., Houston, TX, USA). The measurements were performed in duplicate. Data are expressed in relative values as a percentage of body weight (%). The lean/fat mass ratio was also calculated.

3.7 Serum analysis

Enzymatic colorimetric assays were used for the analysis of glucose, total cholesterol and triglycerides (QCA, Barcelona, Spain), HDL-cholesterol, and LDL/VLDL-cholesterol (Bioassay systems, Hayward, CA, USA). Serum insulin levels were analysed using a hamster insulin ELISA kit (MyBiosource, Bizkaia, Spain).

3.8 N-Glycan analysis

3.8.1 Protein extraction and quantification

Samples containing approximately 65 mg of brain tissue were resuspended in 1 mL of RIPA buffer and subjected to bead beating combined with a freeze–thaw cycle. Three to four 1.4 mm stainless steel beads were added to each sample, followed by a 1 min bead beating cycle at medium speed (Bullet Blender, Cultek, Barcelona, Spain); this step was repeated twice. Samples were then agitated for 1.5 h at 20 °C and centrifuged at 16,000× *g* for 20 min. Proteins in the supernatant were precipitated overnight with TCA/acetone. The obtained pellet was resuspended in 50 mM ABC and the concentration was quantified using the Bradford method.

3.8.2 De-N-Glycosylation and labelling of N-Glycans

Sample denaturation, de-N-glycosylation, labelling with Rapifluor-MS (RFMS), and purification were performed in accordance with the Waters Corporation “GlycoWorks RapiFluor-MS N-Glycan Kit Care and Use

Manual" (p/n 715004793) (Waters, Milford, MA, USA). Briefly, the glycoproteins were denatured at 90 °C for 3 min in the presence of 5% (*w*/*v*) RapiGest. De-N-glycosylation was then conducted at 50 °C for 5 min, with the addition of 1.2 µL of Rapid PNGase F. The digested samples were directly subjected to RFMS labelling without purification by adding 6 µL of RFMS reagent. The reaction was then allowed to proceed at room temperature for 5 min. A GlycoWorks µElution Plate was used for the SPE Clean-up procedure. Glycans were eluted with 200 mM ammonium acetate in 5% acetonitrile.

3.8.3 LC-MS/MS

Derivatized samples were analysed using an Agilent UHPLC 1290 Infinity Series coupled to an Agilent qTOF/MS 6550 Series (Agilent Technologies, Santa Clara, CA, USA). Mobile phase A was 50 mM ammonium formate solution, and mobile phase B was acetonitrile. N-glycans were separated on a Waters ACQUITY UPLC BEH amide column (2.1 mm × 150 mm i.d., particle size 1.7 µm). The flow rate was 0.4 mL/min, the injection volume was 20 µL, and the column temperature was set to 60 °C. Initially, the gradient ramped mobile phase A from 25 to 46%, over 35 min. From 35 to 36.5 min, the gradient ramped from 46 to 100% solvent A and the flow rate was lowered to 0.2 mL/min. A 100% solvent A was held constant from 36.5 to 39.5 min, after which the percentage of solvent A decreased to 25%, from 39.5 min to 43.1 min. The flow rate was then increased back to 0.4 mL/min from 43.1 to 47.6 min and solvent A was held constant at 25%. Lastly, the parameters were held constant from 47.6 to 55.0 min. The qTOF operated in positive electrospray ionisation mode (ESI+), and mass spectra were recorded between m/z 300–1700 at 1.5 spectra/s. The source conditions were 25 psi for nebuliser gas, 200 °C for gas temperature, 12 L/min for gas flow, 250 °C for sheath gas temperature, 12 L/min for sheath gas flow, 3500 V for capillary voltage, and 500 V for nozzle voltage. Additionally, tandem mass experiments (MS/MS) using data dependence

acquisition at a collision energy of 30 eV from the 10 most intense ions were used for identification purposes.

3.8.4 Data processing of LC-MS Data

The MS data were first processed using Agilent MassHunter Qualitative Analysis B.07 software. For each sample, total ion chromatograms (TIC) containing MS/MS fragmentation data were deconvoluted using the "find molecular feature" algorithm to find chromatographic peaks that could potentially be N-glycans. The resulting list of entities containing the MS/MS data was exported and loaded to Simglycan software v.5.93 (Premier Biosoft, San Francisco, CA, USA) for molecular and structural elucidation. Simglycan is a high throughput structural identification tool that uses a built-in database with theoretical fragmentation profiles to provide the most likely structure candidates [51]. The results obtained from Simglycan were matched against the GlycoStore database (https://www.glycostore.org (accessed on 24 March 2022)) to refine the identification results. GlycoStore was able to provide elution property information for over 850 unique structures including standardized retention times, expressed as glucose units (GU), for the RFMS-labelled glycans [52]. After the identification process of N-glycans on brain samples, 72 N-glycans were identified. Then, the exact mass $[M + H]^+$, $[M + 2H]^{2+}$ or $[M + 3H]^{3+}$ of these structures were extracted on all samples using Agilent Mass Hunter Quantitative software (B.07) to create a refined matrix of quantitative data for statistical purposes. Finally, the data matrix obtained containing the area of each identified N-glycan was normalized by dividing the peak area of each N-glycan with the sum of the area of all N-glycans in each sample.

3.9 Lipidomics analysis

3.9.1 Sample preparation

Samples were extracted using an adapted Folch procedure [53,54,55]. Approximately 150 mg of brain tissue samples were extracted with 1500

µL of chloroform:methanol (2:1, *v*/*v*) containing internal standard mixture (Lipidomix SPLASH®, Avanti Polar Lipids, Birmingham, AL, USA) and homogenized using a bead beating method. Next, 300 µL of water with NaCl (0.9%) was added and centrifuged at 15,000 rpm for 10 min to promote liquid phase separation. The lower phase was recovered, evaporated to dryness, and reconstituted with methanol:methyl-tert-butyl ether (9:1) for LC-MS analysis.

3.9.2 LC-MS

Samples were analysed using an Agilent UHPLC 1290 Infinity Series coupled to an Agilent qTOF/MS 6550 Series (Agilent Technologies, Santa Clara, CA, USA). The chromatographic separation consists of an elution with a ternary mobile phase containing water with 10 mM ammonium formate and 0.1% formic acid (solvent A), methanol (solvent B), and 2-propanol (solvent C). The stationary phase was a C18 column (Kinetex EVO C18 Column, 2.6 µm, 2.1 mm × 100 mm) that allows the sequential elution of the more hydrophobic lipids such as lysophospholipids, sphingomyelins, phospholipids, diglycerides, triglycerides, and cholesteryl esters, among others. The flow rate was 0.6 mL/min, the injection volume was 2 µL, and the column temperature was set to 60 °C. The gradient employed was 0–0.5 min, 55–45% A + 10% B; 0.5–1.5 min, 45–42.8% A + 10–9.5% B; 1.5–1.6 min, 42.8–34% A + 9.5–7.5% B; 1.6–5 min, 34–31.8% A + 7.5–7% B; 5–5.1 min, 31.8–18.6% A + 7–4% B; 5.1–7.5 min, 18.6–16.4% A + 4–3.5% B; 7.5–9 min, 16.4% A + 3.5% B; 9–9.5 min, 16.4–0% A + 3.5–0% B; 9.5–11.5 min, 0% A + 0% B; 11.5–11.6 min, 0–45% A + 0–10% B; and 24.75–29.25, 55–45% A + 10% B. The qTOF operated in positive electrospray ionisation mode (ESI+), and mass spectra were recorded between m/z 300–1700 at 3 spectra/s. The source conditions were 35 psi for nebuliser gas, 225 °C for gas temperature, 11 L/min for gas flow, 300 °C for sheath gas temperature, 12 L/min for sheath gas flow, 3500 V for capillary voltage, and 500 V for nozzle voltage.

3.9.3 Data processing of LC-MS data

The MS data were processed using both Agilent MassHunter Qualitative and Quantitative Analysis B.07 software. The identification of lipid species was performed by matching their accurate mass and tandem mass spectrum, when available, to Metlin-PCDL from Agilent containing more than 40,000 metabolites and lipids. LipidCreator workbench was also used for targeted exact mass list generation [56]. In addition, chromatographic behaviour of pure standards for each family and bibliographic information was used to ensure their putative identification. After putative identification of lipids, these were quantified in terms of internal standard response ratio using one internal standard for each lipid family by using Agilent Mass Hunter Quantitative software (B.07) to create a refined matrix of quantitative data for statistical purposes.

3.10 Statistical analysis

Differences in energy intake, and biometric and serum parameters between the CTRL hamsters and the HFD hamsters, after 8 weeks, were analysed using Student's *t*-test. At the endpoint (week 12), Student's *t*-test was used to evaluate differences in energy intake, hepatic lipid content, biometric parameters, and serum parameters for the three pairs of conditions: HFD vs. CTRL, MED vs. CTRL, and MED vs. HFD. Differences in steatosis scores were evaluated using the Chi-squared test.

The same statistical analysis procedure was employed for both the N-glycan and lipidomics analyses. After the data processing, the normalized data matrices containing 72 identified-glycan-identified entities and 192 lipidic species were separately loaded on Mass Profiler Professional (MPP) software v.15.1 (Agilent Technologies, Santa Clara, MA, USA). Further data normalization was carried out which consisted of transforming data to a log2 scale. To determine the statistically significant differences ($p < 0.05$), a pairwise comparison with Student's *t*-test was performed between HFD and CTRL, MED and CTRL, and, lastly, MED vs. HFD.

4. CONCLUSIONS

In this study, the global brain N-glycome and lipid profile were determined. Using LC-MS/MS, 72 glycans and 192 lipids were identified based on informative MS/MS data. Statistically significant differences were observed in 18 N-glycans and 53 lipids between groups HFD, MED, and CTRL. Results suggested that a short MED diet intervention barely modified the N-glycan and lipid profile on animals that were previously fed with a HFD, confirming that the HFD, administrated before the MED, had more impact on the N-glycan and lipid composition than the MED nutritional intervention itself. The tendencies observed should be confirmed with a longer-term MED after a HFD to elucidate whether the MED can reverse or modify the brain N-glycan and lipid pattern more effectively.

Regarding the N-glycan profile, most sialylated and fucosylated structures were decreased in HFD-fed groups, whereas most oligomannose structures were increased. These tendencies are commonly observed in ageing studies, suggesting that a HFD can produce events that occur in the ageing process as well as in age-related diseases.

Most of the identified brain lipids belonged to the PC and PE lipid species. PC and PE are the most abundant phospholipids in mammalian cell membranes and more specifically, PC are the most abundant lipids in the brain. Previous studies have reported that certain brain regions are not depots for dietary lipids, as the blood barrier serves as a metabolic shield to the brain. Nevertheless, a statistically significant increase was observed in 48 lipids in the HFD group compared to the CTRL group. Further research could determine if these shifts in the lipid profile entail relevant functional brain changes. Changes observed in both the lipidomic and glycomic brain profile could potentially be caused by the alteration of the gut microbiota after the exposure to a HFD, as a state of dysbiosis would lead to increased insulin resistance and inflammation, leading to an

alteration of the nervous system through the gut-brain axis. However, to confirm this hypothesis, studies including metagenomics and metabolomics should be conducted. Additional studies including diets supplemented with antioxidants could also be of interest. Obesity is known to be associated with an increase in cerebral oxidative stress levels, which may enhance neurodegeneration [46]. Some studies have evaluated the neuroprotective action of dietary supplements containing antioxidants (i.e., resveratrol) [47]. In future studies, with HFD-fed animals supplemented with antioxidants, we could assess the modulations induced on lipidomic and glycomic brain profiles to broaden our understanding of the neuroprotection of antioxidants.

Author Contributions

Conceptualization, M.S., A.C., N.C. and P.H.; methodology, B.P., E.F.-R., J.M.-P. and N.B.; formal analysis, B.P. and E.F.-R.; writing—original draft preparation, B.P.; writing—review and editing, B.P., M.S., A.C., N.C. and P.H.; supervision, M.S., N.C. and P.H.; funding acquisition, A.C. and N.C. All authors have read and agreed to the published version of the manuscript.

Funding

This work was financially supported by the Centre for the Development of Industrial Technology (CDTI) of the Spanish Ministry of Science and Innovation under a grant agreement: TECNOMIFOOD project. CER-2019-1010). BP is supported by a fellowship from the Vicente Lopez Program (Eurecat).

Institutional Review Board Statement

The Animal Ethics Committee of the Technological Unit of Nutrition and Health of Eurecat (Reus, Spain) and the Generalitat de Catalunya approved all procedures (DAAM 10026, 18 July 2018). The experimental protocol complied with the ARRIVE guidelines, followed the 'Principles of

laboratory animal care' and was carried out in accordance with the EU Directive 2010/63/EU for animal experiments.

Acknowledgments

We gratefully acknowledge the help of Yaiza Tobajas, Anna Antolín, Iris Triguero, Cristina Egea, and Gertruda Chomiciute, who are laboratory technicians at the Technological Unit of Nutrition and Health of Eurecat, for their technical support.

Conflicts of Interest

The authors declare no conflict of interest.

REFERENCES

1. D'innocenzo, S.; Biagi, C.; Lanari, M. Obesity and the Mediterranean Diet: A Review of Evidence of the Role and Sustainability of the Mediterranean Diet. *Nutrients* **2019**, *11*, 1306.
2. Afshin, A.; Sur, P.J.; Fay, K.A.; Cornaby, L.; Ferrara, G.; Salama, J.S.; Mullany, E.C.; Abate, K.H.; Abbafati, C.; Abebe, Z.; et al. Health effects of dietary risks in 195 countries, 1990–2017: A systematic analysis for the Global Burden of Disease Study 2017. *Lancet* **2019**, *393*, 1958–1972.
3. Mu, M.; Xu, L.F.; Hu, D.; Wu, J.; Bai, M.J. Dietary Patterns and Overweight/Obesity: A Review Article. *Iran. J. Public Health* **2017**, *46*, 869.
4. Thaler, J.P.; Yi, C.X.; Schur, E.A.; Guyenet, S.J.; Hwang, B.H.; Dietrich, M.O.; Zhao, X.; Sarruf, D.A.; Izgur, V.; Maravilla, K.R.; et al. Obesity is associated with hypothalamic injury in rodents and humans. *J. Clin. Investig.* **2012**, *122*, 153–162.
5. Karlsson, H.K.; Tuominen, L.; Tuulari, J.J.; Hirvonen, J.; Parkkola, R.; Helin, S.; Salminen, P.; Nuutila, P.; Nummenmaa, L. Obesity is associated with decreased μ-opioid but unaltered dopamine D2 receptor availability in the brain. *J. Neurosci.* **2015**, *35*, 3959–3965.
6. McLean, F.H.; Campbell, F.M.; Langston, R.F.; Sergi, D.; Resch, C.; Grant, C.; Morris, A.C.; Mayer, C.D.; Williams, L.M. A high-fat diet induces rapid changes in the mouse hypothalamic proteome. *Nutr. Metab.* **2019**, *16*, 26.
7. Freeman, L.R.; Haley-Zitlin, V.; Rosenberger, D.S.; Granholm, A.-C. Damaging effects of a high-fat diet to the brain and cognition: A review of proposed mechanisms. *Nutr. Neurosci.* **2014**, *17*, 241.
8. Sikalidis, A.K.; Maykish, A. The Gut Microbiome and Type 2 Diabetes Mellitus: Discussing a Complex Relationship. *Biomedicines* **2020**, *8*, 8.
9. Rutsch, A.; Kantsjö, J.B.; Ronchi, F. The Gut-Brain Axis: How Microbiota and Host Inflammasome Influence Brain Physiology and Pathology. *Front. Immunol.* **2020**, *11*, 3237.
10. Antoniazzi, L.; Arroyo-Olivares, R.; Bittencourt, M.S.; Tada, M.T.; Lima, I.; Jannes, C.E.; Krieger, J.E.; Pereira, A.C.; Quintana-Navarro, G.; Muñiz-Grijalvo, O.; et al. Adherence to a Mediterranean diet, dyslipidemia and

inflammation in familial hypercholesterolemia. *Nutr. Metab. Cardiovasc. Dis.* **2021**, *31*, 2014–2022.
11. Serra-Majem, L.; Roman, B.; Estruch, R. Scientific evidence of interventions using the Mediterranean diet: A systematic review. *Nutr. Rev.* **2006**, *64*, S27–S47.
12. Romagnolo, D.F.; Selmin, O.I. Mediterranean Diet and Prevention of Chronic Diseases. *Nutr. Today* **2017**, *52*, 208–222.
13. Rosato, V.; Temple, N.J.; La Vecchia, C.; Castellan, G.; Tavani, A.; Guercio, V. Mediterranean diet and cardiovascular disease: A systematic review and meta-analysis of observational studies. *Eur. J. Nutr.* **2019**, *58*, 173–191.
14. Huo, R.; Du, T.; Xu, Y.; Xu, W.; Chen, X.; Sun, K.; Yu, X. Effects of Mediterranean-style diet on glycemic control, weight loss and cardiovascular risk factors among type 2 diabetes individuals: A meta-analysis. *Eur. J. Clin. Nutr.* **2015**, *69*, 1200–1208.
15. Tangney, C.C.; Kwasny, M.J.; Li, H.; Wilson, R.S.; Evans, D.A.; Morris, M.C. Adherence to a Mediterranean-type dietary pattern and cognitive decline in a community population. *Am. J. Clin. Nutr.* **2011**, *93*, 601.
16. Gao, X.; Chen, H.; Fung, T.T.; Logroscino, G.; Schwarzschild, M.A.; Hu, F.B.; Ascherio, A. Prospective study of dietary pattern and risk of Parkinson disease. *Am. J. Clin. Nutr.* **2007**, *86*, 1486–1494.
17. Scarmeas, N.; Stern, Y.; Mayeux, R.; Luchsinger, J.A. Mediterranean diet, Alzheimer disease, and vascular mediation. *Arch. Neurol.* **2006**, *63*, 1709–1717.
18. Valls-Pedret, C.; Lamuela-Raventós, R.M.; Medina-Remón, A.; Quintana, M.; Corella, D.; Pintó, X.; Martínez-González, M.Á.; Estruch, R.; Ros, E. Polyphenol-rich foods in the Mediterranean diet are associated with better cognitive function in elderly subjects at high cardiovascular risk. *J. Alzheimers Dis.* **2012**, *29*, 773–782.
19. Dias, A.M.; Pereira, M.S.; Padrão, N.A.; Alves, I.; Marcos-Pinto, R.; Lago, P.; Pinho, S.S. Glycans as critical regulators of gut immunity in homeostasis and disease. *Cell. Immunol.* **2018**, *333*, 9–18.
20. Scott, H.; Panin, V.M. The role of protein N-glycosylation in neural transmission. *Glycobiology* **2014**, *24*, 407–417.
21. Ednie, A.R.; Bennett, E.S. Modulation of voltage-gated ion channels by sialylation. *Compr. Physiol.* **2012**, *2*, 1269–1301.
22. Tucholski, J.; Simmons, M.S.; Pinner, A.L.; Haroutunian, V.; McCullumsmith, R.E.; Meador-Woodruff, J.H. Abnormal N-linked glycosylation of cortical AMPA receptor subunits in schizophrenia. *Schizophr. Res.* **2013**, *146*, 177–183.
23. Lichnerova, K.; Kaniakova, M.; Park, S.P.; Skrenkova, K.; Wang, Y.X.; Petralia, R.S.; Suh, Y.H.; Horak, M. Two N-glycosylation sites in the GluN1 subunit are essential for releasing N-methyl-D-aspartate (NMDA) receptors from the endoplasmic reticulum. *J. Biol. Chem.* **2015**, *290*, 18379–18390.
24. Gu, W.; Fukuda, T.; Isaji, T.; Hang, Q.; Lee, H.H.; Sakai, S.; Morise, J.; Mitoma, J.; Higashi, H.; Taniguchi, N.; et al. Loss of α1,6-fucosyltransferase decreases hippocampal long term potentiation: Implications for core fucosylation in the regulation of AMPA receptor heteromerization and cellular signaling. *J. Biol. Chem.* **2015**, *290*, 17566–17575.
25. Inaba, H.; Kai, D.; Kida, S. N-glycosylation in the hippocampus is required for the consolidation and reconsolidation of contextual fear memory. *Neurobiol. Learn. Mem.* **2016**, *135*, 57–65.

26. Barboza, M.; Krueger, M.R.; Honeycutt, M.; Lebrilla, C.B.; Raybould, H. Multi-omics Studies Reveal Altered Hippocampal N-Glycosylation in High Fat Diet-Induced Obese Mice. *FASEB J.* **2020**, *34*, 1.
27. Castellanos, D.B.; Martín-Jiménez, C.A.; Rojas-Rodríguez, F.; Barreto, G.E.; González, J. Brain lipidomics as a rising field in neurodegenerative contexts: Perspectives with Machine Learning approaches. *Front. Neuroendocrinol.* **2021**, *61*, 100899.
28. Shamim, A.; Mahmood, T.; Ahsan, F.; Kumar, A.; Bagga, P. Lipids: An insight into the neurodegenerative disorders. *Clin. Nutr. Exp.* **2018**, *20*, 1–19.
29. Borg, M.L.; Omran, S.F.; Weir, J.; Meikle, P.J.; Watt, M.J. Consumption of a high-fat diet, but not regular endurance exercise training, regulates hypothalamic lipid accumulation in mice. *J. Physiol.* **2012**, *590*, 4377–4389.
30. Bravo, E.; Cantafora, A.; Calcabrini, A.; Ortu, G. Why prefer the golden Syrian hamster (Mesocricetus auratus) to the Wistar rat in experimental studies on plasma lipoprotein metabolism? *Comp. Biochem. Physiol. Part B Comp. Biochem.* **1994**, *107*, 347–355.
31. Yang, H.; Mayneris-Perxachs, J.; Boqué, N.; del Bas, J.M.; Arola, L.; Yuan, M.; Türkez, H.; Uhlén, M.; Borén, J.; Zhang, C.; et al. Combined Metabolic Activators Decrease Liver Steatosis by Activating Mitochondrial Metabolism in Hamsters Fed with a High-Fat Diet. *Biomedicines* **2021**, *9*, 1440.
32. Harvey, D.J.; Merry, A.H.; Royle, L.; Campbell, M.P.; Dwek, R.A.; Rudd, P.M. Proposal for a standard system for drawing structural diagrams of N- and O-linked carbohydrates and related compounds. *Proteomics* **2009**, *9*, 3796–3801.
33. Lee, J.; Ha, S.; Kim, M.; Kim, S.-W.; Yun, J.; Ozcan, S.; Hwang, H.; Ji, I.J.; Yin, D.; Webster, M.J.; et al. Spatial and temporal diversity of glycome expression in mammalian brain. *Proc. Natl. Acad. Sci. USA* **2020**, *117*, 28743–28753.
34. Albach, C.; Klein, R.A.; Schmitz, B. Do Rodent and Human Brains Have Different N-Glycosylation Patterns? *Biol. Chem.* **2001**, *382*, 187–194.
35. Kleene, R.; Schachner, M. Glycans and neural cell interactions. *Nat. Rev. Neurosci.* **2004**, *5*, 195–208.
36. Edri-Brami, M.; Rosental, B.; Hayoun, D.; Welt, M.; Rosen, H.; Wirguin, I.; Nefussy, B.; Drory, V.E.; Porgador, A.; Lichtenstein, R.G. Glycans in sera of amyotrophic lateral sclerosis patients and their role in killing neuronal cells. *PLoS ONE* **2012**, *7*.
37. Lundström, S.L.; Yang, H.; Lyutvinskiy, Y.; Rutishauser, D.; Herukka, S.K.; Soininen, H.; Zubarev, R.A. Blood plasma IgG Fc glycans are significantly altered in Alzheimer's disease and progressive mild cognitive impairment. *J. Alzheimer's Dis.* **2014**, *38*, 567–579.
38. Váradi, C.; Nehéz, K.; Hornyák, O.; Viskolcz, B.; Bones, J. Serum N-Glycosylation in Parkinson's Disease: A Novel Approach for Potential Alterations. *Molecules* **2019**, *24*, 2220.
39. Dotz, V.; Lemmers, R.F.H.; Reiding, K.R.; Hipgrave Ederveen, A.L.; Lieverse, A.G.; Mulder, M.T.; Sijbrands, E.J.G.; Wuhrer, M.; van Hoek, M. Plasma protein N-glycan signatures of type 2 diabetes. *Biochim. Biophys. Acta-Gen. Subj.* **2018**, *1862*, 2613–2622.
40. Lee, J.C.; Park, S.M.; Kim, I.Y.; Sung, H.; Seong, J.K.; Moon, M.H. High-fat diet-induced lipidome perturbations in the cortex, hippocampus,

hypothalamus, and olfactory bulb of mice. *Biochim. Biophys. Acta-Mol. Cell Biol. Lipids* **2018**, *1863*, 980–990.

41. Dahdah, N.; Gonzalez-franquesa, A.; Samino, S.; Gama-perez, P.; Herrero, L.; Perales, J.C.; Yanes, O.; Malagón, M.D.M.; Garcia-roves, P.M. Effects of lifestyle intervention in tissue-specific lipidomic profile of formerly obese mice. *Int. J. Mol. Sci.* **2021**, *22*, 3694.
42. van der Veen, J.N.; Kennelly, J.P.; Wan, S.; Vance, J.E.; Vance, D.E.; Jacobs, R.L. The critical role of phosphatidylcholine and phosphatidylethanolamine metabolism in health and disease. *Biochim. Biophys. Acta-Biomembr.* **2017**, *1859*, 1558–1572.
43. Suárez-García, S.; Caimari, A.; del Bas, J.M.; Suárez, M.; Arola, L. Serum lysophospholipid levels are altered in dyslipidemic hamsters. *Sci. Rep.* **2017**, *7*, 10431.
44. Kim, H.J.; Kim, J.H.; Noh, S.; Hur, H.J.; Sung, M.J.; Hwang, J.T.; Park, J.H.; Yang, H.J.; Kim, M.S.; Kwon, D.Y.; et al. Metabolomic analysis of livers and serum from high-fat diet induced obese mice. *J. Proteome Res.* **2011**, *10*, 722–731.
45. Kim, H.Y.; Kim, M.; Park, H.M.; Kim, J.; Kim, E.J.; Lee, C.H.; Yoon Park, J.H. Lysophospholipid profile in serum and liver by high-fat diet and tumor induction in obesity-resistant BALB/c mice. *Nutrition* **2014**, *30*, 1433–1441.
46. Estruch, R.; Ros, E.; Salas-Salvadó, J.; Covas, M.-I.; Corella, D.; Arós, F.; Gómez-Gracia, E.; Ruiz-Gutiérrez, V.; Fiol, M.; Lapetra, J.; et al. Primary Prevention of Cardiovascular Disease with a Mediterranean Diet Supplemented with Extra-Virgin Olive Oil or Nuts. *N. Engl. J. Med.* **2018**, *378*, e34.
47. Kris-Etherton, P.M.; Dietschy, J. Design criteria for studies examining individual fatty acid effects on cardiovascular disease risk factors: Human and animal studies. *Am. J. Clin. Nutr.* **1997**, *65*, 1590S–1596S.
48. Mast, N.; Shafaati, M.; Zaman, W.; Zheng, W.; Prusak, D.; Wood, T.; Ansari, G.A.S.; Lövgren-Sandblom, A.; Olin, M.; Bjorkhem, I.; et al. Marked variability in hepatic expression of cytochromes CYP7A1 and CYP27A1 as compared to cerebral CYP46A1. Lessons from a dietary study with omega 3 fatty acids in hamsters. *Biochim. Biophys. Acta* **2010**, *1801*, 674–681.
49. Laos, S.; Caimari, A.; Crescenti, A.; Lakkis, J.; Puiggròs, F.; Arola, L.; Del Bas, J.M. Long-term intake of soyabean phytosterols lowers serum TAG and NEFA concentrations, increases bile acid synthesis and protects against fatty liver development in dyslipidaemic hamsters. *Br. J. Nutr.* **2014**, *112*, 663–673.
50. Kleiner, D.E.; Brunt, E.M.; Van Natta, M.; Behling, C.; Contos, M.J.; Cummings, O.W.; Ferrell, L.D.; Liu, Y.-C.; Torbenson, M.S.; Unalp-Arida, A.; et al. Design and validation of a histological scoring system for nonalcoholic fatty liver disease. *Hepatology* **2005**, *41*, 1313–1321.
51. Apte, A.; Meitei, N.S. Bioinformatics in Glycomics: Glycan Characterization with Mass Spectrometric Data Using SimGlycan. *Methods Mol. Biol.* **2010**, *600*, 269–281.
52. Zhao, S.; Walsh, I.; Abrahams, J.L.; Royle, L.; Nguyen-Khuong, T.; Spencer, D.; Fernandes, D.L.; Packer, N.H.; Rudd, P.M.; Campbell, M.P. GlycoStore: A database of retention properties for glycan analysis. *Bioinformatics* **2018**, *34*, 3231–3232.
53. Tarancon-Diez, L.; Rodríguez-Gallego, E.; Rull, A.; Peraire, J.; Viladés, C.; Portilla, I.; Jimenez-Leon, M.R.; Alba, V.; Herrero, P.; Leal, M.; et al.

Immunometabolism is a key factor for the persistent spontaneous elite control of HIV-1 infection. *EBioMedicine* **2019**, *42*, 86–96.

54. Tarancón-Diez, L.; Rull, A.; Herrero, P.; Vazquez-Alejo, E.; Peraire, J.; Guillén, S.; Navarro-Gomez, M.L.; Viladés, C.; Muñoz-Fernandez, M.Á.; Vidal, F. Early antiretroviral therapy initiation effect on metabolic profile in vertically HIV-1-infected children. *J. Antimicrob. Chemother.* **2021**, *76*, 2993–3001.
55. Samarra, I.; Masdevall, C.; Foguet-Romero, E.; Guirro, M.; Riu, M.; Herrero, P.; Canela, N.; Delpino-Rius, A. Analysis of oxylipins to differentiate between organic and conventional UHT milks. *Food Chem.* **2021**, *343*, 128477.
56. Peng, B.; Kopczynski, D.; Pratt, B.S.; Ejsing, C.S.; Burla, B.; Hermansson, M.; Benke, P.I.; Tan, S.H.; Chan, M.Y.; Torta, F.; et al. LipidCreator workbench to probe the lipidomic landscape. *Nat. Commun.* **2020**, *11*, 2057.

SUPPLEMENTARY MATERIAL

Supplementary Table 1. Composition of the diets used in the study. NFD, normal fat diet; HFD, high-fat diet; MED, Mediterranean-like Diet; EVOO, extra-virgin olive oil.

	NFD	**HFD**	**MED**
Energy			
Protein, % of kcal	21.6	21.2	21.3
Carbohydrate, % of kcal	67.2	55.9	55.6
Fat, % of kcal	11.3	22.9	23.1
Kcal/g	3.6	3.9	3.9
Ingredients (g/kg)			
Casein	220	233	230
L-Cystine	3	3.2	3.2
Corn Starch	380	291	291
Maltodextrin	100	106	106
Dextrose, monohydrate	50	53	53
Sucrose	100	106	106
Cellulose	50	53	51
Coconut Oil	7.74	5.3	5.3
Flaxseed Oil	5.16	4.2	4.2
Safflower Oil, linoleic	30.1	10.6	10.6
Lard	0	76.4	7.5
EVOO	0	0	50
Walnuts	0	0	20
Fish oil	0	0	6
Cholesterol	0.03	0.98	0.21

Vitamin Mix, AIN-93-VX (94047)	10	10.6	10.6
Choline Bitartrate	2.5	2.65	2.65
Mineral Mix, AIN-93G-MX (94046)	35	37.15	37.15
Potassium Citrate, monohydrate	5	5.3	5.3
Magnesium Oxide	1.2	1.27	1.27
Ferric Citrate	0.3	0.32	0.32
Cupric Carbonate	0.01	0.011	0.011
Fat profile			
Saturated fat (g/kg)	8.71	35.8	20.6
Monounsatured fat (g/kg)	5.74	40.7	46.1
Polyunsaturated fat (g/kg)	26.1	19.6	29.0
Unsaturated to saturated fat ratio	3.65	1.68	3.65

Supplementary Table 2. Fatty acid profile of the virgin olive oil included in the MED. SFAs, saturated fatty acids; MUFAs, monounsaturated fatty acids; PUFAs, polyunsaturated fatty acids.

Fatty acid	**%**
C14:0	0,0
C16:0	14,4
c9-C16:1	1,2
C17:0	0,1
c9-C17:1	0,2
C18:0	2,0
c9-C18:1	70,2
c9,12-C18:2	10,5
C18:3 n3	0,6
C20:0	0,4
C20:1	0,3
C22:0	0,1
C24:0	0,1
SFAs	17,0
MUFAs	71,9
PUFAs	11,1
TOTAL	100

Supplementary Table 3. Nutritional information of the walnuts included in the MED. SFAs, saturated fatty acids; MUFAs, monounsaturated fatty acids; PUFAs, polyunsaturated fatty acids.

	100 g
Energetic value (Kcal)	685
Proteins (g)	15
Total fat (g)	65
SFAs (g)	6.4
MUFAs (g)	10
PUFAs (g)	48
Carbohydrates (g)	4.0
Sugars (g)	2.9
Dietary fiber (g)	12
Salt (g)	0.02

Supplementary Table 4. Nutritional information of MEG-3™ '30' n-3 Food Oil included in the MED.

Energy content total Energy content total **Content in:**	kJ/100 g kcal/100 g	3'687 897
Fat	g/100 g	99.7
-> thereof saturated fatty acids	g	27.4
-> thereof mono-unsaturated fatty acids	g	22.5
-> thereof poly-unsaturated fatty acids	g	40.7
-> thereof trans fatty acids[1]	g	0
-> thereof cholesterol[1]	mg	530
Carbohydrates	g/100 g	0
-> thereof sugars	g	0
-> thereof polyols	g	0
-> thereof starch	g	0
Fibre	g/100 g	0
Protein	g/100 g	0
Salt (Sodium content x 2.5)	g/100 g	0

Supplementary Table 5. Identified brain N-glycans. Employed glycan nomenclature: F- Fucose; G- Galactose; S- N-Acetylneuraminic acid; Ga- a-linked Galactose; A1- Monoantennary, A2- Biantennary, B, bisecting GlcNAc linked α1-4 to α1-3 mannose. Numbers with parentheses indicate the preceding monosaccharide's linkage while those not in parentheses indicate the preceding characteristic's number. For example, F(6)A3G(4)3S(3,3,3)3 represents a core fucosylated triantennary glycan with 3 galactoses directly attached to antennae,

and the three antennae terminated with an N-glycolylneuraminic acid. Employed glycan nomenclature for glycan composition: HexNAc- N-Acetylhexosamine; Hex- Hexose; NeuAc- N-Acetylneuraminic acid; Fuc- Fucose; Gal- Galactose; GlcNAc- N-Acetylglucosamine; Man- Mannose.

Name	Composition	Precursor m/z
-	HexNAc2 Hex3	611.7628
M4	GlcNAc2 Man4	692.7899
M5	GlcNAc2 Man5	773.8161
-	HexNAc2 Hex4 NeuAc1	816.7985
F(6)M5	Fuc1 GlcNAc2 Man5	846.8442
M6 D1 (putative)	GlcNAc2 Man6	854.8422
M6D3	GlcNAc2 Man6	854.8434
F(6)A2	Fuc1 GlcNAc4 Man3	887.8706
A2[6]G(4)1	Gal1 GlcNAc4 Man3	895.872
A3	GlcNAc5 Man3	916.3829
M7 (putative)	GlcNAc2 Man7	935.8692
M7D3	GlcNAc2 Man7	935.8699
F(6)A2[3]G(4)1	Gal1 Fuc1 GlcNAc4 Man3	968.8977
A2G(4)2	Gal2 GlcNAc4 Man3	976.8975
F(6)A3	Fuc1 GlcNAc5 Man3	989.411
-	HexNAc4 Hex5 Fuc1 NeuAc3	991.3839
-	HexNAc7 Hex7 Fuc1	1011.0655
-	HexNAc3 Hex4 Fuc1 NeuAc1	1012.9059
F(6)A3G(4)3S(3,3)2	NeuAc2 Gal3 Fuc1 GlcNAc5 Man3	1016.0619
M8 D2,D3	GlcNAc2 Man8	1016.8943
M8	GlcNAc2 Man8	1016.8956
F(6)M5A1G(4)1	Fuc1 Gal1 GlcNAc3 Man5	1029.4121
	HexNAc8 Hex7	1029.7350
-	HexNAc6 Hex7 Fuc1 NeuAc1	1040.0698
-	NeuAc1 Hex1 HexNAc4 Hex3	1041.9283
F(6)A2[3]G1Ga1	Fuc1 Gal2 GlcNAc4 Man3-Isomer 1	1049.9238
F(6)A2[6]G1Ga1	Fuc1 Gal2 GlcNAc4 Man3-Isomer 2	1049.9261
-	HexNAc5 Hex6 NeuAc3	1064.7501
F(6)A2[3]BG(4)1	Gal1 Fuc1 GlcNAc5 Man3	1070.4368
-	HexNAc6 Hex7 NeuAc2	1088.4155
F(6)A4	Fuc1 GlcNAc6 Man3	1090.9519
-	HexNAc3 Hex5 Fuc1 NeuAc1	1093.9325
M9	GlcNAc2 Man9	1097.9217
F(6)M4A1G(4)1Sg(6)1	Fuc1 Gal1 GlcNAc3 Man4 NeuGc1	1101.9299

Name	Composition	Precursor m/z
-	HexNAc3 Hex6 NeuGc1	1110.419
F(6)A3G(4)3S(3,3,3)3	NeuAc3 Gal3 Fuc1 GlcNAc5 Man3	1113.0953
F(6)A2[6]G(4)1S(6)1	Fuc1 Gal1 GlcNAc4 Man3 NeuAc1-Isomer 1	1114.4457
F(6)A2[3]G(4)1S(3)1	Fuc1 Gal1 GlcNAc4 Man3 NeuAc1-Isomer 2	1114.4462
-	HexNAc6 Hex5 Fuc1 NeuAc3	1126.7695
-	HexNAc8 Hex8 Fuc1	1132.4403
-	HexNAc5 Hex4 NeuAc1	1143.4665
-	HexNAc5 Hex6 NeuAc4	1161.7798
-	HexNAc6 Hex6 Fuc1 NeuAc3	1180.7875
-	HexNAc4 Hex5 Fuc1 NeuAc1	1195.9816
-	HexNAc5 Hex6 Fuc1 NeuAc4	1210.1249
-	HexNAc5 Hex4 Fuc1 NeuAc1 -Isomer 1	1215.9866
F(6)A2[6]BG(4)1S(6)1	NeuAc1 Gal1 Fuc1 GlcNAc5 Man3-Isomer 2	1215.9891
F(6)A4G(4)4S(3,3,3)3	NeuAc3 Gal4 Fuc1 GlcNAc6 Man3-Isomer 1	1234.8057
F(6)A3G(4)3Lac1S3	NeuAc3 Gal4 Fuc1 GlcNAc6 Man3-Isomer 2	1235.1454
M11 a3D1,[D2(1),D3(1)],a2D4(2)	GlcNAc2 Man11	1259.9943
-	HexNAc4 Hex5 NeuAc2	1268.4994
-	HexNAc6 Hex7 NeuAc4 -Isomer 1	1283.491
-	HexNAc6 Hex7 NeuAc4 -Isomer 2	1283.4952
-	HexNAc8 Hex9 Fuc3	1283.8297
A2G(4)2Sg(3,6)2	NeuGc2 Gal2 GlcNAc4 Man3- Isomer 1	1283.9852
A2G(4)2Sg(6,6)2	NeuGc2 Gal2 GlcNAc4 Man3- Isomer 2	1283.9866
-	HexNAc7 Hex7 Fuc1 NeuAc3	1302.8351
A3G(4)3S(6)1	NeuAc1 Gal3 GlcNAc5 Man3	1304.9926
-	HexNAc6 Hex5 Fuc2	1325.9973
FA4G(4,4,4,4)4S(3,3,3,3)4	NeuAc4 Gal4 Fuc1 GlcNAc6 Man3	1331.838
F(6)A2G(4)2S(6,6)2	NeuAc2 Gal2 Fuc1 GlcNAc4 Man3-Isomer 1	1341.0211
F(6)A2G(4)2S(3,3)2	NeuAc2 Gal2 Fuc1 GlcNAc4 Man3-Isomer 2	1341.0214
F(6)A2G(4)2Sg(6,6)2	Fuc1 Gal2 GlcNAc4 Man3 NeuGc2-Isomer 1	1357.016
F(6)A2G(4)2Sg(3,6)2	Fuc1 Gal2 GlcNAc4 Man3 NeuGc2-Isomer 2	1357.5054
-	HexNAc5 Hex4 NeuAc2 Fuc1	1361.5341
-	HexNAc5 Hex5 NeuAc2	1370.0424
F(6)A3G(4)3S(3)1	Fuc1 Gal3 GlcNAc5 Man3 NeuAc1	1378.0222
-	HexNAc6 Hex7 Fuc2 NeuAc4	1380.5217
	HexNAc6 Hex3 Fuc1 NeuAc2	1382.0477
-	HexNAc4 Hex5 NeuAc3	1414.0498
F(6)A2BG(4)2S(6,6)2	NeuAc2 Gal2 Fuc1 GlcNAc5 Man3	1442.5621
-	HexNAc5 Hex6 Fuc1 NeuAc3	1669.6472

UNIVERSITAT ROVIRA I VIRGILI
EXPLORING THE ROLE OF GLYCANS: A NEW FRONTIER IN DISEASE BIOMARKER RESEARCH
Beatrix Paton Jimenez

Chapter 3

To determine glycan signatures for reliable risk stratification of COVID-19 patients and to identify patients who are more likely to progress to a critical stage

UNIVERSITAT ROVIRA I VIRGILI
EXPLORING THE ROLE OF GLYCANS: A NEW FRONTIER IN DISEASE BIOMARKER RESEARCH
Beatrix Paton Jimenez

PREFACE

In this last chapter, we focused on deepening the role of N-glycans in infectious diseases, specifically in COVID-19. The emergence of the COVID-19 pandemic in 2020, led to the opportunity to evaluate the profile of N-glycans in COVID-19 patients. While most studies focused on elucidating how glycosylation affects the proteins of the SARS-CoV-2 virus, we examined N-glycan signatures in the host. We analysed the total plasma N-glycome composition from COVID-19 patients and evaluated its potential as a biomarker for the development of the disease (**Manuscript 4**).

Building on the findings of a prior study that established fetuin-A as an accurate biomarker of the critical clinical progression of COVID-19, we considered that the glycan signature of fetuin-A could potentially surpass the total plasma N-glycome signature in accuracy for predicting disease development. Therefore, we performed a site-specific glycan analysis of human fetuin-A, aiming to look for differences in the glycosylation pattern between groups of severity (**Manuscript 5**). This study allowed us to explore the field of glycoproteomics, adding a new dimension to our research. The use of two complementary fields, glycomics and glycoproteomics, contributed to our understanding of glycosylation in COVID-19. Additionally, we continued to uphold our cross-cutting objectives, by examining glycans in plasma from COVID-19 patients, further assessing the viability of glycomic studies in different organisms.

Manuscript 4

Fucosylated N-glycans as early biomarkers of COVID-19 severity

Beatrix Paton, Pol Herrero, Joaquim Peraire, Antoni del Pino, Sílvia Chafino, Javier Martinez-Picado, Fréderic Gómez-Bertomeu, Anna Rull, Núria Canela and Manuel Suárez

Article

Published in Frontiers in Immunology

Impact Factor: 8.787; Q1, Viral Immunology

(2023) 14:1204661

doi: 10.3389/fimmu.2023.1204661

Fucosylated N-glycans as early biomarkers of COVID-19 severity

Beatrix Paton [1], Pol Herrero [1], Joaquim Peraire [2 3 4 5], Antoni Del Pino [1], Silvia Chafino [2 3 4], Javier Martinez-Picado [4 6 7 8 9], Fréderic Gómez-Bertomeu [2 3 4 5], Anna Rull [2 3 4 5], Núria Canela [1], Manuel Suárez [3 10]

1 Eurecat, Centre Tecnològic de Catalunya, Centre for Omic Sciences (Joint Unit Eurecat- Universitat Rovira i Virgili), Unique Scientific and Technical Infrastructure (ICTS), Reus, Spain.

2 Hospital Universitari de Tarragona Joan XXIII (HJ23), Tarragona, Spain.

3 Institut Investigació Sanitària Pere Virgili (IISPV), Tarragona, Spain.

4 Centro de Investigación Biomédica en Red de Enfermedades Infecciosas (CIBERINFEC), Instituto de Salud Carlos III, Madrid, Spain.

5 Universitat Rovira i Virgili (URV), Tarragona, Spain.

6 IrsiCaixa AIDS Research Institute, Badalona, Spain.

7 Germans Trias i Pujol Research Institute (IGTP), Badalona, Spain.

8 University of Vic-Central University of Catalonia (UVic-UCC), Vic, Spain.

9 Catalan Institution for Research and Advanced Studies (ICREA), Barcelona, Spain.

10 Universitat Rovira i Virgili, Departament de Bioquímica i Biotecnologia, Nutrigenomics Research Group, Tarragona, Spain.

* Correspondence: Dr Anna Rull and Dr Núria Canela

ABSTRACT

Background: The pathological mechanisms of SARS-CoV-2 in humans remain unclear and the unpredictability of COVID-19 progression may be attributed to the absence of biomarkers that contribute to the prognosis of this disease. Therefore, the discovery of biomarkers is needed for reliable risk stratification and to identify patients who are more likely to progress to a critical stage.

Methods: Aiming to identify new biomarkers we analysed N-glycan traits in plasma from 196 patients with COVID-19. Samples were classified into three groups according to their severity (mild, severe and critical) and obtained at diagnosis (baseline) and at 4 weeks of follow-up (postdiagnosis), to evaluate their behaviour through disease progression. N-glycans were released with PNGase F and labelled with Rapifluor-MS, followed by their analysis by LC-MS/MS. The Simglycan structural identification tool and Glycostore database were employed to predict the structure of glycans.

Results: We determined that plasma from SARS-CoV-2-infected patients display different N-glycosylation profiles depending on the disease severity. Specifically, levels of fucosylation and galactosylation decreased with increasing severity and Fuc1Hex5HexNAc5 was identified as the most suitable biomarker to stratify patients at diagnosis and distinguish mild from critical outcomes.

Conclusion: In this study we explored the global plasma glycosignature, reflecting the inflammatory state of the organs during the infectious disease. Our findings show the promising potential of glycans as biomarkers of COVID-19 severity.

1. INTRODUCTION

Three significant coronavirus outbreaks have been documented to date, with the most recent being caused by the 2019 novel coronavirus (2019-nCoV, also known as SARS-CoV-2), which is known to cause the Coronavirus Disease-2019 (COVID-19) (1). Since the start of the pandemic in 2020, over 6.6 million deaths from COVID-19 have been reported globally, resulting in one of the major global health crises of the 21st century (2). In most cases, SARS-CoV-2 infection is accompanied by a variety of symptoms, including fever, cough, and general malaise (3). Acute lung injury and acute respiratory distress syndrome appear in more severe COVID-19 instances, which can induce morbidity and mortality due to pneumonia and inflammation caused by damage to the alveolar lumen (4, 5).

The pathophysiology of COVID-19 still needs to be better understood, which will lead to better clinical and therapeutic approaches for patients, improved management of healthcare resources, as well as advancements in vaccination strategy. The SARS-CoV-2 vaccinations that are currently available have been crucial for controlling the pandemic, but their long-term effectiveness and delivery methods are still being tested (6, 7). Additionally, it remains unclear if an association exists between having certain risk factors and an increased death rate, and why some COVID-19 patients can fight the infection while others require hospitalization. Therefore, prognostic and predictive biomarkers must be identified to promptly detect patients who are more likely to evolve to a critical state of the disease (8, 9).

Within this framework, omics datasets, such as proteomics, lipidomics and metabolomics have been used to improve the understanding of the immunopathogenesis and the host immune response to SARS-CoV-2, and study the biological factors that contribute to a worse prognosis of patients with COVID-19 (9–11). In addition to these omics techniques, the detection

of glycomic alterations could potentially extend the knowledge of COVID-19. Plasma glycomic changes are considered biomarkers for a variety of illnesses, including diabetes, systemic lupus erythematosus, colorectal cancer, and cardiovascular disease (12–16). Beyond being used as a biomarker, the circulating glycome on plasma has been shown to mediate and drive significant immunological functions (17). Plasma glycoproteins are released from organs and enter the circulation by active secretion or leakage. Several studies have shown that glycosylation of such circulating glycoproteins can reflect the inflammatory states of these organs during chronic diseases (18). The study of the glycoprofile in COVID-19 has received some attention, specifically in serum immunoglobulin Gs (IgGs). Afucosylated Fc N-glycans in IgGs specific for SARS-CoV-2-spike protein have been found to be more prevalent in critically ill patients (19), and total IgG N-glycome composition has been reported to be different between mild and severe disease patients (20). Additionally, levels of galactose and sialic acid structures on IgGs have been reported to predict the development of a poor COVID-19 disease (21).

Samples were collected during the first and second waves of the COVID-19 pandemic in Spain, which started in March 2020 and October 2020, respectively. During this period, alpha and beta (lineages B.1.1.7 and B.1.351, respectively) were the predominant circulating variants (22) and patients were still not vaccinated against COVID-19, as vaccines were not made available until later in the year (23). This cohort was initially used in a previous study in which metabolomics, lipidomics and proteomics analyses were conducted to identify key molecules involved in the mechanistic pathways of the disease. Specific molecules related to complement and coagulation cascades, platelet activation, cell adhesion, acute inflammation, energy production (Krebs cycle and Warburg effect), amino acid catabolism and lipid transport were identified as fingerprints of the acute disease. Additionally, fetuin-A, inter-α-trypsin, glutamic acid and cholesteryl ester 18:0 were collectively proposed as a novel panel of

biomarkers to differentiate mild from critical COVID-19 outcomes (9). To enrich the knowledge about COVID-19 progression and extend the list of potential biomarkers, our study focused on analysing the total plasma N-glycome composition of 196 patients at diagnosis and at 4 weeks postdiagnosis, to assess if it can help stratify COVID-19 patients and evaluate whether it can act as a biomarker for the development of COVID-19. We aimed to obtain a global plasma glycosignature, instead of exclusively focusing on the IgG N-glycome, to reflect the inflammatory state of the organs during the infectious disease.

2. RESULTS

The sample size employed in this study consisted of 196 COVID-19 patients, classified into three groups according to their severity (mild, severe and critical) (9). Disease progression was evaluated at 4 weeks postdiagnosis for 122 of the aforementioned patients. Firstly, the glycosignature in COVID-19 patients was presented, followed by a comparison between groups of severity at diagnosis and an evaluation of potential glycosignatures to indicate disease severity in COVID-19 at diagnosis. Additionally, the N-glycan profile at 4 weeks postdiagnosis was evaluated to explore the potential of total plasma N-glycome to act as a biomarker for COVID-19 disease progression. N-glycan compositions detected by mass spectrometry were reported as follows: Hex [hexose, either galactose (Gal), or mannose (Man)], HexNAc [N-acetylhexosamine], Fuc [fucose] and Neu5Ac [N-acetylneuraminic acid].

2.1 N-linked glycosylation variations among COVID-19 patients at diagnosis

The N-glycan profile at diagnosis was evaluated to explore the prognostic potential of total plasma N-glycome as a biomarker for COVID-19 disease severity. Patients were classified at diagnosis as mild (n=56), severe (n=105) and critical (n=35) (24). Total plasma N-glycan composition was determined by LC-MS/MS analysis of RFMS-labelled glycans, confirming

structures with MS/MS data. A total of 36 structures were identified in all patients (Supplementary Table 1) and 13 additional structures were detected but could not be accurately annotated. The most abundant structures in all the samples were biantennary and were specifically Neu5Ac2Hex5HexNAc4 followed by Neu5Ac1Hex5HexNAc4 and Fuc1Hex3HexNAc4. A total of 22 N-glycans were found to be statistically significant between groups at diagnosis (Figure 1). These 22 N-glycans were further tested as potential biomarkers for COVID-19 for their ability to predict the disease course at diagnosis.

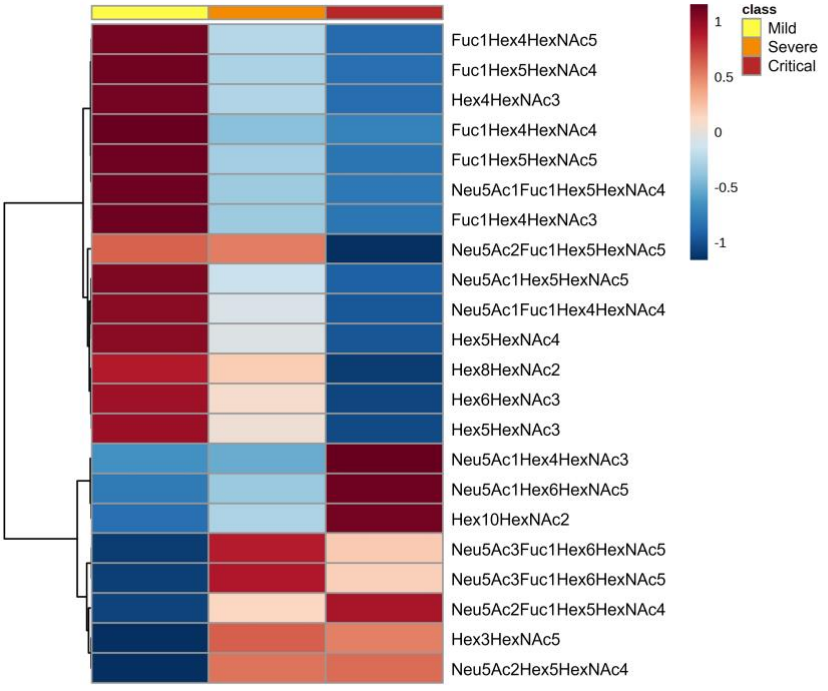

Figure 1. N-glycan signatures associated with COVID-19 disease severity. Heatmap plotting the significant relative abundance of N-glycans increasing or decreasing at diagnosis in accordance with disease severity. Significant differences ($p < 0.05$) between mild, severe and critical COVID-19 groups of patients were determined by Kruskal-Wallis test. Columns indicate the degree of disease severity: mild (left), severe (centre) and critical (right) groups. Mean values for each compound in each COVID-19 group (columns) are colour-coded based on relative abundance, low (blue) and high (red).

2.2 Plasma N-glycosylation profile at diagnosis aids in the stratification of patients and predicts COVID-19 prognosis

A random forest analysis was used to evaluate the effectiveness of the statistically significant total plasma N-glycans as predictive biomarkers to indicate disease severity in COVID-19 at diagnosis. Results indicated that the top 3 N-glycans with the highest discriminatory power between groups were Fuc1Hex5HexNAc5 and Hex6HexNAc3, which decrease with increasing severity, and Neu5Ac1Hex4HexNAc3, which increases with severity (Figure 2).

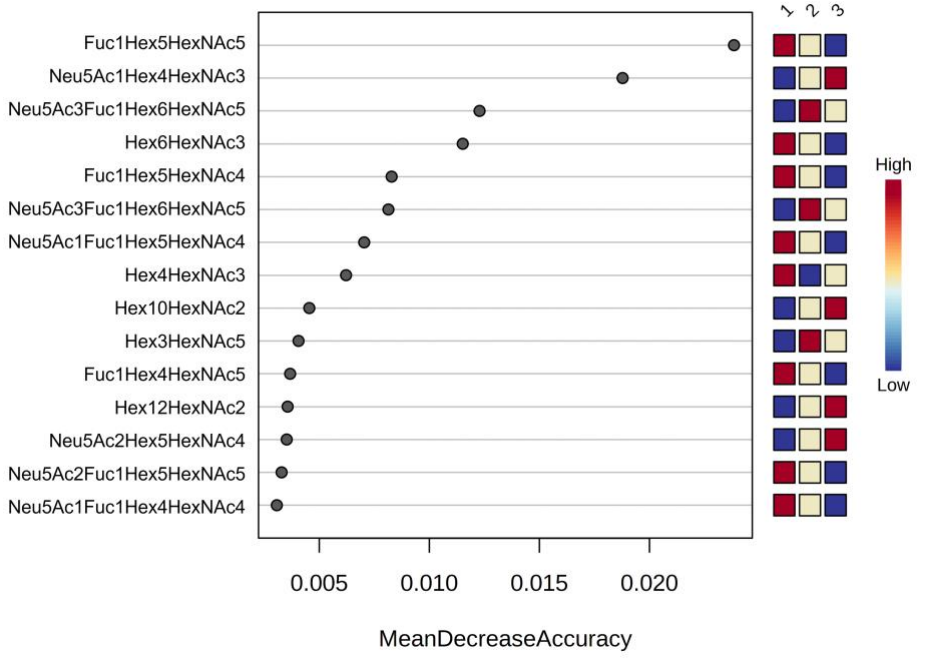

Figure 2. Random forest analysis. Random forest modelling of the top 15 significant N-glycans with the highest discriminatory power between groups (1 = mild, 2 = severe and 3 = critical). Coloured boxes on the right indicate the relative concentrations of the corresponding N-glycan in each group.

Subsequently, prediction models were built to evaluate the predictive efficacy of some of the N-glycans with the highest classification accuracy. Receiver operating characteristic (ROC) curves were generated through a

binary logistic regression analysis comparing the mild vs. critical groups, severe vs. critical groups and mild vs. severe groups (Table 1; Figure 3). The ROC curve analysis was performed for an individual N-glycan and for the ratio of two N-glycans. The ratio was computed as it was able to provide more information than the two corresponding N-glycans alone. These ratios were computed for all possible N-glycan pairs and the top-ranked ratio (based on p-values) was selected for further biomarker analysis.

Table 1. ROC curve analysis data obtained for a selected N-glycan and a ratio between two selected N-glycans showing the area under the curve (AUC) scores, significance, specificity and sensitivity.

COVID-19 group	N-glycan/s	AUC	Significance	Sensitivity (%)	Specificity (%)
Mild vs Critical	Fuc1Hex5HexNAc5	0.880	<0.001	73.1	90.9
	Fuc1Hex5HexNAc4/Hex10HexNAc2	0.881	<0.001	88.5	78.8
Severe vs Critical	Fuc1Hex5HexNAc5	0.793	<0.001	77.9	57.6
	Fuc1Hex5HexNAc4/Hex10HexNAc2	0.750	<0.001	79.2	72.7
Mild vs Severe	Fuc1Hex5HexNAc5	0.666	0.02	73.1	67.5
	Fuc1Hex5HexNAc4/Hex10HexNAc2	0.701	0.002	73.1	64.9

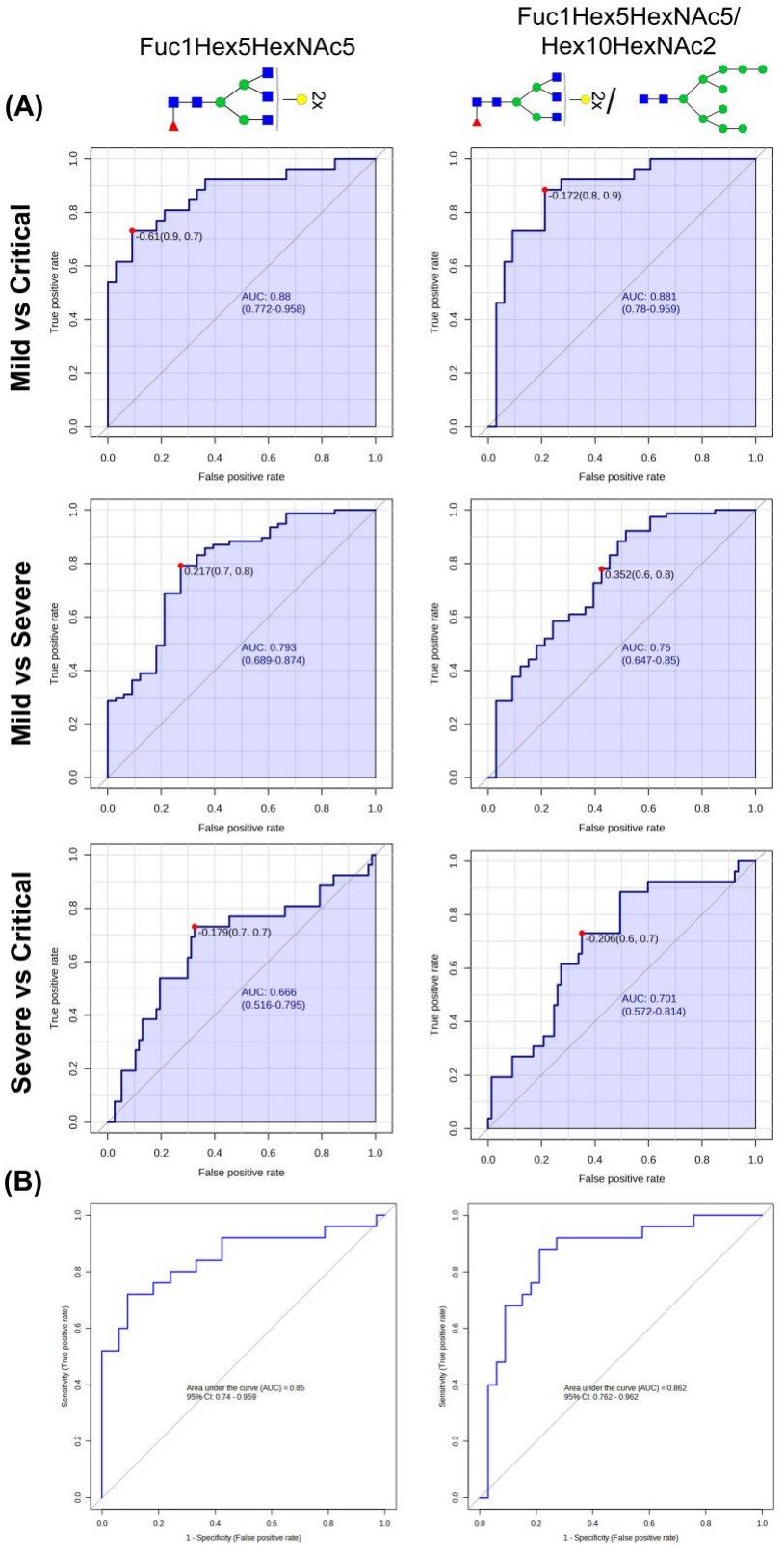
(A)
Fuc1Hex5HexNAc5
Fuc1Hex5HexNAc5/
Hex10HexNAc2
Mild vs Critical
Mild vs Severe
Severe vs Critical
-0.61(0.9, 0.7)
AUC: 0.88
(0.772-0.958)
-0.172(0.8, 0.9)
AUC: 0.881
(0.78-0.959)
0.217(0.7, 0.8)
AUC: 0.793
(0.689-0.874)
0.352(0.6, 0.8)
AUC: 0.75
(0.647-0.85)
-0.179(0.7, 0.7)
AUC: 0.666
(0.516-0.795)
-0.206(0.6, 0.7)
AUC: 0.701
(0.572-0.814)
True positive rate
False positive rate
(B)
Area under the curve (AUC) = 0.85
95% CI: 0.74 - 0.959
Area under the curve (AUC) = 0.862
95% CI: 0.762 - 0.962
Sensitivity (True positive rate)
1 - Specificity (False positive rate)

Figure 3. N-glycan biomarkers to indicate COVID-19 severity at diagnosis. **(A)** Receiver operating characteristic (ROC) curves analyses of Fuc1Hex5HexNAc5 and Fuc1Hex5HexNAc5/Hex10HexNAc2 for distinguishing COVID-19 patients between groups of severity. **(B)** Binary logistic regression modelling analysis testing the accuracy of Fuc1Hex5HexNAc5 and Fuc1Hex5HexNAc5/Hex10HexNAc2 to differentiate mild from critically ill patients with COVID-19 in a randomly selected set of patients. For the N-glycan cartoons, green circles denote mannose, yellow circles denote galactose, blue squares denote N-acetylglucosamine, red triangles denote fucose, and purple diamonds denote N-acetylneuraminic acid.

The ratio of Fuc1Hex5HexNAc4/Hex10HexNAc2 was the top-ranked ratio ($p<0.001$), showing a high capacity to differentiate between mild and critical patients, with an AUC of 0.881 and a specificity and a sensitivity of 90.9 and 73.1%, respectively. Similarly, Fuc1Hex5HexNAc5, individually, was also optimal to distinguish between mild from critical patients (AUC = 0.88; $p<0.001$) (Table 1; Figure 3A). In the random forest analysis, Fuc1Hex5HexNAc5 was considered to be the N-glycan with the highest classification accuracy.

Regarding the other two pairwise comparisons, severe vs critical and mild vs severe, more biomarkers should be considered to rapidly identify the clinical progression of patients at an early stage, as AUCs ranged between 0.666 and 0.793. Next, a regression model was performed in a randomly selected set of patients to validate the accuracy of these aforementioned N-glycans to properly predict mild and critical outcomes at diagnosis. Results indicated that the ratio Fuc1Hex5HexNAc4/Hex10HexNAc2 (AUC=0.862, $p<0.001$, specificity=78.8% and sensitivity=88.0%) and Fuc1Hex5HexNAc5 (AUC=0.85, $p<0.001$, specificity=90.9% and sensitivity=72.0%) could be suitable biomarkers to distinguish mild from critical outcomes (Figure 3B).

2.3 N-linked glycosylation variations among COVID-19 patients at 4 weeks postdiagnosis

The N-glycan profile at 4 weeks postdiagnosis was evaluated to explore the potential of total plasma N-glycome to act as a biomarker for COVID-19 disease course prediction. A total of 18 N-glycans were found to be statistically significant between groups at 4 weeks postdiagnosis, 15 of which were also significantly altered at diagnosis. The progression of these 15 N-glycans at diagnosis and at 4 weeks for the different groups of severity is shown in Figure 4. The aforementioned N-glycans (Fuc1Hex5HexNAc5 and Hex10HexNAc2) that were tested as potential biomarkers using a regression model were altered at diagnosis and at 4 weeks postdiagnosis. Fuc1Hex5HexNAc5 showed the same tendency at both time points, decreasing with increasing severity. Differently, Hex10HexNAc2 increased with increasing severity at diagnosis and at 4 weeks postdiagnosis. Interestingly, for both N-glycans, the significance of the alterations was higher at diagnosis than at 4 weeks. The remaining 13 N-glycans altered at both time points showed similar tendencies at diagnosis and at 4 weeks postdiagnosis (Figure 4). More specifically, all the statistically significant fucosylated structures decreased with increasing severity at diagnosis and at 4 weeks, except for Neu5Ac3Fuc1Hex6HexNAc5 which increased with increasing severity.

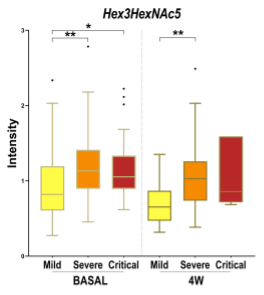
Hex3HexNAc5
Intensity
Mild Severe Critical Mild Severe Critical
BASAL 4W

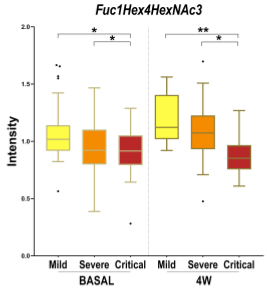
Fuc1Hex4HexNAc3
Intensity
Mild Severe Critical Mild Severe Critical
BASAL 4W

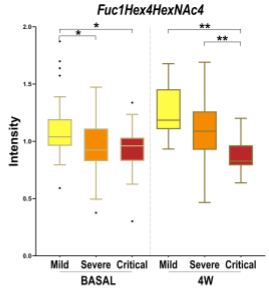
Fuc1Hex4HexNAc4
Intensity
Mild Severe Critical Mild Severe Critical
BASAL 4W

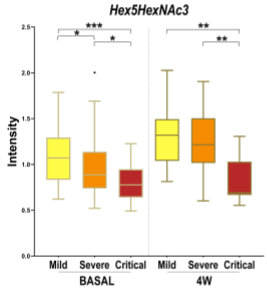
Hex5HexNAc3
Intensity
Mild Severe Critical Mild Severe Critical
BASAL 4W

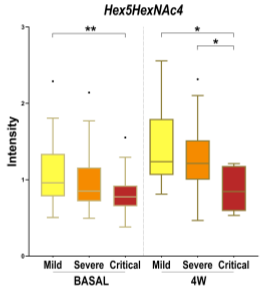
Hex5HexNAc4
Intensity
Mild Severe Critical Mild Severe Critical
BASAL 4W

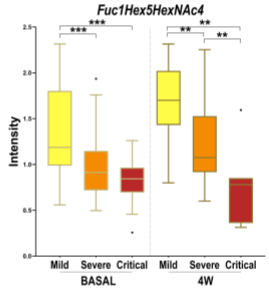
Fuc1Hex5HexNAc4
Intensity
Mild Severe Critical Mild Severe Critical
BASAL 4W

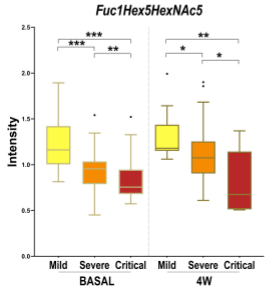
Fuc1Hex5HexNAc5
Intensity
Mild Severe Critical Mild Severe Critical
BASAL 4W

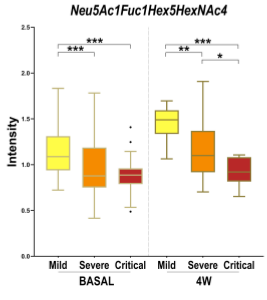
Neu5Ac1Fuc1Hex5HexNAc4
Intensity
Mild Severe Critical Mild Severe Critical
BASAL 4W

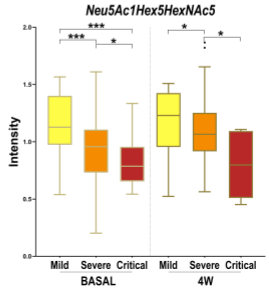
Neu5Ac1Hex5HexNAc5
Intensity
Mild Severe Critical Mild Severe Critical
BASAL 4W

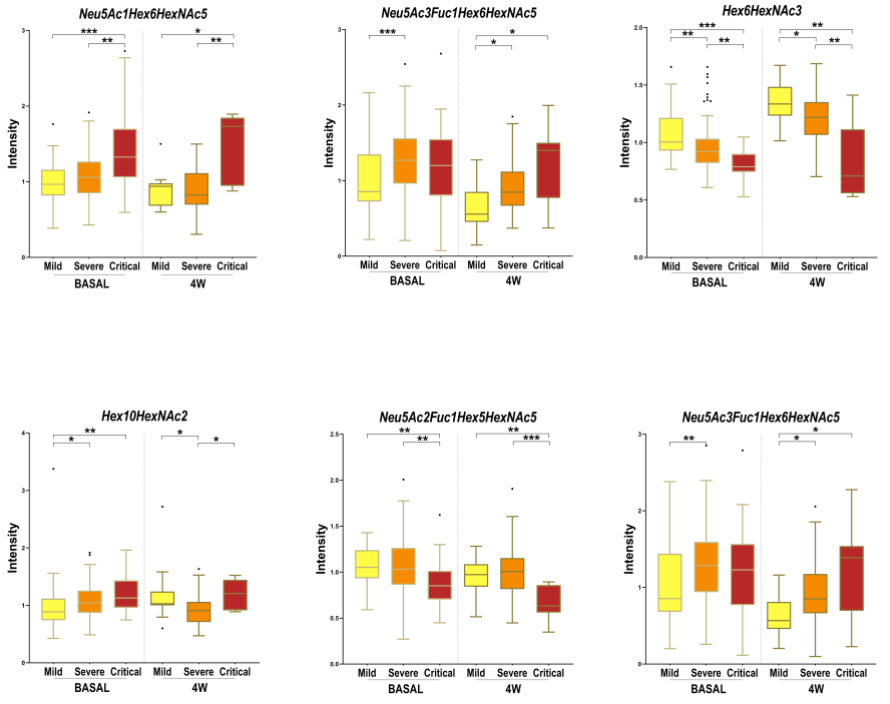

Figure 4. Box-and-whisker plots showing N-glycan abundance levels in COVID-19 patients. Relative abundance of total plasma N-glycans in different COVID-19 severities (mild, severe and critical) at diagnosis (BASAL) and at 4 weeks postdiagnosis (4W). Kruskal-Wallis, *p-value < 0.05; **p-value < 0.01 ***p-value < 0.001.

Three additional N-glycans were altered only at 4 weeks between severity groups, specifically Hex4HexNAc5 and NeuAc1Hex4HexNAc5, which increased with severity and Hex7HexNAc2, which decreased with severity. To obtain a global picture of the observed significant alterations at diagnosis and at 4 weeks postdiagnosis, glycan structures were grouped by their traits in terms of bisecting GlcNAc (N-acetylglucosamine), oligomannose-type, fucosylation, galactosylation and sialylation (Figure 5). Total plasma bisecting GlcNAc structures significantly decreased in critical patients when compared with mild and severe ones at diagnosis, whereas the trend shifted at 4 weeks postdiagnosis, increasing in severe patients compared to mild ones. A similar pattern was observed for fucosylation

and galactosylation, both decreasing with increasing severity at diagnosis and at 4 weeks postdiagnosis. Notably, a greater significance between groups of severity was observed at diagnosis than at 4 weeks. Differently, oligomannose structures increased with severity at diagnosis and showed no significant alterations between groups at 4 weeks postdiagnosis. No significant changes were observed in sialylation.

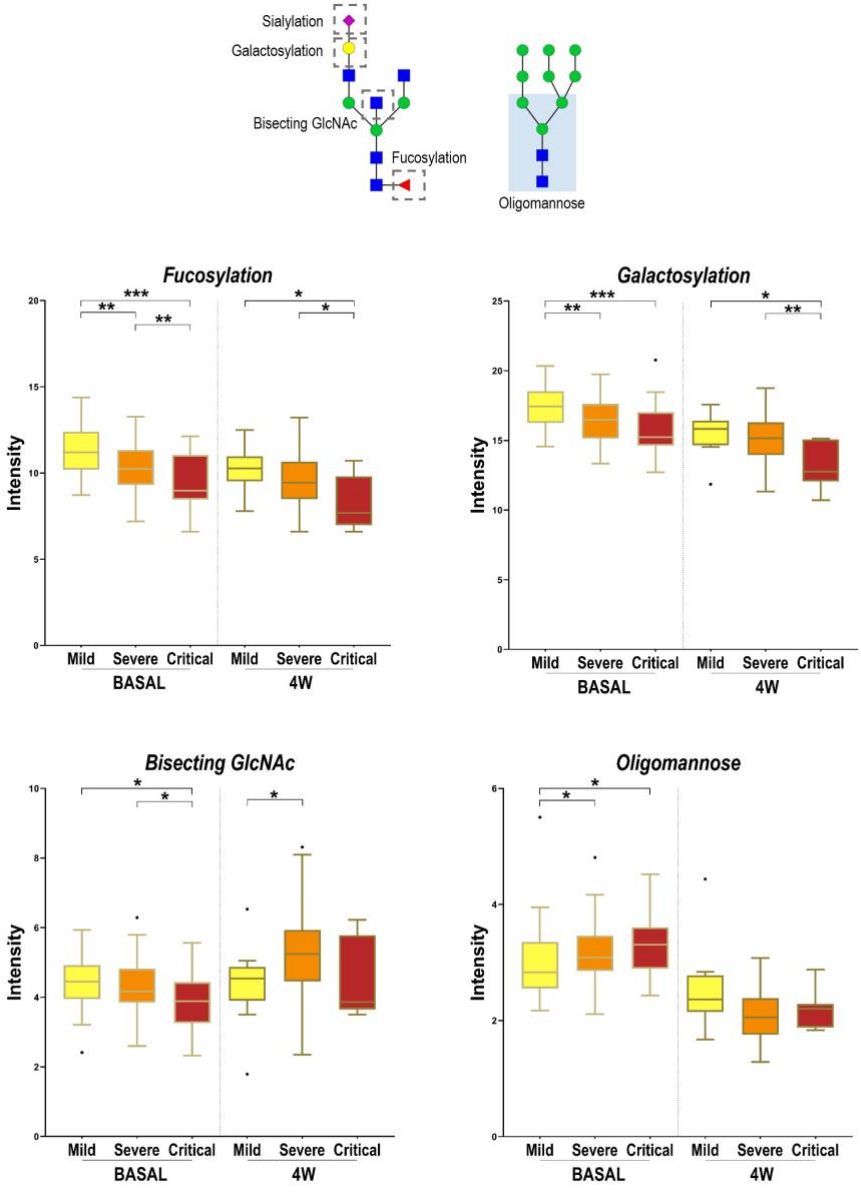

Figure 5. Alterations in four N-glycan families according to disease severity. Relative abundance of total Bisecting GlcNAc, fucosylation, galactosylation and

oligomannose structures in different COVID-19 severities (mild, severe and critical) at diagnosis (BASAL) and at 4 weeks postdiagnosis (4W). Kruskal-Wallis, *p-value < 0.05; **p-value < 0.01; ***p-value < 0.001. For the N-glycan cartoons, green circles denote mannose, yellow circles denote galactose, blue squares denote N-acetylglucosamine, red triangles denote fucose, and purple diamonds denote N-acetylneuraminic acid.

3. DISCUSSION

We have demonstrated that total plasma from SARS-CoV-2-infected patients displays different glycosylation profiles that can be detected at diagnosis and at 4 weeks postdiagnosis, aiding in the stratification of patients and with potential to predict COVID-19 prognosis. A total of 15 N-glycans were statistically significant between groups at diagnosis as well as at 4 weeks postdiagnosis, showing a similar trend at both time points. We determined that fucosylated and galactosylated structures significantly decreased in critical patients when compared with mild and severe ones. In line with our results, a deficiency of IgG galactosylation has been observed in COVID-19 patients (25) that display a poor disease course (21), showing that agalactosylation on IgG is associated with the activation of the lectin-initiated complement pathway in the development of inflammatory diseases (25, 26). Moreover, we found that agalactosylated structures were increased in critical patients compared to moderate and mild ones. Levels of galactosylation in IgG are, in fact, one of the most prominent glycosylation alterations observed in several chronic inflammatory and autoimmune diseases (27). Regarding fucosylation, recent studies on IgG glycome show a decrease in fucosylation in SARS-CoV-2 infected patients, which upregulates antibody-dependent cell cytotoxicity (ADCC) in acute immune responses (25). Also, in accordance with our results at diagnosis, glycans with bisecting GlcNAc have been reported to be significantly lower in COVID-19 cases, compared to controls, potentially causing a decrease in the modulation of the inflammatory response among COVID-19 patients (25). Loss of sialylation

in total IgG Fc has been observed in severe patients compared to mild ones (21, 25). The ability of IgG to participate in complement-dependent cytotoxicity (CDC) activity via C1q binding is decreased in the absence of sialylation, increasing the activation of the lectin-initiated alternative complement pathway (28). In our study, some sialylated N-glycans increased with severity and others decreased with severity at diagnosis. No significant differences in sialylation were reported at 4 weeks postdiagnosis. With the obtention of a global plasma glycosignature, we potentially observed the inflammatory state of the organs during the disease. The tendencies observed were similar to those reported in the IgG N-glycome, indicating that the IgG N-glycan profile can be obtained without purifying IgG, thus simplifying the sample preparation.

Other prognostic biomarkers have been proposed for COVID-19 based on metabolomics, lipidomics and proteomics analyses (9, 29–31). In a previous study from this same cohort of patients, fetuin-A, inter-α-trypsin inhibitor 3, glutamic acid and cholesterol ester 18:0 were reported to be the most accurate biomarkers of the critical clinical progression of COVID-19 (9). The addition of Fuc1Hex5HexNAc5 or Fuc1Hex5HexNAc4/Hex10HexNAc2 to this set of biomarkers could potentially improve the prediction of mild and critical outcomes. Moreover, these glycans were significantly altered between groups at diagnosis and at 4 weeks postdiagnosis, showing the same tendency at both time points. Interestingly, for these N-glycans, the significance of the alterations was higher at diagnosis than at 4 weeks, showing the potential of these glycans to become biomarkers that can be detected at early stages.

It is crucial to account for potential confounding factors that can influence the interpretation of the results. We specifically looked for the influence of pre-existing health conditions that could impact COVID-19 severity and affect biomarker levels. A few patients in the cohort presented comorbidities such as diabetes, cardiovascular disease or cancer. We observed that N-glycans Hex3HexNAc5 and Hex4HexNAc5 were affected by these comorbidities. However, most of the significantly altered N-

glycans between groups of severity, including all fucosylated N-glycans, were not biased by the presence of other comorbidities. Importantly, no associations were observed between any underlying medical conditions and the proposed biomarkers, Fuc1Hex5HexNAc5 and Fuc1Hex5HexNAc4/Hex10HexNAc2. Future studies should be designed to minimise the impact of confounding factors. The validation of the obtained results using larger and well-characterised multicentric cohorts will help account for population heterogeneity and increase the generalisability of findings. These studies will also help to determine the impact of different SARS-CoV-2 variants in total plasma glycosylation, as in the moment of sample recruitment the circulating variants were mainly alpha and beta. Additionally, future longitudinal studies including analysis of samples before and after infection would be useful to determine whether these structures could be employed as preinfection biomarkers to predict the critical clinical progression of COVID-19. However, it is important to note the difficulty implied in obtaining a sample from an individual before and after the SARS-CoV-2 infection. On the other hand, the analysis of samples from healthy volunteers, who have never been diagnosed with the disease, could aid in the identification of biomarkers that are highly specific to COVID-19 infection, as well as help control for confounding factors that may be present in COVID-19 positive patients. Finally, additional studies in the vaccinated population should focus on breakthrough infections requiring hospitalization, as well as measuring the effectiveness of vaccines to prevent infection and hospitalization. Overall, this study reveals a novel risk screening system based on the plasma N-glycome signature, able to assess the stratification of COVID-19 patients and discriminate the progression of the disease at diagnosis. The reported minimally invasive blood biomarker has the potential to improve and optimise the management of healthcare resources and vaccination strategies in COVID-19.

4. METHODS

4.1 Study design and classification criteria

A total of 196 patients with SARS-CoV-2 infection who had positive polymerase chain reaction (PCR) confirmation within the first 21 days of infection make up the COVID-19 patient cohort. Patients were categorised into 3 groups of severity (mild (n=56), severe (n=105) and critical (n=35)), according to the inclusion criteria described in "Diagnosis and Treatment Protocol for COVID-19 Patients (version 8 trial)" (24). Additionally, disease progression was evaluated at 4 weeks postdiagnosis for 122 of the aforementioned patients (mild (n=22), severe (n=82) and critical (n=18)). The severity classification changed for 49 patients during the 4 weeks postdiagnosis, with 16 patients changing from mild to severe, 32 from severe to critical and one from critical to severe. Data from patients were stored in a database with information about the hospitalization, including the symptoms that were present at the time of admission, radiological findings, the severity of pneumonia, the need for oxygen therapy, the medical treatment received, as well as demographic information and previously diagnosed diseases of interest (9). Patients' demographic and relevant clinical data are summarised in Supplementary Table 2. Briefly, the cohort median age increased with COVID-19 severity and the female sex predominated in the mild and critical groups. Hypertension was the most common comorbidity in all groups and more predominant in severe and critical patients. Drug administration and the need for oxygen and aggressive treatments were consistent with the severity of the disease. A total of 25 patients from the cohort died from COVID-19. The serum biochemical composition was also characterised at the time of admission in the entire cohort, including both routine and inflammatory parameters. The most significant differences in the blood pattern were observed between mild and critical patients (9).

4.2 Samples recruitment

The sampling protocol consisted of a clinical evaluation, blood cell count, and standard biochemical parameters at inclusion (baseline). Serum

samples were stored at -80°C at BioBank - Institut d'Investigació Sanitària Pere Virgili (IISPV) facilities until analysed (9).

4.3 Ethics

Protocols were carried out in accordance with the recommendations of the Ethical and Scientific Committees from each participating institution and were approved by the Committee for Ethical Clinical Research following the rules of Good Clinical Practice from the IISPV (079/2020, CEIm IISPV). The CEIm IISPV is an independent committee, which oversees the correct adherence to the ethical standards governing clinical trials and research projects that are carried out in our environment, specifically in terms of its methodology, ethics and laws. Its members include both health and non-health professionals. All subjects or their relatives gave written informed consent in accordance with the Declaration of Helsinki (9).

4.4 Reagents

Ammonium bicarbonate (ABC), ammonium formate and formic acid (LC-MS grade) were purchased from Sigma-Aldrich (St. Louis, MO, USA). Acetonitrile (LC-MS grade) was purchased from Merck (Darmstadt, Germany). The water used throughout the study was purified with a Milli-Q system from Millipore (Burlington, MA, USA).

4.5 De-N-glycosylation and labelling of N-glycans

The release and labelling of N-glycans were done using a method previously described (32). Briefly, total protein was quantified with the Bradford assay. Sample denaturation, de-N-glycosylation, labelling with Rapifluor-MS (RFMS), and purification were performed in accordance with the Waters Corporation "GlycoWorks RapiFluor-MS N-Glycan Kit Care and Use Manual" (p/n 715004793). Briefly, 15 µg of protein were denatured at 90°C for 3 min in the presence of 5% (w/v) RapiGest. De-N-glycosylation was then conducted at 50°C for 5 min, by adding 1.2 µL of Rapid PNGase F. Subsequently, the digested samples were directly labelled with 6 µL of RFMS reagent without the need for purification. The reaction proceeded at room temperature for 5 min before using a GlycoWorks µElution Plate for

the SPE Clean-up procedure. Glycans were eluted with 200 mM ammonium acetate in 5% acetonitrile.

4.6 LC-MS/MS

The LC-MS/MS analysis was carried out using a previously described analytical method (32). Derivatised samples were analysed using an Agilent UHPLC 1290 Infinity Series coupled to an Agilent qTOF/MS 6550 Series (Agilent Technologies, Santa Clara, CA). N-glycans were separated on a Waters ACQUITY UPLC BEH amide column (2.1 mm × 150 mm i.d., particle size 1.7 μm), using 50 mM ammonium formate solution (mobile phase A) and 100% acetonitrile (mobile phase B). The analysis was performed at a flow rate of 0.4 mL/min, with an injection volume of 20 μL, and the column temperature set at 60°C. The chromatographic gradient began by ramping mobile phase A from 25% to 46% over a period of 35 minutes. From 35 to 36.5 min, the gradient ramped from 46 to 100% solvent A and the flow rate was lowered to 0.2 mL/min. 100% solvent A was held constant from 36.5 to 39.5 min, after which the percentage of solvent A decreased to 25%, from 39.5 min to 43.1 min. The flow rate was then increased back to 0.4 mL/min from 43.1 to 47.6 min and solvent A was held constant at 25%. Lastly, the parameters were held constant from 47.6 to 55.0 min. The qTOF operated in positive electrospray ionisation mode (ESI+), and mass spectra were recorded between m/z 300–1700 at 1.5 spectra/s. The source conditions were set as follows: nebuliser gas at 25 psi, gas temperature at 200°C, gas flow at 12 L/min, sheath gas temperature at 250°C, sheath gas flow at 12 L/min, capillary voltage at 3500 V, and nozzle voltage at 500 V. Additionally, tandem mass experiments (MS/MS) using data dependence acquisition at a collision energy of 30 eV from the 10 most intense ions were used for identification purposes.

4.7 Data processing of LC-MS data

The MS data were first processed using Agilent MassHunter Qualitative Analysis B.07 software. For the identification of N-glycans, total ion chromatograms (TIC) containing MS/MS fragmentation data were

deconvoluted using the "find molecular feature" algorithm, which detected chromatographic peaks considered to be N-glycans. The resulting list of entities containing the MS/MS data was exported and loaded to Simglycan software for molecular and structural elucidation. Simglycan is a high-throughput structural identification tool that uses a built-in database with theoretical fragmentation profiles to predict the structure of glycans (33). Additionally, the Simglycan results were matched against the GlycoStore database (https://www.glycostore.org) to refine the identification results. GlycoStore provided elution property information for over 850 unique structures including standardised retention times, expressed as glucose units (GU), for the RFMS-labelled glycans (34). Following the identification process, 36 N-glycans were identified in human plasma and 13 additional structures were detected but could not be annotated. Subsequently, the exact masses [M+H]+, [M+2H]2+ or [M+3H]3+ of these structures were extracted on all samples using Agilent Mass Hunter Quantitative software (B.07) to generate a refined matrix of quantitative data for statistical purposes. Finally, the obtained data matrix, which included the peak area for each identified N-glycan, was normalised by dividing the peak area of each N-glycan by the sum of the peak areas of all N-glycans within each respective sample.

4.8 Statistical analysis

Non-parametric Kruskal-Wallis test was used to assess significant differences between groups of severity, employing Mass Profiler Professional (MPP) software v.15.1 (Agilent Technologies, Massachusetts, USA). Graphical representations were generated with GraphPad Prism software (version 9.0, GraphPad Inc., San Diego, CA) and Metaboanalyst 5.0. Both SPSS (version 21.0, SPSS Inc., Chicago, IL) and Metaboanalyst were employed to perform random forest analyses, and create binary logistic regression models and ROC curves to evaluate the potential accuracy of the selected biomarkers for predicting COVID-19 severity. Kruskal-Wallis test and $\chi 2$ test were used to determine the demographic and clinical features differences between groups of severity. The

Spearman's correlation coefficient, used to measure the association between the study cohort variables and groups of severity, was performed with SPSS. Results were considered statistically significant at $p < 0.05$.

Data availability statement

The datasets presented in this study can be found in online repositories. The names of the repository/repositories and accession number(s) can be found here: GPST000341 (Glycopost).

Ethics statement

The studies involving human participants were reviewed and approved by the Ethics Research Committee (CEIM Institut d'Investigació Sanitària Pere Virgili). The patients/participants provided their written informed consent to participate in this study.

Author contributions

Conception and design of the study, PH, NC, AR and MS. Methodology, BP, JP, AdP, SC, JM-P and FG-B. Formal Analysis, BP and AdP. Writing – Original Draft Preparation, BP. Writing – Review and Editing, BP, PH, NC, AR and MS. Supervision, PH, NC, AR and MS. Funding Acquisition, AR and PH. All authors contributed to the article and approved the submitted version.

Funding

BP is supported by a fellowship from the Vicente Lopez Program (Eurecat). This work was financially supported by the Catalan Government through the funding grant ACCIÓ-Eurecat (Project PRIV-COVIDOMICS), and also by the COVIDOMICS' project supported by Direcció General de Recerca i Innovació en Salut (DGRIS), Departament de Salut, Generalitat de Catalunya (PoC-6-17). The research was also supported by the Programa de Suport als Grups de Recerca AGAUR (2021SGR01404), the SPANISH AIDS Research Network [RD16/0025/0006]-ISCIII-FEDER (Spain) and the CIBER -Consorcio Centro de Investigación Biomédica en Red- (CB21/13/00020, CB21/13/00063), Instituto de Salud Carlos III, Ministerio de Ciencia e Innovación and Unión Europea – NextGenerationEU. AR is supported by a grant from IISPV through the

project “2019/IISPV/05” (Boosting Young Talent), by GeSIDA through the “III Premio para Jóvenes Investigadores 2019” and by the Instituto de Salud Carlos III (ISCIII) under grant agreement “CP19/00146” through the Miguel Servet Program.

Acknowledgments

We gratefully acknowledge the help of Salvador Fernández, researcher at Centre for Omic Sciences Unit at Eurecat, for his support with the statistical analysis.

Conflict of interest

The authors declare that the research was conducted in the absence of any commercial or financial relationships that could be construed as a potential conflict of interest.

REFERENCES

1. Wang C, Horby PW, Hayden FG, Gao GF. A novel coronavirus outbreak of global health concern. Lancet (London, England) (2020) 395(10223):470. doi:10.1016/S0140-6736(20)30185-9
2. World Health Organization. COVID-19 Weekly Epidemiological Update (2022). Edition 123 https://www.who.int/publications/m/item/covid-19-weekly-epidemiological-update [Accessed January 16, 2023].
3. Chen N, Zhou M, Dong X, et al. Epidemiological and clinical characteristics of 99 cases of 2019 novel coronavirus pneumonia in Wuhan, China: a descriptive study. Lancet (London, England) (2020) 395(10223):507. doi:10.1016/S0140-6736(20)30211-7
4. Xu XW, Wu XX, Jiang XG, et al. Clinical findings in a group of patients infected with the 2019 novel coronavirus (SARS-Cov-2) outside of Wuhan, China: retrospective case series. BMJ. (2020) 368. doi:10.1136/BMJ.M606
5. Wölfel R, Corman VM, Guggemos W, et al. Virological assessment of hospitalized patients with COVID-2019. Nature (2020) 581(7809):465-469. doi:10.1038/s41586-020-2196-x
6. Krammer F. SARS-CoV-2 vaccines in development. Nature (2020) 586(7830):516-527. doi:10.1038/s41586-020-2798-3
7. Ssentongo P, Ssentongo AE, Voleti N, et al. SARS-CoV-2 vaccine effectiveness against infection, symptomatic and severe COVID-19: a systematic review and meta-analysis. BMC Infect Dis (2022) 22(1). doi:10.1186/S12879-022-07418-Y
8. Kermali M, Khalsa RK, Pillai K, Ismail Z, Harky A. The role of biomarkers in diagnosis of COVID-19 – A systematic review. Life Sci (2020) 254:117788. doi:10.1016/J.LFS.2020.117788
9. Reverté L, Yeregui E, Olona M, et al. Fetuin-A, inter-α-trypsin inhibitor, glutamic acid and ChoE (18:0) are key biomarkers in a panel distinguishing mild from critical coronavirus disease 2019 outcomes. Clin Transl Med (2022) 12(1):e704. doi:10.1002/CTM2.704

10. Rana R, Tripathi A, Kumar N, Ganguly NK. A Comprehensive Overview on COVID-19: Future Perspectives. Front Cell Infect Microbiol (2021) 11. doi:10.3389/FCIMB.2021.744903
11. Lin B, Liu J, Liu Y, Qin X. Progress in understanding COVID-19: insights from the omics approach. Crit Rev Clin Lab Sci (2021) 58(4):242-252. doi:10.1080/10408363.2020.1851167
12. Hu M, Lan Y, Lu A, Ma X, Zhang L. Glycan-based biomarkers for diagnosis of cancers and other diseases: Past, present, and future. Prog Mol Biol Transl Sci (2019) 162:1-24. doi:10.1016/BS.PMBTS.2018.12.002
13. Trbojevic Akmacic I, Ventham NT, Theodoratou E, et al. Inflammatory bowel disease associates with proinflammatory potential of the immunoglobulin G glycome. Inflamm Bowel Dis (2015) 21(6):1237-1247. doi:10.1097/MIB.0000000000000372
14. Vučkovïc F, Krištïc J, Gudelj I, et al. Association of systemic lupus erythematosus with decreased immunosuppressive potential of the IgG glycome. Arthritis Rheumatol (2015) 67(11):2978-2989. doi:10.1002/art.39273
15. Lemmers RFH, Vilaj M, Urda D, et al. IgG glycan patterns are associated with type 2 diabetes in independent European populations. Biochim Biophys acta Gen Subj (2017) 1861(9):2240-2249. doi:10.1016/j.bbagen.2017.06.020
16. Akinkuolie AO, Buring JE, Ridker PM, Mora S. A novel protein glycan biomarker and future cardiovascular disease events. J Am Heart Assoc (2014) 3(5). doi:10.1161/JAHA.114.001221
17. Giron LB, Papasavvas E, Azzoni L, et al. Plasma and Antibody Glycomic Biomarkers of Time to HIV Rebound and Viral Setpoint. AIDS (2020) 34(5):681. doi:10.1097/QAD.0000000000002476
18. Lauc G, Pezer M, Rudan I, Campbell H. Mechanisms of disease: The human N-glycome. Biochim Biophys Acta (2016) 1860(8):1574-1582. doi:10.1016/J.BBAGEN.2015.10.016
19. Larsen MD, de Graaf EL, Sonneveld ME, et al. Afucosylated IgG characterizes enveloped viral responses and correlates with COVID-19 severity. Science (2021) 371(6532). doi:10.1126/science.abc8378
20. Petrović T, Alves I, Bugada D, et al. Composition of the immunoglobulin G glycome associates with the severity of COVID-19. Glycobiology (2021) 31(4):372-377. doi:10.1093/GLYCOB/CWAA102
21. Vicente MM, Alves I, Gaifem J, et al. Altered IgG glycosylation at COVID-19 diagnosis predicts disease severity. Eur J Immunol (2022) 52(6):946-957. doi:10.1002/EJI.202149491
22. Aleem A, Akbar Samad AB, Slenker AK. Emerging Variants of SARS-CoV-2 And Novel Therapeutics Against Coronavirus (COVID-19). StatPearls Publishing (2022).
23. Gencat. Vaccines against COVID-19 (2021). https://canalsalut.gencat.cat/ca/salut-a-z/v/vacuna-covid-19/ciutadania/vacunes/index.html#googtrans(ca%7Cen) [Accessed January 3, 2023].
24. Wang G-Q, Zhao L, Wang X, Jiao Y-M, Wang F-S. Diagnosis and Treatment Protocol for COVID-19 Patients (Tentative 8th Edition): Interpretation of Updated Key Points. Infect Dis Immun (2021) 1(1):17. doi:10.1097/ID9.0000000000000002

25. Hou H, Yang H, Liu P, et al. Profile of Immunoglobulin G N-Glycome in COVID-19 Patients: A Case-Control Study. Front Immunol (2021) 12. doi:10.3389/fimmu.2021.748566
26. Nimmerjahn F, Anthony RM, Ravetch J V. Agalactosylated IgG antibodies depend on cellular Fc receptors for in vivo activity. Proc Natl Acad Sci U S A (2007) 104(20):8433-8437. doi:10.1073/pnas.0702936104
27. Seeling M, Brückner C, Nimmerjahn F. Differential antibody glycosylation in autoimmunity: sweet biomarker or modulator of disease activity? Nat Rev Rheumatol (2017) 13(10):621-630. doi:10.1038/NRRHEUM.2017.146
28. Kaneko Y, Nimmerjahn F, Ravetch J V. Anti-inflammatory activity of immunoglobulin G resulting from Fc sialylation. Science (2006) 313(5787):670-673. doi:10.1126/SCIENCE.1129594
29. Barberis E, Timo S, Amede E, et al. Large-Scale Plasma Analysis Revealed New Mechanisms and Molecules Associated with the Host Response to SARS-CoV-2. Int J Mol Sci. (2020) 21(22):1-25. doi:10.3390/IJMS21228623
30. Shen B, Yi X, Sun Y, et al. Proteomic and Metabolomic Characterization of COVID-19 Patient Sera. Cell (2020) 182(1):59-72.e15. doi:10.1016/J.CELL.2020.05.032
31. López-Hernández Y, Monárrez-Espino J, Oostdam ASH van, et al. Targeted metabolomics identifies high performing diagnostic and prognostic biomarkers for COVID-19. Sci Rep. (2021) 11(1). doi:10.1038/S41598-021-94171-Y
32. Paton B, Foguet-Romero E, Suarez M, et al. Brain N-Glycosylation and Lipidomic Profile Changes Induced by a High-Fat Diet in Dyslipidemic Hamsters. Int J Mol Sci. (2023) 2;24(3):2883. doi: 10.3390/ijms24032883
33. Apte A, Meitei NS. Bioinformatics in glycomics: glycan characterization with mass spectrometric data using SimGlycan. Methods Mol Biol (2010) 600:269-81. doi:10.1007/978-1-60761-454-8_19.
34. Zhao S, Walsh I, Abrahams JL, et al. GlycoStore: A database of retention properties for glycan analysis. Bioinformatics (2018) 34(18):3231-3232. doi:10.1093/bioinformatics/bty319

SUPPLEMENTARY MATERIAL

Supplementary Table 1. N-glycan profile in COVID-19 patients. Hex, hexose (either galactose (Gal), or mannose (Man)); Fuc, fucose; HexNAc, N-acetylhexosamine; Neu5Ac, N-acetylneuraminic acid.

Glycan composition	m/z	Glycan Mass
Fuc1Hex3HexNAc4	887.867	1462.539
Fuc1Hex4HexNAc3	867.353	1421.512
Fuc1Hex4HexNAc4	968.894	1624.592
Fuc1Hex4HexNAc5	1070.433	1827.671
Fuc1Hex5HexNAc4	1049.920	1786.645
Fuc1Hex5HexNAc5	1151.458	1989.721
Hex10HexNAc2	1178.946	2044.697

Hex3HexNAc4	814.838	1316.481
Hex3HexNAc5	916.377	1519.559
Hex4HexNAc2	692.784	1072.374
Hex4HexNAc3	794.325	1275.456
Hex4HexNAc4	895.864	1478.533
Hex5HexNAc2	773.812	1234.429
Hex5HexNAc3	875.350	1437.506
Hex5HexNAc4	976.890	1640.586
Hex6HexNAc2	854.838	1396.482
Hex6HexNAc3	956.382	1599.569
Hex7HexNAc2	935.864	1558.533
Hex8HexNAc2	1016.890	1720.585
Hex9HexNAc2	1097.917	1882.639
Neu5Ac1Fuc1Hex4HexNAc3	1012.901	1712.607
Neu5Ac1Fuc1Hex4HexNAc4	1114.440	1915.685
Neu5Ac1Fuc1Hex5HexNAc4	1195.468	2077.741
Neu5Ac1Hex4HexNAc3	939.872	1566.549
Neu5Ac1Hex4HexNAc4	1041.411	1769.627
Neu5Ac1Hex5HexNAc4	1122.439	1931.683
Neu5Ac1Hex5HexNAc5	1297.007	2280.819
Neu5Ac1Hex6HexNAc3	1101.924	1890.653
Neu5Ac1Hex6HexNAc5	1305.003	2296.811
Neu5Ac2Fuc1Hex5HexNAc4	1341.015	2368.835
Neu5Ac2Fuc1Hex5HexNAc5	1442.561	2571.927
Neu5Ac2Hex5HexNAc4	1267.987	2222.779
Neu5Ac2Hex6HexNAc5	1450.556	2587.917
Neu5Ac3Fuc1Hex6HexNAc5	1113.091	3025.068
Neu5Ac3Hex6HexNAc5	1596.105	2879.015
NeuAc1Hex5HexNAc3	1020.898	1728.601

Supplementary Table 2. Demographic and clinical features of COVID-19 study cohort.

Variables	COVID-19 group			
	Mild (n=56)	**Severe (n=105)**	**Critical (n=35)**	**P value**
Male	28 (50.0)	71 (67.6)	20 (67.7)	n.s.
Age, years	52.0 (39.3-63.8)	66.0 (51.5-66.0)	64.0 (53.0-75.0)	<0.001
Comorbidities – no. (%)				

Obesity	10 (17.9)	27 (25.8)	10 (28.6)	<0.001
Metabolic syndrome	0 (0)	7 (6.7)	N.D.	<0.001
Diabetes mellitus	9 (16.1)	22 (21.0)	7 (20.0)	<0.001
Hypertension	16 (28.6)	57 (54.3)	16 (45.7)	0.008
Cardiovascular disease	5 (8.9)	14 (13.3)	6 (17.1)	<0.001
COPD	2 (3.6)	16 (15.2)	5 (14.3)	<0.001
Cancer	5 (8.9)	12 (11.4)	3 (8.6)	<0.001
HIV	0 (0)	1 (1.0)	1 (2.9)	<0.001
COVID-19 Symptoms				
Fever	32 (57.1)	74 (70.5)	26 (74.3)	<0.001
Cough	24 (42.9)	66 (62.9)	22 (62.9)	0.021
Fatigue	14 (25.0)	30 (28.6)	10 (28.6)	<0.001
Dyspnea	19(33.9)	64 (61.0)	29 (82.9)	0.021
Anosmia	10 (17.9)	10 (9.5)	2 (5.7)	<0.001
Oxygen therapy and intensive care				
Oxygen required	7(12.5)	57 (54.3)	30(85.7)	<0.001
Low-flow oxygen administration (Ventimask or nasal prongs)	4(7.1)	34 (32.4)	5 (14.3)	<0.001
High-flow oxygen administration/NIMV	0(0)	20 (19.0)	4 (11.4)	<0.001
MV/intubation	2(3.6)	15(14.3)	21 (60.0)	<0.001
Vasopressors or dialysis required	2(3.6)	7 (6.7)	8 (22.9)	<0.001
Mortality				
Exitus	2 (3.6)	14 (13.3)	9 (25.7)	<0.001
Medicines subscribed				
Hydroxychloroquine	3 (5.4)	16 (15.2)	6 (17.1)	<0.001
Azithromycin	15 (26.8)	57 (54.3)	7 (20.0)	0.007
Lopinavir/ritonavir	1 (1.8)	13 (12.4)	5 (14.3)	<0.001
Tocilizumab	0 (0)	12 (11.4)	5 (14.3)	<0.001
Interferon	0 (0)	0 (0)	1 (2.9)	<0.001
Corticosteroids	13 (23.2)	74 (70.5)	18 (51.4)	<0.001
Remdesivir	3 (5.4)	34 (32.4)	8 (22.9)	<0.001

Data are presented as n (%) or median (interquartile range: 25-75). P values comparing mild, severe and critical patients were computed using non-parametric Kruskal-Wallis test for continuous data and c2 test for categorical data. P value < 0.05 was considered significant. COPD, chronic obstructive pulmonary disease; NIMV, non-invasive mechanical ventilation; MV, mechanical ventilation.

Manuscript 5

Site-Specific glycan analysis of human fetuin-A in COVID-19 patients: Implications for disease severity prediction

Article

In preparation

ABSTRACT

Severe acute respiratory syndrome coronavirus 2 (SARS-CoV-2) infection leads to diverse clinical manifestations, ranging from mild symptoms to severe multiorgan failure in critical cases. Several biomarkers have been associated with coronavirus disease 2019 (COVID-19), including human fetuin-A (hFet) and the global plasma N-glycan profile, which have emerged as potential biomarkers for differentiating mild from critical COVID-19 outcomes. Aiming to characterise the glycosylation profile of hFet and identify specific glycosylation patterns associated with specific COVID-19 outcomes, we conducted a site-specific glycan analysis of hFet in COVID-19 patients with different disease severities (mild, severe and critical). Our findings revealed distinct glycan structures at specific glycosylation sites of hFet that correlated with mild and critical COVID-19 cases. Additionally, two disialylated N-glycan and O-glycan structures were found to be significantly decreased in severe patients compared to mild and severe ones. This study highlights the significance of hFet glycosylation patterns in predicting COVID-19 outcomes, helping improve our understanding of crucial molecular interactions and networks underlying disease manifestation and progression.

1. INTRODUCTION

The ongoing coronavirus disease 2019 (COVID-19) pandemic caused by severe acute respiratory syndrome coronavirus-2 (SARS-CoV-2) has posed significant challenges to global healthcare systems [1]. The wide spectrum of disease severity observed in COVID-19 patients, ranging from mild respiratory symptoms to critical illness requiring intensive care, highlights the urgent need to identify reliable biomarkers for predicting disease outcomes [2]. Understanding the mechanistic pathways underlying immune dysregulation and complications caused by SARS-CoV-2 infection is crucial but still poses significant challenges [3].

A recent study identified human fetuin-A (hFet) as a potential biomarker for differentiating between mild and critical COVID-19 outcomes [4]. hFet, a highly glycosylated protein predominantly synthesized in the liver, is involved in various physiological processes, including calcium metabolism [5,6] and insulin signalling [7]. Increased levels of hFet have been associated with an increased risk of cardiovascular disease (CVD) [8] and incident type 2 diabetes (T2DM) [9]. Moreover, hFet has garnered significant attention as a potential metabolic biomarker [10,11]. However, the specific glycosylation patterns of hFet and their association with COVID-19 severity have yet to be investigated.

A site-specific glycan analysis offers a unique approach to elucidate the glycosylation profile of hFet and its potential relevance in COVID-19 outcomes. By characterizing the glycan structures at specific glycosylation sites of hFet, valuable insights into the glycosylation alterations associated with COVID-19 cases could be identified. In this study, our main objective was to perform a comprehensive site-specific glycan analysis of hFet in COVID-19 patients with varying disease severities. Specifically, we aimed to identify specific glycosylation patterns that correlate with mild or critical COVID-19 outcomes. For this, we tested two methods to analyse hFet in

plasma: an in-solution digestion of total plasma and an in-gel digestion of isolated hFet using two-dimensional gel electrophoresis (2D-PAGE). Notably, on the selected set of samples, metabolomics, lipidomics, proteomics and N-glycomics analyses were previously conducted to identify key molecules involved in the mechanistic pathways of the disease. From these studies, a novel panel of biomarkers, including hFet, was proposed to differentiate mild from critical COVID-19 outcomes. Biomarkers inter-α-trypsin, glutamic acid, cholesteryl ester 18:0 and N-glycan Fuc1Hex5HexNAc5 were the remaining contributors to this panel [4,12]. Together with the site-specific glycan analysis, this holistic approach enhances the robustness and depth of our study, enabling us to help uncover crucial molecular interactions and networks that contribute to the disease's manifestation and progression.

2. MATERIALS AND METHODS

2.1 Samples

Plasma samples were obtained from SARS-CoV-2 infected patients. The study was approved by the Committee for Ethical Clinical Research following the rules of Good Clinical Practice from the IISPV (079/2020, CEIm IISPV). All subjects or their relatives gave written informed consent in accordance with the Declaration of Helsinki [4]. Patients were classified into three groups according to their severity: mild, severe and critical. Five individuals were analysed for each severity group, except for the critical group, for which 4 samples were analysed.

2.2 Reagents

hFet (alpha-2-HS glycoprotein; Uniprot Code: P02765), dithiothreitol (DTT), iodoacetamide (IAA), trifluoroacetic acid (TFA), formic acid (FA) and ammonium bicarbonate (ABC) were purchased from Sigma-Aldrich (St.

Louis, MO, USA). Acetonitrile (ACN) was purchased from Biosolve (Valkenswaard, The Netherlands). Sequencing-grade trypsin and Glu-C were obtained from Promega (Madison, WI) and New England Biolabs (Ipswich, MA), respectively.

2.3 2-Dimensional PAGE

Plasma samples were diluted in 7 mol/L urea, 2 mol/L thiourea, 4% (wt/vol) CHAPS and 65 mmol/L DTT. The protein solution was mixed with 1.8% (by volume) pH 2–4 ampholytes, 0.45% (by volume) pH 9–11 ampholytes, and 0.9% (by volume) pH 3–10 ampholytes (SERVALYT®, SERVA). Bromophenol blue was added at 0.3% (wt/vol) before spinning samples at 16,000g for 5 min; 135 μL of supernatant (containing 300 μg protein) was used for 2-dimensional (2D)-PAGE with 7-cm pH 3–6 immobilized pH gradient (IPG) strips (BIO-RAD). Rehydration was performed for 15 h, followed by isoelectric focusing with a Multiphor (GE Healthcare) at 300 V for 30 min, followed by a gradient increasing to 1,000 V for 30 min, further increasing to 5,000 V for 1 h 30 min. The voltage was then held at 5,000 V for 40 min, up to 8 kVh. After isoelectric focusing, immobilized pH gradient strips were incubated in equilibration solution [4 mol/L urea, 0.26 mol/L thiourea, 50 mmol/L Tris (pH 6.8), 30% (by volume) glycerol, 2% (wt/vol) SDS, 130 mmol/L DTT, 0.3% (wt/vol) bromphenol blue] for 20 min. Proteins were then separated by NuPAGE Bis-Tris mini protein gels (4%–12% (wt/vol), Thermo Fisher), during 50 minutes at 200 V constant.

2.4 In-gel digestion

The bands of interest were carefully cut into ~1 mm cubes and transferred into sample tubes. These gel cubes were destained with Milli Q water (x2 15 min cycle washes with shaking) and water/ACN 1:1 (v/v) (x2 15 min cycle washes with shaking). Gel cubes were next dehydrated by the addition of ACN (x1 10 min cycle wash with shaking), and rehydrated with 100 mM

ABC. After 5 min, an equal volume of ACN was added, samples were shaked for 15 min and dried in a vacuum concentrator. Reduction of protein disulfide bonds was carried out with 10 mM DTT in 100 mM ABC at 56 °C for 45 min and subsequent alkylation was performed with 55 mM IAA in 100 mM ABC at room temperature for 30 min (in complete darkness). After removing the IAA, gel pieces were washed twice by dehydrating and rehydrating them using ABC and ACN, respectively. Next, samples were vacuum dried prior to digestion. Sequencing grade modified trypsin (Promega) and Glu-C (New England Biolabs) (both at 12.5 ng/µL in 50 mM ABC) were added to cover the dehydrated gel pieces on ice, and allowed to rehydrate on ice for 45 min. Excess buffer and trypsin were then removed and replaced with sufficient 50 mM ABC buffer to cover the gel pieces, before incubating overnight at 37 °C. On the following day, samples were washed with 25 mM ABC followed by an equal volume of ACN, and incubated with shaking for 15 min. The resulting tryptic peptides were extracted from the gel by equilibrating the samples with 50% ACN and 5% FA for 20 min in a 37 °C shaker. The extraction was performed twice and samples then were vacuum dried. For the LC-MS analysis, samples were resuspended in 0.05% v/v TFA.

2.5 LC-MS and MS/MS Analysis

Peptides were separated on a Dionex Ultimate 3000 nano UHPLC system (Thermo Scientific). An EASY-Spray column with dimensions 75 µm x 50 cm, 2 µm particle size (Thermo Scientific) was used with a flow rate of 250 nL/min at 45 °C. A 147-min gradient was utilized, with 0.1% FA in LC-MS grade water as solvent A, and 20% water, 80% ACN, 0.1% FA as solvent B. The gradient was set as follows: 0-6.6 min., 2% B isocratic; 6.6-105 min., 2-36% B; 105-125 min., 36-60% B; 125-126 min., 60-95% B; 126-131 min., 95% B isocratic; 131-132 min., 95-2% B; and 131-147 min., 2% B isocratic.

Peptides from the nano LC were analysed on a benchtop Q Exactive hybrid quadrupole-Orbitrap mass spectrometer using the Nanospray Flex ion source. Samples were analyzed in positive-ion mode. The conditions for data dependent acquisition (DDA) were as follows: chromatographic peak width was set at 20 s and the Full MS conditions were with a resolution of 70,000, AGC target of 3e6, maximum IT (injection time) of 60 ms, scan range of 375 to 1,500 m/z. The dd-MS2 conditions were with a resolution of 35,500, AGC target of 1e5, maximum IT of 60 ms, loop count of 10 (i.e. Top 10), isolation window of 2.0 m/z, fixed first mass of 120.0 m/z and normalised collision energy (NCE) was stepped at 27, 30 and 33 in a high-energy collision dissociation (HCD) cell. The DDA settings were with minimum intensity threshold of 3.3e4 ions, charge exclusion: unassigned, 1, >8, peptide match: preferred, dynamic exclusion: 30 s.

2.6 Data Analysis

The data was analysed using Byonic software (v.4.3.4) with fully specific cleavage enabled and choosing the appropriate cleavage sites for each protease. Tryptic/Glu-C digests were searched against the FASTA sequences of hFet. Oxidation of methionine, deamidation of asparagine and glutamine were used as rare variable modifications and carbamidomethylation of cysteine as a fixed modification. The specific databases used were provided from the Byonic software (N-glycans: 57 human plasma, O-glycans: 70 human). A precursor mass tolerance of 10 ppm was set, and a fragment mass tolerance of 20 ppm. A maximum of 3 missed cleavages was allowed, as well as 2 common modifications per peptide, and 1 rare modification per peptide.

When manually confirming the results, close attention was paid to oxonium ions detected in each MS/MS spectra. Specifically, oxonium ions for Neu5Ac (m/z 292.1026 and 274.0921) were checked for all matches containing more than one fucose but no sialic acid, to rule out false assignment as

multiple fucoses. The relative abundance of peptides was assessed by calculating the area under the curve. To ensure consistent glycoform abundance measurements and mitigate any ionization variations, the same peptide backbone was employed for each site. This approach also served to validate the assignments, as all positively identified peptides were cross-referenced with the raw data and confirmed.

2.7 Statistical analysis

Non-parametric Kruskal-Wallis test was used to assess significant differences between groups of severity, employing Mass Profiler Professional (MPP) software v.15.1 (Agilent Technologies, Massachusetts, USA) and MetaboAnalyst 5.0. Graphical representations were generated with GraphPad Prism software (version 9.0, GraphPad Inc., San Diego, CA) and MetaboAnalyst 5.0. Results were considered statistically significant at $p < 0.05$.

3. RESULTS

In this study we performed a site-specific glycan analysis of hFet from 14 patients categorized into three different groups: mild (n=5), severe (n=5) and critical (n=4). The aim was to determine whether the glycan structures at different glycosylation sites of hFet differed between groups of severity, for which we employed 2D-PAGE and LC-MS/MS. Glycan compositions were reported as follows: Hex [hexose, either galactose (Gal), or mannose (Man)], HexNAc [N-acetylhexosamine], Fuc [fucose] and NeuAc [Nacetylneuraminic acid].

3.1 Site-specific characterization of glycosylation on hFet

The major circulating form of hFet is most likely a two-polypeptide-chain protein with a heavy chain (A chain) comprised of 300 residues and a light chain (B chain) consisting of 27 residues (Figure 1A). This circulating form of hFet contains a propeptide (connecting peptide) attached to the A chain. The A and B chains are linked by a single disulfide linkage [13]. A variety of posttranslational modifications (PTMs) modify hFet, including two N-glycosylation sites and two O-glycosylation sites in the A-chain, and one O-glycosylation site in the B-chain (Figure 1A) [13,14]. Although Uniprot reports in HFet eight putative glycosylation sites (N156, N176, T270, S280, S293, T339, T341 and S346) [15], Lin et al. identified the following glycosylation sites in hFet from serum: N156, N176, T256, T270 and S346. Differently, in our study we identified a total of 5 modifications: two N-glycosylation sites (N156 and N176) and three O-glycosylation sites (T270, S280 and S293), all from the A chain of hFet.

We tested two different approaches for the analysis of hFet in plasma, including an in-solution digestion of total plasma and an in-gel digestion of hFet isolated using 2D-PAGE. As hFet is an abundant protein in human plasma [16], an in-solution digestion of total plasma was tested, proving to be insufficient for the determination of all the glycosylations occurring in hFet. Therefore, 2D-PAGE was employed to isolate hFet, which proved to be a successful approach for its isolation in all samples (Figure 1B). We tested two combinations of proteolytic enzymes for the fetuin digestion after carefully inspecting the fetuin amino acid sequences: Glu-C with Lys-C and Glu-C with trypsin. The combination of Glu-C and trypsin proved to be the best option, generating a set of peptides with a suitable length for subsequent sequencing by LC-MS/MS. After enzymatic digestion, the peptide mixtures were subjected to HCD fragmentation.

As well as identifying the glycosylation sites and glycan composition, we assessed the relative abundance of the different glycopeptides across

severity groups. The list of all glycopeptides determined can be found in Table S1.

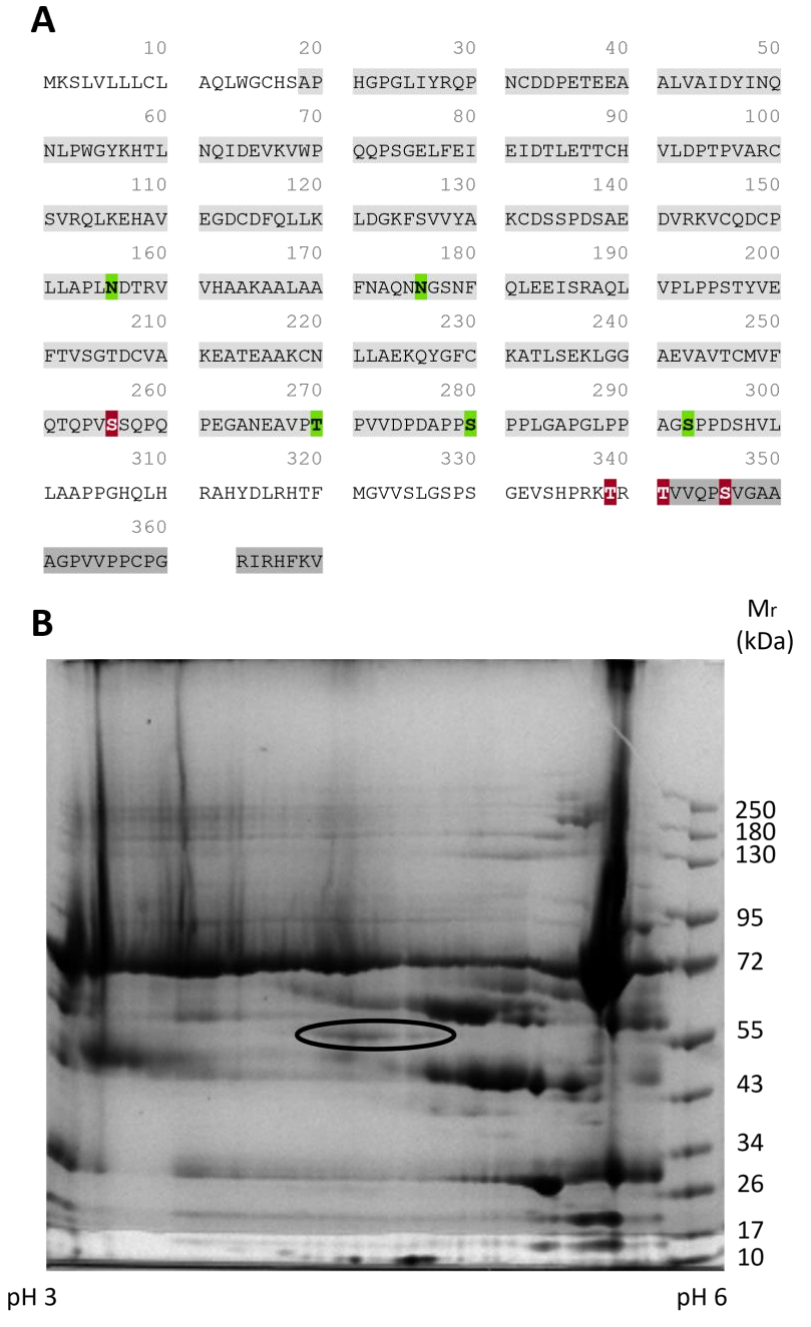

Figure 1. (**A**) FASTA sequence of hFet. In this study, modifications were identified in 5 different glycosylation sites: two N-glycosylations (sites N156 and N176 on chain A) and three O-glycosylations (sites T270, S280 and S293 on chain A), all highlighted in green. Glycosylation sites reported in other studies but not observed in ours, were highlighted in red. Chain A and B are highlighted in light and darker grey, respectively. (**B**) 2D-PAGE image of proteins present in a plasma sample from the severe COVID-19 group. hFet spot is highlighted in the center of the image.

3.2 Comparison of the glycosylation profile between groups of severity

The observed site-specific glycosylation patterns in hFet standard and in the three groups of COVID-19 severity are depicted in Figures 2 and 3. Focusing first on N-glycosylation (Figure 2), sites N156 and N176 contain complex N-glycans but differ in their structural composition and level of microheterogeneity. In all groups and consistent with previous reports [13], sialylated complex type structures were found to be predominant, while less abundant core-fucosylated glycoforms were present across all groups. Differently, on site N176, non-fucosylated HexNAc(4)Hex(5) was observed only in critical patients.

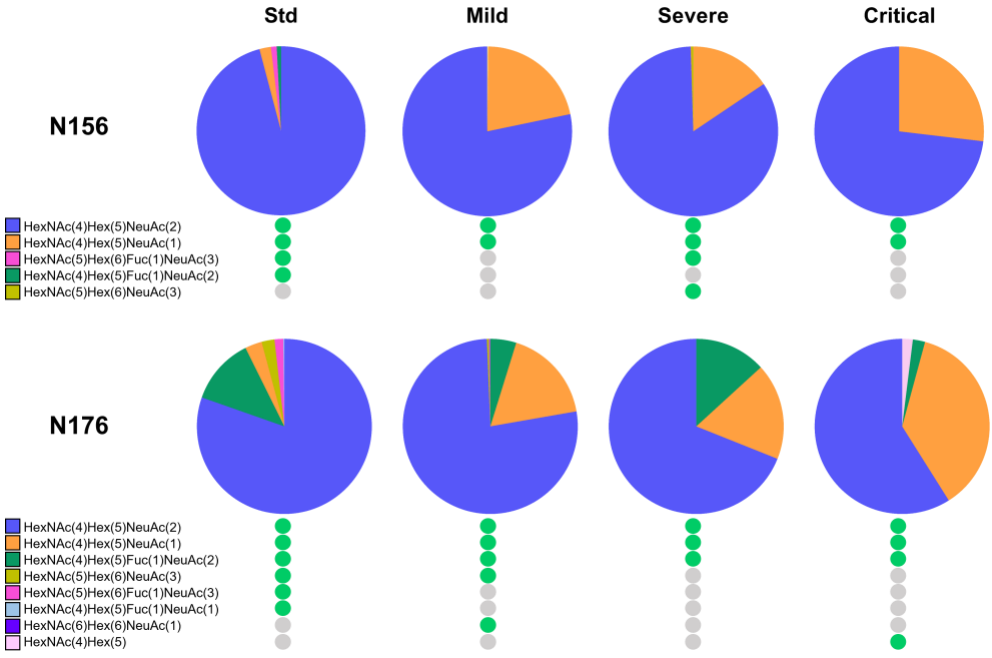

Figure 2. Site-specific N-linked glycosylation on sites N156 and N176 in COVID-19 patients (mild, severe and critical severity groups) and in hFet standard. Occupancy and unoccupancy of an N-linked glycan on a specific site and group is represented in green and grey dots, respectively. The pie charts summarise the quantification of these glycans in each group and site. HexNAc, N-acetylhexosamine; Hex, hexose; NeuAc, N-acetylneuraminic acid; Std, hFet standard.

The heterogeneity of the fetuin glycosylation patterns is further increased by the presence of O-glycosylation. As previously mentioned, we reported three O-glycosylation sites: T270, S280 and S293. The most abundant structures on these sites were mucin-type core 1 O-glycans with one or two sialic acids. More specifically, disialylated were especially abundant on T270, whereas S280 and S293 were mostly harboured by monosialylated structures. Site T270 had a very similar pattern in mild and severe patients, but differed in critical patients, in which disialylated structures were considerably more abundant. Differences in the O-glycosylation patterns between groups of severity were rather marginal on site S280. Lastly, differences on site S293 were characteristic for the presence of structure

HexNAc(6)Hex(4) in mild and severe groups but not in the critical group (Figure 3).

Differences in glycan abundance in the difference sites were measured in the three groups of severity. The observed tendencies are shown in Figure 4A. Statistically significant differences were only observed for two glycans; N-glycan HexNac(4)Hex(5)NeuAc(2) on site N156 and O-glycan HexNAc(1)Hex(1)NeuAc(2) on site T270. Both these structures were significantly decreased in critical patients compared to mild and severe ones. To potentially observe additional significant alterations, differences were measured for each site, obtaining significant differences between severity groups in the abundance of glycans on sites S280 and S293 (Figure 4B). Both sites showed a significant decrease in the abundance of their respective O-glycans with the increase of COVID-19 severity.

Figure 3. Site-specific O-linked glycosylation on sites T270, S280 and S293 in COVID-19 patients (mild, severe and critical severity groups) and in hFet standard. Occupancy and unoccupancy of an O-linked glycan on a specific site and group is represented in green and grey dots, respectively. The pie charts summarise the quantification of these glycans in each group and site. HexNAc, N-acetylhexosamine; Hex, hexose; NeuAc, N-acetylneuraminic acid; Std, hFet standard.

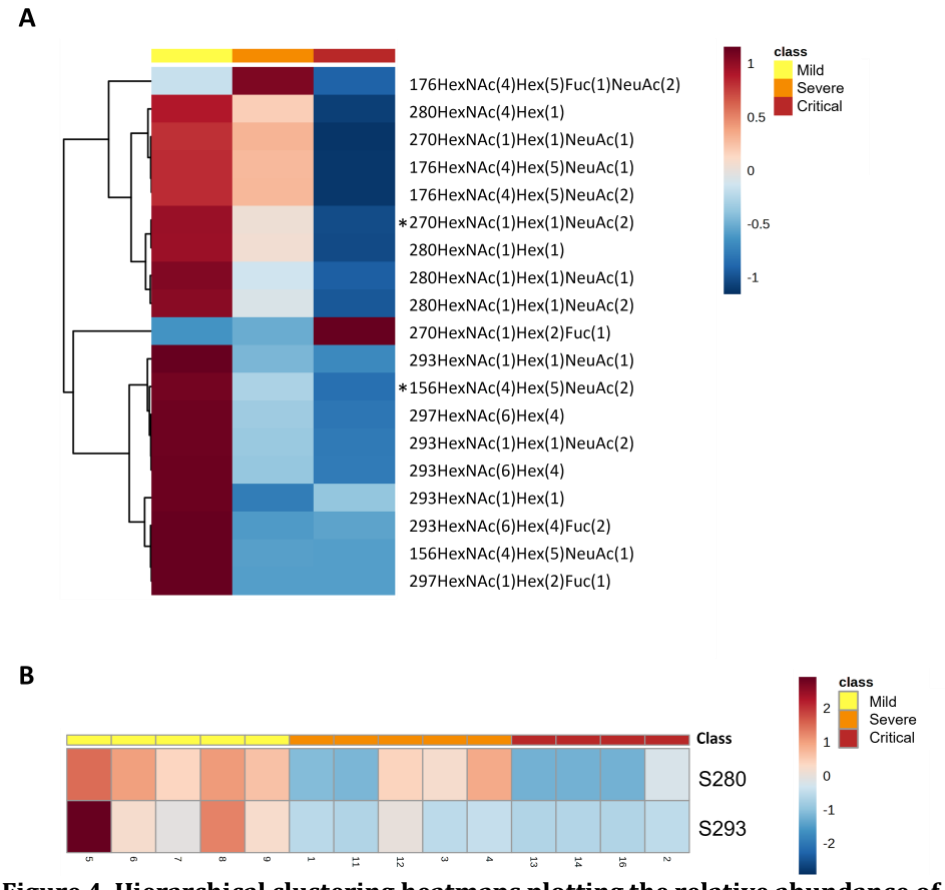

Figure 4. **Hierarchical clustering heatmaps plotting the relative abundance of different glycans in hFet, in accordance with disease severity.** (**A**) Heatmap plotting glycosylations present in more than 3 out of 5 samples in at least one group of severity. Only group averages are shown. Rows show the location of the glycan (3-digit number), followed by the composition of the glycan. Significant differences ($p < 0.05$) between groups are indicated with an asterisk (*). (**B**) Heatmap plotting the significant relative abundance of O-glycans in O-glycosylated sites 280 and 293 in hFet, in accordance with disease severity. For both heatmaps (A and B), significant differences ($p < 0.05$) between mild, severe and critical COVID-19 groups of patients were determined by Kruskal-Wallis test. Columns indicate the degree of disease severity: mild (left), severe (centre) and critical (right) groups. Mean values for each glycosylation in each COVID-19 group (columns) are colour-coded based on relative abundance, low (blue) and high (red). Samples are not clustered to show the natural contrast among groups.

4. DISCUSSION

hFet is a well-known negative acute-phase protein [17] observed in several inflammatory conditions, such as pediatric hemolytic-uremic syndrome, pneumococcal pneumonia [10], chronic inflammatory bowel disease [18], rheumatoid arthritis [19], septicemia [20], as well as in COVID-19 [4]. The decrease of hFet in severe COVID-19 patients may be due to its consumption during inhibition of dystrophic calcification attesting to its general role in tissue chaperoning [21].

In the context of COVID-19, calcification occurring in the lungs of some severe and critically ill patients, has been reported [22,23]. The exact mechanisms underlying this phenomenon are not fully understood, however a potential mechanism related to the regulation of calcification exists [24]. During inflammation, cell damage results in the release of calcium and phosphate from the damaged cells, promoting dystopic calcification, while simultaneous energy depletion leads to diminished formation of pyrophosphate, a natural inhibitor of calcification [24,25]. Pyrophosphate, along with magnesium and hFet, collectively prevent extracellular calcification [26]. hFet plays a crucial role in this process by binding to calcium and phosphate ions, inhibiting dystrophic calcification [27]. Additionally, hFet forms calciprotein particles (CPP), which can be cleared from the system, further contributing to the regulation of calcification processes [28]. Desialylation acts as a regulatory signal, triggering the degradation and subsequent clearance of hFet after its binding to calcium and phosphate [24]. This phenomenon may explain the observed decrease in sialylated glycan structures in most sites among critical patients in our study. Therefore, the observed desialylation could be responsible for the clearance of hFet in critical patients, as observed in the previous study on the same patient cohort [4].

Site-specific N- and O-glycoproteomic studies of plasma proteins can enhance our understanding of protein glycosylation implications in both normal physiological and pathophysiological conditions. These studies serve as valuable diagnostic tools, enabling the detection and discovery of relevant glycopeptides that can serve as biomarker candidates. This, in turn, forms the basis for targeted quantitative glycoproteomic analyses, facilitating site-specific monitoring of glycosylation alterations during disease progression.

Further studies should include a larger sample size to firmly establish hFet glycosylation patterns can become a marker of COVID-19 severity. Additionally, the use of 2D-PAGE is semi-quantitative at best, hence more accurate results could be obtained with the use of a stable heavy isotope labelled synthetic fetuin A peptide. Addressing these limitations in future studies will be essential to gain more comprehensive insights into the role of glycosylation in hFet.

5. CONCLUSION

In this study we conducted a site-specific glycan analysis of hFet in COVID-19 patients with different disease severities (mild, severe and critical). We aimed to characterise the glycosylation profile of plasma hFet and pinpoint distinct glycosylation patterns linked to particular COVID-19 outcomes. We characterised the composition of 2 N-glycosylation and 3 O-glycosylation hFet sites in all groups of severity. Additionally, we report significantly decreased levels of sialylated N- and O-glycans on sites N156 and T270 in critical patients compared to mild and severe ones. Lastly, a significant decrease of the glycan composition on sites S280 and S293 was observed in critical patients compared to mild and severe ones. These results suggest that the observed desialylation could potentially be responsible for the clearance of hFet in critical patients. Our findings may help to better understand the function of hFet glycosylation in COVID-19 and could open

up new avenues for more accurate diagnostic approaches based on glycosylation profiles.

REFERENCES

1. Wang C, Horby PW, Hayden FG, Gao GF. A novel coronavirus outbreak of global health concern. Lancet (London, England). 2020;395: 470. doi:10.1016/S0140-6736(20)30185-9

2. Kermali M, Khalsa RK, Pillai K, Ismail Z, Harky A. The role of biomarkers in diagnosis of COVID-19 – A systematic review. Life Sci. 2020;254: 117788. doi:10.1016/J.LFS.2020.117788

3. Domingo P, Mur I, Pomar V, Corominas H, Casademont J, de Benito N. The four horsemen of a viral Apocalypse: The pathogenesis of SARS-CoV-2 infection (COVID-19). EBioMedicine. 2020;58. doi:10.1016/J.EBIOM.2020.102887

4. Reverté L, Yeregui E, Olona M, Gutiérrez-Valencia A, Buzón MJ, Martí A, et al. Fetuin-A, inter-α-trypsin inhibitor, glutamic acid and ChoE (18:0) are key biomarkers in a panel distinguishing mild from critical coronavirus disease 2019 outcomes. Clin Transl Med. 2022;12: e704. doi:10.1002/CTM2.704

5. Schinke T, Amendt C, Trindl A, Pöschke O, Müller-Esterl W, Jahnen-Dechent W. The serum protein alpha2-HS glycoprotein/fetuin inhibits apatite formation in vitro and in mineralizing calvaria cells. A possible role in mineralization and calcium homeostasis. J Biol Chem. 1996;271: 20789–20796. doi:10.1074/JBC.271.34.20789

6. Reynolds JL, Skepper JN, McNair R, Kasama T, Gupta K, Weissberg PL, et al. Multifunctional roles for serum protein fetuin-A in inhibition of human vascular smooth muscle cell calcification. J Am Soc Nephrol. 2005;16: 2920–2930. doi:10.1681/ASN.2004100895

7. Mathews ST, Chellam N, Srinivas PR, Cintron VJ, Leon MA, Goustin AS, et al. Alpha2-HSG, a specific inhibitor of insulin receptor autophosphorylation, interacts with the insulin receptor. Mol Cell Endocrinol. 2000;164: 87–98. doi:10.1016/S0303-7207(00)00237-9

8. Jensen MK, Bartz TM, Mukamal KJ, Djoussé L, Kizer JR, Tracy RP, et al. Fetuin-A, type 2 diabetes, and risk of cardiovascular disease in older adults: the cardiovascular health study. Diabetes Care. 2013;36: 1222–1228. doi:10.2337/DC12-1591

9. Wang Y, Koh WP, Jensen MK, Yuan JM, Pan A. Plasma Fetuin-A Levels and Risk of Type 2 Diabetes Mellitus in A Chinese Population: A Nested Case-Control Study. Diabetes Metab J. 2019;43: 474. doi:10.4093/DMJ.2018.0171

10. Janapatla RP, Hsu MH, Liao WT, Chien KY, Lee HY, Chiu CH. Low Serum Fetuin-A as a Biomarker to Predict Pneumococcal Necrotizing Pneumonia and Hemolytic Uremic Syndrome in Children. Medicine (Baltimore). 2016;95: e3221. doi:10.1097/MD.0000000000003221

11. Laughlin GA, McEvoy LK, Barrett-Connor E, Daniels LB, Ix JH. Fetuin-A, a new vascular biomarker of cognitive decline in older adults. Clin Endocrinol (Oxf). 2014;81: 134–140. doi:10.1111/CEN.12382

12. Paton B, Herrero P, Peraire J, Del Pino A, Chafino S, Martinez-Picado J, et al. Fucosylated N-glycans as early biomarkers of COVID-19 severity. Front Immunol. 2023;14: 1204661. doi:10.3389/FIMMU.2023.1204661

13. Lin YH, Franc V, Heck AJR. Similar Albeit Not the Same: In-Depth Analysis of Proteoforms of Human Serum, Bovine Serum, and Recombinant Human Fetuin. J Proteome Res. 2018;17: 2861–2869. doi:10.1021/ACS.JPROTEOME.8B00318/ASSET/IMAGES/LARGE/PR-2018-00318F_0005.JPEG

14. Hoffmann M, Marx K, Reichl U, Wuhrer M, Rapp E. Site-specific O-Glycosylation Analysis of Human Blood Plasma Proteins. Mol Cell Proteomics. 2016;15: 624–641. doi:10.1074/MCP.M115.053546

15. Bateman A, Martin MJ, Orchard S, Magrane M, Ahmad S, Alpi E, et al. UniProt: the Universal Protein Knowledgebase in 2023. Nucleic Acids Res. 2023;51: D523–D531. doi:10.1093/NAR/GKAC1052

16. Chekol Abebe E, Tilahun Muche Z, Behaile T/Mariam A, Mengie Ayele T, Mekonnen Agidew M, Teshome Azezew M, et al. The structure, biosynthesis, and biological roles of fetuin-A: A review. Front Cell Dev Biol. 2022;10.

doi:10.3389/FCELL.2022.945287

17. Lebreton JP, Joisel F, Raoult JP, Lannuzel B, Rogez JP, Humbert G. Serum concentration of human alpha 2 HS glycoprotein during the inflammatory process: evidence that alpha 2 HS glycoprotein is a negative acute-phase reactant. J Clin Invest. 1979;64: 1118. doi:10.1172/JCI109551

18. Ma P, Feng YC. Decreased serum fetuin-A levels and active inflammatory bowel disease. Am J Med Sci. 2014;348: 47–51. doi:10.1097/MAJ.0000000000000195

19. Sato H, Kazama JJ, Wada Y, Kuroda T, Narita I, Gejyo F, et al. Decreased levels of circulating alpha2-Heremans-Schmid glycoprotein/Fetuin-A (AHSG) in patients with rheumatoid arthritis. Intern Med. 2007;46: 1685–1692. doi:10.2169/INTERNALMEDICINE.46.6269

20. Wang H, Sama AE. Anti-inflammatory role of Fetuin-A in Injury and Infection. Curr Mol Med. 2012;12: 625. doi:10.2174/156652412800620039

21. Rudloff S, Jahnen-Dechent W, Huynh-Do U. Tissue chaperoning-the expanded functions of fetuin-A beyond inhibition of systemic calcification. Pflugers Arch. 2022;474: 949–962. doi:10.1007/S00424-022-02688-6

22. Messina F, Calabrese G, Turano L, Tebala C, Arcadi N. A pulmonary hamartoma in Covid-19 pneumonia: an interesting case studied with computed tomography. Radiol Case Reports. 2021;16: 942. doi:10.1016/J.RADCR.2021.01.051

23. Moreno BG, Weiland GB, Alegre MLS, Rodríguez JEV. Accelerated pulmonary ossification as a sequela of sars-cov-2 pneumonia. Radiol Cardiothorac Imaging. 2021;3. doi:10.1148/RYCT.2021200598/ASSET/IMAGES/LARGE/RYCT.20212005 98.FIG2.JPEG

24. Ricken F, Can AD, Gräber S, Häusler M, Jahnen-Dechent W. Post-translational modifications glycosylation and phosphorylation of the major hepatic plasma protein fetuin-A are associated with CNS inflammation in children. PLoS One. 2022;17. doi:10.1371/JOURNAL.PONE.0268592

25. Ghadially FN. As you like it, Part 3: A critique and historical review of

calcification as seen with the electron microscope. Ultrastruct Pathol. 2001;25: 243–267. doi:10.1080/019131201300343874

26. Babler A, Schmitz C, Buescher A, Herrmann M, Gremse F, Gorgels T, et al. Microvasculopathy and soft tissue calcification in mice are governed by fetuin-A, magnesium and pyrophosphate. PLoS One. 2020;15. doi:10.1371/JOURNAL.PONE.0228938

27. Jahnen-Dechent W, Heiss A, Schäfer C, Ketteler M. Fetuin-A regulation of calcified matrix metabolism. Circ Res. 2011;108: 1494–1509. doi:10.1161/CIRCRESAHA.110.234260

28. Jahnen-Dechent W, Büscher A, Köppert S, Heiss A, Kuro-o M, Smith ER. Mud in the blood: the role of protein-mineral complexes and extracellular vesicles in biomineralisation and calcification. J Struct Biol. 2020;212. doi:10.1016/J.JSB.2020.107577

SUPPLEMENTARY MATERIAL

Supplementary Table 1. List of all modified peptide isoforms on human fetuin-A (hFet). Peptides were detected in human fetuin-A standard and COVID-19 patients (mild, severe and critical).

N-glycosylation				
Peptide Sequence (N156)	**Modifications**	**Obs. m/z**	**Product Charge**	**Retention Time (min)**
D.VRKVCQDCPLLAPLnD.T	2xCarboxymethyl [C5; C8]; 1xHexNAc(4)Hex(5)NeuAc(2) [N15]	1368.908	3	86.95
D.VRKVCQDCPLLAPLnD.T	2xCarboxymethyl [C5; C8]; 1xHexNAc(4)Hex(5)NeuAc(1) [N15]	1271.879	3	76.64
D.VRKVCQDCPLLAPLnD.T	2xCarboxymethyl [C5; C8]; 1xHexNAc(5)Hex(6)Fuc(1)NeuAc(3) [N15]	1227.503	4	97.48
D.VRKVCQDCPLLAPLnD.T	2xCarboxymethyl [C5; C8]; 1xHexNAc(4)Hex(5)Fuc(1)NeuAc(2) [N15]	1417.597	3	86.33
D.CPLLAPLnDTR.V	1xCarboxymethyl [C1]; 1xHexNAc(5)Hex(6)Fuc(2)NeuAc(2) [N8]	1378.221	3	84.13
Peptide Sequence (N176)				
K.AALAAFNAQNnGSNFQLEE.I	1xHexNAc(4)Hex(5)NeuAc(2) [N11]	1405.232	3	114.48
K.AALAAFNAQNnGSNFQLEE.I	1xHexNAc(4)Hex(5)Fuc(1)NeuAc(2) [N11]	1058.438	4	116.15
K.AALAAFNAQNnGSNFQLEE.I	1xHexNAc(4)Hex(5)NeuAc(1) [N11]	981.4055	4	99.7
K.AALAAFNAQNnGSNFQLEE.I	1xHexNAc(5)Hex(6)NeuAc(3) [N11]	1218.238	4	136.01
K.AALAAFNAQNnGSNFQLEE.I	1xHexNAc(5)Hex(6)Fuc(1)NeuAc(3) [N11]	1222.494	4	137.17
K.AALAAFNAQNnGSNFQLEE.I	1xHexNAc(4)Hex(5)Fuc(1)NeuAc(1) [N11]	1356.896	3	99.56
K.AALAAFNAQNnGSNFQLE.E	1xHexNAc(6)Hex(6)NeuAc(1) [N11]	1454.595	3	112.9
K.AALAAFNAQNnGSNFQLEE.I	1xHexNAc(4)Hex(5) [N11]	1211.177	3	86.64

O-glycosylation				
Peptide Sequence (T270)	**Modifications**	**Obs. m/z**	**Product Charge**	**Retention Time (min)**
E.GANEAVPtPVVDPDAPPSPPLGAPGLPPAGSPPDSHVLLAAPPGHQLHR.A	1xHexNAc(1)Hex(1)NeuAc(2) [T8]	817.2604	7	98.71
E.GANEAVPtPVVD.P	1xHexNAc(1)Hex(1)NeuAc(1) [T8]	912.9085	2	84.25
E.GANEAVPtPVVDPDAPPSPPLGAPGLPPAGSPPDSHVLLAAPPGHQLHR.A	1xHexNAc(2)Hex(2)NeuAc(2) [T8]	869.4153	7	98.57
E.GANEAVPtPVVD.P	1xHexNAc(1)Hex(2)Fuc(1) [T8]	921.4195	2	84.19
E.GANEAVPtPVVDPDAPPSPPLGAPGLPPAGSPPDSHVLLAAPPGHQLHR.A	1xHexNAc(2)Hex(2)NeuAc(1) [T8]	827.8348	7	94.85
E.GANEAVPtPVVDPDAPPSPPLGAPGLPPAGSPPDSHVLLAAPPGHQLHR.A	1xHexNAc(4)Hex(1) [T8]	821.1171	7	99.83
E.AVPtPVVDPD.A	1xHexNAc(3)Hex(3)Fuc(2)NeuAc(2) [T4]	993.7491	3	94.05
E.AVPtPVVD.P	1xHexNAc(4)Hex(4)Fuc(3)NeuAc(1) [T4]	996.425	3	106.32
E.AVPtPVVD.P	1xHexNAc(1)Hex(1)NeuAc(3) [T4]	679.2911	3	96.04
Peptide Sequence (T280)				
E.GANEAVPTPVVDPDAPPsPPLGAPGLPPAGSPPDSHVLLAAPPGHQLHR.A	1xHexNAc(1)Hex(1)NeuAc(2) [S18]	817.2623	7	98.71
E.GANEAVPTPVVDPDAPPsPPLGAPGLPPAGSPPDSHVLLAAPPGHQLHR.A	1xHexNAc(1)Hex(1)NeuAc(1) [S18]	1085.545	5	94.85
D.APPsPPLGAPGLPPAGSPPDSHVLLAAPPGHQLHR.A	1xHexNAc(4)Hex(4)Fuc(3) [S4]	1061.713	5	101.61
E.GANEAVPTPVVDPDAPPsPPLGAPGLPPAGSPPDSHVLLAAPPGHQLHR.A	1xHexNAc(1)Hex(1) [S18]	1027.329	5	93.08
E.GANEAVPTPVVDPDAPPsPPLGAPGLPPAGSPPD.S	1xHexNAc(1)Hex(2)Fuc(1) [S18]	1276.273	3	121.43
E.GANEAVPTPVVDPDAPPsPPLGAPGLPPAGSPPDSHVLLAAPPGHQLHR.A	1xHexNAc(2)Hex(2)NeuAc(2) [S18]	869.4208	7	97.54
E.GANEAVPTPVVDPDAPPsPPLGAPGLPPAGSPPDSHVLLAAPPGHQLHR.A	1xHexNAc(2)Hex(2)NeuAc(1) [S18]	1158.56	5	94.42
E.GANEAVPTPVVDPDAPPsPPLGAPGLPPAGSPPDSHVLLAAPPGHQLHR.A	1xHexNAc(2)Hex(1)Fuc(1) [S18]	1097.142	5	102.01
E.GANEAVPTPVVDPDAPPsPPLGAPGLPPAGSPPDSHVLLAAPPGHQLHR.A	1xHexNAc(4)Hex(1) [S18]	1149.161	5	99.25
D.PDAPPsPPLGAPGLPPAGSPPDSHVLLAAPPGHQLHR.A	1xHexNAc(6)Hex(4) [S6]	1097.722	5	95.94
E.GANEAVPTPVVDPDAPPsPPLGAPGLPPAGSPPDSHVLLAAPPGHQLHR.A	1xHexNAc(2)Hex(1)Fuc(1)NeuAc(1) [S18]	1155.365	5	98.9
Peptide Sequence (T293)				
E.AVPTPVVDPDAPPSPPLGAPGLPPAGsPPDSHVLLAAPPGHQLHR.A	1xHexNAc(1)Hex(1)NeuAc(1) [S27]	1011.316	5	95.07
D.PDAPPSPPLGAPGLPPAGsPPDSHVLLAAPPGHQLHR.A	1xHexNAc(6)Hex(4) [S19]	914.9424	6	96.26
D.PDAPPSPPLGAPGLPPAGsPPDSHVLLAAPPGHQLHR.A	1xHexNAc(6)Hex(4)Fuc(2) [S19]	963.619	6	98.84
E.AVPTPVVDPDAPPSPPLGAPGLPPAGsPPDSHVLLAAPPGHQLHR.A	1xHexNAc(1)Hex(1)NeuAc(2) [S27]	1069.532	5	99.22
E.AVPTPVVDPDAPPSPPLGAPGLPPAGsPPDSHVLLAAPPGHQLHR.A	1xHexNAc(1)Hex(1) [S27]	953.0952	5	93.08
E.AVPTPVVDPDAPPSPPLGAPGLPPAGsPPDSHVLLAAPPGHQLHR.A	1xHexNAc(2)Hex(2)NeuAc(2) [S27]	816.4016	7	98.57
D.PDAPPSPPLGAPGLPPAGsPPDSHVLLAAPPGHQLHR.A	1xHexNAc(6)Hex(3)Fuc(1) [S19]	782.0954	7	98.37
E.AVPTPVVDPDAPPSPPLGAPGLPPAGsPPDSHVLLAAPPGHQLHR.A	1xHexNAc(1)Hex(2)Fuc(1) [S27]	1014.716	5	94.85
D.PDAPPSPPLGAPGLPPAGsPPDSHVLLAAPPGHQLHR.A	1xHexNAc(3)Hex(2)Fuc(4) [S19]	856.7583	6	106.12
E.AVPTPVVDPDAPPSPPLGAPGLPPAGsPPDSHVLLAAPPGHQLHR.A	1xHexNAc(1)Hex(1)Fuc(1)NeuAc(1) [S27]	1040.522	5	98.35
D.PDAPPSPPLGAPGLPPAGsPPDSHVLLAAPPGHQLHR.A	1xHexNAc(4)Hex(3)Fuc(2) [S19]	1042.504	5	93.08
E.AVPTPVVDPDAPPSPPLGAPGLPPAGsPPDSHVLLAAPPGHQLHR.A	1xHexNAc(5)Hex(5)Fuc(3) [S27]	1332.825	5	104.11
E.AVPTPVVDPDAPPSPPLGAPGLPPAGsPPDSHVLLAAPPGHQLHR.A	1xHexNAc(3)Hex(2)Fuc(1)NeuAc(1) [S27]	1154.16	5	106.31
D.PDAPPSPPLGAPGLPPAGsPPDSHVLLAAPPGHQLHR.A	1xHexNAc(4)Hex(3)Fuc(2) [S19]	1042.504	5	91.9
D.PDAPPSPPLGAPGLPPAGsPPDSHVLLAAPPGHQLHR.A	1xHexNAc(6)Hex(3)Fuc(1) [S19]	1367.913	4	96.06
E.AVPTPVVDPDAPPSPPLGAPGLPPAGsPPDSHVLLAAPPGHQLHR.A	1xHexNAc(2)Hex(2)Fuc(1)NeuAc(2) [S27]	976.6449	6	98.95

UNIVERSITAT ROVIRA I VIRGILI
EXPLORING THE ROLE OF GLYCANS: A NEW FRONTIER IN DISEASE BIOMARKER RESEARCH
Beatrix Paton Jimenez

GENERAL DISCUSSION

UNIVERSITAT ROVIRA I VIRGILI
EXPLORING THE ROLE OF GLYCANS: A NEW FRONTIER IN DISEASE BIOMARKER RESEARCH
Beatrix Paton Jimenez

GENERAL DISCUSSION

Glycans, crucial players in various biological processes, have emerged as significant biomarkers with wide-ranging applications in biomedical research and clinical settings [1–3]. These carbohydrates contribute to essential cellular communication, immune responses, and disease progression [4,5]. Through the study and analysis of glycans as biomarkers, valuable insights into an organism's physiological and pathological states are obtained, facilitating the development of novel diagnostic tools and therapeutic interventions. The relevance of altered glycosylation patterns extends across numerous diseases, encompassing cancer, cardiovascular disorders, autoimmune diseases, and infectious diseases [3,6,7]. Detecting changes in glycans can provide critical indications of disease initiation, progression, or prognosis, with the added benefit of potential use for early detection and patient stratification. Moreover, the early manifestation of glycan alterations in disease makes them particularly valuable for early-stage identification. Their significance is further emphasized by their potential to serve as key indicators for identifying therapeutic targets in drug development. Understanding the specific glycosylation changes associated with various diseases can effectively guide the design of targeted therapies focused on modulating distinct glycan-related pathways. The integration of glycan analysis into the study of any disease, can potentially uncover novel avenues for therapeutic intervention and diagnostic tools, as well as fostering a more comprehensive understanding of the intricate relationship between glycans and disease pathogenesis.

Taking this into account, the first objective contemplated exploring the alterations in the N-glycome, related to the process of ageing and age-related conditions (**Chapter 1**). Firstly, we compiled alterations in N-glycosylation profiles associated with age-related diseases, including cancer, type 2 diabetes mellitus (T2DM), metabolic syndrome, and chronic

inflammatory diseases, while also discussing common techniques for determining and characterising protein glycosylation (**Manuscript 1**). This review showed how glycosylation is a potential factor in disease progression and how these post-translational modifications (PTMs) can serve as diagnostic and prognostic biomarkers for multifactorial diseases. Overall, galactosylation and sialylation are frequently altered in ageing and various age-related diseases, with a specific decrease observed with age, Alzheimer's disease (AD) and rheumatoid arthritis (RA) patients, but an increase seen in amyotrophic lateral sclerosis (ALS) patients [8–11]. Conversely, fucosylation generally increases in several cancer types but decreases in inflammatory bowel disease (IBD) and T2DM patients [12–15]. Comparing glycans levels in specific diseases across clinical studies often yields inconsistent results, partially due to the diversity of the glycome in different populations and environments. Nonetheless, glycan traits hold promise as a new avenue for understanding complex diseases systematically, as changes in glycosylation patterns can reflect the real-time status of complex interactions involved in disease development. The analysis of glycans is challenging due to their complex and heterogenous structures and the use of diverse methodologies for their determination leads to low comparability between studies, hindering clear results. Techniques like capillary electrophoresis (CE), ion mobility spectrometry (IMS), nuclear magnetic resonance (NMR), and mass spectrometry (MS) are employed for glycomic analysis [16–21], with MS being considered the most promising due to its versatility in chromatographic separation and ionization techniques.

This comprehensive evaluation of the reported N-glycosylation alterations associated with age-related diseases led to exploring the effects of a high-glucose diet (HGD) on ageing, employing the animal model *C. elegans* (**Manuscript 2**). Several risk factors contribute to the development of diseases, including obesity, hypertension, dyslipidaemia, and hyperglycaemia, which can be induced with the consumption of a high-

glucose diet [22,23]. Reducing sugar intake and maintaining a balanced diet can play a crucial role in promoting healthy ageing and reducing the risk of age-related diseases [24,25]. We conducted a multi-omics study, encompassing N-glycomics, proteomics, and lipidomics, along with gene expression analysis and lifespan determination. For this, we employed three *C. elegans* strains with different lifespans: N2, CF1038 and CB1370. Compared to the control diet, we found that worms fed a HGD had 29%, 12%, and 19% shorter lifespans, respectively. Similar findings have been observed in previous HGD research [26]. Notably, oligomannosidic and paucimannosidic structures were the most abundant subgroups of N-glycans in all groups. Some N-glycan species, such as Hex6HexNAc2 (GLY17), responded differently to HGD and ageing in strain-specific ways. Furthermore, N-glycan profiles exhibited variations throughout embryonic phases, suggesting critical lifestyle changes and developmental processes in the worm. We also observed changes in vitellogenins, which play crucial roles in lipid transport and reproduction, across strains and diets, indicating their involvement in lifespan regulation and response to HGD. Proteomic data analysis revealed modifications in pathways related to catabolic processes, energy production, translation, and RNA processing, suggesting an adaptive response to elevated glucose levels. Additionally, HGD impacted lipid metabolism, with strain-specific changes in triglyceride levels. Throughout the analyses, a general trend emerged, with more significant alterations observed on day 5, coinciding with the egg-laying adult stage. These changes are likely due to the higher metabolic rates exhibited by adult *C. elegans* compared to an ageing stage. Notably, changes induced by the diet were more prominent from day 5 to day 12, as glucose, a major energy source for *C. elegans*, is more actively utilized in HGD-fed adults. Through an integrative analysis, positive correlations were observed between triglycerides (TG) and N-glycans in HGD-fed N2 and CF strains, compared to the respective control groups. Additionally, proteins involved in lipid transport showed drastically different correlations with different lipid families, potentially indicating a

distruption in the lipid transport activity. Overall, this study sheds light on the intricate relationship between nutrition, multi-omics responses, gene expression, and lifespan in *C. elegans*. The changes observed in the N-glycome, proteome, and lipidome, as well as alterations in critical transcription factors and pathways, provide valuable insights into the molecular mechanisms underlying the organism's response to HGD and its impact on aging. However, more research is required to fully comprehend the activities and relationships of individual genes, pathways, and metabolic processes in *C. elegans*.

To further provide insights into the biological relevance of glycan modifications, glycosylation patterns were evaluated in different animal models and matrices. An unparalleled level of complexity exists in the development, organisation, and regulation of the brain, in which N-glycosylation is a crucial player. Understanding the specific N-glycan species involved is essential. Hence, this study aimed to comprehensively explore brain protein N-glycosylation by investigating how a High-Fat Diet (HFD) impacts N-glycan and lipid profiles in the brain (**Chapter 2, Manuscript 3**). Additionally, the research sought to assess the changes that occur when transitioning from a HFD to a Mediterranean-like diet (MED). This investigation has the potential to provide valuable insights into the brain's plasticity and its ability to recover when exposed to diverse lifestyle patterns, initially with a HFD and later transitioning to a healthier MED. The study revealed statistically significant differences in 18 N-glycans and 53 lipids between groups HFD, MED, and CTRL. Additionally, results indicated that a short MED intervention had minimal impact on modifying the N-glycan and lipid profile in animals previously fed with a HFD. A longer-term MED after a HFD could reveal if the MED can effectively reverse or modify the brain N-glycan and lipid pattern. Regarding the N-glycan profile, the HFD-fed groups showed a decrease in most sialylated and fucosylated structures but an increase in most oligomannose structures. These changes resembled trends observed in

ageing studies [27–29], indicating that the HFD may induce events similar to those observed in ageing and age-related diseases.

Most of the identified brain lipids belonged to the PC and PE lipid species, which are abundant phospholipids in mammalian cell membranes. PC, in particular, is one of the most abundant lipid in the brain [30]. Despite the blood-brain barrier acting as a metabolic shield to the brain [31], there was a statistically significant increase in 48 lipids in the HFD group compared to the CTRL group. Further research is needed to determine if these lipid profile shifts are associated with relevant functional brain changes. These findings stimulate further questions about the potential crosstalk between glycosylation and lipid metabolism in the brain.

Having explored the intricate role of glycosylation in response to a high-glucose diet in *C. elegans*, we could draw parallels to the investigation of glycosylation in the brain of hamsters under the influence of a HFD. The converging trends in both studies suggest that dietary composition plays a critical role in shaping glycosylation patterns, influencing organismal responses across species. Overall, the parallels and distinctions observed between these two studies underscore the significance of glycosylation as a conserved and sensitive regulatory mechanism in response to dietary variations. Understanding glycosylation dynamics in different animal models provides a comprehensive view of the multifaceted roles this post-translational modification plays in shaping cellular functions, metabolic responses, and potentially neurological outcomes.

The translational potential of glycosylation research from model organisms to human subjects underscores its relevance in tackling global health challenges and advancing precision medicine [32]. In the wake of the ongoing COVID-19 pandemic, the investigation of glycosylation took on an even greater significance, as emerging evidence suggested that this PTM may play a pivotal role in the progression and clinical outcomes of SARS-CoV-2 infection [33]. Notably, in the context of infectious diseases such as COVID-19, glycosylation of viral proteins and host glycoproteins plays a

vital role in viral entry, immune evasion, and host-pathogen interactions [34]. The analysis of glycosylation patterns in COVID-19 patients can offer a deeper understanding of how glycosylation influences disease outcomes and immune responses. The third objective aimed to determine glycan signatures for reliable risk stratification of COVID-19 patients and to identify patients who are more likely to progress to a critical stage (**Chapter 3**). The identification of specific glycan biomarkers associated with severe COVID-19 cases may facilitate patients clustering and enable the development of targeted therapies aimed at mitigating the detrimental effects of the disease. Targeting glycan-related pathways could potentially modulate the inflammatory response, enhance antiviral immunity, or improve the clearance of viral particles, leading to better clinical outcomes for patients with severe COVID-19. The investigation of glycosylation in COVID-19 could hold promising implications for advancing personalised medicine and optimising patient care in the future.

Taking this into account, we have demonstrated that total plasma from SARS-CoV-2-infected patients exhibits distinct glycosylation profiles, which can be detected at both the time of diagnosis and four weeks post-diagnosis (**Manuscript 4**). These profiles offer valuable insights for patient stratification and have the potential to predict COVID-19 prognosis. Specifically, 15 N-glycans showed statistically significant differences between patient groups at both time points, with higher significance observed at diagnosis, indicating their potential as early-stage biomarkers. Notably, fucosylated and galactosylated structures were significantly decreased in critical patients compared to mild and severe cases, while agalactosylated structures were increased in critical patients. The observed glycosylation patterns align with previous studies on COVID-19 patients, linking certain glycan alterations with poor disease outcomes and inflammatory processes [35]. Furthermore, sialylated N-glycans exhibited varying changes with disease severity at diagnosis but did not show significant differences at four weeks post-diagnosis. Obtaining a global

plasma glycosignature allowed us to assess the inflammatory state of organs during the disease, and these glycan trends mirrored those observed in IgG N-glycome, suggesting a simplified sample preparation process for obtaining IgG N-glycan profiles. In the context of other proposed prognostic biomarkers for COVID-19, such as metabolomics, lipidomics, and proteomics analyses [36–38], the addition of specific glycans could potentially enhance the prediction of mild and critical outcomes. Future studies should explore the impact of different SARS-CoV-2 variants on total plasma glycosylation, especially as new variants emerge. Longitudinal studies, including analysis of samples before and after infection, could provide insights into the potential use of these glycan structures as preinfection biomarkers for predicting critical disease progression. Overall, our study unveils a novel risk screening system based on the plasma N-glycome signature, which can stratify COVID-19 patients and predict disease progression at diagnosis. This minimally invasive blood biomarker has the potential to optimize healthcare resource management and vaccination strategies for COVID-19.

In this same cohort of patients, fetuin-A has been reported to be an accurate biomarker of the critical clinical progression of COVID-19, decreasing with increasing severity [36]. To potentially provide valuable information to the glycomics study, a site-specific glycan analysis of human fetuin-A was performed, aiming to provide information on the specific glycosylation patterns at individual glycoprotein sites (**Manuscript 5**). A site-specific glycan analysis provides valuable information to a glycomics study by offering more detailed and precise insights into the glycan structures attached to specific glycoprotein sites. Site-specific glycan analysis allows researchers to correlate specific glycosylation patterns with the function of glycoproteins. This information is particularly important in disease studies, where changes in glycosylation at specific sites may be associated with disease progression, severity, or response to therapy. We examined the composition of N-glycosylation and O-glycosylation at two and three fetuin-A sites, respectively, in mild, severe

and critical COVID-19 patients. Our findings revealed significantly decreased levels of sialylated N- and O-glycans on sites N156 and T270 in severe patients compared to mild and severe cases. Additionally, a significant decrease in the glycan composition on sites S280 and S293 was observed in severe patients compared to the other groups. Desialylation serves as a regulatory signal, leading to the degradation and clearance of fetuin-A after it binds to calcium and phosphate [39]. This phenomenon could explain the observed decrease in sialylated glycan structures in several sites among critical patients. These results provide valuable insights into the function of fetuin-A glycosylation in COVID-19 and may pave the way for new diagnostic approaches based on glycosylation profiles.

Some limitations exist in the studies included in this thesis, which should be addressed. In terms of sample size and diversity, expanding the sample pool to include larger and more diverse populations would strengthen the generalizability of the findings and enhance the reliability of glycan-based biomarkers. Moreover, while the use of model organisms like *C. elegans* and hamsters offers valuable insights into glycosylation processes and their roles in biological functions, it is essential to acknowledge that the glycomic landscape may differ between these models and humans. For instance, while both *C. elegans* and mammals share a common core glycosylation machinery [40], the differences in glycan structures reflect the evolutionary divergence between organisms. Extrapolating results from model organisms to human diseases requires caution and validation in human studies. Also, glycans are highly diverse and heterogeneous, making the analysis and interpretation of glycomic data challenging. The intricacy of glycan structures can result in some glycoforms being overlooked or not well characterised. Software tools and advanced data processing techniques play a crucial role in addressing the complexity of glycosylation and capturing glycomic variations.

The findings we present in this thesis open up avenues for future research, particularly in the context of clinical translation. The glycan-based risk stratification approach for COVID-19 patients **(Manuscript 4)** warrants validation in larger, diverse patient cohorts to assess its robustness and generalizability. Prospective longitudinal studies could provide valuable insights into the predictive power of glycan signatures for disease progression, treatment response, and long-term outcomes. Additionally, in-depth mechanistic studies are essential to unravel the underlying molecular pathways through which glycosylation influences disease outcomes. Investigating the glycosylation-related changes in protein function, immune responses, and host-pathogen interactions could provide a deeper understanding of disease pathogenesis. Standardization of glycomic analysis methodologies is critical to ensure the reproducibility and comparability of results across different studies. For this aim we compilated the existing reports on N-glycan alterations in **Manuscript 1**, although the field of glycomics would benefit from more efforts to establish reference glycan databases, standardized protocols, and quality control measures.

This thesis contributes significantly to our understanding of glycosylation in various contexts, ranging from age-related diseases and dietary influences to COVID-19. The study of the N-glycome in different animal models and matrices, suggested that dietary composition plays a critical role in shaping glycosylation patterns across species. Notably, the use of glycans as potential biomarkers was highlighted with the proposal of an N-glycan signature for the stratification of COVID-19 patients. Furthermore, the integration of N-glycome data with other omics datasets, such as proteomics or lipidomics, provides a more comprehensive view of the biological processes and helps uncover complex relationships between glycosylation and other molecular mechanisms.

REFERENCES

1. Li X, Wang H, Russell A, Cao W, Wang X, Ge S, et al. Type 2 Diabetes Mellitus is Associated with the Immunoglobulin G N-Glycome through Putative Proinflammatory Mechanisms in an Australian Population. Omi A J Integr Biol. 2019;23. doi:10.1089/omi.2019.0075
2. Muchena J. Kailemia, Dayoung Park and CBL. Glycans and Glycoproteins as Specific Biomarkers for Cancer. Anal Bioanal Chem. 2017;409: 395–410. doi:doi:10.1007/s00216-016-9880-6
3. Paton B, Suarez M, Herrero P, Canela N, Cairo W, Garozzo D, et al. Glycosylation Biomarkers Associated with Age-Related Diseases and Current Methods for Glycan Analysis. Int J Mol Sci 2021, Vol 22, Page 5788. 2021;22: 5788. doi:10.3390/IJMS22115788
4. Reily C, Stewart TJ, Renfrow MB, Novak J. Glycosylation in health and disease. Nat Rev Nephrol 2019 156. 2019;15: 346–366. doi:10.1038/s41581-019-0129-4
5. Varki A, Gagneux P. Multifarious roles of sialic acids in immunity. Ann N Y Acad Sci. 2012;1253: 16–36. doi:10.1111/J.1749-6632.2012.06517.X
6. Zhang XL, Qu H. The Role of Glycosylation in Infectious Diseases. Adv Exp Med Biol. 2021;1325: 219–237. doi:10.1007/978-3-030-70115-4_11
7. Ząbczyńska M, Link-Lenczowski P, Pocheć E. Glycosylation in Autoimmune Diseases. Adv Exp Med Biol. 2021;1325: 205–218. doi:10.1007/978-3-030-70115-4_10
8. Lemmers RFH, Vilaj M, Urda D, Agakov F, Šimurina M, Klaric L, et al. IgG glycan patterns are associated with type 2 diabetes in independent European populations. Biochim Biophys acta Gen Subj. 2017;1861: 2240–2249. doi:10.1016/j.bbagen.2017.06.020
9. Gindzienska-Sieskiewicz E, Klimiuk PA, Kisiel DG, Gindzienski A, Sierakowski S. The changes in monosaccharide composition of immunoglobulin G in the course of rheumatoid arthritis. Clin Rheumatol. 2007;26: 685–690. doi:10.1007/s10067-006-0370-7
10. Ruhaak LR, Uh HW, Beekman M, Koeleman CAM, Hokke CH, Westendorp RGJ, et al. Decreased levels of bisecting GLcNAc glycoforms of IgG are associated with human longevity. PLoS One. 2010;5: 1–8. doi:10.1371/journal.pone.0012566

11. Baković MP, Selman MHJ, Hoffmann M, Rudan I, Campbell H, Deelder AM, et al. High-throughput IgG Fc N-glycosylation profiling by mass spectrometry of glycopeptides. J Proteome Res. 2013;12: 821–831. doi:10.1021/pr300887z
12. Clerc F, Novokmet M, Dotz V, Reiding KR, de Haan N, Kammeijer GSM, et al. Plasma N-Glycan Signatures Are Associated With Features of Inflammatory Bowel Diseases. Gastroenterology. 2018;155: 829–843. doi:10.1053/j.gastro.2018.05.030
13. Kyselova Z, Mechref Y, Kang P, Goetz JA, Dobrolecki LE, Sledge GW, et al. Breast cancer diagnosis and prognosis through quantitative measurements of serum glycan profiles. Clin Chem. 2008;54: 1166–1175. doi:10.1373/CLINCHEM.2007.087148
14. Hu Y, Ferdosi S, Kapuruge EP, Diaz de Leon JA, Stücker I, Radoï L, et al. Diagnostic and Prognostic Performance of Blood Plasma Glycan Features in the Women Epidemiology Lung Cancer (WELCA) Study. J Proteome Res. 2019. doi:10.1021/acs.jproteome.9b00457
15. Dotz V, Lemmers RFH, Reiding KR, Hipgrave Ederveen AL, Lieverse AG, Mulder MT, et al. Plasma protein N-glycan signatures of type 2 diabetes. Biochim Biophys Acta - Gen Subj. 2018;1862: 2613–2622. doi:10.1016/j.bbagen.2018.08.005
16. Fellenberg M, Behnken HN, Nagel T, Wiegandt A, Baerenfaenger M, Meyer B. Glycan analysis: Scope and limitations of different techniques - A case for integrated use of LC-MS(/MS) and NMR techniques. Anal Bioanal Chem. 2013;405: 7291–7305. doi:10.1007/s00216-013-7164-y
17. Wang H, Li X, Wang X, Liu D, Zhang X, Cao W, et al. Next-Generation (Glycomic) Biomarkers for Cardiometabolic Health: A Community-Based Study of Immunoglobulin G N -Glycans in a Chinese Han Population . Omi A J Integr Biol. 2019;23: 1–11. doi:10.1089/omi.2019.0099
18. Hamid U, Royle L, Saldova, R et. al. A strategy to reveal potential glycan markers from serum glycoproteins associated with breast cancer progression. Glycobiology. 2008;18: 1105–1118. doi:10.1093/glycob/cwn095
19. Šunderić M, Šedivá A, Robajac D, Miljuš G, Gemeiner P, Nedić O, et al. Lectin-based protein microarray analysis of differences in serum alpha-2-macroglobulin glycosylation between patients with colorectal cancer and

persons without cancer. Biotechnol Appl Biochem. 2016;63: 457–464. doi:10.1002/bab.1407

20. De Leoz MLA, An HJ, Kronewitter S, Kim J, Beecroft S, Vinall R, et al. Glycomic approach for potential biomarkers on prostate cancer: Profiling of N-linked glycans in human sera and pRNS cell lines. Dis Markers. 2008;25: 243–258. doi:10.1155/2008/515318
21. Lu JP, Knežević A, Wang YX, Rudan I, Campbell H, Zou ZK, et al. Screening novel biomarkers for metabolic syndrome by profiling human plasma N-glycans in Chinese han and Croatian populations. J Proteome Res. 2011;10: 4959–4969. doi:10.1021/pr2004067
22. Aston LM. Glycaemic index and metabolic disease risk. Proc Nutr Soc. 2006;65: 125–134. doi:10.1079/PNS2005485
23. Venn BJ, Green TJ. Glycemic index and glycemic load: measurement issues and their effect on diet-disease relationships. Eur J Clin Nutr. 2007;61 Suppl 1: S122–S131. doi:10.1038/SJ.EJCN.1602942
24. Noordam R, Gunn DA, Tomlin CC, Maier AB, Mooijaart SP, Slagboom PE, et al. High serum glucose levels are associated with a higher perceived age. Age (Omaha). 2013;35: 189. doi:10.1007/S11357-011-9339-9
25. Cerami A. Hypothesis. Glucose as a mediator of aging. J Am Geriatr Soc. 1985;33: 626–634. doi:10.1111/J.1532-5415.1985.TB06319.X
26. Alcántar-Fernández J, Navarro RE, Salazar-Martínez AM, Pérez-Andrade ME, Miranda-Ríos J. Caenorhabditis elegans respond to high-glucose diets through a network of stress-responsive transcription factors. PLoS One. 2018;13: 1–24. doi:10.1371/journal.pone.0199888
27. Edri-Brami M, Rosental B, Hayoun D, Welt M, Rosen H, Wirguin I, et al. Glycans in sera of amyotrophic lateral sclerosis patients and their role in killing neuronal cells. PLoS One. 2012;7. doi:10.1371/journal.pone.0035772
28. Lundström SL, Yang H, Lyutvinskiy Y, Rutishauser D, Herukka SK, Soininen H, et al. Blood plasma IgG Fc glycans are significantly altered in Alzheimer's disease and progressive mild cognitive impairment. J Alzheimer's Dis. 2014;38: 567–579. doi:10.3233/JAD-131088
29. Váradi C, Nehéz K, Hornyák O et. al. Serum N-Glycosylation in Parkinson's Disease: A Novel Approach for Potential Alterations. Molecules. 2019;24. doi:10.3390/molecules24122220

30. Lee JC, Park SM, Kim IY, Sung H, Seong JK, Moon MH. High-fat diet-induced lipidome perturbations in the cortex, hippocampus, hypothalamus, and olfactory bulb of mice. Biochim Biophys Acta - Mol Cell Biol Lipids. 2018;1863: 980–990. doi:10.1016/j.bbalip.2018.05.007
31. Dahdah N, Gonzalez-franquesa A, Samino S, Gama-perez P, Herrero L, Perales JC, et al. Effects of lifestyle intervention in tissue-specific lipidomic profile of formerly obese mice. Int J Mol Sci. 2021;22: 3694. doi:10.3390/ijms22073694
32. Almeida A, Kolarich D. The promise of protein glycosylation for personalised medicine. Biochim Biophys Acta. 2016;1860: 1583–1595. doi:10.1016/J.BBAGEN.2016.03.012
33. Petrović T, Lauc G, Trbojević-Akmačić I. The Importance of Glycosylation in COVID-19 Infection. Adv Exp Med Biol. 2021;1325: 239–264. doi:10.1007/978-3-030-70115-4_12
34. Reis CA, Tauber R, Blanchard V. Glycosylation is a key in SARS-CoV-2 infection. J Mol Med (Berl). 2021;99: 1023–1031. doi:10.1007/S00109-021-02092-0
35. Hou H, Yang H, Liu P, Huang C, Wang M, Li Y, et al. Profile of Immunoglobulin G N-Glycome in COVID-19 Patients: A Case-Control Study. Front Immunol. 2021;12. doi:10.3389/fimmu.2021.748566
36. Reverté L, Yeregui E, Olona M, Gutiérrez-Valencia A, Buzón MJ, Martí A, et al. Fetuin-A, inter-α-trypsin inhibitor, glutamic acid and ChoE (18:0) are key biomarkers in a panel distinguishing mild from critical coronavirus disease 2019 outcomes. Clin Transl Med. 2022;12: e704. doi:10.1002/CTM2.704
37. Barberis E, Timo S, Amede E, Vanella V V., Puricelli C, Cappellano G, et al. Large-Scale Plasma Analysis Revealed New Mechanisms and Molecules Associated with the Host Response to SARS-CoV-2. Int J Mol Sci. 2020;21: 1–25. doi:10.3390/IJMS21228623
38. López-Hernández Y, Monárrez-Espino J, Oostdam ASH van, Delgado JEC, Zhang L, Zheng J, et al. Targeted metabolomics identifies high performing diagnostic and prognostic biomarkers for COVID-19. Sci Rep. 2021;11. doi:10.1038/S41598-021-94171-Y
39. Ricken F, Can AD, Gräber S, Häusler M, Jahnen-Dechent W. Post-translational modifications glycosylation and phosphorylation of the major

hepatic plasma protein fetuin-A are associated with CNS inflammation in children. PLoS One. 2022;17. doi:10.1371/JOURNAL.PONE.0268592

40. Paschinger K, Yan S, Wilson IBH. N-glycomic complexity in anatomical simplicity: Caenorhabditis elegans as a non-model nematode? Front Mol Biosci. 2019;6: 9. doi:10.3389/FMOLB.2019.00009/BIBTEX

UNIVERSITAT ROVIRA I VIRGILI
EXPLORING THE ROLE OF GLYCANS: A NEW FRONTIER IN DISEASE BIOMARKER RESEARCH
Beatrix Paton Jimenez

CONCLUSIONS

UNIVERSITAT ROVIRA I VIRGILI
EXPLORING THE ROLE OF GLYCANS: A NEW FRONTIER IN DISEASE BIOMARKER RESEARCH
Beatrix Paton Jimenez

CONCLUSIONS

Derived from the obtained results, the conclusions drawn for each objective, are as follows:

Objective 1.1:

1. Based on the initial analysis of the current state of knowledge, a wide variety of glycans are altered in ageing and age-related diseases, suggesting that changes in glycosylation could help distinguish diseases and become potential diagnostic and prognostic biomarkers.
2. The use of a wide range of glycomic methodologies and the lack of an established reference technique leads to low comparability between studies. Nevertheless, mass spectrometry (MS) is increasingly recognised as the most promising technique for glycan analysis, particularly in complex samples lacking characterization.

Objective 1.2:

3. Age-related proteins in wild-type (N2) and short-lived (CF1038) *C. elegans* strains are more drastically affected by a high-glucose diet (HGD) than the long-lived (CB1370) strain.
4. When fed a HGD, vitellogenins, involved in lipid transport activity, are increased in CB1370 strains compared to N2 and CF1038 ones. Additionally, integrative analyses reveal positive correlations between vitellogenins and phosphatidylcholines (PC) and triglycerides (TG) in N2 and CF1038 under HGD conditions.
5. The impact of a HGD on the lipidome, proteome and N-glycome in *C. elegans* varies across strains (N2, CB1370 and CF1038), with more significant changes in aged adults.
6. N-glycans are altered between diets, especially in aged adults, mainly in N2 and CB1370 strains. In N2, N-glycans generally decrease with a HGD across all time points, whereas CB1370 exhibits the opposite tren, increasing with a HGD. Understanding glycosylation patterns in

C. elegans sheds light on the role of nutrition in multi-omics approaches.

Objective 2:

7. The consumption of a high-fat diet (HFD) affects brain N-glycan and lipid profiles in hamsters. Notably, it leads to a decrease in fucosylated and sialylated N-glycan structures in HFD-fed groups, resembling changes seen in ageing.
8. The transition from a HFD to a Mediterranean-like diet (MED) resulted in some observed trends, yet there were no statistically significant changes in the brain N-glycan and lipid profiles of hamsters. This suggests that the duration of the MED intervention was insufficient.

Objective 3.1:

9. In the obtention of a global plasma glycosignature in COVID-19 patients, a decrease in fucosylated and galactosylated structures, along with an increase in agalactosylated structures, is observed in critical patients compared to mild and severe ones.

10. Distinct glycosylation signatures in SARS-CoV-2-infected patients are observed at diagnosis and 4 weeks postdiagnosis. We propose Fuc1Hex5HexNAc5 as the most suitable biomarker to stratify patients at diagnosis and distinguish mild from critical outcomes.

Objective 3.2:

11. Changes in levels of sialylated N- and O-glycans on sites N156 and T270 of human fetuin-A (hFet) distinguish COVID-19 disease severity, suggesting that desialylation could be responsible for the clearance of hFet in critical patients.

The conclusions deriving from the cross-cutting objectives addressed in all studies are as follows:

Objective 4:

12. MS, used for the analysis of glycans (including both N-glycan profiling and site-specific glycan analysis), proves to be a streamlined approach for the analysis of the glycome, allowing us to identify a large number of glycans in complex samples. Furthermore, the employed fragmentation techniques and software tools have allowed us to confidently identify these glycan structures.

Objective 5:

13. The examination of glycans across diverse animal models, including *C. elegans,* golden Syrian hamster and humans, proves to be relevant for deepening our knowledge of ageing, age-related diseases, infectious diseases and enhancing our understanding of the impact of nutrition. Notably, it suggests that dietary composition plays a critical role in shaping glycosylation patterns across species.

LIST OF PUBLICATIONS

Manuscripts included in this thesis

Published papers

Paton B, Suarez M, Herrero P, Canela N. Glycosylation Biomarkers Associated with Age-Related Diseases and Current Methods for Glycan Analysis. Int J Mol Sci. 2021 May 28;22(11):5788. doi: 10.3390/ijms22115788.

Paton B, Foguet-Romero E, Suarez M, Mayneris-Perxachs J, Boqué N, Caimari A, Canela N, Herrero P. Brain N-Glycosylation and Lipidomic Profile Changes Induced by a High-Fat Diet in Dyslipidemic Hamsters. Int J Mol Sci. 2023 Feb 2;24(3):2883. doi: 10.3390/ijms24032883.

Paton B, Herrero P, Peraire J, Del Pino A, Chafino S, Martinez-Picado J, Gómez-Bertomeu F, Rull A, Canela N, Suárez M. Fucosylated N-glycans as early biomarkers of COVID-19 severity. Front Immunol. 2023 Jun 5;14:1204661. doi: 10.3389/fimmu.2023.1204661.

Papers in preparation

Paton B, Herrero P, Arora T, García L, Suárez M, Canela N. Decoding the glycosylation signatures of ageing in *C. elegans* under a high-glucose diet: A multi-omics perspective. Ready to be submitted.

Site-Specific glycan analysis of human fetuin-A in COVID-19 patients: Implications for disease severity prediction. In preparation.

LIST OF CONFERENCES

Paton B, Foguet-Romero E, Suarez M, Mayneris-Perxachs J, Boqué N, Caimari A, Canela N, Herrero P. Brain N-glycosylation and Lipidomics in High Fat Diet-Induced dyslipideamic Hamsters. 2022. 18th International Conference of the Metabolomics Society, Metabolomics 2022. 19th-23rd June 2022, Valencia.

Paton B, Foguet-Romero E, Suarez M, Mayneris-Perxachs J, Boqué N, Caimari A, Canela N, Herrero P. Brain N-glycosylation and Lipidomics in High Fat Diet-Induced dyslipideamic Hamsters. 2022. NuGOweek 2022 Food bioactives for disease prevention: From mechanisms to chrononutrition. 29th August-1st September 2022, Tarragona.

UNIVERSITAT ROVIRA I VIRGILI
EXPLORING THE ROLE OF GLYCANS: A NEW FRONTIER IN DISEASE BIOMARKER RESEARCH
Beatrix Paton Jimenez

UNIVERSITAT ROVIRA i VIRGILI

eurecat
Centre Tecnològic de Catalunya